Universidade Vigo

International Doctoral School

Danica Ciric

DOCTORAL DISSERTATION

Linking Extreme Precipitation Events and the Associated Moisture Transport

Supervised by

Luis Gimeno Presa, PhD

Raquel Olalla Nieto Muñiz, PhD

2019

Universidade de Vigo

International Doctoral School

Dr. Luis Gimeno Presa and Dr. Raquel Olalla Nieto Muñiz,

DECLARE that the present work, entitled ***"Linking Extreme Precipitation Events and the Associated Moisture Transport"***, submitted by Danica Ciric to obtain the title of Doctor, was carried out under their supervision in the PhD programme "Applied Physics".

Ourense, 05 December 2018

The supervisors,

Dr. Luis Gimeno Presa   Dr. Raquel Olalla Nieto Muñiz

To my Family and Friends

‘‘Ништа није немогуће за онога ко има вољу покушати”

–Александар Велики–

Acknowledgements / Agradecimientos

Como autora de esta tesis me gustaría agradecer a todas las personas que estuvieron conmigo, que me apoyaron y que dieron su contribución en diferentes maneras durante los tres años de desarrollo de esta tesis doctoral. Este trabajo no hubiera sido posible completarlo con éxito sin la participación de cada uno de ellos.

En primer lugar, quiero dar las gracias a mis tutores, el Dr. Luis Gimeno y la Dra. Raquel Nieto, por la oportunidad de formar parte del grupo de investigación EPhysLab y por todos conocimientos investigadores y profesionales que aprendí de ellos. También les agradezco por su confianza y apoyo en cada momento durante todo el periodo del doctorado. Lo único que puedo decir es que para mí ha sido un honor y un gran placer estar bajo su tutoría, y de los que creo he ganado, además, una gran amistad.

Me gustaría también dar las gracias a todos mis compañeros del "Laboratorio 13", a aquellos que han estado allí durante todo el periodo de mi doctorado, y a aquellos que han estado en algún período más corto: Anita, Marta, Rogert, Milica, Iago, Lucia, Jorge, Zeinab, Dejanira, Elham, Motjaba, Moha, Natalia, y Aleksandar. Aprendí de cada uno de ellos algo distinto y tenía su apoyo y ayuda siempre cuando lo necesitaba. Gracias, porque habéis hecho que este periodo largo pasase muy rápido y que siempre estuviese rodeada de personas maravillosas. Agradezco especialmente a Marta por su paciencia, ayuda y porque siempre ha estado disponible para resolver todas mis dudas relacionas con el mundo del IDL. Y también merece un agradecimiento distinguido la Dra. Anita Drumond por su colaboración en todos mis trabajos y porque siempre ha estado disponible a ayudarme y darme los mejores consejos profesionales y personales.

Me gustaría dar las gracias a mis queridos vecinos Gloria, Antonio, Iván y Jorge por su cariño, amor y por la oportunidad de tener una "segunda" familia en España.

Por último, no podría dejar de dar las gracias a las personas más importantes en mi vida, mis padres, mi hermana y a Milos. Gracias por vuestro amor, apoyo, porque hayan estado disponibles siempre cuando les necesitaba y por aguantarme y entenderme en

ciertos momentos duros, y especialmente cuando estaba “muy pesada”. Por eso quiero dedicaros esta tesis doctoral a todos vosotros.

También agradezco a todos mis amigos y primos de Serbia que estuvieron conmigo todo este tiempo en la distancia.

Este trabajo ha sido financiado durante estos tres años por la beca de European Commission under the Erasmus Mundus Project Green-Tech-WB: Smart and Green Technologies for Innovative and Sustainable Societies in the Western Balkans (551984-EM-1-2014-1-ES-ERA Mundus-EMA2). También quisiera agradecer a la Universidade de Vigo por el apoyo financiero para la realización de una estancia predoctoral en el “ALFATEC” en Nis, Serbia bajo las ayudas: Estadías en centros de investigación.

Захвалница

Као аутор ове докторске тезе хтела бих да се захвалим свим људима који су током њеног настајања били уз мене, подржавали ме и дали свој допринос у реализацији на различите начине. Сигурно да овај рад не би био успешно завршен без учешћа сваког од њих.

Најпре, велику захвалност дугујем својим менторима др Луис Гимено и др Ракел Нието на прилици да будем део истраживачке групе *EPhysLab* и на све стечено истраживачко и професионално знање које сам добила од њих. Такође, хтела бих да им се захвалим на поверењу и подршци коју сам добила од њих у сваком моменту током трајања студија. Једино што могу да кажем је да ми је била част и велико задовољство бити под њиховим менторством и поврх свега стећи једно велико пријатељство.

Захваљујем се свим мојим колегама из „Лабораторије 13“, онима који су били тамо сво време током мог боравка и онима који су били у одређеном периоду: Анита, Марта, Роџерт, Милица, Иаго, Лусиа, Хорхе, Зеинаб, Дежанира, Елхам, Моштаба, Моха, Наталиа и Александар. Свако од њих ме је научио нешто ново и пружио ми подршку увек када ми је била потребна. Хвала вам што сте учинили да овај период прође брзо и што сам имала прилику да будем окружена дивним особама око себе. Посебно се захваљујем Марти на стрпљењу, помоћи и што је увек била спремна да реши сваку моју недоумицу везану за један мени нови свет зван „*IDL*”. Такође посебну захвалност дугујем др Аниті Друмонд на њеном учешћу у свим мојим радовима и што је увек била ту да ми да најбољи могући савет на професионалном и приватном плану.

Не могу а да не искажем велику захвалност мојим дивном комшијама: Глорији, Антониу, Ивану и Хорхеу на указаној пажњи, љубави и прилици да имам другу породицу у Шпанији.

На крају, посебно се захваљујем најважнијим особама у мом животу, мојим родитељима, сестри и Милошу на безрезервној подршци, љубави и стрпљењу које су имали за мене у одређеним тешким тренутцима, посебно у оним када ме је било тешко поднети. Зато желим да посветим ову докторску дисертацију свима вама.

Такође се захваљујем свим мојим пријатељима и члановима породице из Србије који су били уз мене све ово време.

Ова докторска дисертација је током три године њене реализације била финансирана стипендијом добијеном од стране European Commission under the Erasmus Mundus Project Green-Tech-WB: Smart and Green Technologies for Innovative and Sustainable Societies in the Western Balkans (551984-EM-1-2014-1-ES-ERA Mundus-EMA2). Такође захваљујем Universidade de Vigo на финансијској подршци за реализацију истраживачког боравка у току докторских студија у научно – истраживачком центру „ALFATEC” у Нишу у оквиру програма: Estadías en centros de investigación.

CONTENTS

ABSTRACT

The research presented in this PhD dissertation aims to characterise the transport of moisture from the detected main moisture source regions using a Lagrangian perspective at the regional and global scales, and to link this transport with extreme precipitation events that have recently occurred around the world. The role of anomalous moisture transport for extreme rainfall events that occur due to the impact of climate change is important for current and future research related to the occurrence of intense precipitation, flood events, and accompanying risks in several regions.

This work consists of four published articles in scientific journals included in the SCI list, listed in "Chapter 4: Collection of Publications" of this PhD thesis, and the independent Chapter 5, which presents "A Global Atlas of Precipitation and Contribution of the Main Moisture Sources in the Peak Precipitation Month". The published papers describe moisture transport at the regional scale in two related regions in Europe, the Danube River Basin, and the Mediterranean Basin.

The first studied region is the ***Danube River Basin*** (DRB), an important European catchment and the second largest in Europe by size. Three research activities were conducted in the DRB: i) detection of the main moisture sources for precipitation; ii) ranking the extreme precipitation events; and iii) investigation of the moisture contribution from the Mediterranean Sea to the extreme precipitation events detected.

The ***Mediterranean Basin*** was analysed next. It is one of the main oceanic moisture sources producing continental precipitation (Gimeno et al., 2010, 2012). Its effect on the mean and extreme precipitation on the surrounding continental areas, and the sink for its moisture, were examined.

Finally, in a worldwide study, the role of the major global moisture source regions in the occurrence of extreme precipitation over the continents was investigated. This work forms the basis of the ***Global Atlas of Precipitation and Contribution of the Main Moisture Sources in the Peak Precipitation Month***.

Throughout this work, the Lagrangian model FLEXPART, v9.0, was used to analyse moisture transport for precipitation. The model requires a division of the atmosphere into approximately 2 million virtual air particles recorded every 6 hours, with constant mass and motion along the trajectories allowed by the three-dimensional wind fields inferred by the input model data, the ERA-Interim reanalysis. Following the particles' trajectories in a backward mode, it is possible to detect regions where particles gain moisture along their pathway, thus identifying regions that are the sources of moisture. Tracking particles' forward trajectories allows identification of regions where particles lose moisture, indicating the main moisture sink regions. To identify regions that are moisture sources and sinks, changes in specific humidity along the particles' trajectories were tracked, and the fresh water balance was calculated as evaporation rate minus precipitation rate (E-P). Regions where evaporation exceeds precipitation (E-P > 0) are defined as moisture sources, whereas in moisture sink regions, precipitation exceeds evaporation (E-P < 0).

The main source regions were detected using this methodology by following the backward trajectories of air particles that ultimately reach the DRB. The results show that seven different moisture source regions are responsible for precipitation over the Danube basin: the Danube River Basin itself, the Mediterranean Sea, Caspian Sea, Black Sea, North Atlantic Ocean and two additional sources located over land areas, including part of North Africa, and continental parts of Central and Eastern Europe.

Once the climatological moisture sources for the DRB were identified, the next important step in the study was characterizing the extreme precipitation events (wet spells) over the region, and linking these with the moisture sources. Wet spell events of different durations (1, 3, 5, 7, and 10 days) were detected by applying a ranking methodology developed by Ramos et al. (2014; 2017). Daily precipitation data from the Climate Hazards Group InfraRed Precipitation with Station (CHIRPS) during the period 1981 to 2015 was used. The ensuing ranking was used for two different analyses. The first one was based on the top-ranked 1-day extreme precipitation event, which occurred on 23 September 1996. The roles of the moisture sources for this event were investigated, and a complete synoptic analysis was done to better understand this extraordinary event. The larger second analysis took into consideration the top 100 extreme precipitation events across all time scales (1, 3, 5, 7, and 10 days). In this second analysis, moisture contribution from the Mediterranean Sea only, one of the most evaporative regions in the world, was considered. The analysis was done at the annual and seasonal scales.

The Mediterranean Sea was also investigated in terms of its contribution to climatological and extreme monthly precipitation over the surrounding continental areas. The monthly Multi-Source Weighted-Ensemble Precipitation (MSWEP) database was used to determine climatological and extreme precipitation over the region each month from 1980 to 2015, while the Mediterranean sea's moisture contribution was computed via the FLEXPART Lagrangian model. In this case, the air particles were followed forward from the Mediterranean Sea to compute the moisture that generates precipitation over the continental areas. This study highlighted that the Mediterranean Sea, as a moisture source for precipitation, has a similar spatial pattern for monthly precipitation during both extreme and regular climatological conditions. Moreover, significant differences were recorded over the European continent; in some areas the Mediterranean Sea plays a significant role in extreme precipitation events, but is not an important source of moisture for climatological precipitation.

As mentioned above, in this thesis the characterization of extreme precipitation events started from a regional perspective (Danube River Basin and Mediterranean Sea) and then expanded to a global perspective. For this purpose, a ***Global Atlas of Precipitation and Contribution of the Main Moisture Sources in the Peak Precipitation Month*** was prepared. The Atlas connects the monthly provision of moisture by the main global moisture sources with precipitation during the peak precipitation month (PPM). The study was performed on a grid of 0.25° resolution in longitude and latitude. The forward mode was applied to the Lagrangian trajectories to compute precipitation over continental areas from each moisture source. This data was combined with the MSWEP monthly precipitation dataset to construct the Atlas, which consists of 26 types of maps. Fourteen of these maps are presented in Chapter 5; 12 more are located in Appendix A: Supplementary Material. The first map in the Atlas provides new, much-needed information about the contribution of moisture sources to precipitation on a monthly scale; previously, this information existed only at an annual scale. The following maps detail the PPM grid-by-grid, using MSWEP monthly precipitation data around the globe. The remaining maps aim to better characterize the moisture supply from the main sources during the PPM, both from a climatological point of view and during the occurrence of extreme precipitation events over each grid square.

RESUMEN

La investigación del transporte de humedad a partir de fuentes de humedad detectadas tanto a escala global como regional en las últimas décadas es uno de los temas más estudiados e importantes en hidrología y ciencias del cambio climático. El papel de la cantidad de humedad transportada para la generación de precipitación continental, y más en particular, para la génesis de eventos extremos, en las áreas terrestres circundantes o más lejanas, es crucial para comprender la frecuencia e intensidad de las precipitaciones intensas y/o inundaciones posteriores a las mismas.

Los desastres naturales y los eventos de inundaciones catastróficas que resultan de la precipitación de los eventos extremos pueden volverse más frecuentes y graves en el futuro (Kundzewicz et al., 2006). El estudio y las predicciones de los cambios de precipitación a escala global tienen una función importante para la estimación de los cambios en la frecuencia e intensidad de los extremos de precipitación a lo largo del tiempo (Tu and Chou, 2013), pero los cambios en la frecuencia y el volumen de los extremos de precipitación a escalas regionales representan un reto mayor, y juegan una función importante de incertidumbre en las predicciones climáticas (Smalley and L'Ecuyer, 2015). Debido a estas afirmaciones, la investigación, el monitoreo y la estimación de los extremos de precipitación, tanto a escala global como regional, son cruciales y de igual importancia.

La estructura de esta tesis está organizada en seis capítulos principales dispuestos de la siguiente manera: El Capítulo 1 presenta un breve resumen del ciclo hidrológico y del transporte de humedad en la atmósfera, las precipitaciones medias y extremas distribuidas por todo el mundo. También se revisaron las investigaciones relacionados con la precipitación media y extrema en la región del Mar Mediterráneo. Por último, se presenta una breve revisión sobre las fuentes de humedad más importantes del planeta y su importancia en la precipitación sobre los continentes. El Capítulo 2 incluye los objetivos principales relacionados con los estudios hechos en este trabajo. El Capítulo 3 presenta un resumen de la metodología y técnicas utilizadas para la realización de los diferentes experimentos o análisis. El Capítulo 4 incluye los cuatro artículos publicados

en revistas incluidas en la lista *Science Citation Index* (SCI) que componen el cuerpo de esta tesis doctoral escrita y presentada como compendio de publicaciones según la normativa vigente de la Universidad de Vigo. Los artículos publicados se centran, a modo de resumen, en la ligazón de las precipitaciones extremas en la región del Mediterráneo, y sobre la cuenca del río Danubio (como sub-área de la misma), y la humedad transportada desde la propia cuenca del Mar Mediterráneo para la generación de la precipitación anómala que finalmente deviene en eventos extremos. Finalmente, en el Capítulo 5 se presenta, de modo independiente a las publicaciones del capítulo anterior, un Atlas Global de Precipitación y Contribución de las Principales Fuentes de Humedad en el Mes de Máxima Precipitación. Este último capítulo expande el estudio del papel de las fuentes de humedad en la precipitación extrema a una escala global. En el Capítulo 6 se incluye, para cerrar este manuscrito, un resumen de las principales conclusiones derivadas de los trabajos realizados durante el período de la tesis doctoral, y la propuesta para trabajos futuros siguiendo la misma línea de investigación.

Como ya se ha mencionado en el párrafo anterior, este trabajo consiste en cuatro artículos ya publicados y un Atlas. La descripción de los resultados y el orden de este documento se realizada de un modo cronológico, comenzando por los artículos publicados en primer lugar y terminando con el Atlas, aún en proceso de escritura para ser enviado a una revista de carácter internacional indexada en SCI. Asimismo, el orden también refleja una expansión en el ámbito geográfico de estudio, ya que los tres primeros artículos se centran en análisis más regionales estudiando el transporte de humedad y la asociación con la generación de precipitaciones extremas en la cuenca del rio Danubio, para posteriormente estudiar la cuenca del Mediterráneo en todo su conjunto. Finalmente, el Atlas presenta un análisis a escala global planetaria de la importancia de todas las fuentes de humedad, tanto oceánicas como continentales, en la precipitación extrema.

En primer lugar, se eligió para ser investigada la **cuenca del río Danubio**, ya que es la segunda cuenca hidrográfica más larga de Europa tras el rio Volga, con una longitud de 2.780 km y un caudal medio 6.460 m³/s. Tiene su nacimiento en la Selva Negra en Alemania y desemboca en el Mar Negro en Rumanía, representa pues un río muy internacional, compartiendo su cuenca entre 19 países. Su extensión y posición hace que la cuenca del Danubio tenga una gran importancia en muchos ámbitos, como la disponibilidad de agua, la agricultura, la calidad de la vida humana, etc. La investigación que concierne a esta tesis sobre la cuenca del río Danubio se realizó en tres direcciones diferentes: i) primero se llevó a cabo la detección de las principales fuentes de humedad para la precipitación sobre la cuenca del río Danubio; ii) a continuación se realizó una clasificación de los eventos de precipitación extrema en la cuenca del Danubio para el período de 1980 a 2015, y iii) finalmente se analizó la contribución del Mar Mediterráneo en la generación de los eventos de precipitación extrema detectados sobre la cuenca.

Para la identificación de las fuentes de humedad para la cuenca del río Danubio (DRB), se utilizó el modelo Lagrangiano FLEXPART v9.0 (Stohl and James, 2004, 2005) alimentado con los datos del reanálisis ERA-Interim del European Centre para Medium-Range Weather Forecasts (ECMWF) (Dee et al., 2011). Los datos son accesibles a 1° × 1° grado de longitud y latitud en 61 niveles verticales, de 0.1 a 1000 hPa. Para un primer experimento, el estudio cubre un período temporal de 35 años desde 1980 hasta 2014, debido a la disponibilidad de los datos de ERA-Interim en el momento de la realización del mismo. Para un análisis realizado más adelante, el período de estudio se prolongó hasta 37 años, desde 1980 hasta 2016.

El modelo FLEXPART fue desarrollado inicialmente (Stohl et al., 1998) como un modelo para el cálculo de la dispersión a largas distancias y mesoescalar de los contaminantes liberados en la atmósfera desde fuentes puntuales, como los contaminantes del aire que se producen después de un accidente en una central nuclear. Durante los años posteriores a su desarrollo, el modelo se ha convertido en una herramienta integral utilizada en la rama atmosférica para la investigación del transporte y análisis de la humedad atmosférica, tanto a nivel regional como global. El modelo FLEXPART en su versión 9.0 realiza una división de la atmósfera en aproximadamente dos millones de las partículas de aire virtuales con masa constante, registradas en cada 6 horas, y que son advectadas por el campo de viento definido por los datos con los que el modelo es alimentado. Los movimientos de las partículas a lo largo de las trayectorias son permitidos por el campo de viento tridimensional (horizontal y vertical), así como por los movimientos turbulentos y convectivos

estocásticos superpuestos (más información sobre las parametrizaciones del modelo pueden ser encontrada en la nota técnica al respecto en Stohl et al. (2005)).
A lo largo de las trayectorias, y cada 6 horas, el modelo guarda aquellas variables que los datos de ERA-Interim es capaz de proporcionarnos, como pueden ser la posición (latitud, longitud y altura), temperatura, y humedad específica, entre otros. Así, y con la mente puesta en el cálculo de fuentes y sumideros de humedad, las variables de posición y humedad específica serán las de mayor interés para el fin que se propone en este trabajo. Siguiendo las trayectorias de las partículas, el modelo nos permite detectar regiones donde las partículas ganan o liberan la humedad, identificando las fuentes de humedad o regiones sumideros, respectivamente. El seguimiento de los cambios en la humedad específica (q) a lo largo de las trayectorias, y realizando un cómputo del balance en la vertical (sobre una región a definir) de los mismos, identifica las regiones donde la evaporación excede a la precipitación (E-P > 0), estas regiones se definen como fuentes de humedad, y en caso contrario cuando la precipitación excede la evaporación (E-P < 0) representa las regiones sumidero de humedad.

Así, siguiendo las partículas de aire sobre la cuenca del Danubio (DRB) hacia atrás en el tiempo (análisis backward), se detectaron sus principales regiones fuentes de humedad. Los resultados obtenidos muestran que para el Danubio existen siete fuentes de humedad diferentes: a) cinco ubicadas sobre ríos, mares y océanos: la propia cuenca del Danubio, el Mar Mediterráneo, el Mar Caspio, el Mar Negro y el Océano Atlántico Norte, b) y dos fuentes más sobre tierra: aquella que incluye regiones continentales que rodean a la cuenca del Danubio sobre el Este y Europa Central y una fuente sobre el norte de África. Se comprobó que las contribuciones de las fuentes también son diferentes a lo largo del año. Por lo tanto, durante la temporada de invierno (de octubre a marzo), la humedad dominante en la DRB es aquella que viene del mar Mediterráneo, mientras que durante la temporada de verano (de abril a septiembre) la propia cuenca del Danubio se identificó como la mayor fuente de humedad.

Una vez identificadas las fuentes de humedad climatológicas para el DRB, el siguiente paso importante en el estudio es la investigación del transporte de humedad asociado con los eventos extremos de precipitación en la cuenca, con el objetivo de analizar sus contribuciones en la generación de las precipitaciones extremas. Siguiendo esta idea, en este trabajo hemos realizado una clasificación de eventos de precipitaciones extremas (wet spells) en la cuenca del río Danubio con diferentes duraciones de 1, 3, 5, 7 y 10 días. Para ello se utilizaron valores diarios de precipitación del Climate Hazards Group Infra-Red Precipitation with Station (CHIRPS, Funk et al., 2015). Los datos tienen alta resolución espacial (0.05° en latitud y longitud), y para esta investigación se consideró un período temporal de 35 años, de 1981 a 2015. Para la detección de los eventos de precipitación extrema, se utiliza un índice de clasificación (R) basado en la magnitud de las anomalías de precipitación de cada evento. El índice de clasificación final (R) se obtiene como resultado de multiplicar dos variables: i) el porcentaje de área (A) con anomalías de precipitación mayores que dos desviaciones estándar, y ii) la magnitud media de anomalías de precipitación (M) sobre el área expresada como A. Por lo tanto, el índice de clasificación se puede expresar con la siguiente ecuación: $R = M \times A$. Para el cálculo del índice, solo se tienen en cuenta los puntos de la cuadrícula con una cantidad de precipitación superior a 1 mm/día. Usando los resultados de este ranking se realizaron dos trabajos con puntos de vista independientes. El primero se centró en el evento detectado más intenso, que ocurrió el 23 de septiembre de 1996. Para esa fecha se determinaron sus fuentes particulares de humedad, así como la situación sinóptica que dio lugar a tal evento extremo. Después, el análisis se amplió considerando los primeros 100 eventos del ranking para todas las duraciones, y en qué manera influyó en los mismos el aporte de humedad desde el Mar Mediterráneo.

Análisis del evento de precipitación extrema ocurrido el día 23 de septiembre de 1996

Los resultados de este estudio, como ya se dijo anteriormente, están enfocados en el evento más intenso de precipitación y que fue detectado en el primer lugar del ranking para eventos de duración de un día. El análisis sinóptico de la situación para ese día indica la existencia de una ciclogénesis sobre el sur de Europa (acompañado de una fuerte anomalía en el campo de convergencia), que cruzó la región del Danubio y dio lugar a las precipitaciones extremas. Al mismo tiempo, un fuerte anticiclón estaba posicionado en el Atlántico Norte. El análisis de las anomalías de humedad que dieron origen a las fuertes precipitaciones se realizó utilizando el método backward usando las salidas de modelo Lagrangiano FLEXPART v9.0. Los resultados del estudio demuestran que, en este día el sistema recibió un aporte de humedad anómalo desde tres fuentes marítimas: el Mar Mediterráneo, el Mar Negro y el Océano Atlántico Norte. Esta última fuente de humedad desde el Océano Atlántico no es habitual, lo que llevó a un análisis pormenorizado de esta anomalía. Se encontró que las condiciones sinópticas ocurridas con anterioridad al evento y durante el mismo apoyaron la ocurrencia de este evento excepcional. A la derecha del ciclón sobre el Danubio se encontraba un anticiclón que perduró durante al menos 10 días antes del evento y que actuó como una cinta transportadora de humedad desde el Atlántico hasta el Mediterráneo, donde fue captada por el ciclón. Esa humedad sobre el Atlántico se justifica por la ocurrencia del huracán Hortense durante los días anteriores al evento (del 9 al 14 de septiembre 1996) y que se transformó en un ciclón extratropical que llegó hasta las costas europeas dejando una cantidad de humedad anómala en la zona. Esta sería luego transportada hacia el Mediterráneo por un sistema de bajas presiones secundario que ocurrió inmediatamente después del huracán, asociado con un río atmosférico y que toma la humedad dejada por el huracán y la transporta a la cuenca del rio Danubio.

<u>Análisis de los 100 primeros eventos de precipitación extrema sobre la cuenca del Danubio</u>

El segundo estudio considera los primeros 100 casos del mismo ranking hecho para la cuenca Danubio y analiza la relación entre los eventos extremos detectados y el transporte de humedad anómalo originado desde el Mar Mediterráneo. Este estudio cubre el período temporal 1981-2015. La contribución de la humedad anómala desde el Mediterráneo se realizó a través del cómputo de los cambios de humedad en las trayectorias simuladas por el modelo Lagrangiano FLEXPART en modo hacia adelante (forward) en el tiempo, analizando las partículas que salen del Mar Mediterráneo y llegan a la cuenca del Danubio. Como se mencionó anteriormente, el estudio toma en cuenta los primeros 100 casos de la clasificación en diferentes escalas de tiempo (diferentes duraciones) de 1, 3, 5, 7 y 10 días. El período del tiempo para el seguimiento de las trayectorias se ajusta en función de la duración de los eventos, por lo que, para los eventos extremos de duración de 1 día, el tiempo de integración considerado es de 1 día, para aquellos con una duración de 3 días el tiempo es de 3 días, y así hasta los 10 días. La importancia del Mar Mediterráneo como fuente para las precipitaciones extremas registradas se confirma con el hecho de que entre el 84% y el 93% de los eventos analizados fueron suministrados por humedad anómala desde esta fuente. La relación establecida entre el transporte de humedad anómalo desde el Mar Mediterráneo y los eventos extremos resaltó que el mayor número de los mismos ocurrieron durante el invierno. En particular, de los 100 casos analizados, ocurrieron en invierno 36 para los eventos con duración de 1 día, 42 para los de 3 días, 46 para los de 5 días, 39 para aquellos de 7 días, y finalmente 43 casos para eventos de 10 días. Sin embargo, no es en esta estación cuando el Mediterráneo aporta más humedad porcentualmente, ocurriendo ésta en un 100% de los casos en la época de verano y primavera. En general, los resultados también sugieren que el Mar Mediterráneo tiene una contribución más significativa en la generación de los eventos de precipitación extrema con una duración más larga que en aquellos con una duración más corta.

En segundo lugar en esta tesis se investigó el **Mar Mediterráneo** como fuente principal de humedad para producir la precipitación continental (Gimeno et al., 2010, 2012), con el propósito de estudiar su influencia sobre la precipitación media y extrema en todas sus áreas continentales circundantes, y no solo sobre la cuenca del Danubio. En la literatura existen diversos trabajos en los que se pone de manifiesto el importante papel que juega el Mediterráneo como fuente de humedad tanto a escala global como regional (como también queda reflejado en los resultados presentados anteriormente) debido a su posición subtropical (e.g. Mehta and Yang, 2008; Trigo et al., 2006). La investigación relacionada con esta región se centra, en este trabajo, en analizar la contribución de la humedad procedente del mar Mediterráneo en la precipitación mensual, tanto climatológica como extrema, en su área continental circundante y sobre la que tiene influencia. Debido a esto, es muy importante comprender previamente el patrón de precipitación, la intensidad y la frecuencia en toda la región mediterránea mensualmente. Con este fin se utilizó la base de datos de precipitación mensual MSWEP (Beck et al., 2017a) para determinar la precipitación en términos climatológicos y las precipitaciones extremas (media de los cinco años de lluvia más alta) en cada punto de rejilla sobre la región de interés.

La precipitación media mensual mostró, como cabía esperar, una clara dicotomía entre el invierno y el verano. En general durante el invierno, los valores más altos de precipitación se registraron a lo largo de la costa atlántica europea y partes de Europa

Central debido a la precipitación frontal típica asociada con los ciclones en los límites norte y este de la cuenca y sobre la región del Fertile Crescent debido a sistemas convectivos. Sin embargo, durante el verano, el patrón muestra sus valores máximos afectando prácticamente todo el continente euroasiático, a excepción de las penínsulas Ibérica y de Anatolia y la región norte de África. El análisis de la media mensual de los valores extremos de precipitación mostró un patrón similar al climatológico.
Cuando se analiza la relación entre la climatología y los eventos extremos, se hace evidente que la precipitación extrema modula, en algunas partes de la región del Mediterráneo continental, los valores climatológicos medios. Este comportamiento es evidente en las regiones áridas y semiáridas, incluido el sur de la Península Ibérica tanto en verano como en invierno, cuando los eventos extremos generan valores tres veces superiores a la precipitación media. Sobre las penínsulas de Anatolia y del sur de Grecia, esto ocurre en verano. Sin embargo, también es destacable el hecho de que sobre algunas regiones esta relación alcanza valores bajos, lo que indica que, a lo largo del período analizado (36 años), la precipitación es bastante regular sobre las mismas. Esto ocurre en terrenos elevados como los Alpes y las montañas de los Cárpatos y Escandinavia, donde las precipitaciones cuando ocurren son siempre copiosas.

Para la estimación de la contribución de humedad desde el Mediterráneo se usaron las salidas del modelo Lagrangiano FLEXPART v9.0 y se siguieron las trayectorias de las partículas que salen de la cuenca hacia adelante en el tiempo durante 10 días mediante el cálculo de ($E-P < 0$) sobre la región continental. El análisis se realizó para un periodo de 36 años, desde 1980 a 2015, ambos incluidos, en una resolución espacial de 0.25º en longitud y latitud.
El análisis de la contribución del Mediterráneo a la precipitación continental mostró que durante el invierno, los principales sumideros de humedad se encuentran en la región noreste del Mediterráneo con una clara dirección hacia el oriente causado por vientos predominantes del oeste. Durante el verano, además de registrarse valores más bajos, las áreas afectadas son más locales (con un alto impacto en la región alpina, la Península Ibérica oriental, Oriente Medio y el norte de África). La contribución de la humedad del Mediterráneo a la precipitación extrema muestra un patrón geográfico similar en ambas estaciones a su climatología; mostrándose una sobre-estimación de la humedad para la precipitación modelada por FLEXPART en comparación con datos de

MSWEP sobre las regiones áridas (recordar que lo que se calcula en este trabajo es la humedad disponible para la precipitación que a falta de mecanismos de inestabilidad no precipitaría).
Cuando se comparan los valores de precipitación extrema (modelados y de MSWEP), como cabe esperar, los modelados son más bajos porque sólo se están calculando las cantidades de precipitación continental con origen en el Mar Mediterráneo (cuando una región puede tener una o varias fuentes de humedad).
La proporcionalidad entre los valores modelados climatológicos y extremos muestra que la contribución del Mar Mediterráneo a los eventos extremos durante los meses de verano es más pronunciada en la Península Ibérica, en la costa de Oriente Medio y en las regiones desérticas del norte de África, donde puede los valores extremos llegan a ser hasta tres veces mayores que la media climatológica. Aparece un caso interesante en las regiones alpinas, en los Balcanes y Grecia, donde la proporción muestra un comportamiento opuesto durante el invierno y el verano. Durante el invierno, el Mar Mediterráneo aporta hasta cinco veces más humedad para la precipitación durante los eventos extremos, mientras que durante el verano la contribución es bastante similar a la climatológica (proporción cercana a la unidad). En Europa Central y Occidental durante el invierno la relación también es cercana a la unidad, lo que muestra que los valores medios y extremos exhiben cantidades bastante similares.
En resumen, los resultados mostraron que el patrón espacial de la contribución de la lluvia de la fuente mediterránea es similar para los años de precipitación extrema en comparación con la climatología. Sin embargo, se producen diferencias significativas a nivel local, especialmente en cualquier región europea donde el Mediterráneo no sea una fuente regular de humedad para la precipitación climatológica, pero sí una fuente importante en años de precipitaciones extremas.

Finalmente, el análisis de la contribución de las principales fuentes de humedad a la precipitación extrema continental se expandió a una escala global. Los resultados se muestran en el Capítulo 5 de esta tesis como un Atlas de la precipitación para todo el mundo, titulado: **“Un Atlas Global de Precipitación y Contribución de las Fuentes Principales de Humedad en el Mes de Precipitación Máxima”**. Para formar este Atlas global, se utilizaron los datos mensuales de precipitación de MSWEP y los campos de E-P < 0 obtenidos a partir de las trayectorias calculadas del modelo

Lagrangiano FLEXPART v9.0. El Atlas proporciona una visualización exhaustiva del papel que tiene el transporte de humedad desde las principales fuentes globales en la ocurrencia de las precipitaciones extremas en áreas continentales a escala global.

En primer lugar se realizó una nueva detección de las fuentes de humedad globales mes a mes siguiendo la metodología de Gimeno et al. (2010). La metodología aplicada para detección las fuentes mensuales se basa en el cálculo de los máximos de la divergencia del flujo de humedad integrado en la vertical (VIMF, de sus siglas en inglés), en vez de usar la climatología anual utilizada en Gimeno et al. (2010) en el que se definían unas fuentes fijas. En este trabajo las fuentes son identificadas mes a mes y su extensión diferirá por tanto a lo largo del año. Los datos de reanálisis de ERA-Interim (Dee et al., 2011) del ECMWF usados para el cálculo de la divergencia de VIMF se extienden desde enero de 1980 hasta diciembre de 2016, con una resolución espacial de 1° × 1° grados en latitud y longitud. Para la definición de las fuentes de humedad se aplicó un umbral mensual basado en el percentil 50 de la divergencia de VIMF para las fuentes oceánicas y en el percentil 40 para las continentales. Esto difiere de Gimeno et al. (2010) que usa un umbral fijo de 750 mm/año y 500 mm/año para las fuentes oceánicas y terrestres, respectivamente. La elección de los percentiles 50 y 40 se basa en el intento de encontrar un percentil común a la menor distancia del umbral utilizado en el trabajo anteriormente citado. Así pues, se identificaron un total de 14 fuentes principales de humedad, 11 oceánicas: NPAC (Pacífico Norte), SPAC (Pacífico Sur), MEXCAR (Golfo de México y Mar Caribe), NATL (Atlántico Norte), SATL (Atlántico Sur), ZANAR (Corriente de Zanzíbar y Mar Arábigo), AGU (Corriente de Agulhas), IND (Océano Índico), CORALS (Mar del Coral), MED (Mar Mediterráneo), REDS (Mar Rojo), y 3 fuentes más en tierra: SAM (América del Sur), SAHEL (Sahel región) y SAFR (África Sur).

Una vez definidas las principales fuentes de humedad también se detectaron los sumideros asociados a cada una de ellas utilizando, como ya se ha comentado antes, los campos de E-P < 0 calculados desde las salidas del modelo Lagrangiano que conforma la base de esta tesis. La caracterización de los sumideros se realiza para cada mes del año, generando 12 mapas en total por fuente de humedad (para simplificar, en el Capítulo 5 de esta tesis se presentan solo los mapas de enero y julio, mientras que los mapas para los otros meses se pueden encontrar en el Apéndice A: Material Suplementario marcados de la figura A.4.1 a la figura A.4.12).

Con el fin de describir las características de la precipitación global en términos climatológicos, tanto a escala anual como mensual, se utilizó la base de datos de precipitación MSWEP (Beck et al., 2017a). Usando los datos de la climatología de precipitación mensual de MSWEP se detectó punto a punto de grid (0.25 grados) el mes que muestra la precipitación máxima, al que se denominará a partir de ahora como "Mes de Precipitación Máxima" (PPM, en sus siglas en inglés de Peak Precipitation Month). Los resultados muestran claramente el movimiento de la ITCZ (Zona de Convergencia Intertropical) que se produce en los PPMs entre diciembre y febrero (verano austral) en latitudes de 10°S a 30°S grados en el centro de América del Sur, Sudáfrica y el norte de Australia; y durante julio y agosto (verano boreal) sobre el sur de Asia, el Sahel y África Central, y entre 5°N y 30°N en América. Más al norte, prácticamente en todo el continente asiático, el norte de Europa y el norte y centro de América del Norte, los PPMs se ocurren para los meses entre junio y agosto. Es interesante observar que la región del Mar Mediterráneo y el norte de Norte américa exhiben el patrón más diverso.

Como se comentó anteriormente, para estimar la contribución de la precipitación desde cada fuente de humedad detectada en cada punto de la rejilla se obtuvieron los campos E-P < 0 utilizando los resultados de FLEXPART para el período 1980-2016. Agregando los valores de E-P < 0 para todas las fuentes detectadas para cada PPM, se realizó un mapa de la contribución para la precipitación por cada una de las fuentes principales durante el PPM de cada punto de rejilla. Los resultados muestran que algunas áreas durante el PPM son afectadas por tan solo una fuente, mientras que hay otras afectadas por dos o más. Por ejemplo, el área de América del Norte, donde la mayoría de los PPM son en julio, solo se ve afectada por una única fuente, el Pacífico Norte. Por otro lado, hay regiones donde durante el PPM contribuyen dos o más fuentes de humedad, por ejemplo, es el caso de la región del sur de la Península Arábica, Irak, Irán y Kazajstán donde el PPM es marzo y la humedad para la precipitación es aportada desde las fuentes del Mar Rojo y la zona de la Corriente de Zanzíbar y el Mar de Arabia.

El siguiente paso en la construcción de este Atlas fue el cálculo de la fuente preferente de humedad para el mes de precipitación máxima (PPM) en cada punto de la rejilla. La fuente de humedad que contribuye más a la precipitación en cada punto de la rejilla se denota pues como la “Fuente Preferente” (PS). Los resultados muestran que en la costa atlántica europea, desde la Península Ibérica hasta la Península Escandinava, la fuente preferente es el Océano Atlántico Norte, mientras que para Europa del Norte hasta Eurasia y para África del Norte la fuente preferente de la humedad es el Mar Mediterráneo. La fuente del Atlántico Norte extiende su gran influencia en los PPM sobre la cuenca del río Amazonas, mientras que la fuente de humedad del Atlántico Sur prevalece sobre la mayor parte del este de Sudamérica y sobre África Central. Por otro lado, para Sudáfrica, la fuente preferente es la Corriente de Agulhas.

Para mostrar la importancia de la contribución de humedad de las fuentes principales durante los PPMs se realizó también el cálculo del porcentaje de la contribución de cada fuente. El propósito de este cálculo es mostrar qué porcentaje de la cantidad de precipitación en el PPM se debe a la humedad proveniente de cada una de las fuentes de humedad detectadas. También se calculó el porcentaje de la contribución de la fuente preferente para cada cuadrícula en comparación con todas las fuentes detectadas. Los valores porcentuales más altos indican que en esas áreas las grandes cantidades de precipitación para los PPMs provienen de la fuente preferente detectada.

Por ultimo en el Atlas son incorporados los mapas que muestran la media de precipitación para los 5 años de máxima y de mínima precipitación para cada punto de rejilla en el PPM utilizando datos de MSWEP. Para estos años de extremos de precipitación se tomaron también los valores medios de los campos de E-P < 0 calculados a partir de las salidas del modelo Lagrangiano FLEXPART para las fuentes preferentes detectadas. Se observa que la distribución geográfica de la precipitación es similar, indicando que el modelo FLEXPART y la metodología utilizada para calcular la humedad que produce la precipitación continental procedente de las principales fuentes de humedad es válida tanto para el análisis de valores medios como para el caso de extremos de precipitación, captando las variabilidades espaciales y temporales con gran exactitud.

LIST OF FIGURES

LIST OF TABLES

ACRONYMS

AGU	Agulhas Current
Anom. CHIRPS	Daily precipitation anomaly value from the CHIRPS precipitation dataset
Anom. PFLEX	Daily anomalous (E-P < 0) value obtained via Lagrangian experiment
CHIRPS	Climate Hazards Group Infra-Red Precipitation with Station data dataset
CORALS	Coral Sea
CRU	Climate Research Unit
DOI	Digital Object Identifier
DRB	Danube River Basin
EASAC	European Academies' Science Advisory Council
ECMWF	European Centre for Medium-Range Weather Forecast
EEA	European Environment Agency
EPhysLab	Environmental Physical Laboratory
ERA	European Centre for Medium-Range Weather Forecasting Re-Analysis
FLEXPART	FLEXible PARTicle dispersion model
GCM	General Circulation Model
GFS	Global Forecast System
GRIB	General Regularly-distributed Information in Binary form
IND	Indian Ocean
IPCC	Intergovernmental Panel on Climate Change
IVT	Vertically Integrated Horizontal Water Vapour Transport
JRC	Journal Citation Reports
MED	Mediterranean Sea
MEXCAR	Mexico Caribbean
MSWEP	Multi-Source Weighted-Ensemble Precipitation
NATL	North Atlantic
NPAC	North Pacific
PET	Potential Evapotranspiration

PFLEX	Climatological monthly moisture contribution during the peak precipitation month obtained by the Lagrangian experiment
PFLEX-PS	Moisture contribution of preferred source in peak precipitation month
PFLEX-PSMax	Mean precipitation values of preferred source obtained by the Lagrangian experiment for the five years of maximum precipitation
PFLEX-PSMin	Mean precipitation values of preferred source obtained by the Lagrangian experiment for the five years of minimum precipitation
PMSWEP	Monthly climatological precipitation values of peak precipitation month obtained from MSWEP dataset
PMSWEP-Max	Mean precipitation for the detected five years with maximum precipitation from MSWEP dataset
PMSWEP-Min	Mean precipitation for the detected five years with minimum precipitation from MSWEP dataset
PPM	Peak Precipitation Month
PRE	Precipitation
PS	Preferred Source
REDS	Red Sea
SAFR	South Africa
SAHEL	Sahel region
SAM	South America
SATL	South Atlantic
SCI	Science Citation Index
SPAC	South Pacific
VIMF	Vertical Integrated Moisture Flux
WRF	Weather Research and Forecasting
ZANAR	Zanzibar Current and Arabian Sea

1

Introduction

1.1 The hydrological cycle and precipitation on Earth

The hydrological cycle refers to the process of water circulation and exchange through the hydrosphere, atmosphere, and lithosphere, and plays a major role in the generation of freshwater continental precipitation. This process regulates an uninterrupted supply of water and maintains surface and underground water levels. Consistency in the hydrological cycle and precipitation patterns are crucial for life on Earth (Palazzi and Provenzale, 2016). Although there is abundant water on Earth, only about 2.5% of it is potable fresh water (Oki and Kanae, 2006).

Solar heating causes evaporation from oceans and lakes and transpiration of water vapour into the atmosphere. After this process, water cools and condenses into precipitable warm or cold cloud particles; in this manner, freshwater returns to the Earth's surface through precipitation as rain or snow, completing the cycle (e.g. Huntington and Williams, 2012; Peixoto and Oort, 1992). Figure 1.1 shows the annual average water exchange between oceans and land. The amount of water vapour depends on factors such as latitude, or the local characteristics, such as land cover, geomorphology, or ecosystem (Bengtsson, 2010).

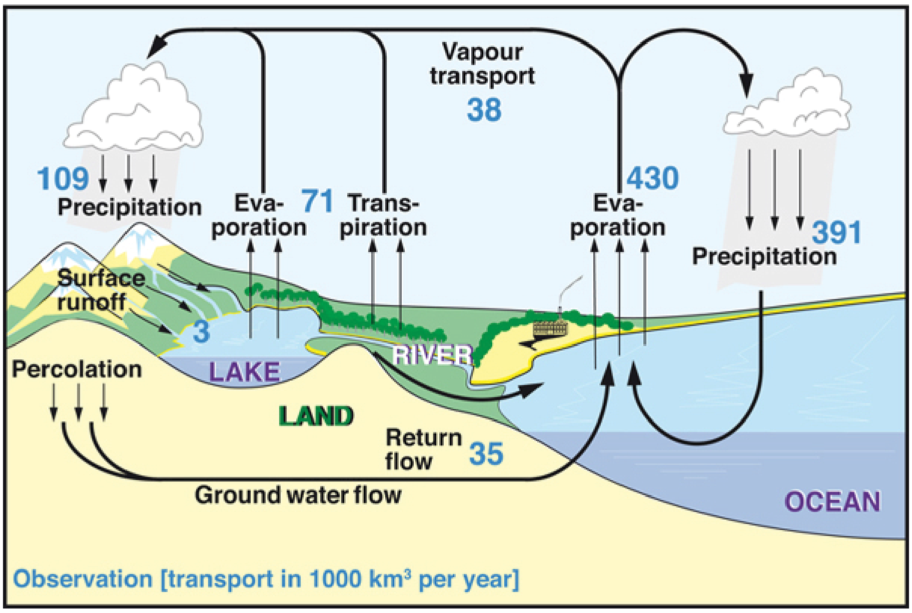

Figure 1.1. The hydrological cycle (units: 103 km^3/year). Water evaporates and transpires from the ocean and lakes into the atmosphere and returns in the form of precipitation. Figure from Bengtsson (2010), modified from Baumgartner and Reichel (1975).

The hydrological cycle of oceans behaves differently than the hydrological cycle of continents (Bengtsson, 2010). Oceans play an important role within the hydrological cycle, since they cover 70% of the Earth's surface (Stewart, 2008) and contain about the 97% of the Earth's water (Costello et al., 2010). The other 3% is stored in glaciers (2%) and as surface water, groundwater, and soil moisture (less than 1%) (Table 1.1). Freshwater fluxes into the ocean include direct water supply from rivers and lakes on the continents; submarine melting and melting of sea ice; water runoff; and direct precipitation in the form of rainfall and snowfall. Thus, the ocean is the dominant source of moisture for precipitation over the continents and in the global hydrological cycle (Gimeno et al., 2010). Only 10% of water that evaporates from the oceans falls over land; the majority (90%) falls over the ocean. Because of this, the oceans – where the evaporation rate exceeds the precipitation rate – are the main source of moisture for continental precipitation (Gimeno et al., 2012).

Table 1.1. Earth's water supply in the Earth (percentage by volume). Table from Huntington and Williams (2012), adjusted from U.S. Geological Survey Circular 536 (http://pubs.usgs.gov/circ/1967/0536/report.pdf).

Source	Percentage by Volume
Oceans	97. 2
Freshwater:	
Glacier ice	2.15
Subsurface water	0.625
Surface water	0.017
Atmosphere	0.001
Subtotal (fresh water)	2.793
Total	~100.0

Precipitation is one of the most important components of the water cycle (Trenberth et al., 2003) and a crucial variable in climatic and weather studies (Becker et al., 2012). Precipitation measurements must be reliable and precise for studying climate trends and variability, managing water resources, and forecasting climate or weather (e.g. Sun et al., 2018). The global annual average precipitation is estimated to be around 1000 mm: a study by Michaelides et al. (2009) shows 1050 mm/year, while Legates and Willmott (1990) state 1123 mm/year. The distribution of precipitation varies around the world; each of Earth's regions receive a different amount of rainfall. The regions with the highest estimated precipitation are near to the equator, in the tropics, where strong solar heating causes heavy prolonged rainfall and frequent thunderstorms. Annual precipitation in the tropics is usually between 2500 and 10,000 mm/year, influenced by monsoons. In these regions, coastal areas receive 90% of the annual precipitation – about 3500 mm/year. These regions therefore have the highest annual precipitation on Earth (Ogino et al., 2016). The regions with the lowest amount of annual precipitation are at high latitudes within the polar regions, where the air mass is cold and does not contain much water vapour. A similar situation exists in desert regions of the subtropics, where there are high atmospheric pressure levels and clouds cannot form, reducing precipitation. The estimated total annual precipitation in these regions, both hot and cold regions, is around 250 mm/year. In cold regions, the lowest amounts of precipitation occur in Antarctica and central Greenland, with an average of less than 73 mm/year (Turner and Marshall, 2011); the Central Arctic region receives less than 150 mm/year (Serezze and Hurst, 2000). In arid and semi-arid regions, the average precipitation for 40% of Africa is less than 100 mm/year (Blanc and Perez, 2007), while in the Arabian Peninsula region (Gunawardhana et al., 2018) it reaches 130 mm/year. The mid-latitudes are characterized by moderate precipitation levels; precipitation in these regions is associated with frontal depressions developing. This belt includes regions where cold, polar air masses dominate in the cold season, and warm, tropical air masses dominate in the hot season (Khlebnikova, 2009). In this belt, the total annual precipitation is estimated to be around 2500 mm/year, with regions of East Asia and North America having the highest precipitation (Chen et al., 2004). Figure 1.2 shows the mean annual precipitation across Earth.

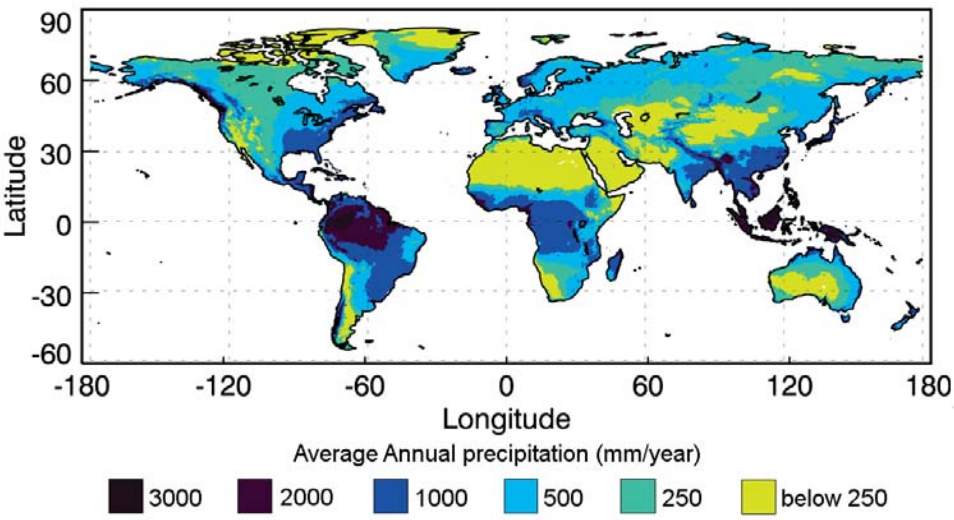

Figure 1.2. Mean annual precipitation over the continents (mm/year), shown at a 0.25° latitude-longitude grid. Data from MSWEP database.

As precipitation varies greatly across time and space (Becker et al., 2012), a detailed knowledge of its frequency, intensity, and spatial distribution is required to better understand and assess its impact on localised extreme precipitation events and for adaptation to climate change (Samlley and L'Ecuyer, 2015). Several studies that used global circulation models under a futuristic climate changes, showed that, in general, wet areas are likely to get wetter, while dry zones are likely to get drier (Held and Soden, 2006). According to Dore (2005), and the Intergovernmental Panel on

Climate Change (IPCC, 2007), the following significant changes are occurring in the global precipitation patterns: i) an increase in precipitation of approximately 20% in high latitudes (Eastern Africa, Central Asia, etc.); ii) a decrease in precipitation in subtropical areas (China, Australia, and some Pacific regions); and iii) a significant variation in precipitation over equatorial regions (e.g. increased precipitation variance in the Amazon, and Southeast Asia).

Increased precipitation is usually connected with an increased rainfall frequency and severity. Therefore, it is important to investigate the origin and impacts of increased precipitation at selected locations.

1.1.1 Extreme precipitation

Climate change is one of the main challenges today, and its impact on the natural environment and human society is widely recognised by the scientific community. One of the main characteristics of climate change is the variation in both climatological and extreme climate variables (Santos and Costa, 2014). Understanding how climate change affects climate extremes is important for maintaining normal life and human activity. It is also necessary for the development, management, and monitoring of unexpected and extreme weather situations (Toreti and Desiato, 2008).

Over time, precipitation changes in volume, type (for instance, rain, snow, etc.), intensity, and/or frequency, influence both the natural environment and human society (Trenberth, 2011). Floods and drought represent extreme hydrological events. Drought can be defined as an extreme lack of precipitation over an extended period, causing a significant soil moisture deficit and negative impacts on the natural ecosystem, hydrological balance, agriculture, and human society (Drumod et al., 2016; IPCC, 2012). Depending on how it is measured or defined, drought may be characterized as hydrological, meteorological, agricultural, or socioeconomic (Ebi and Bowen, 2016). In contrast, floods are usually associated with heavy precipitation caused by meteorological systems (e.g. extreme cyclones, tropical storms, atmospheric rivers, convective systems, orographic rainfall), and may have serious consequences, resulting in huge socioeconomic losses worldwide and significant human health impacts, including, in worst cases, the loss of human life (Zhao et al., 2009). It is important to distinguish between extreme precipitation and so-called ‘flash flood’ events. The former significantly impact society and the environment, while the latter are usually short events of intense rainfall, which may lead to huge socioeconomic losses. Flash flood events may therefore be more destructive than extreme precipitation events (Marengo et al., 2009).

There are different approaches to analysing extreme precipitation, and these approaches define extreme precipitation events differently. One definition is that an extreme precipitation event occurs when, during one day, 20% or more of the seasonal mean precipitation falls in a given location (Carvalho et al., 2002). The European Academies' Science Advisory Council Policy Report (EASAC, 2013), defines extreme precipitation events in two categories: i) short term, when a huge amount of precipitation falls in a period from a few hours until one day at one location (this could be caused by strong atmospheric water vapour convergence); and ii) long term, when a huge amount of precipitation falls in a period from weeks to months over the same location, leading to an accumulation precipitation in quantities sufficient enough to cause floods and impact the environment and society.

Generally, short and long term precipitation events are significantly connected, as short precipitation events are required for prolonged precipitation. In a trend analysis of precipitation, the EASAC Policy Report (2013) and the IPCC report (2007) show that short and isolated events have increased across the world (Figure 1.3).

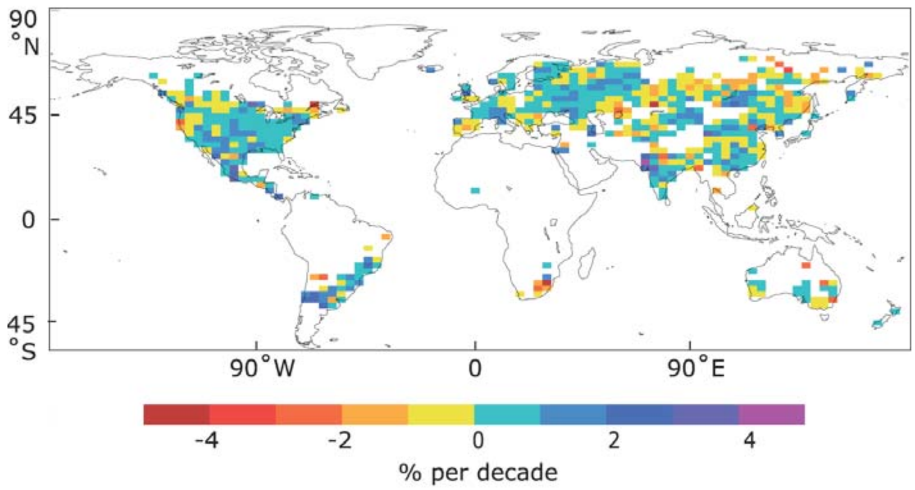

Figure 1.3. Worldwide trend of single short precipitation events' contribution to total precipitation, measured in percentage per decade for the period 1951-2003. Figure from EASAC Policy Report (2013).

Another analysis showed that global precipitation (with exception of the Antarctic region) has increased at a rate of 0.89 mm/decade, although comparison with inter-annual and multi-decadal variation shows that this change is still within an acceptable range (New et al., 2001). Although most terrestrial areas on Earth have suffered an increase in precipitation, there are some important exceptions: Amazonia, western South America, tropical North Africa, and southern Africa (Kidda and Huffman, 2011). In most regions where a significant increase in monthly or seasonal precipitation has been detected, the probability of increase in the precipitation amount falling during heavy and extreme precipitation events was even higher (Dore, 2005). Moreover, in some areas there was no detected increase in total precipitation (monthly or seasonal), but there was a significant increase in the frequency and intensity of 1 day extreme precipitation events (Easterling et al., 2000). Frich et al. (2001) suggested that a significant increase in total precipitation exists in areas affected by extreme daily rainfall. This precipitation increase is especially notable in the mid- and high latitudes. It is determined by a significant increase in mean annual total precipitation, and in the annual maximum precipitation depending on the total number of 5-day precipitation events.

Today, an increase in extreme precipitation events can be observed in many parts of the world. For instance, in the United Kingdom a significant increase was found in both short (1 day) and long (10 day) extreme precipitation events (Fowler and Ekström, 2009). The same increasing trend of extreme precipitation events was also found in other European regions such as Switzerland, Italy, and Spain, although the spatial patterns were not homogeneous (Kundzewicz et al., 2006). A 10-45% increase in heavy rainfall events was observed in Australia between 1910 and 1995 (Hennessy et al., 1999). In eastern and northwest China, the annual rate of extreme precipitation events increased by 10-20%, mainly in the summer (Wang and Zhou, 2005). In Russia, the frequency of extreme precipitation events during winter and spring increased by 20-40% of the typical mean regional value (Zolotokrylin and Cherenkova, 2017). In the European part of Russia, in the Aral-Caspian region, and Siberia, the total precipitation of 5-day extreme precipitation events has increased from 10-40% (Shmakin and Popova, 2006).

1.2 Climatological and extreme precipitation in the Mediterranean region

The fifth IPCC report (Kovats et al., 2014) indicates that Europe is one of the areas notably affected by climate change, reflected in strong changes in the hydrological cycle (Christensen et al., 2007). These changes caused an increase in heavy and extreme precipitation events in most of Europe, especially in the central (including the Mediterranean region) and eastern parts during winter (EEA, 2017). According to regional precipitation scenarios under a changing climate future, two regions in Europe will experience a significant increase in winter precipitation. These are the northeast and the northwest parts of the Mediterranean coast (Parry, 2000).

The Mediterranean climate is very diverse, with notable differences in precipitation over the whole region. The average annual precipitation is around 1-2 mm/day, but the highest precipitation (3-5 mm/day) is recorded in mountainous regions on the European side of the sea basin, while the lowest values (~0.5 mm/day) are located over semi-arid and arid regions in North Africa (Dayan et al., 2015). A clear seasonal pattern can be observed: precipitation is higher from October to March, when the western Mediterranean Sea has 20% more precipitation than the eastern Mediterranean (Xoplaki et al., 2004). At a monthly scale, the highest monthly climatological precipitation values (3-5 mm/day) occur during November in the western Mediterranean and during December over the central and eastern Mediterranean (Mehta and Yang, 2008).

The Mediterranean basin is an area where the extreme precipitation events contribute a large proportion of total precipitation (Hertig et al., 2013). Usually, extreme precipitation events in this region are caused by advection (Eshel and Farrell, 2000) and/or because of convective precipitation (Llasat et al., 2014). This means that monitoring and studying changes in precipitation extremes is a particularly important challenge for the Mediterranean area. In addition to being scientifically relevant, these events have a significant impact on the environment and society, as noted in the previous chapter.

Recently, extreme precipitation and flood events were detected in many Mediterranean regions. For instance, in the Alpine region 40% of the total annual precipitation resulted from extreme precipitation events with an estimated duration of 10 days (Frei et al., 2000). Furthermore, several studies showed specific flood events in the region – for example, June 2000 in Spain (Milelli et al., 2006); August 2002 in Greece (Lasda et al., 2010); November 2014 in Italy (Faccini et al., 2015); and Serbia, Bosnia, and Croatia in May 2014 (Stadtherr et al., 2016).

1.3 Major moisture sources for continental precipitation

To better comprehend the atmospheric aspects of the water cycle and the progress of its phases through time, it is crucial to thoroughly understand the exchange mechanisms of water between oceans and the atmosphere, and how these processes affect land via precipitation (e.g. Gimeno, 2014; Palazzi and Provenzale, 2016). This should be considered from a climatology perspective, as well as for studying and possibly predicting extreme precipitations. Understanding the link between oceanic and continental moisture sources at the global scale and precipitation over land is key to understanding the atmospheric branch of the hydrological cycle (e.g. Gimeno et al., 2010; van der Ent and Savenije, 2013). Thus, identifying the major oceanic sources of precipitation is especially important for areas that are undergoing changes in the hydrological cycle due to climate change (Gimeno et al., 2013). Given the importance of this topic, many studies have investigated the major oceanic and terrestrial water sources for precipitation and their corresponding sink regions at global (Gimeno et al., 2010; van der Ent et al., 2010) and regional scales (e.g. Drumond et al., 2014; Gomez-Hernandez et al., 2013; Sodemann and Zubler, 2010).

Gimeno et al. (2010) and Castillo et al. (2014) identified 12 major oceanic moisture sources around the world (see Figure 1.4) based on the maximum values of annual divergence flux of moisture. They highlighted that, in global terms, moisture source regions exhibit asymmetrical and specific roles to precipitation over land. For example, the North Atlantic Ocean was found to be the major moisture source for many parts of the world, from Mexico to some regions of Eurasia, and from the Arctic region to the Amazon. In contrast, some small moisture sources can provide moisture for precipitation on vast continental areas. This is the case with the Mediterranean and Red

Seas. Their findings also highlighted that some regions receive moisture only from one or two source regions (for instance, Europe, eastern North America, and Australia), while continental monsoon areas (such as India and tropical Africa) receive moisture from multiple source regions.

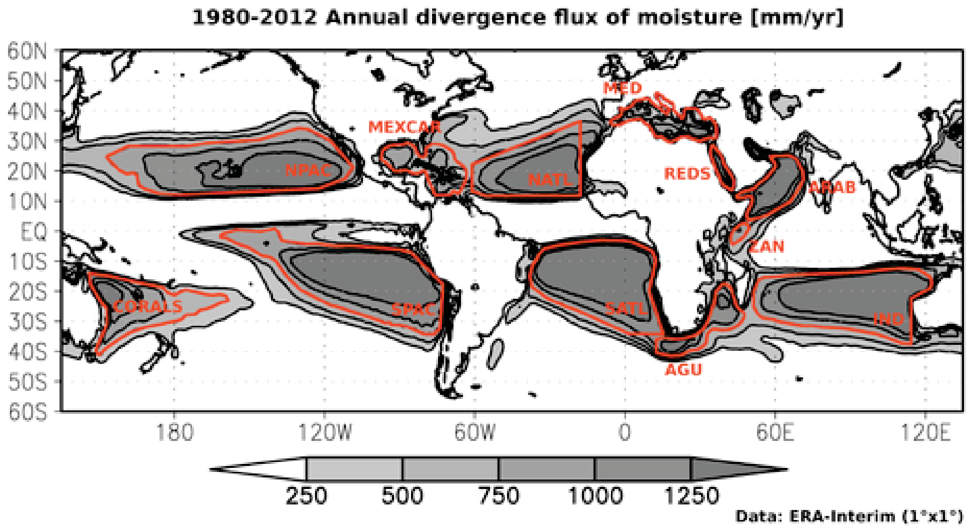

Figure 1.4. The main global oceanic source regions, identified according to maximum annual divergence flux of moisture, 1980-2012. The sources of moisture are: CORALS (Coral Sea), NPAC (North Pacific), SPAC (South Pacific), MEXCAR (Mexico Caribbean), NATL (North Atlantic), SATL (South Atlantic), ARAB (Arabian Sea), ZAN (Zanzibar Current), AGU (Agulhas Current), IND (Indian Ocean), MED (Mediterranean Sea), and REDS (Red Sea). Figure from Castillo et al. (2014).

Major moisture sources for precipitation over land at the global scale have been well characterized in recent years (Gimeno et al., 2010). However, their contribution to extreme precipitation over continental areas has not been well investigated. This study aims to address this gap and attempts to characterise the moisture contribution of detected sources to extreme precipitation events at the global and regional scales.

2

Objectives

It is important to examine and diagnose extreme and intense precipitation at both the global and regional scales. The precipitation-evapotranspiration cycle of a given location depends on the moisture supply from oceanic and terrestrial surrounding moisture source regions. One of the main methods of analysing extreme weather events, such as extreme precipitation events, is identifying the main moisture sources at the global and regional scales (Gimeno, 2013). Therefore, given that moisture is essential for extreme precipitation events, it is critical that we better understand changes in moisture transport from identified moisture source regions (oceanic and/or continental).

This work evaluates the role of moisture sources for extreme precipitation, starting from a regional point of view and moving to a global study. To investigate changes in annual and extreme precipitation at the regional scale in this study, the Mediterranean area and its sub-region, the Danube River Basin (DRB), were chosen.

We selected the Mediterranean region because the Mediterranean Sea is one of the major sources of oceanic moisture for continental precipitation (Gimeno et al., 2010, 2012) and plays an important role as a moisture source at the global and regional scales because of its sub-tropical position (Mehta and Yang, 2008; Trigo et al., 2006). Throughout the year, the Mediterranean Sea releases more moisture through evaporation than the amount it receives through precipitation. The evaporation intensity of the Mediterranean as a moisture source is strongly connected with the precipitation intensity over the Mediterranean region, including its sub-regions (Lionello et al., 2006): the Mediterranean Sea itself, the European part of the Mediterranean region, North Africa, Middle East coast, and the DRB (area of interest in the present work). Because of this, it is very important to understand the precipitation pattern, intensity, and frequency over the entire Mediterranean region.

At the sub-regional scale, it must be noted that the DRB is the second-longest catchment in Europe and represents an international river that shares its catchment between 19 countries. It is hugely important in many spheres, such as water availability, agriculture, and quality of human life. From a hydrological point of view, it is particularly interesting because its precipitation characteristics (peak values around 2000 mm/day) are strongly connected with warm, humid air masses coming from the Mediterranean Sea (Brilly, 2010). The influence of the Mediterranean Sea on water balance in the Danube is especially strong in the central and lower basin (Lucarini, et al., 2008). Therefore, we chose to study the DRB as an important part of the hydrological cycle of the Mediterranean Sea and as a significant sink for moisture from the Mediterranean, both climatological and during extreme events.

The main objectives of the **regional analysis** of this dissertation are:

(1) To identify the main oceanic and continental sources of moisture for the DRB.

Specific objectives related with this main objective are:

- To describe the annual cycle of potential evapotranspiration (PET) and precipitation (PRE) and differences between them over the DRB.
- To identify the main moisture source regions for the DRB and analyse their seasonal variability.
- To investigate the contribution of each detected moisture source to continental precipitation over the DRB.

This objective corresponds to the first of the articles that constitute the corpus of this PhD thesis: “Tracking the Origin of Moisture over the Danube River Basin Using a Lagrangian Approach” by D. Ciric, M. Stojanovic, A. Drumond, R. Nieto, and L. Gimeno, published in 2016 in Atmosphere 7(12), 162, doi:10.3390/atmos7120162.

(2) To analyse the contribution of moisture from the Mediterranean Sea to extreme precipitation events over the DRB.

The following specific objectives are related to this main objective:

- To make a daily ranking of extreme precipitation events (wet spells) of different durations, from 1 to 10 days, for the period from 1981 to 2015.
- To select the most intense extreme event and analyse the moisture source anomalies responsible for its development.
- To study the role of local and non-local synoptic conditions during the event.
- To select the top 100 extreme precipitation events of each duration (1 to 10 days) and calculate climatological and anomalous moisture contributions from the Mediterranean Sea during each.
- To compute the percentage of moisture supply from the Mediterranean Sea to each precipitation event for all time scales.

This objective corresponds to the second and third papers presented in this PhD thesis. These articles were titled "Wet Spells and Associated Moisture Sources Anomalies across Danube River Basin" by D. Ciric, R. Nieto, A.M. Ramos, A. Drumond, and L. Gimeno published in 2017 in Water 9, 615, doi:10.3390/w9080615; and "Contribution of Moisture from Mediterranean Sea to Extreme Precipitation Events over Danube River Basin" by D. Ciric, R. Nieto, A.M. Ramos, A. Drumond, and L. Gimeno published in 2018 in Water 10(9), 1182; doi:10.3390/w10091182.

(3) To analyse the contribution of the Mediterranean Sea to climatological and extreme monthly precipitation over the surrounding continental areas.

To achieve this, the specific objectives are:

- To quantify the contribution from the Mediterranean Sea to monthly precipitation over its surrounding continental areas using a grid.
- To determine the percentage of this contribution to extreme monthly continental precipitation using a grid.

This objective is addressed in the fourth article presented in this PhD thesis, entitled “The Mediterranean Moisture Contribution to Climatological and Extreme Monthly Continental Precipitation” by D. Ciric, R. Nieto, L. Losada, A. Drumond, and L. Gimeno published in 2018 in Water 10(4), 519, 1-19, doi:10.3390/w10040519.

After the Mediterranean regional analysis, including the DRB, was conducted, we expanded the study to identify the monthly role of the main oceanic and continental moisture sources to extreme precipitation on a **global scale**. These results are included Chapter 5 of this text, as a global atlas.

The last objective of this PhD is:

(4) To analyse the monthly contribution of the main moisture sources to extreme continental precipitation.

The following specific objectives pertain to this fourth main objective:

- To identify the major global oceanic and terrestrial moisture sources at a monthly scale, based on maximum monthly vertical integrated moisture flux divergence (VIMF).
- To quantify, using a grid, the monthly contribution of all detected moisture sources to precipitation over continental areas worldwide.
- To detect, using a grid, the month with maximum climatological precipitation (peak month) using MSWEP data.
- To detect, using a grid, the dominant moisture source during the peak precipitation month.
- To detect, using a grid, the contribution of the dominant source to extreme precipitation during the peak precipitation month.
- To detect, using a grid, the five years with maximum and minimum precipitation value during the peak precipitation month, using precipitation data from the MSWEP database.

- To use a grid to detect the contribution of the dominant moisture source to the precipitation in the peak precipitation month for the five years of maximum and minimum precipitation.

3

Methodology

3.1 Identification of the main moisture sources and sinks using a Lagrangian approach: FLEXPART model

To better understand the source-sink relationship, it is crucial to choose the most suitable approach to investigate moisture transport and their anomalies from a moisture source to its receptor sink. Gimeno et al. (2010) proposed the Lagrangian FLEXible PARTicle dispersion model (FLEXPART) for this type of research, showing that it is more suitable than other existing approaches (for instance, Eulerian, box, or isotope models; see their work for more precise details).

FLEXPART was widely used in recent years for different purposes, but it was initially designed for computing the long-range and mesoscale transport of air pollutants originating from point sources (Stohl et al., 1998), for example in the case of a nuclear power plant accident (Stohl et al., 2005). Since then, the use of the FLEXPART model has progressed; it has been used in many different atmospheric fields, ranging from air pollution studies (Pan et al., 2014; Seibert and Frank, 2004; Stohl et al., 2003) to other fields related to atmospheric transport, such as studies of global or regional water cycles (Chen et al., 2013; Dirmeyer and Brubaker, 2007; Gimeno et al., 2010; Martin-Gomez et al., 2016; Nieto et al., 2010a), stratosphere-troposphere exchange (Bourqui, 2006; Castro et al., 2011; Huang and Cui, 2015), among others.

The Lagrangian method is one of the two numerical water vapour tracer methods available for identifying the origin of moisture that reaches a specific area (Gimeno et al., 2012). Compared to the other, Eulerian methods, the Lagrangian method has the advantage that there is no induced numerical diffusion. Another important advantage is the resolution independence of the Lagrangian method, which allows computation of air particles at a very small resolution (extending from point, line, area, or bigger moisture sources) (see the user guide for FLEXPART version 3.1 by Stohl, 1999).

In addition to numerical methods for identifying source-sink relationships, other techniques are also available, such as analytic (box) methods and physical water vapour tracers (isotope method). These methods also provide interesting and useful information for moisture transport analysis. All analytic methods are based on the equation of the vertically integrated balance of water vapour (Burde and Zangvil, 2001):

$$\frac{\partial(w)}{\partial t} + \frac{\partial(wu)}{\partial x} + \frac{\partial(wv)}{\partial y} = E - P \tag{3.1}$$

where w denotes the amount of water vapour in a column of air of unit base area, u denotes the water vapour-weighted zonal wind, v is the water vapour-weighted meridional wind, E represents evaporation, and P is precipitation. The equation can be used to independently calculate the moisture reaching the target area from outside (advection) and from inside (recycling). Therefore, the box method allows the identification of moisture inflow and outflow over a selected region, but its main weakness is its inability to provide information about the physical processes that occur inside the selected box. The isotopes method, on the other hand, does not consider convection and rainwater evaporation.

A more detailed explanation of the Lagrangian model is presented in the next sections, but a complete comparison with other approaches (Eulerian, box model, or isotopes), including advantages and weakness (see Table 3.1) can be found in the comprehensive study by Gimeno et al. (2012).

Table 3.1. Summary of the main advantages and limitations of the methods used to detect source and sink regions of atmospheric moisture. Taken from Gimeno et al. (2012).

Type		Advantages	Limitations
Analytical Box Models		✓ Simple, as few parameters are required, and they consider grid based spatial variability	✓ Neglects in-boundary processes; ✓ Some are based on the well mixed assumption (the local source of water is well mixed with all other sources of water in the whole vertical column) ✓ most are only valid for monthly or longer timescales
Physical Water Vapour Tracers		✓ Simplicity ✓ Global coverage ✓ Include vertical processes ✓ Reanalysis input data (high spatiotemporal resolution) ✓ Enable the combination of GCM sand Lagrangian Rayleigh models	✓ Sensitivity of the isotopic signal ✓ Calculation time ✓ Availability of data for validation; ✓ Does not account for convection and rain water evaporation/equilibration
Numerical Water Vapour Tracers	***Eulerian***	✓ Detailed atmospheric processes ✓ Realistic moisture circulation.	✓ Dependent on the model bias ✓ Global forcing is required ✓ Poor representation of short-timescale hydrological cycle parameters ✓ Does not include the remote sources of water for a region.
	Lagrangian	✓ High spatial resolution moisture source diagnostics ✓ Quantitative interpretation of the moisture origin allowed not limited by a specific RCM domain and spin-up ✓ Establishment of source-receptor relationship can be easily assessed as budgets can be traced along suitably defined trajectory ensembles ✓ Net freshwater flux can be tracked from a region both forward and backward in time ✓ Realistic tracking of air parcels; ✓ Computationally efficient compared to performing multi-year GCM simulations or reanalyses ✓ More information provided than a purely Eulerian description of the velocity fields ✓ Parallel use of information from Eulerian tagging methods allowed.	✓ Sensitivity of moisture flux computations leads to increases in data noise for shorter time periods or smaller regions ✓ Simple method does not provide a diagnostic of the surface moisture fluxes ✓ Surface fluxes under (over) estimation if dry (cold) air masses tracking as the budget is not closed ✓ Evaporation rates are based on calculations rather than observations in some methods; ✓ Evaporation and precipitation are not clearly separable (in some methods) ✓ Movement and extraction of water does not depend on the physical tendencies included in the reanalysis data.

The Lagrangian method has been widely and successfully used to detect moisture source regions at the global scale (e.g., Castillo et al., 2014; Gimeno et al., 2013; Stohl and James, 2005) and regional scale in different climatic regions, for instance those that have suffered long drought periods – such as the Sahel (Nieto et al., 2006), the Fertile Crescent (Salah et al., 2018), and different parts of Brazil (Drumond et al., 2008, 2010). The Lagrangian method has also been used to provide historic climatic data through ice-cores (Nieto et al., 2010b; Sodemann and Stohl, 2009), in regions which have an impact on water availability, such as river basins (Sorí et al., 2017a,b,c; 2018; Stohl and James, 2005), in regions characterised by episodes of intense precipitation (Bohlinger et al., 2017; Ciric et al. 2017; Huang and Cui, 2015; Sodemann et al., 2009) or areas of complex orography (e.g. the Alps, by Sodemann and Zubler, 2010), and over the Arctic (Gimeno et al., 2015; Gimeno-Sotelo et al., 2018; Vázquez et al., 2016, 2017, 2018; Wegman et al., 2015). This wide, and growing, number of publications prove that this is the most suitable approach with which to analyse the moisture source-sink relationship.

3.1.1 Model setup and simulation

FLEXPART is an off-line model optimised for use with input data from the European Centre for Medium-Range Weather Forecasts (ECMWF). Forecast and analysis of input data are stored in a gridded binary format (GRIB) on a latitude/longitude grid and on indigenous ECMWF levels. Other meteorological fields from the Global Forecast System (GFS) and the Weather Research and Forecasting (WRF) regional models (Brioude et al., 2013) may also be used as input data. Since the research focus of this PhD thesis is the atmospheric branch of the hydrological cycle, the input data that was used is ERA-Interim reanalysis data from the ECMWF (Dee et al., 2011). ERA-Interim reanalysis data are accessible at 6 h time intervals at 60 vertical levels resolution from the surface (1000 hPa) to 0.1 hPa at 1° horizontal resolution (in latitude and longitude). Many studies state that ERA-Interim data are the most suitable data for performing experiments in terms of water balance (Lorenz and Kunstmann, 2012; Trenberth et al., 2011).

The FLEXPART model is based on the Lagrangian method; its main purpose is tracking particles along their trajectories in the atmosphere. Basically, the Lagrangian approach considers the atmosphere as a large number of homogeneous elements (air particles or parcels), each with constant mass (m) and a known position at each moment in time along the trajectory (Figure 3.1).

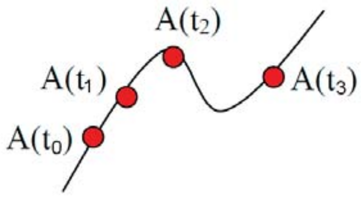

Figure 3.1. Schematic representation of a single particle's trajectory over time. Adapted from Gomez-Hernandez (2013).

To construct the particles' trajectories, the model uses the 3D wind fields (one vertical dimension and two horizontal) of the input data, interpolating on its momentary position (namely Lagrangian grid) to track the particle. Thus, for model computation, the input data must contain three-dimensional fields such as superimposed stochastic turbulent and convective motions, horizontal and vertical wind components, temperature, and specific humidity. The particle advection in FLEXPART is based on the simple equation of movement along a trajectory, as shown in equation (3.2):

$$\frac{\partial}{\partial t}\vec{X} = \vec{v}\left[\vec{X}(t)\right] \tag{3.2}$$

where t is time, $\vec{X}$ is the vector position, and $\vec{v}$ is the wind vector.

The Lagrangian method allows study of moisture transport from the atmosphere to the destination (moisture-sink relationship) using the three-dimensional coordinate system, where the position of an air particle is constantly tracked along its trajectory. In addition to requiring three-dimensional fields, FLEXPART also needs two-dimensional fields (as indicated in several technical guides, see Brioude et al., 2013; Stohl et al., 2005). These two-dimensional fields include surface pressure, total cloud cover, 10 m horizontal wind components, 2 m temperature and dew point temperature, large scale and convective precipitation, sensible heat flux, east/west and north/south surface stress, topography, land-sea-mask, and sub-grid standard deviation of topography.

In addition, FLEXPART records outputs data for each particle at 6 h intervals along its trajectory (00, 06, 12, and 18 UTC). These variables are listed in Table 3.2.

Table 3.2. Summary of output parameters for the FLEXPART model, v9.0.

Outputs fields	
Parameter(abbreviation)	*Units*
Latitude (Lat)	°
Longitude (Lon)	°
Height (H)	m
Topographic Height (TH)	m
Potential Vorticity (PV)	10^{-6}(m^2 K/s kg)
Specific Humidity (q)	g/kg
Density of the air (ρ)	kg/m^3
Mixing height (hmixi)	m
Temperature (T)	K

During its years of development, the FLEXPART model has advanced and improved in many technical parameters. A more detailed explanation of the model's physical and technical parameters may be found in the technical note of Stohl et al. (2005) and in other technical notes available at the official FLEXPART webpage (https://www.flexpart.eu/wiki).

3.1.2 Using the FLEXPART tool to detect moisture sources and sinks

Much of this work is based on using outputs from the FLEXPART model to analyse moisture transport between sources and sinks. The global FLEXPART experiment was done in the Environmental Physical Laboratory (EPhysLab) at the University of Vigo, Spain. To perform the experiments, the ERA-Interim reanalysis data (Dee et al., 2011) was used for a longer period of 37 years, from 1980-2016. The period before 1980 is absent from this study because the lack of satellite data led to bad quality results (Bengtsson et al., 2004).

FLEXPART model v. 9.0 tracks approximately 2 million particles with constant mass in the atmosphere. Information about these particles (Table 3.2) is recorded at 6 h time intervals (00, 06, 12 and 18 UTC). Essentially, the model calculates surface freshwater flux (E-P) using information about the particles' trajectories or an absolute value of specific humidity (q).

Recorded changes to the specific humidity (q) of each particle's trajectory over time allow increasing moisture trough evaporation (e) or decreasing trough precipitation (p) to be identified. This is schematized in Figure 3.2(a). This relationship may be expressed by equation (3.3):

$$(e-p)=m\left(\frac{dq}{dt}\right) \tag{3.3}$$

where m indicates particle and dt indicates the 6 h time interval.
By summing all (*e*-*p*) values of particles in an atmospheric column over a target region (for instance with area A, as in Figure 3.2(b)), it is possible to calculate the total surface freshwater flux (E-P). This is shown in equation (3.4) (Stohl and James, 2004):

$$(E-P)\approx\frac{\sum_{k=1}^{k}(e-p)}{A} \tag{3.4}$$

where E represents evaporation rate and P represents precipitation rate per unit area, and K is the total number of particles that reach a target region (A).

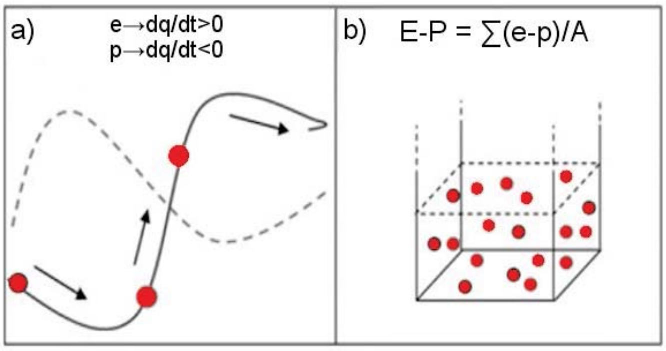

Figure 3.2. Schematic representation of Lagrangian calculation of (E-P) as variation of the specific moisture of air particles along the trajectories integrated over vertical atmospheric columns. a) Tracking method scheme, where the solid grey line represents the particle's trajectory, and the grey dotted line indicates moisture content. b) Vertical atmospheric column filled with many particles with different moisture content. Adapted from Duran-Quesada et al. (2010).

The FLEXPART model allows us to follow particles along their trajectories backward and forward in time. Following them in reverse shows the source of atmospheric humidity over a target region. By tracking the air particles in reverse, we can identify the locations where they gain moisture along their trajectories toward the selected area (the source). In this way, all grid points where the balance of E-P is positive (E-P > 0) indicate moisture source regions for the target area. The second possibility is to track particles forward in time to answer the question: where is the destination (sink) of the moisture that flows from a selected source? When tracking particles forward, all values where E-P < 0 indicate where loss of moisture. This allows for identification of the main moisture sink regions.

Both reverse and forward analysis are computed by adding (E-P) values above or below 0, respectively) during an integration time of the trajectories. The most widely used integration time in Lagrangian analysis (not only for FLEXPART outputs) is derived from the average residence time of water vapour in the atmosphere, normally considered to be around 10 days (Numaguti, 1999; Trenberth, 1999). The total E-P, integrated over days 1 to n (n from 1 to 10), is used for analysis. It is also possible to analyse a shorter time segment, for example, the spatial pattern for days 1 to 5: $(E\text{-}P)_{i5}$. These results would show where the particles gain or lose moisture during the fifth day of the trajectories. However, the results derived from these Lagrangian approaches are very sensitive to the integration time that is used in the analyses; it is possible that an over- or underestimation occurs for some regions (Läderach and Sodemann, 2016; van der Ent and Tuinenburg, 2017). The use of different integration times to find moisture sources/sinks could alter the initial results, analyses, and subsequent interpretations.

3.2 Ranking of extreme precipitation events (wet spells)

In this thesis, we ranked extreme precipitation events over the Danube River Basin based on the method developed by Ramos et al. (2014; 2017). This method was initially applied to rank multi-day extreme precipitation events over the Iberian Peninsula, considering daily normalised precipitation anomalies using daily gridded precipitation data for the Iberian Peninsula from 1950 to 2008, with a grid of 0.2 degrees.

To rank events over the Danube River Basin, daily values from the Climate Hazards Group Infra-Red Precipitation with Station (CHIRPS) dataset (Funk et al., 2015) were used for a 35 year period, from 1981 to 2015. This dataset spans from 50°S to 50°N in all longitudes and is accessible in 0.05° × 0.05° spatial resolution, from 6-

hourly to 3-monthly aggregates. Three types of precipitation information are combined in the CHIRPS database: precipitation climatology data, in situ rain gauge data, and precipitation measurements obtained via satellite. The high resolution and daily availability of precipitation data make this database able to detect extreme precipitation events with high precision (Katsanos et al., 2016).

To perform the ranking, three main steps were conducted:

1. For each grid point in the domain area, the daily normalised precipitation anomaly was calculated (N). This N represents the difference between precipitation values for a certain day and the daily mean climatological values. This value was then divided by the daily standard deviation climatological value. Only grid points with precipitation greater than 1 mm were considered.

2. To obtain wet spell events with longer duration (3, 5, 7, and 10 days) we computed the accumulated anomalies for a certain period (NCC), adding the N values for different periods.

3. The final step of the ranking method was calculating the precipitation magnitude of each event (R), where R represents the final ranking index. This R-index was obtained by multiplying two variables: 1) the area (A), expressed as a percentage, with precipitation anomalies above two standard deviations; and 2) the mean value of precipitation anomalies (M) over the area (A). The index can be expressed using the following equation:

$$R = A \times M \tag{3.5}$$

The R ranking index was computed for extreme precipitation events of different durations (Table 3.3) as the sum of normalized precipitation anomalies for the length duration of the event – in our case 1, 3, 5, 7, and 10 days. For example, a 5 day event consisted of the precipitation anomalies of the analysed day and four days before it to make a total of five days. Therefore, an event that occurred on 24 September 1996 would include the precipitation anomalies for 24, 23, 22, 21, and 20 September 1996. A detailed explanation of the ranking development and methodology is available in studies by Ramos et al. (2014; 2017).

Table 3.3. The top 10 extreme precipitation events of different durations over the Danube River Basin.

Duration	1 Day		3 Days		5 Days		7 Days		10 Days	
Ranking	R	Date	R	Date	R	Date	R	Date	R	Date
1	198.65	23 Sep 1996	249.95	24 Sep 1996	254.85	24 Sep 1996	298.19	1 Jan 1996	325.98	23 Aug 2005
2	168.81	28 Dec 2014	228.27	23 Sep 1996	254.22	25 Sep 1996	290.71	15 Dec 1990	317.66	18 Dec 1990
3	156.70	6 Nov 1985	224.59	25 Sep 1996	251.71	26 Sep 1996	277.60	2 Jan 1996	315.91	24 Aug 2005
4	155.58	1 Mar 2008	206.04	11 Feb 1984	237.58	14 Dec 1990	273.79	14 Dec 1990	313.98	4 Jan 1996
5	142.60	18 Feb 1994	204.39	6 Nov 1985	234.92	23 Jan 1998	260.72	7 May 1987	313.50	15 Dec 1990
6	140.42	27 Nov 1983	198.54	8 Jan 2010	231.42	27 Sep 1996	260.69	27 Sep 1996	301.29	17 Dec 1990
7	138.02	6 May 1987	198.36	6 May 1987	230.92	23 Sep 1996	258.47	24 Sep 1996	300.85	16 Dec 1990
8	137.91	14 Mar 2013	195.88	10 Feb 1984	227.95	22 Jan 1998	257.33	16 Dec 1990	298.32	14 Dec 1990
9	136.17	2 Mar 2014	195.15	29 Oct 1990	222.08	30 Oct 1990	256.91	28 Sep 1996	298.17	22 Aug 2005
10	131.77	27 Mar 1993	193.43	31 Oct 1994	221.67	31 Oct 1990	256.87	25 Sep 1996	290.89	12 May 1991

3.3 Detection of maximum precipitation

Using the global precipitation database the from Multi-Source Weighted-Ensemble Precipitation (MSWEP) (Beck et al., 2017a), we calculated the five years that exhibited maximum precipitation value over the regions of the Mediterranean Sea that lost moisture for precipitation, calculated by the Lagrangian experiment. A 0.25° latitude-longitude grid and monthly scale was used, and the computation was conducted for the period 1980-2015.

The MSWEP dataset is relatively new, having been accessible for use from the beginning of 2017. This database was designed for analysing hydrological fields at a 0.25° × 0.25° spatial resolution and covers the temporal period from 1979 until the present. Several characteristics distinguish it from other precipitation databases: i) it combines the advantages of a wide range of precipitation data sources to provide reliable precipitation estimates around the world, including satellite, gauge, and reanalysis data; ii) it corrects for gauge under-catch and orographic effects using Q streamflow information from 13762 stations that are available across the globe; and iii) it has a high (0.25°) spatial resolution and a 3 h temporal resolution.

3.4 Supplementary databases

ERA-Interim datasets:

Data for running FLEXPART: As mentioned previously, we used ERA-Interim data (Dee et al., 2011) from the ECMWF to run the FLEXPART model. This dataset is available at 1° × 1° spatial resolution at 6 h time intervals. It covers two temporal periods used in this thesis: 1980-2014 and 1980-2016. The model required 3D fields, including horizontal and vertical wind and specific humidity data; and 2D fields, including surface pressure, total cloud cover, 10 m horizontal wind components, 2 m temperature and dew point temperature, large-scale and convective precipitation, sensible heat flux, east/west and north/south surface stress, topography, land-sea-mask, and sub-grid standard deviation of topography.

Other ERA-Interim datasets:

- The eastward and northward water vapour flux from ERA-Interim was used at daily and monthly scale to calculate the VIMF and its divergence. For the most extreme wet spell event (23 September 1996) over the DRB, we computed the daily VIMF and its divergence to show the climatology and anomaly of this specific day. Maximum values of climatological monthly VIMF divergence were used to detect the major monthly moisture source regions for continental precipitation. These data are available at: https://www.ecmwf.int/en/forecasts/datasets/archivedatasets/reanalysisdatasets/era-interim.
- ERA-Interim daily data was used to diagnose atmospheric circulation. Two sets were used, one at 1° × 1° longitude and latitude for Sea Level Pressure (*SLP*) data and Geopotential Height (*Z*) at 850 hPa; and a second at 0.75° × 0.75° for specific humidity (*q*), zonal (*u*), and meridional (*v*) winds was used to calculate vertically integrated horizontal water vapour transport (*IVT*) from 1000 to 300 hPa.

Additional datasets were used to complete the investigation described in this work. A list of the supplementary data, data access points, and specific data use is given below:

<u>Precipitation data:</u>

- Daily precipitation data from CHIRPS (Funk et al., 2015). The database represents a combination of global climatological precipitation information, satellite-based measurements, and in situ rain gauge data. It has a high resolution of 0.05° longitude and latitude. The high resolution made it convenient for high-precision ranking of extreme precipitation events over the Danube River Basin. Data were obtained from http://chg.geog.ucsb.edu/data/chirps/.

- Monthly Multi-Source Weighted-Ensemble Precipitation (MSWEP) database (Beck et al., 2017a) at 0.25° × 0.25° resolution. The period used was 1980-2015. It combines gauges, satellites, and atmospheric reanalysis precipitation information. It was used to detect the peak precipitation month over each grid point and to compute monthly climatology, extreme, and minimum precipitation values (by the mean composite of the 5 highest and lowest monthly values). Available upon request from: http://www.gloh2o.org/.

- Monthly precipitation (PRE) data from the Climate Research Unit (CRU. TS3.23) at 0.5° × 0.5° degree spatial resolution from 1980-2015 was used to calculate the annual cycle of E-P over the Danube River Basin. Available at http://www.cru.uea.ac.uk/data.

<u>Evapotranspiration data:</u>

- Potential evapotranspiration (PET) data from the Climate Research Unit (CRU T.S 3.23). Data are freely available at 0.5° × 0.5° latitude and longitude at monthly scale at http://www.cru.uea.ac.uk/data. The period between 1980-2015 was used to calculate the annual cycle of E-P over the Danube River Basin.

All variables used are listed in Table 3.4.

Table 3.4. Summary of the databases used in this dissertation.

Type of data and Database	**Spatial resolution** (in degrees)	**Temporal resolution**	**Period**	**Data access**
Precipitation				
CHIRPS	0.05° × 0.05°	daily	1981-2015	http://chg.geog.ucsb.edu/data/chirps
MSWEP	0.25° × 0.25°	monthly	1980-2015	http://www.gloh2o.org
CRU TS3.23	0.5° × 0.5°	monthly	1980-2014	http://www.cru.uea.ac.uk/data
Potential Evapotranspiration	0.5° × 0.5°	monthly	1980-2014	http://www.cru.uea.ac.uk/data
CRU TS3.23				
ERA-Interim data	0.75° × 0.75° 1° × 1°	daily and monthly	1980-2016	http://apps.ecmwf.int/datasets/data/interim-full-daily/levtype=sfc
Sea Level Pressure (*SLP*) Geopotential Height (*Z*) Specific Humidity (*q*) Zonal wind (*u*) Meridional wind (*v*) Vertical integral of eastward (*uq*) and northward (*vq*) water vapour flux				

3.5 Statistical analysis

In this work, the Student's statistic test (*t-test*) (Decremer et al., 2014) was used. The analysis was applied in order to assess whether the relationship between precipitation anomalies over the Danube River Basin (Anom. CHIRPS) and anomalous moisture contribution from the Mediterranean Sea (Anom. PFLEX) was significant. The computation was conducted for the top 100 extreme precipitation events of different durations (1, 3, 5, 7, and 10 days) over the Danube River Basin.

4

Publications

This section presents part of the main results of the study performed in this PhD work, which have been published as independent research articles in four different journals included in Journal Citation Reports (JCR). The main purpose of the investigation is to characterise the contribution of moisture sources to extreme precipitation. The papers listed below do not appear in order of publication; thus, there are some inconsistencies in study periods because the output data from FLEXPART experiments was updated during the creation of this PhD thesis, and the databases available for research were supported in different periods. Table 4.1 lists these publications and gives information about each article: authors, title, journal of publication, and DOI number. A detailed description of the journals' characteristics is presented in Table 4.2. The supplementary material linked to each article is given in Appendix A: Supplementary Material.

The first article is "**Tracking the Origin of Moisture over the Danube River Basin Using a Lagrangian Approach**" by **D. Ciric**, M. Stojanovic, A. Drumond, R. Nieto, L. Gimeno, published in ***2016*** in ***Atmosphere*** 7(12), 162, doi:10.3390/atmos7120162. In this study, we characterized the main climatological moisture sources for the Danube River Basin and their contribution to precipitation over the region at a seasonal scale.

Table 4.1. List of publications

Authors	**Title**	**Journal of publication and year**	**DOI number**
D. Ciric M.Stojanovic, A. Drumond, R. Nieto, L. Gimeno	"Tracking the Origin of Moisture over the Danube River Basin Using a Lagrangian Approach"	*Atmosphere (2016)*	*10.3390/atmos7120162*
D. Ciric, R. Nieto, A.M. Ramos, A. Drumond, L. Gimeno	"Wet Spells and Associated Moisture Sources Anomalies across Danube River Basin"	*Water (2017)*	*10.3390/w9080615*
D. Ciric, R. Nieto, A.M. Ramos, A. Drumond, L. Gimeno	"Contribution of Moisture from Mediterranean Sea to Extreme Precipitation Events over Danube River Basin"	*Water (2018)*	*10.3390/w10091182*
D. Ciric, R. Nieto, L. Losada, A. Drumond, L. Gimeno	"The Mediterranean Moisture Contribution to Climatological and Extreme Monthly Continental Precipitation"	*Water (2018)*	*10.3390/w10040519*

The second article is titled: "**Wet Spells and Associated Moisture Sources Anomalies across Danube River Basin**" by **D. Ciric**, R. Nieto, A.M. Ramos, A. Drumond, L. Gimeno published in ***2017*** in ***Water*** 9, 615, doi:10.3390/w9080615. In this paper, we report on our ranking of extreme precipitation events (wet spells) for the Danube River Basin for the period 1981 to 2015. The events are ranked on different time scales (from 1 to 10 days), but an individual analysis is made for the most intense 1-day wet spell, which occurred on 23 September 1996. A synoptic analysis accompanied the study to complete the knowledge of the extreme and exceptional event.

The third article from the presented list is titled "**Contribution of Moisture from Mediterranean Sea to Extreme Precipitation Events over Danube River Basin**" by **D. Ciric**, R. Nieto, A.M. Ramos, A. Drumond, and L. Gimeno. This article was published in ***2018*** in the journal ***Water*** 10(9), 1182; doi: 10.3390/w10091182. This study is based on characterizing how moisture from the Mediterranean basin contributed to the top 100 extreme precipitation events with durations of 1, 3, 5, 7, and 10 days over the Danube River Basin.

The fourth and last article of this compendium is entitled "**The Mediterranean Moisture Contribution to Climatological and Extreme Monthly Continental Precipitation**" by **D. Ciric**, R. Nieto, L. Losada, A. Drumond, and L. Gimeno, published in ***2018*** in ***Water*** 10(4), 519, 1-19, doi:10.3390/w10040519. The focus of this work is investigating the role of the Mediterranean basin as a moisture source in extreme precipitation over the surrounding continental areas. It was conducted at a monthly scale with a spatial resolution of 0.25˚ longitude and latitude.

Table 4.2. Summary of the journals' characteristics.

Journal	Category	Journal overview
Atmosphere (open access journal of scientific studies related to the atmosphere)	Environmental Science	- Publisher: MDPI Basel, Switzerland - Current Impact Factor: 1.704 - 5-year Impact Factor: 1.775 - Cite Score 2017 (Scopus): **Q2** - ISSN: 2073-4433
Water (open access journal on water science and technology, including the ecology and management of water resources)	Water Science and Technology and Aquatic Science	- Publisher: MDPI Basel, Switzerland - Current Impact Factor: 2.069 - 5-year Impact Factor: 2.250 - Cite Score 2017 (Scopus): **Q1** - ISSN: 2073-4441

Finally, this PhD thesis includes an analysis of the role of the major oceanic and terrestrial moisture source regions to monthly maximum precipitation at the global scale. This section is not included as a publication; the results are presented in **Chapter 5** of this dissertation, entitled: "**A Global Atlas of Precipitation and Contribution of the Main Moisture Sources in the Peak Precipitation Month**".

atmosphere

Article

Tracking the Origin of Moisture over the Danube River Basin Using a Lagrangian Approach

Danica Ciric [1,*], Milica Stojanovic [1], Anita Drumond [1], Raquel Nieto [1,2] and Luis Gimeno [1]

[1] Environmental Physics Laboratory (EPhysLab), Facultade de Ciencias, Universidad de Vigo, Ourense 32004, Spain; smilica@alumnos.uvigo.es (M.S.); anitadru@uvigo.es (A.D.); rnieto@uvigo.es (R.N.); l.gimeno@uvigo.es (L.G.)

[2] Department of Atmospheric Sciences, Institute of Astronomy, Geophysics and Atmospheric Sciences, University of São Paulo, São Paulo 05508-090, Brazil

* Correspondence: cdanica@alumnos.uvigo.es; Tel.: +34-988-387-208

Academic Editor: Anthony R. Lupo
Received: 16 November 2016; Accepted: 8 December 2016; Published: 14 December 2016

Abstract: In this study, we investigate the sources of moisture (and moisture for precipitation) over the Danube River Basin (DRB) by means of a Lagrangian approach using the FLEXPART V9.0 particle dispersion model together with ERA-Interim reanalysis data to track changes in atmospheric moisture over 10-day trajectories. This approach computes the budget of evaporation-minus-precipitation by calculating changes in specific humidity along forward and backward trajectories. We considered a time period of 34 years, from 1980 to 2014, which allowed for the identification of climatological sources and moisture transport towards the basin. Results show that the DRB mainly receives moisture from seven different oceanic, maritime, and terrestrial moisture source regions: North Atlantic Ocean, North Africa, the Mediterranean Sea, Black Sea, Caspian Sea, the Danube River Basin, and Central and Eastern Europe. The contribution of these sources varies by season. During winter (October–March) the main moisture source for the DRB is the Mediterranean Sea, while during summer (April–September) the dominant source of moisture is the DRB itself. Moisture from each source has a different contribution to precipitation in the DRB. Among the sources studied, results show that the moisture from the Mediterranean Sea provides the greatest contribution to precipitation in the basin in both seasons, extending to the whole basin for the winter, but being more confined to the western side during the summer. Moisture from the Caspian and Black Seas contributes to precipitation rather less.

Keywords: moisture sources and sinks; Lagrangian approach; precipitation; FLEXPART; Danube River Basin

1. Introduction

The global hydrological cycle is both an important element of the climate system and a decisive driver of water resources, which is why there is such intense interest in hydrology and meteorology for understanding the origin of moisture for precipitation over different regions of interest [1–3]. Europe is no exception, and many studies have shown a decreasing trend in precipitation over Central and Southern Europe, increasing over Northern Europe [4].

Rivers represent an important part of the global hydrological cycle, returning about 35% of continental precipitation to the oceans. Rivers also have a significant socio-economic role, in industrial activity, transportation, agriculture, and domestic fresh water supplies [5]. Because of climate change, the hydrological cycles of river basins vary over time, affecting their physical condition at regional scales [6]. The River Danube has a length of 2870 km and a catchment area of around 817,000 km^2 (as shown in Figure 1), and is the second longest river in Europe. A total of

19 countries (Germany, Austria, Slovakia, Hungary, Croatia, Serbia, Montenegro, Romania, Bulgaria, Moldova, Ukraine, Poland, Czech Republic, Switzerland, Italy, Slovenia, Bosnia-Herzegovina, Albania, Macedonia) constitute the Danube River Basin (DRB), making it the world's most international river basin [7]. Connected to 27 large and over 300 smaller tributaries (the DRB district), the river plays an important role in the ecological balance of the region, having a number of important socio-economic contributions as a waterway, a natural resource, and a source of energy [8].

The climate of the DRB is very diverse, with Atlantic influences in the western upper basin, and a Mediterranean influence in the southern part of the central and lower basin. Its proximity to the Mediterranean Sea means that the DRB receives high precipitation throughout the year [9].

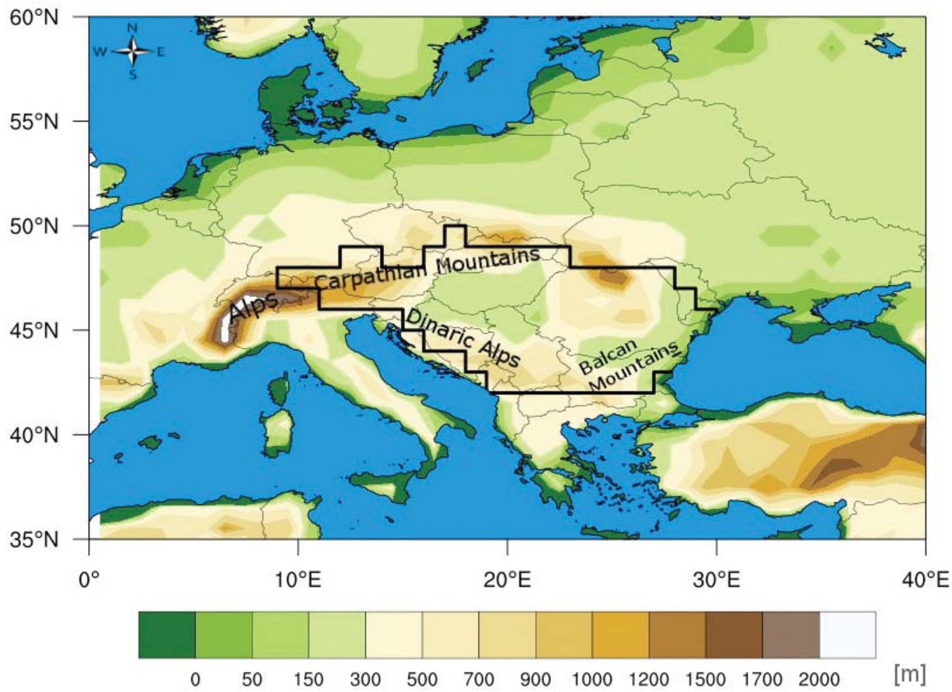

Figure 1. The black line indicates the Danube river basin. The colors are related to elevation (in meters).

River flow in the Danube is mainly a function of precipitation and evaporation in the Danube catchment. The mean annual rainfall throughout the catchment is strongly dependent on orography; one-third of the basin consists of mountains with the remainder being hills and plains. The total annual precipitation is estimated at about 2000 mm per year in the high parts (the Alps in the West, the Dinaric-Balkan mountain chains in the south, and the Carpathian Mountains in the north), about 500 mm per year in the plains, and less than 600 mm in the Danube delta. The annual mean evaporation is estimated at between 450 and 650 mm per year [8].

Many previous studies, using observational data in the DRB, have attempted to explain the effects of changes in precipitation and temperature on the flow regime, and on the possible changes in the natural drivers with impacts on water resources, water availability, extreme hydrological events, the quality of the water resources, and the ecosystem in the DRB [10].

It is very important to know the origin of the atmospheric moisture and the precipitation that occurs over a given region as they represent important elements of the atmospheric hydrological, so changes in the precipitation in one region may be dependent of changes in sources of moisture. The knowledge of the moisture sources is crucial to justify physically the changes in precipitation both for current and future climates [3].

Given the importance of the DRB in the moisture budget, the main objective of this paper is to track the origin of moisture for precipitation over the DRB. The identification of moisture sources can be accomplished by using a wide range of methods, which includes "analytical and box models", "physical water vapor tracers" (isotopes), and "numerical water vapor tracers". In the review by

Gimeno et al. [3] a detailed review and comparison of the different approaches was done concluding that the Lagrangian approaches provide the more realistic source-sink relationships. In this paper, we have used the Lagrangian method developed by Stohl and James [11,12]. Using this method, Stohl and James studied the main flooding events and periods with intensive precipitation in central Europe, including the area around and within the DRB [11]. This approach has been extensively and successfully used in many regions throughout the world, including the Orinoco river basin [13], the Sahel [14], China [15], Iceland [16], Central America [17], the Mediterranean region [18], and the Sahelian Sudan region [19].

Specific objectives are (i) the identification of the major climatological source of moisture for the DRB for the 34-year period from 1980 to 2014 by tracking the air masses that ultimately reach the DRB backwards in time; (ii) to analyse the seasonal variability of these sources by comparing two seasons: the summer (April–September) and the winter (October–March); and (iii) to study the influences on the different moisture sources for precipitation at a subregional scale in the basin by tracking the air masses departing each source region and reaching the DRB forwards in time.

2. Data and Methodology

This study is based on the method developed by Stohl and James [11,12], which uses the Lagrangian particle dispersion model FLEXPART V9.0 [12] together with ERA-interim reanalysis data from the European Centre for Medium-Range Weather Forecasts (ECMWF) [20] at a 1° horizontal resolution on 61 vertical levels from 0.1 to 1000 hPa. The analysis covers a 34-year period from October 1980 to September 2014. Our aim is to use this Lagrangian approach to determine the major moisture sources for the DRB, and the relative contributions of these to the precipitation.

The method has been widely used in a number of studies [13,21,22], and consists of dividing the atmosphere into a large number of air particles (approximately 2.0 million) with constant mass, which must take into account any changes in the density and volume of the air. The particles are transported using a 3-dimensional wind field. The transport time of the particles is limited to 10 days, this being the average period of residence of water vapor in the atmosphere [23]. The specific humidity (q) and the position of all the particles are recorded at 6-h intervals. Changes in specific humidity (q) with time ($e\text{-}p = m\, dq/dt$), where m is the mass of the particle, help us to identify those particles that lose moisture through precipitation (p) or receive it through evaporation (e) over each particle trajectory. By adding the (e-p) of all the particles existing in the atmosphere over the area of interest, we obtain the total (E-P) field, where (E) indicates the evaporation rate and (P) indicates the precipitation rate per unit area. The two main limitations of the method are (i) that we cannot calculate E and P separately and (ii) its reliability strongly depends on the quality of the input data. However, with such a large number of air particles it is hoped that any errors may cancel each other out given the number of particles contained in an atmospheric column [24].

Using the Lagrangian model FLEXPART we can identify the origins of the particles observed over the DRB via the backward analysis, which allows us to identify where the air masses gain humidity along their trajectories from their moisture source areas. Positive values of (E-P) indicate those areas where evaporation dominates over precipitation. Through backward tracking, the particles over the target area (DRB) are returned to their source regions where they gain humidity, and using the annual averages of (E-P) > 0 for the period 1980–2014 we can identify the source regions.

In order to identify the boundaries of the moisture source regions, we used the 90% percentile of the annual averages of (E-P) > 0 for the backward experiment, which corresponds to a contour line of 0.06 mm/day. Although the definition of the threshold is arbitrary, this statistical procedure is valid and has successfully been applied in many previous studies using the same approach (e.g., [21]).

The Lagrangian forward experiment is used to identify where moisture is lost (precipitation exceeds evaporation) by the air masses that originate in each moisture source region, and reveals the moisture sinks. Negative values of (E-P) indicate those areas where precipitation exceeds evaporation. A more detailed description of the use of backward and forward analysis to track moisture can be found in any of the many articles published in recent years describing this approach (e.g., Drumond et al. [24] for the Amazon Basin).

3. Results

Due to the seasonality of the precipitation, the pattern of moisture sources is likely to vary over the year. The minimum potential evapotranspiration (PET) is in December and the maximum is in July, while for the annual cycle of precipitation (PRE) the minimum is in February and the maximum is in June as illustrated on Figure 2. To calculate PRE, PET, and the difference between them (P-E), we used the Climatic Research Unit (CRU) (TS3.23) [25] climate data set with a spatial resolution of 0.5 degrees. The annual cycle of P-E can help us to justify the definition of two annual seasons: a Winter season when P-E > 0 (from October to March), and a Summer season when P-E < 0 (from April to September). The winter season encompasses the period October 1980 to March 2014, and the summer season refers to April 1981 to September 2014.

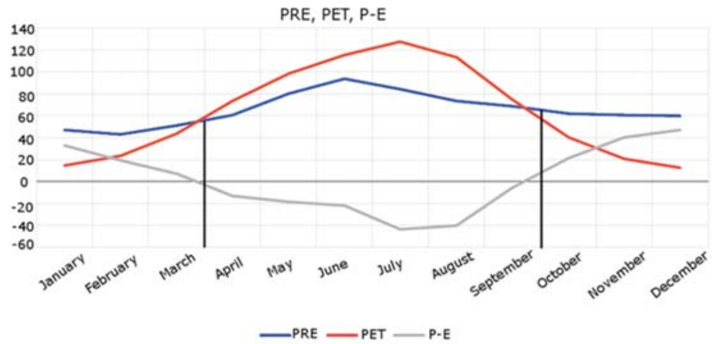

Figure 2. The climatological annual cycle of precipitation (PRE, blue line), potential evapotranspiration (PET, red line) and their difference (P-E, grey line) averaged over the Danube River Basin (DRB) for 1980–2014. Data from Climatic Research Unit (CRU). Scale in mm/day. Vertical red lines indicate the two identified seasons: summer from April to September and winter from October to March.

We tracked the air masses over the DRB backward in time to identify the sources. The areas characterised by the reddish colours represent regions where (*E-P*) > 0, meaning that evaporation exceeds precipitation in the net moisture budget (moisture source), while areas characterised by the blueish colours represent regions where (*E-P*) < 0, meaning that precipitation exceeds evaporation in the net moisture budget of the tracked air particles (moisture sinks). After identifying the sources of moisture over the DRB through backward analysis, forward analyses were applied to those particles leaving each source moving towards the target area (DRB) in order to estimate the contribution of each of these sources to moisture loss over the DRB. The annual values of 10-day integrated atmospheric moisture budget obtained via backward experiment from the DRB for the 34-year period October 1980–September 2014 are shown on Figure 3.

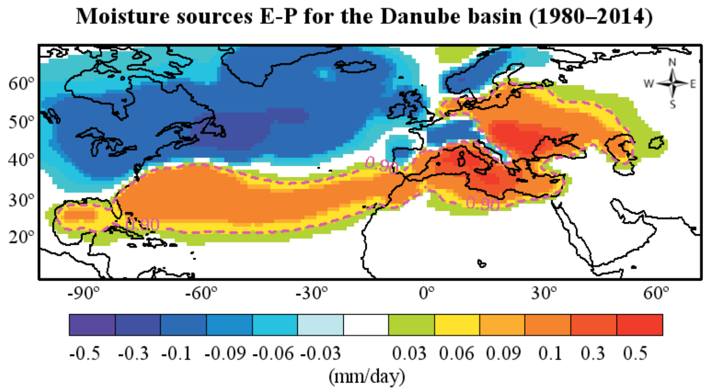

Figure 3. Climatological annual 10-day integrated (*E-P*) obtained from the backward DRB experiment for the period October 1980 to September 2014. The pink dashed contour line delimits the source areas selected using the 90th percentile of the (*E-P*) > 0 values (i.e., 0.06 mm/day).

According to the threshold of 0.06 mm/day, which corresponds to the 90% percentile of the annual averages of (*E-P*) > 0 obtained from the backward experiment, and the methodology described above, the DRB mainly receives moisture from seven different oceanic, maritime, and terrestrial moisture source regions: North Atlantic Ocean (NATL), North Africa (NAF), Mediterranean Sea (MED), Black Sea (BS), Caspian Sea (CS), Danube River Basin (DRB), and Central and Eastern Europe (hereafter Rest of Land, RestL). These regions are shown in Figure 4.

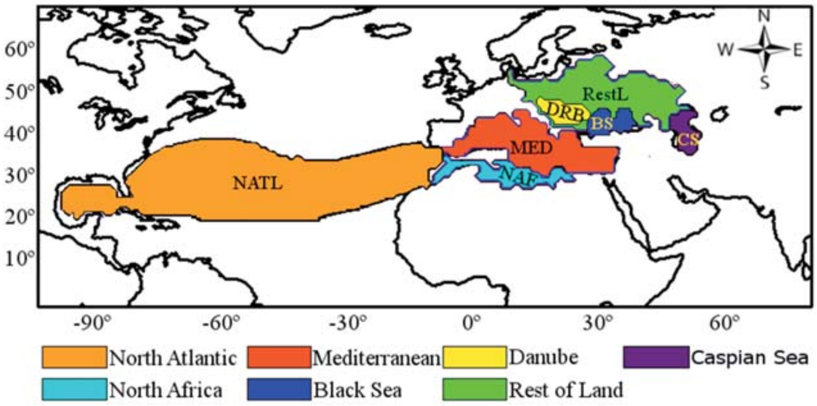

Figure 4. Schematic representation of moisture sources for the DRB identified in Figure 2.

The Lagrangian analysis of moisture sources at a seasonal scale (Figure 5a,c) shows that during the winter the dominant source of moisture for the DRB is the Mediterranean Sea, where the moisture uptake (*E-P* > 0) is greater than 0.3 mm/day, while during the summer the main source is the Danube basin itself where the moisture uptake exceeds 0.5 mm/day. The results show that (*E-P* > 0) over the North Atlantic is greater than 0.1 mm/day during the winter but less than 0.09 mm/day for the summer. The uptakes for the Rest of Land and the Black Sea are higher in the winter (approximately 0.3 mm/day) than in the summer, when they are insignificant. North Africa and the Caspian Sea are minor sources in both seasons.

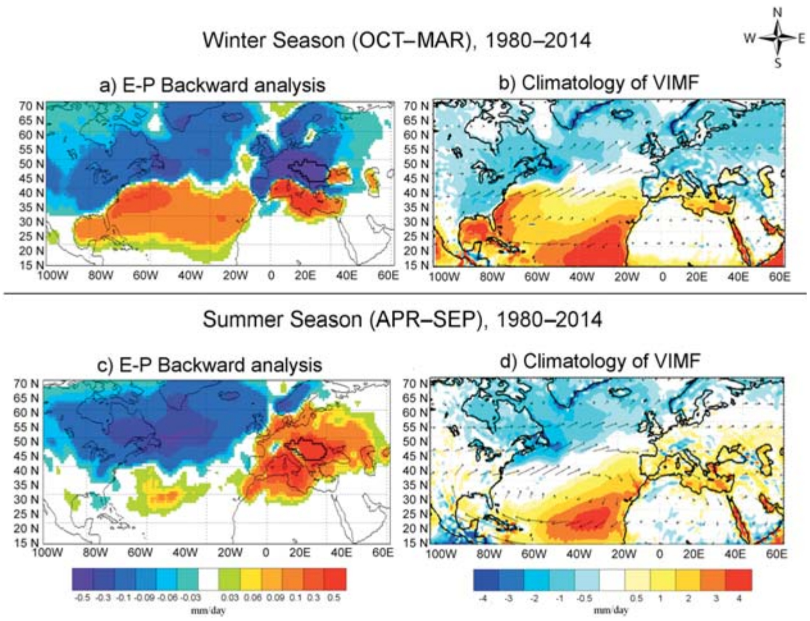

Figure 5. (**a**–**d**) Climatological seasonal values of 10-day integrated atmospheric moisture budget (*E-P*) obtained via backward trajectories from the DRB for (**a**) winter and (**c**) summer, and climatological seasonal vertically integrated moisture flux (vectors; in kg·m^{-1}·s^{-1}) and its divergence (shaded; in mm/day) for (**b**) winter and (**d**) summer seasons. Data obtained from ERA-Interim. Thick black contour in (**a**) and (**c**) indicates the DRB.

By comparison with the vertically integrated moisture flux (VIMF) (see Figure 5b,d), the most important regions of divergence (where evaporation exceeds precipitation) are over the Mediterranean Sea and the North Atlantic. The area of divergence over the North Atlantic is in accordance with the source moisture area during the winter (Figure 5b), with a moisture flux that originates in the North Atlantic and proceeds to the region of the Danube. In the summer (Figure 5d), when the North Atlantic source is weak, we note that the area of divergence over the North Atlantic is not as strong as in the winter, while over the Danube there is a small area of convergence.

The map of VIMF shows that the value of convergence (when precipitation exceeds evaporation) over the Danube exceeds 1 mm/day during the winter season, decreasing in size in summer and even showing a small region of divergence.

The contribution of each source of moisture for each of the 10 days of the backward analysis is shown in Figure 6, indicating the importance of each source along its trajectory for the period 1980–2014 (Figure 6a) and for two seasons: winter (October–March; Figure 6b) and summer (April–September; Figure 6c). This contribution is calculated as the integral of evaporation-minus-precipitation over the ten-day back-trajectory. In these figures, the abscissa shows each of the 10 days for which the *E-P* contribution of each source to the target region is calculated, and the ordinate shows the values of integrated $(E\text{-}P)_{1\text{-}10}$ for each of the seven sources in mm/day. Figure 6a (annual contribution) shows that RestL (Rest of Land), MED (Mediterranean Sea), and the Danube itself are the most important sources at the beginning of the ten-day period, while NATL (North Atlantic Ocean) is an important moisture source from the fourth day, becoming the most intense by day ten. The supply of moisture from BS (Black Sea), CS (Caspian Sea), and NAF (North Africa), although always positive, is lower than for the other regions. In the winter (October–March; Figure 6b), the Mediterranean Sea is clearly the most important source from the second day, and has a maximum contribution at day three. The North Atlantic begins to be an important moisture source from the third day and continues being so up to day ten. The Danube and RestL are not important sources on the first day of transport, but from the second day they start to contribute in a minor way to the supply. Although the Black Sea shows positive values throughout the ten days, its overall contribution is low. The most important contribution in summer (April–September; Figure 6c) is the Danube itself and the Rest of Land. The maximum contribution of these sources is seen on day one and they are significant up to the sixth day, after which their contribution diminishes somewhat.

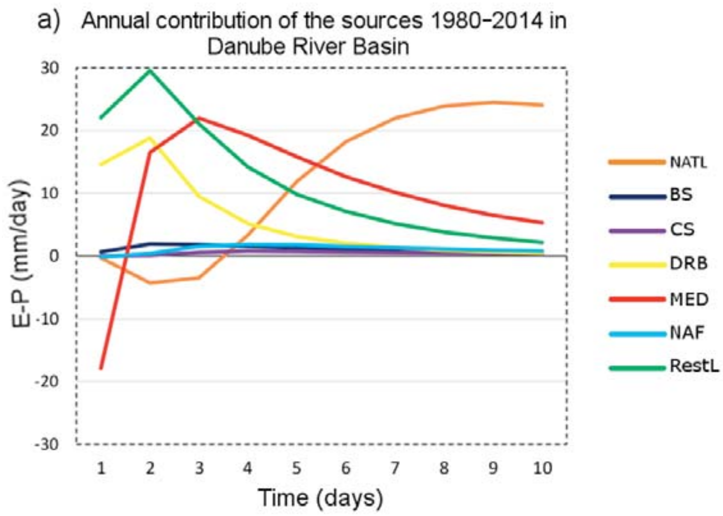

Figure 6. *Cont.*

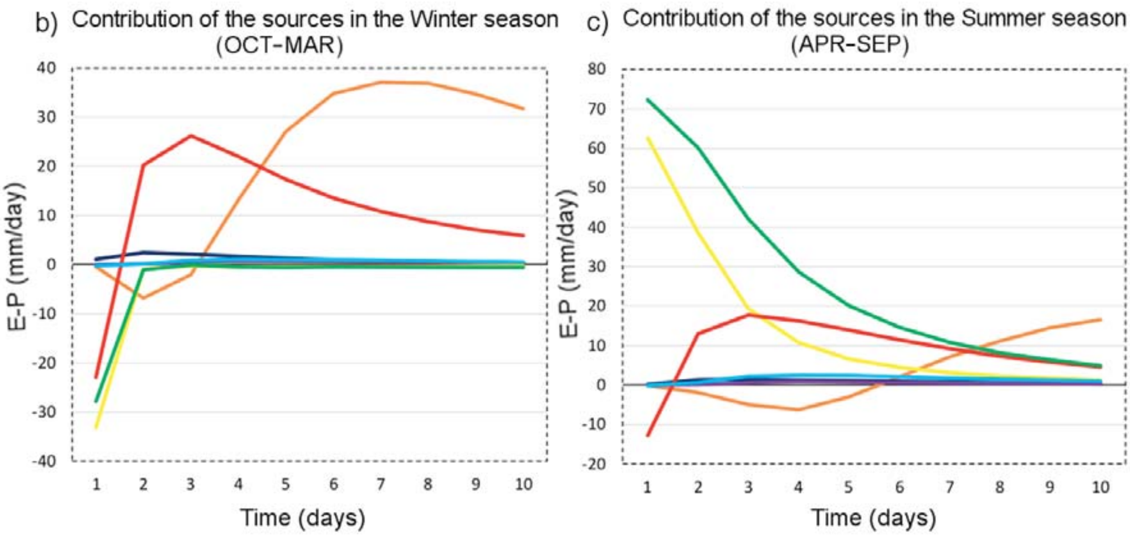

Figure 6. Absolute values of $(E\text{-}P)_{1\text{-}10}$ time series calculated backwards for the moisture over the DRB area and integrated over the regions of interest: NATL (North Atlantic Ocean) orange line, BS (Black Sea) dark blue line, CS (Caspian Sea) violet line, DRB (Danube River Basin) yellow line, MED (Mediterranean Sea) red line, NAF (North Africa) blue line, and RestL (Rest of Land) green line in mm/day. (**a**) Annual 10-day integrated *E-P* moisture contribution of the sources for the period 1980–2014. (**b**) 10-day integrated *E-P* moisture contribution for winter. (**c**) 10-day integrated *E-P* moisture contribution for the summer in mm/day.

The Mediterranean Sea is not a significant moisture source on the first day, but from the second day up to the end of the ten-days period it becomes much more significant. For the first six days the North Atlantic does not make any contribution to the target area, but from day six to day ten its contribution is on the increase. The Black Sea, Caspian Sea, and North Africa contribute throughout the ten-day period but the amounts are smaller.

The contribution of each source in percentage terms is shown in Figure 7. For each source we used the mean values for winter and summer for the whole of the period 1980–2014, and then for this period we calculated the average for each year. We used average values for each source for the whole period 1980–2014 to calculate the percentage contribution of each identified source. The percentage contribution for each source was obtained as the sum of all sources divided by the average value of each source, expressed in percentage terms. All seven sources have an influence on the DRB. From the Figure 7 it can be seen that in winter the Mediterranean Sea is the major source (31%) followed by the Black Sea, the Danube, and the North Atlantic, and that there are three minor sources: North Africa, Rest of Land (Central and Eastern Europe), and the Caspian Sea. The contribution of the sources in the summer is rather different, with the DRB itself being the most important (51%), followed by Rest of Land (21%) and the Mediterranean Sea (11%) as intermediate sources. The other sources contribute a much smaller percentage.

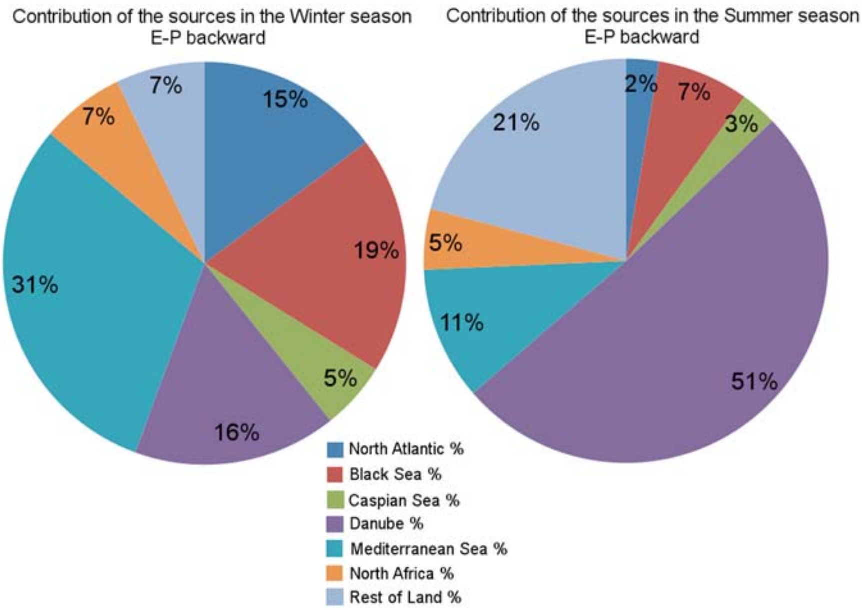

Figure 7. Moisture uptake over the sources obtained from *E-P* backward analysis for the DRB for winter and summer in percentage terms (%).

The various moisture source regions considered can contribute in different ways to precipitation in different subregions inside the Danube basin, and this can also vary for both seasons. An estimate of the moisture provided by the air particles from each source region for precipitation in the basin can be achieved using forward trajectories over 10 days of (*E-P*) for the 34-year period (Figure 8). The Lagrangian forward experiment identifies where moisture is lost (where precipitation exceeds evaporation) from the air masses from each moisture source region, enabling their moisture sinks to be identified. Because we are interested in precipitation, only negative values of *E-P* budget are displayed (the white areas of the maps represent regions where the (*E-P*) fields have low or positive values).

The contribution of the Atlantic Ocean to the target area differ between winter and summer. In winter, the Atlantic has a strong impact on the whole basin, its effects being most strongly felt in the southwestern subregion. During the summer, the spatial pattern is similar but the intensity is lower, and the Atlantic source has no impact at all in the southern part of the basin. The particles from the Black and Caspian Sea sources lose moisture over almost the whole basin during the winter, but the amounts are lower than for the Atlantic. The Black Sea loses more moisture than the Caspian Sea, especially in the center of the river basin. During the summer, these sources have a low impact in the basin area. In the central northern part of the basin, the greatest contribution is from the Danube source itself during the summer. Although the Mediterranean is the most significant source for the whole basin in both seasons, its influence is stronger in winter. During the summer, the maximum values are located over the northwestern and northern parts of the basin. Finally, the North African source has an impact over the whole of the target area in both winter and summer, but the amounts are low, while the Rest of Land contribution reaches the central and northern part of the basin during winter, but during summer it only reaches the western part of the DRB.

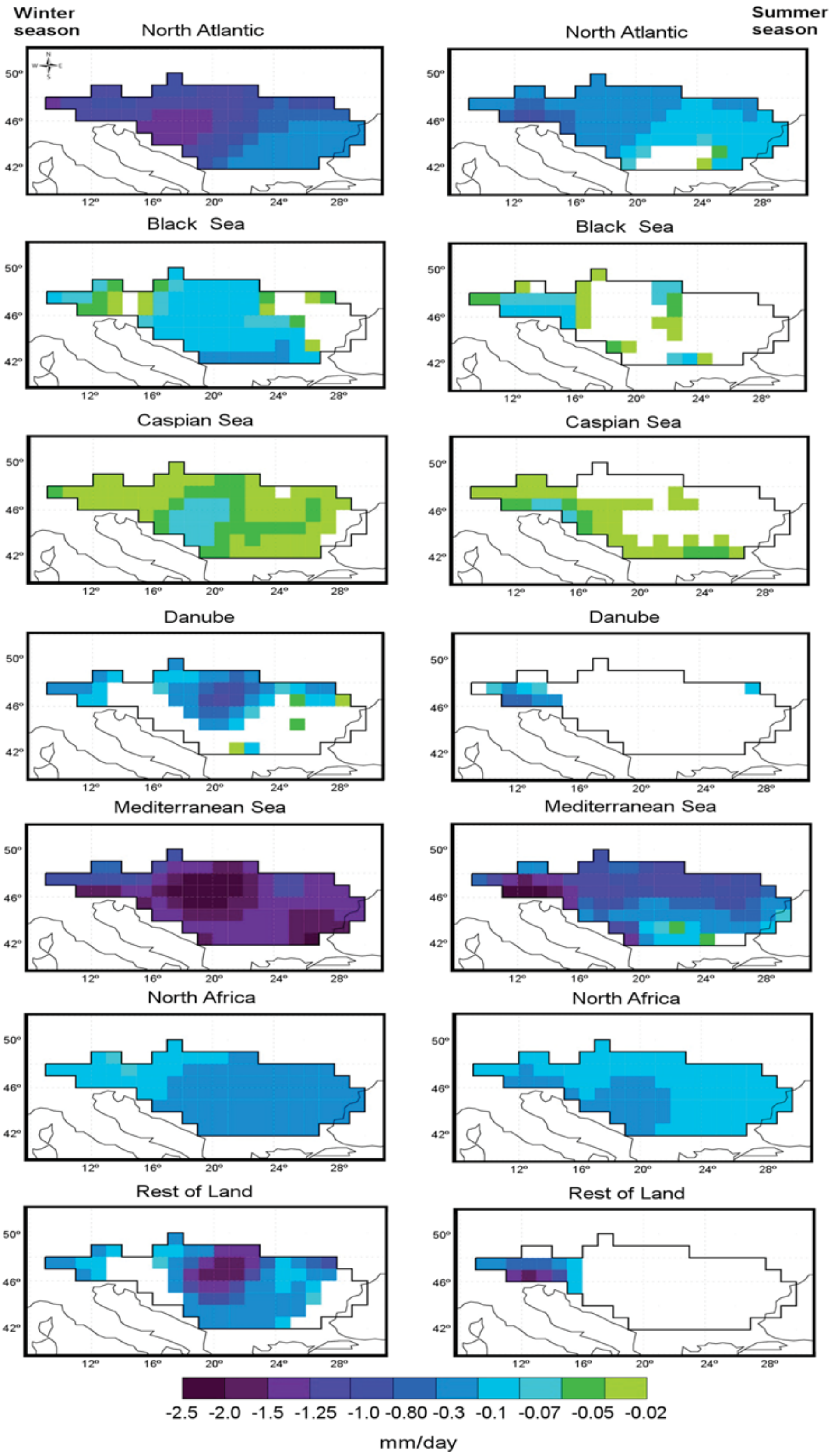

Figure 8. Seasonal average values of *E-P* < 0 for the period 1980–2014 determined from the forward Lagrangian experiment for: NATL, BS, CS, DRB, MED, NAF, and Rest of Land. The **left-hand panels** relate to the winter, while the **right-hand panels** relate to the summer months. Only negative values are shown to reflect sink regions. The thick black line delimits the DRB area. Scale is mm/day.

4. Discussion and Conclusions

We used a Lagrangian approach based on the FLEXPART model to track water vapor in the atmosphere and to diagnose its sources and sinks for the DRB. In this approach we applied the method of Stohl and James [11,12] with the Era-Interim dataset [12].

The results show that the DRB mainly receives moisture from seven different oceanic, maritime, and terrestrial moisture source regions: North Atlantic Ocean, North Africa, Mediterranean Sea, Black Sea, Caspian Sea, Danube River Basin, and Rest of Land (Central and Eastern Europe). For each source, we calculated the percentage contribution of the total moisture supplied to the DRB. The contribution of these sources varies by season. During the winter (October–March), the main moisture source for the DRB is the Mediterranean Sea, while during the summer (April–September) the dominant source of moisture is the DRB itself.

Moisture from each source has a different contribution to precipitation in the Danube. Results show that the air particles from the Mediterranean Sea provide the greatest moisture losses in the basin in both seasons, extending to the whole of the basin for the winter, but being more confined to the western side during the summer. Moisture from the Caspian Sea and the Black Sea contributes the least to precipitation in the Danube basin in both seasons.

Our findings are in agreement with previous studies using this methodology to identify the moisture sources for different regions over Europe. Drumond et al. [26] analysed the main sources and sinks of moisture over the Mediterranean region in the period 1980–2000, showing the role of the Central Mediterranean Sea as the dominant moisture source for the Balkan Peninsula during the wet season, and Sodemann et al. [27] showed the major importance of the Mediterranean source for the moisture sources of the Southern Alps in a seven-year period analysis (from 1995 to 2002).

The DRB is a major source of moisture for itself during the summer, but this moisture does not contribute in any significant way to precipitation in the region overall.

Acknowledgments: D. Ciric and M. Stojanovic are supported by European Commission under the Erasmus Mundus project Green-Tech-WB: Smart and Green technologies for innovative and sustainable societies in Western Balkans (551984-EM-1-2014-1-ES-ERA Mundus-EMA2). R. Nieto acknowledges the support of the CNPq grant 314734/2014-7 by the Brazilian government. A. Drumond acknowledges funding by the Spanish Government and FEDER through the SETH (CGL2014-60849-JIN) project.

Author Contributions: R. Nieto, A. Drumond, and L. Gimeno conceived and designed the experiments; D. Ciric and M. Stojanovic performed the experiments and analysed the data; D. Ciric, M. Stojanovic, L. Gimeno, R. Nieto, and A. Drumond wrote the paper.

Conflicts of Interest: The authors declare no conflict of interest. The founding sponsors had no role in the design of the study; in the collection, analyses, or interpretation of data; in the writing of the manuscript, and in the decision to publish the results.

Abbreviations

The following abbreviations are used in this manuscript:

BS	Black Sea
CRU	Climatic Research Unit
CS	Caspian Sea
DRB	Danube River Basin
E	Evaporation
ERA	European Centre for Medium-Range Weather Forecasting Re-Analysis
FLEXPART	FLEXible PARTicle dispersion model
MED	Mediterranean Sea
NAF	North Africa
NATL	North Atlantic Ocean
P	Precipitation
PET	Potential evapotranspiration
PRE	Precipitation

References

1. Christensen, J.H.; Christensen, O.B. Severe summertime flooding in Europe. *Nature* **2003**, *421*, 805–806. [CrossRef] [PubMed]
2. Schär, C.; Vidale, P.L.; Lüthi, D.C.; Frei, C.; Häberli, C.; Liniger, M.A.; Appenzeller, C. The role of increasing temperature variability in European summer heatwaves. *Nature* **2004**, *427*, 332–336. [CrossRef] [PubMed]
3. Gimeno, L.; Stohl, A.; Trigo, R.M.; Dominguez, F.; Yoshimura, K.; Yu, L.; Drumond, A.; Duran-Quesada, A.M.; Nieto, R. Oceanic and terrestrial sources of continental precipitation. *Rev. Geophys.* **2012**, *50*, 1–41. [CrossRef]
4. Nikolova, N.; Vassilev, S. Variability of summer-time precipitation in Danube plain, Bulgaria. *J. Geogr. Instit. Jovan Cvijic Serbian Acad. Sci.* **2005**, *54*, 19–32. [CrossRef]
5. Gibson, J.J.; Aggarwal, P.; Hogan, J.; Herczeg, A. Isotope studies in large river basins: A new global research focus. EOS, Transactions. *Eos Trans. Am. Geophys. Union* **2002**, *83*, 613–617. [CrossRef]
6. Fan, J.; Huang, Q.; Cui, S.; Guo, A. Detecting runoff variation in Weihe River basin, China. *Proc. Int. Assoc. Hydrol. Sci.* **2015**, *368*, 233–238.
7. Lucarini, V.; Danihlik, R.; Kriegerova, I.; Speranza, A. Hydrological cycle in the Danube basin in present-day and XXII century simulations by IPCCAR4 global climate models. *J. Geophys. Res. Atmos.* **2008**, *113*. [CrossRef]
8. Rîmbu, N.; Boroneanţ, C.; Buţă, C.; Dima, M. Decadal variability of the Danube river flow in the lower basin and its relation with the North Atlantic Oscillation. *Int. J. Climatol.* **2002**, *22*, 1169–1179. [CrossRef]
9. The Danube Basin. Available online: http://www.danubebox.org/ (accessed on 8 June 2016).
10. Pistocchi, A.; Beck, H.; Bisselink, B.; Gelati, E.; Lavalle, C.; Feher, J. *Water Scenarios for the Danube River Basin: Elements for the Assessment of the Danube Agriculture-Energy-Water Nexus*; Publications Office of the European Union: Luxembourg, 2015. [CrossRef]
11. Stohl, A.; James, P. A Lagrangian analysis of the atmospheric branch of the global water cycle. Part I: Method description, validation, and demonstration for the August 2002 flooding in central Europe. *J. Hydrometeorol.* **2004**, *5*, 656–678. [CrossRef]
12. Stohl, A.; James, P. A Lagrangian analysis of the atmospheric branch of the global water cycle: Part II: Moisture transports between Earth's ocean basins and river catchments. *J. Hydrometeorol.* **2005**, *6*, 961–984. [CrossRef]
13. Nieto, R.; Gallego, D.; Trigo, R.M.; Ribera, P.; Gimeno, L. Dynamic identification of moisture sources in the Orinoco basin in equatorial South America. *Hydrol. Sci. J.* **2008**, *53*, 602–617. [CrossRef]
14. Nieto, R.; Gimeno, L.; Trigo, R.M. A Lagrangian identification of major sources of Sahel moisture. *Geophys. Res. Lett.* **2006**, *33*, L18707. [CrossRef]
15. Drumond, A.; Nieto, R.; Gimeno, L. Sources of moisture for China and their variations during drier and wetter conditions in 2000–2004: A Lagrangian approach. *Clim. Res.* **2012**, *50*, 215–225. [CrossRef]
16. Nieto, R.; Gimeno, L.; Gallego, D.; Trigo, R. Contributions to the moisture budget of air masses over Iceland. *Meteorol. Z.* **2007**, *16*, 37–44. [CrossRef]
17. Duran-Quesada, A.M.; Gimeno, L.; Amador, J.A.; Nieto, R. Moisture sources for Central America: Identification of moisture sources using a Lagrangian analysis technique. *J. Geophys. Res. Atmos.* **2010**, *15*, D05103. [CrossRef]
18. Nieto, R.; Gimeno, L.; Drumond, A.; Hernandez, E. A Lagrangian identification of the main moisture sources and sinks affecting the Mediterranean area. *WSEAS Trans. Environ. Dev.* **2010**, *6*, 365–374.
19. Salih, A.A.M.; Zhang, Q.; Tjernström, M. Lagrangian tracing of Sahelian Sudan moisture sources. *J.Geophys. Res. Atmos.* **2015**, *20*, 6793–6808. [CrossRef]
20. Dee, D.P.; Uppala, S.M.; Simmons, A.J.; Berrisford, P.; Poli, P.; Kobayashi, S.; Andrae, U.; Balmaseda, M.A.; Balsamo, G.; Bauer, P.; et al. The ERA-Interim reanalysis: Configuration and performance of the data assimilation system. *Q. J. R. Meteorol. Soc.* **2001**, *137*, 553–597. [CrossRef]
21. Drumond, A.; Nieto, R.; Gimeno, L.; Ambrizzi, T. A Lagrangian identification of major sources of moisture over Central Brazil and La Plata Basin. *J. Geophys. Res. Atmos.* **2008**, *113*, D14128. [CrossRef]
22. Gimeno, L.; Nieto, R.; Drumond, A.; Castillo, R.; Trigo, R. Influence of the intensification of the major oceanic moisture sources on continental precipitation. *Geophys. Res. Lett.* **2013**, *40*, 1–8. [CrossRef]
23. Numaguti, A. Origin and recycling processes of precipitating water over the Eurasian continent: Experiments using an atmospheric general circulation model. *J. Geophys. Res. Atmos.* **1999**, *104*, 1957–1972. [CrossRef]

24. Drumond, A.; Marengo, J.; Ambrizzi, T.; Nieto, R.; Moreira, L.; Gimeno, L. The role of the Amazon Basin moisture in the atmospheric branch of the hydrological cycle: A Lagrangian analysis. *Hydrol. Earth Syst. Sci.* **2014**, *18*, 2577–2598. [CrossRef]
25. Harris, I.; Jones, P.D.; Osborn, T.J.; Lister, D.H. Updated high-resolution grids of monthly climatic observations—the CRU TS3.10 Dataset. *Int. J. Climatol.* **2014**, *34*, 623–642. [CrossRef]
26. Gómez-Hernández, M.; Drumond, A.; Gimeno, L.; Garcia-Herrera, R. Variability of moisture sources in the Mediterranean region during the period 1980–2000. *Water Resour. Res.* **2013**, *49*, 6781–6794. [CrossRef]
27. Sodemann, H.; Zubler, E. Seasonal and inter-annual variability of the moisture sources for Alpine precipitation during 1995–2002. *Int. J. Climatol.* **2010**, *30*, 947–961. [CrossRef]

water

MDPI

Article

Wet Spells and Associated Moisture Sources Anomalies across Danube River Basin

Danica Ciric [1,*], Raquel Nieto [1], Alexandre M. Ramos [2], Anita Drumond [1] and Luis Gimeno [1]

1 EPhysLab (Environmental Physics Laboratory), Facultade de Ciencias, Universidade de Vigo, 32004 Ourense, Spain; rnieto@uvigo.es (R.N.); anitadru@uvigo.es (A.D.); l.gimeno@uvigo.es (L.G.)
2 Instituto Dom Luiz, Universidade de Lisboa, 1749-016 Lisboa, Portugal; amramos@fc.ul.pt
* Correspondence: cdanica@alumnos.uvigo.es; Tel.: +34-988-387-248

Received: 29 May 2017; Accepted: 15 August 2017; Published: 17 August 2017

Abstract: The Danube River Basin is the second longest catchment basin in Europe and exhibits intense climatological diversity. In recent decades, the frequency and intensity of daily precipitation extremes have suffered from an increment in many parts of the world, including Central and Eastern Europe. Wet spells are defined by the number of consecutive rainy days with different thresholds. The identification of wet spells and their trends in the rainfall time is very important for many sectors, such as agriculture, ecology, hydrology and water resources. Wet spells can lead to extreme events and cause floods and other disasters. In this study, we will attempt to characterise global precipitation in the context of wet spells and associated precipitation depth of wet spells in the Danube River Basin area using daily precipitation data, as well as analysing different approaches to identifying wet spells. The ten most intense wet spells were detected, and the most intense, which occurred on 23 September 1996, was studied in depth in terms of precipitation and associated anomalies, the synoptic situation and the anomalous transport of moisture using a Lagrangian approach. The existence of a marked west-east dipole in the field of sea level pressure between the Atlantic Ocean and the eastern Mediterranean leads to the anomalous moisture transport from the Northern Atlantic Ocean to the Mediterranean Sea, where a higher available amount of moisture existed, and subsequently penetrated within the low positioned over the Danube River Basin. In addition, an Atmospheric River was also responsible for the wet conditions in the Danube River Basin. The combination of all these factors was responsible for the extreme precipitation linked with the wet spell.

Keywords: wet spell; precipitation; moisture sources; atmospheric rivers; anomalies; danube river basin

1. Introduction

Extreme precipitation events in Central Europe, including the area inside of the Danube River Basin (DRB), have become very common in the last few decades and have usually been associated with related phenomena, such as flooding, landslides, storms, significant material damage and human sacrifices. One of the primary causes of extreme weather events may be a consequence of global climate changes [1]. It is known that climate change is one of the major causes of increasing temperatures, precipitation amounts and variability of precipitation events. The Danube River Basin has a very diverse climate and notably variable precipitation characteristics because of the proximity of the Atlantic Ocean, Mediterranean Sea and Alps mountain range [2]. Thus, the significant amount of precipitation in the basin area throughout the whole year may be due to the impact of these factors. When the annual precipitation scale is considered, it is clear that those months with the maximum amount of precipitation usually occur during the summer. This phenomenon is especially highlighted in the low-lying part of the Danube River Basin, where convective precipitation makes a significant contribution to the total amount of precipitation [3]. Conversely, the months with minimum precipitation occur in mid-winter (January and February), when the Asiatic region of high pressure disables the movement of air masses from the Atlantic to the east. The average value of annual precipitation for the Danube River Basin is estimated as 2300 mm in the high mountains and approximately 400 mm in the delta region. Precipitation values above 2000 mm appear in the Upper Danube Basin in the high Alpine regions and in the Central Danube Regions on the southern oriented mountain chains of the Julian Alps and Dinaric system (Figure 1), which are exposed to the influence of humid-warm air masses originating in the Mediterranean [2,4].

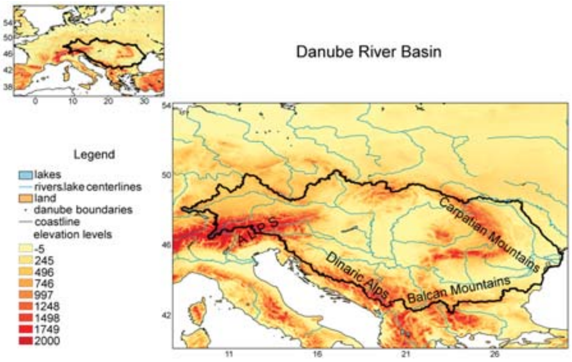

Figure 1. Black line indicates the boundaries of the Danube River Basin. Colours represent elevation levels in metres.

To understand the mechanism of increase in mean and extreme precipitation, it is important to analyse wet spell events on different time scales and their associated precipitation magnitude [5]. Europe is similar to global trends, in that increases in average and extreme rainfall and their variability are expected for areas in the middle northern portion, signifying an increasing risk of flooding; alternatively, in southern regions, less precipitation and frequent dry spell periods may lead to increasing drought trends [1].

The primary and most common reason for river flooding in Central Europe, including the area of the Danube River Basin, is heavy precipitation events, with the exception being snow melting during the winter period. It is important to stress that those heavy rain events of different duration (in the range of one to several days) usually result in a large amount of precipitation per square metre. The most significant conditions are certainly intensity, magnitude and spatial-temporal distribution of precipitation, but also, significant roles have specific conditions within the river basin at the moment of heavy precipitation [6]. In recent years, the largest floods in the area of the Danube River Basin occurred in 2002, 2006, 2013 and 2014. As a consequence, all of the associated areas experienced economic losses in the range of billions of euros and, what is much worse, suffered human causalities [7]. Many authors have studied these flood events, their causes and impacts [8,9]. Generally, two main reasons are cited as leading to the extreme flood events. The floods which occurred in 2002 and 2006 were induced by a huge amount of precipitation falling over a short time period, which produced a massive single flood event in the territory of the Danube River Basin. In contrast, the 2010 flood occurred as a consequence of a high number of rainfall events during the whole year, which caused a large number of flood events throughout the area of the Danube, economic losses around two billion euros, and 35 causalities [7].

As previously indicated, when extreme precipitation events are analysed, two terms (or factors) should be taken into consideration: (i) if the event occurs during a short period (hours or less than one day in extreme situations) which happens as a result of a strong convergence of atmospheric water vapour with local dynamic processes, or (ii) if it occurs during a prolonged time period, when the extreme precipitation is related to huge amounts of precipitation occurring over several weeks, months or seasons; in this last case, the duration of rainfall is the primary reason for the accumulation of large amounts of precipitation, which impacts nature and society through flood events [10].

There is no precise and generally accepted method for the calculation and identification of extreme precipitation events. Some authors [11,12] have used the highest recorded precipitation amount at some rain gauge stations as the selection criteria, whereas others have utilised the socioeconomic impacts of extreme precipitation events as their criterion [13]. Typically, all methodologies for ranking and identifying extreme precipitation events at least require daily precipitation values [1]. However, ranking and analysing extreme precipitation events (wet spell events) does not depend solely on available daily precipitation data, but additionally requires dataset resolution to characterise the precipitation [14] and the chosen criteria for the methodology. There have been many studies in recent years that have given attention to extreme precipitation events in the context of wet spells and associated accumulation precipitation in wet spells events. In these studies, the authors have used different methodologies for the analysis of wet spells. One method uses IDF curves (Intensity-Duration-Frequency) for characterisation and the study of wet spells behaviour [15]. In this study, they used the term "duration" to refer to a number of consecutive rainy days in the context of one day or more, not in reference to the actual duration of rainfall events. Another approach has used precipitation anomalies to identify extreme wet or dry spells and defines wet spell events as events with a minimum of three consecutive days with precipitation anomalies more than one standard deviation (std) from daily precipitation [16].

Understanding the atmospheric moisture transport is fundamental for explaining the nature of the precipitation during extreme events [17]. The Lagrangian approach has been broadly and satisfactorily used during the last several years to compute changes in moisture along trajectories and to identify sources of moisture or sinks, all around the globe [18]. Although other approaches (such as box models and isotopes) could be used with a similar purpose, the Lagrangian model supports an important benefit: it is able to compute the track of the moisture in time and permits the identification of the main moisture sources. More information about the comparison between certain methodologies can be found in Gimeno et al. [19].

In this study, for the identification and selection of wet spell events, we used the methodology developed by Ramos et al. [20,21] for the ranking of high-resolution daily precipitation extremes. The long time period analysed was from 1981 to 2015. The main objectives of this work are (i) to rank wet spell events in regards to different time scales in duration from 1 to 10 days for the whole area of the Danube River Basin using a daily precipitation dataset in high resolution and (ii) to analyse moisture source anomalies for the most intense wet spell event using a Lagrangian approach.

2. Data and Methods

2.1. Precipitation Dataset

In this work, we used the daily precipitation dataset from the Climate Hazards Group Infra-Red Precipitation with Station data (CHIRPS) project [22]. CHIRPS is a relatively new precipitation database, which has been accessible since the beginning of 2015. This database was developed by the USAID Famine Early Warning System Network with the support of scientists at the University of California Santa Barbara (Santa Barbara, CA, USA). To calculate the wet spell events with major precision, the resolution of the daily precipitation database used is critical, which is the main reason to choose the CHIRPS dataset instead of other available daily databases. It is considered the new environmental record for analysing and monitoring extreme events [22]. The CHIRPS database is in a $0.05° \times 0.05°$ degree spatial resolution in latitude and longitude from 6-hourly to 3-monthly aggregates, which makes it a unique daily database.

This database presents a combination of three types of precipitation information: global climatologies, satellite-based measurements and in situ rain gauge data. The database used for calculation wet spells events covers a temporal period from January 1981 until December 2015.

The CHIRPS dataset has been successfully used in recent publications to validate other common datasets in areas that present extreme climate or complex topography. For instance, CHIRPS has been used to quantify the impact of decreasing precipitation trends and increasing temperatures trends in the Greater Horn in Africa [22], and it validated using the data from 21 ground stations in Northeast Brazil [23]. CHIRPS dataset has also been used it to obtain a comprehensive evaluation of eight high spatial resolution precipitation products in an Alpine catchment, the Adige Basin in Italy [24], and to validate a hydrological model to simulate stream flow in a complex topography [25]. Additionally, the same database was successfully used for the analysis of precipitation extremes over Cyprus [26] and Bhutan [27].

2.2. Ranking of Wet Spell Extreme Precipitation Events

This ranking of wet spell events in the area of the Danube River Basin is based on the method developed by Ramos et al. [20,21], which used daily-normalised precipitation anomalies for the ranking of multi-day extreme precipitation events according to the accumulated amount of precipitation and the spatial distribution in the Iberian Peninsula.

The ranking is based on the magnitude of an event (R), which is obtained after considering the area affected as well as its intensity in every grid point, and taking into account the daily-normalised departure from climatology. This method [20] for the Iberian Peninsula was partially adapted from another approach [28], that has suggested some criteria to classify each day in terms of extremeness using different meteorological variables. The use of normalised precipitation departures from the seasonal climatology allows us to measure the rarity of an event given by the standardised precipitation anomalies. With this standardisation, we are assured of the different statistical distribution of daily areal precipitation among different areas that are being studied. Therefore, it [20,21] can be applied easily to other regions of the world using different gridded precipitation datasets (model data or observations), and the use of different time scales [21] is directly applicable to assess persistent precipitation episodes over a certain region.

To obtain a final R index to calculate the wet spell events in different durations, several steps should be applied prior to the final ranking (as in [20,21]). In the first step, we calculated daily normalised precipitation anomalies (N) for each grid point as the difference between the precipitation values for the day under analysis and the daily mean climatological value and later divided by the daily standard deviation climatological value. With this we ensure the different statistical distribution of daily areal precipitation among different areas of the Danube basin are taken into account and can easily be compared. The use of standardised precipitation anomalies to evaluate heavy large-scale rainfall events was already used with success by other authors in central Europe [6]. Therefore, we are confident that this methodology [21] reflects wet spell events in the Danube River Basin particularly well.

Furthermore, for this computation, only grid points with precipitation amounts above 1 mm were considered. The reference period that we took into account is the complete period of the CHIRPS precipitation data from 1981 until 2015. The noise in both time series has been smoothed by applying a 7-day running mean to the climatological series. Thus, climatological normalised precipitation anomalies are computed, taking into account each day and each grid point. The final daily index, according to which wet spell events were ranked, was:

$$R = A \times M \tag{1}$$

where A denotes the area in percentage which has precipitation anomalies above two standard deviations, and M is the mean value of these precipitation anomalies over A.

In a second step, we have also computed the accumulated precipitation anomalies for a certain period (NCC): that is, N added during different time periods. NCC represents in our case the wet spell events on different time scales. Finally, in the last step, we performed the ranking of wet spell events according to the final index R, which computed the magnitude of precipitation for each wet spell event in different durations. The main idea is to sum the daily normalised anomalies (see previous paragraph) over different time scales (2 to 10 days) to allow ranking the different anomalous precipitation on multi-day periods. For each time scale's (2 to 10) accumulated precipitation standardised anomalies, the magnitude of the wet spell event is *R* obtained after multiplying: (1) the area (*A*), expressed as the percentage that has accumulated precipitation anomalies (computed over different time scales) higher than two standard deviations and (2) the mean value of these accumulated precipitation anomalies (*M*), considering only grid points with precipitation anomalies of more than two standard deviations.

Wet spell events on the time scales from 1 day until a maximum of 10 days have been calculated, but for the sake of simplicity only 1, 3, 5, 7, and 10 days of length are presented in this study (time periods between 7 and 10 days are the typically synoptic time scale). These different multi-day extreme rankings will show that specific extreme events at shorter time scales (e.g., 2–3 days) may be absent from the top ranks at longer time scales lists (e.g., 10 days) and others that appear at long time scales are not present at shorter time scales.

Furthermore, we should make clear that the ranking of wet spell events illustrated in this paper is not related to economic impacts and/or human impacts, such as causalities, injuries or homelessness. The rankings of wet spell events are constituted by the daily high precipitation amount and the associated spatial extension.

2.3. Moisture Sources Anomalies

The second part of this work is to compute precipitation anomalies of moisture sources for the identified wet spell events in different time scales. The moisture source anomalies are computed using the Lagrangian FLEXPART V9.0 model. To track the changes in atmospheric moisture along trajectories the approach uses ERA-Interim reanalysis data from ECMWF (European Centre for Medium-Range Weather Forecast), which are accessible at approximately 80 km (T255 spectral) on 60 vertical levels from the surface up to 0.1 hPa, available at each 6-hour time interval [29]. The model developed by Stohl and James [30,31] consists of dividing the global atmosphere into approximately 2 million particles (air masses), which are transported by the three dimensional wind field along their trajectories. Transport time of the trajectories were limited to 10 days, as this is the mean water vapour lifetime in the atmosphere [32]. Changes in specific humidity (q) and locations of air particles were recorded every 6 h. The increases (e) and decreases (p) in moisture along each trajectory may be expressed by changes in specific humidity (q) by the equation:

$$\mathrm{e} - \mathrm{p} = \mathrm{m}\ \mathrm{dq}/\mathrm{dt} \tag{2}$$

where *m* is the mass of the particle. By adding (e − p) values of all air particles residing at each time step over a specific area (in this case, over an area of 1.0 × 1.0 degrees in latitude and longitude), it is possible to obtain the instantaneous values of the (E − P) balance, where (E) denotes evaporation and (P) the precipitation rate per unit area.

According to Stohl and James [30,31], this approach has two main disadvantages: (1) it is not possible to make separate calculations of E and P, and (2) the results are highly dependent on the input data quality. In addition, the fluctuations in q along individual trajectories may also occur for numerical reasons (e.g., because of the interpolation of q). However, such numerical noise may be partly mitigated by the large numbers of particles contained in an atmospheric column. A more detailed description of the use of this Lagrangian approach and backward/forward analysis for tracking moisture can be found in many research studies which have used this method for tracking variation and/or identification of moisture sources in many different worldwide regions, such as the Mediterranean region [33], Central America [34], Iberian Peninsula [35], Iceland [36], Greenland [37], China [38], and Niger River basin [39].

To calculate the anomalies for the wet spells detected, the first step is to compute the 35-years climatology (1981–2015) for the moisture sources over the Danube River Basin for those specific days of interest (daily climatological value). Precipitation anomalies of moisture sources were calculated as the difference between the E − P > 0 value (backward analysis) for the day/days of the wet spell events and the daily climatological value.

3. Results

3.1. Detection of the Wet Spells

Table 1 presents the top ten extreme wet spells for the area of interest, the Danube River basin, for five accumulated periods of the lengths of 1, 3, 5, 7 and 10 days. The date that appears for each wet spell indicates the final day of each event. For instance, the wet spell event with a length of 3 days on 24 September 1996 (top 1) signifies that this event includes accumulated precipitation anomalies for that day (24 September 1996) and the two previous days: 23 and 22 September 1996, that is, 3 days in total. The same is true for longer periods.

Table 1. The top ten wet spell events in the Danube River Basin (DRB) according to the different length of the events (1, 3, 5, 7, and 10 days). Column denoted with **A** corresponds to area of the DRB in percentages that had precipitation anomalies above 2 std (standard deviation). Column **M** corresponds to mean magnitude of precipitation anomalies of A, and the last column denoted with **R** represents the final index of ranking of wet spell events. The final column (R) is the magnitude of the events. In bold are represented wet spell events in different durations that we took into consideration and all events include the most anomalous one for the 1-day ranking identified event with an initial day on 23 September 1996.

		A(%) = Area	M = Mean Magnitude	R = index of Ranking
(a)	**1 day duration–Wet Spell Events**			
1	**23 September 1996**	**44.87**	**4.43**	**198.65**
2	28 December 2014	50.92	3.32	168.81
3	6 November 1985	40.26	3.89	156.70
4	1 March 2008	40.48	3.84	155.58
5	18 February 1994	44.66	3.19	142.60
6	27 November 1983	40.79	3.44	140.42
7	6 May 1987	36.20	3.81	138.02
8	14 March 2013	43.32	3.18	137.91
9	2 March 2014	31.11	4.38	136.17
10	27 March 1993	38.96	3.38	131.77
(b)	**3 day duration–Wet Spell Events**			
1	**24 September 1996**	**53.11**	**4.71**	**249.95**
2	**23 September 1996**	**51.06**	**4.47**	**228.27**
3	**25 September 1996**	**47.25**	**4.75**	**224.59**
4	11 February 1984	44.50	4.63	206.04
5	6 November 1985	51.45	3.97	204.39
6	8 January 2010	47.44	4.18	198.54
7	6 May 1987	49.73	3.99	198.36
8	10 February 1984	43.52	4.50	195.88
9	29 October 1990	48.53	4.02	195.15
10	31 October 1994	51.43	3.76	193.43
(c)	**5 day duration–Wet Spell Events**			
1	**24 September 1996**	**53.66**	**4.75**	**254.85**
2	**25 September 1996**	**53.45**	**4.76**	**254.22**
3	**26 September 1996**	**53.67**	**4.69**	**251.71**
4	14 December 1990	55.32	4.29	237.58
5	13 January 1998	51.67	4.55	234.92
6	**27 September 1996**	**48.54**	**4.77**	**231.42**
7	**23 September 1996**	**51.73**	**4.46**	**230.92**
8	22 January 1998	53.15	4.29	227.95
9	30 October 1990	53.80	4.13	222.08
10	31 October 1990	53.84	4.12	221.67

Table 1. *Cont.*

		A(%) = Area	M = Mean Magnitude	R = index of Ranking
(d)	**7 day duration–Wet Spell Events**			
1	1 January 1996	70.41	4.24	298.19
2	15 December 1990	64.51	4.51	290.71
3	2 January 1996	69.34	4.00	277.60
4	14 December 1990	61.43	4.46	273.79
5	7 May 1987	61.21	4.26	260.72
6	**27 September 1996**	**54.59**	**4.78**	**260.69**
7	**24 September 1996**	**54.73**	**4.72**	**258.47**
8	16 December 1990	59.21	4.35	257.33
9	**28 September 1996**	**54.33**	**4.73**	**256.91**
10	**25 September 1996**	**54.11**	**4.75**	**256.87**
(e)	**10 days duration–Wet Spell Events**			
1	23 August 2005	68.21	4.78	325.98
2	18 December 1990	66.39	4.78	317.66
3	24 August 2005	66.78	4.73	315.91
4	4 January 1996	72.31	4.34	313.98
5	15 December 1990	65.40	4.79	313.50
6	17 December 1990	65.41	4.61	301.29
7	16 December 1990	65.68	4.58	300.85
8	14 December 1990	62.07	4.81	298.32
9	22 August 2005	64.18	4.65	298.17
10	12 May 1991	60.77	4.79	290.89

Focusing on the results (Table 1), it can be observed that the most significant wet spell event for the length of 1 day occurred on 23 September 1996 (in bold). This event is present in all ranking time scales, although in different positions. For the 3-day ranking, it appears in the second position. The top event is, in this case, 24 September 1996, but it is worth noting that it includes the two previous days (23 and 22 September 1996 in the calculation). Thus, it is ultimately the same event. For the 5-day ranking, the same event occurs for the 1, 2, 3, 6 and 7 positions; and for the 7-day ranking, it appears in the 6, 7, 9 and 10 position. Accordingly, we focused our attention on this extreme event, 23 September 1996, to analyse the anomalies in the accumulated precipitation field at different time scales, as well as the moisture source anomalies.

As previously mentioned, the R index corresponds to R = A $\times$ M, where A is the percentage of the area with precipitation anomalies higher than 2 std, and M is the mean magnitude for the area A. For instance, the top ranked wet spell event of one day duration (23 September 1996) had a R index of R = 198.65, which corresponds to the 44.87% of area (A) of the Danube River Basin with precipitation anomalies above 2 std and 4.43 mean magnitude (M) of the area marked with A. All magnitude values for the top 10 positions of wet spell events in duration from 1 to 7 days are shown in Table 1.

Moreover, we also need to emphasise that a specific wet spell events at a shorter time scale could not appear in the top ranking of wet spell events with longer lengths due to accumulated amount of precipitation over multi-day extreme precipitation events. That finding means that any of individual precipitation days which are included in the multi-day wet spell events are not equally represented on the highest position of the ranking at the individual daily scale.

From the results in Table 1, we can compare the domain of the affected area that shows anomalous precipitation for the wet spell events at shorter and longer time scales. The top ten events for 1-day length ranking have affected less than 50% of the Danube River Basin area. On this 1-day time scale, the top wet spell event in the ranking does not affect the largest percentage of affected area A = 44.87%; instead, the second ranked event affects the largest percentage of area (A = 50.92%) in comparison with the top ten events in the 1-day time scale. On the other side, for wet spell events calculated for longer time scales, for instance, for the 7-day length, the first ranking event exhibited the biggest affected area (A = 70.41%). Additionally, from Table 1, it is possible to say that the area affected by the wet spells is higher with longer lengths of calculation. Wet spell events of shorter or longer lengths of time affect smaller or bigger percentages of the DRB area respectively. Also, from Table 1, we can notice that the most anomalous event for the 1-day ranking (23 September 1996) does not appear in the top 10 ranking wet spell events on time scale for the duration of 10 days. In this last time scale the event of 23 September 1996 has position 18 and 19. So, we can conclude that the most anomalous wet spell for the 1-day ranking was also anomalous at a 7-days period of ranking, but at the 10-days period of ranking other events appear more extreme.

3.2. Wet Spell Event 23 September 1996

3.2.1. Precipitation

As previously discussed, this paper focuses from this point forward on the 23 September 1996 wet spell event. Figure 2 shows the accumulated precipitation during this wet spell event for 1-day's duration, as well as 3-day, 5-day and 7-day (Figure 2a–d, respectively). The accumulated precipitation maximum was recorded on the western part of the Danube River Basin area with an amount of precipitation over 100 mm/day, reaching 150 mm/day in the all-time scales and reaches the southern part of the DRB for the wet spell event with duration of 7 days. Intense precipitation with values over 100 mm/day also occurred over the eastern part of the domain.

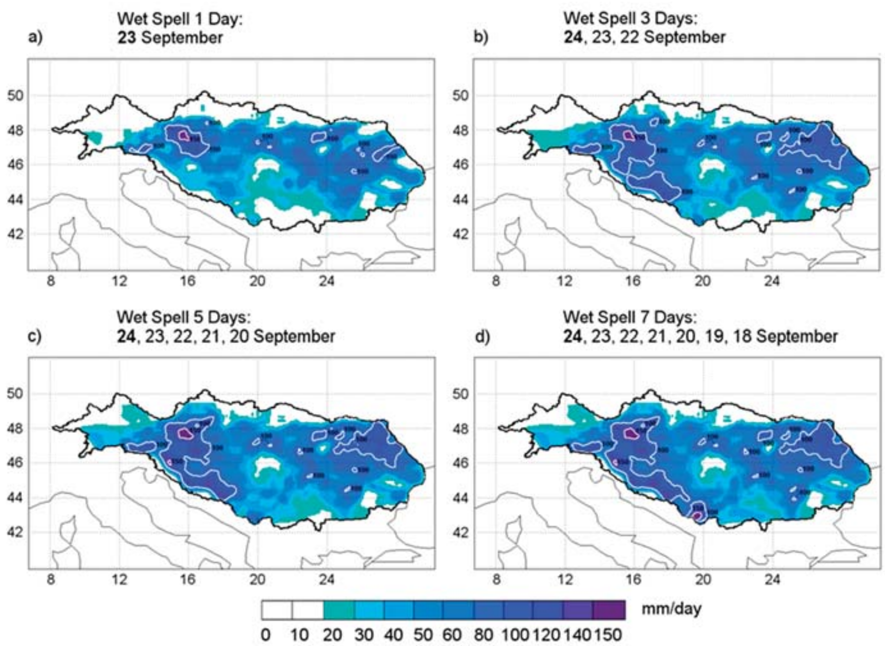

Figure 2. Accumulated precipitation (shaded, mm/day) for the 23 September 1996 wet spell event in duration of one, three, five and seven days, on the area of the DRB (Danube River Basin). White contour line corresponds to the accumulated precipitation amount of 100 and 150 mm/day. Daily data from CHIRPS in a 0.05° degree spatial resolution in latitude and longitude.

Figure 3 shows the mean daily precipitation anomalies for the Danube River Basin area for the whole period of the CHIRPS precipitation dataset for the 23 September 1996 wet spell event at durations of one, three, five and seven days. The largest positive precipitation anomalies are stressed for the wet spell events with shorter durations, one and three days (Figure 3a,b respectively), where the magnitude of the anomalies are in a range of 30 until more than 60 mm/day over the main area of the Danube River Basin. Wet spell events on the longer time scales (Figure 3c,d) also showed positive values of mean daily precipitation anomalies but with considerably less value, lower than 20 mm/day.

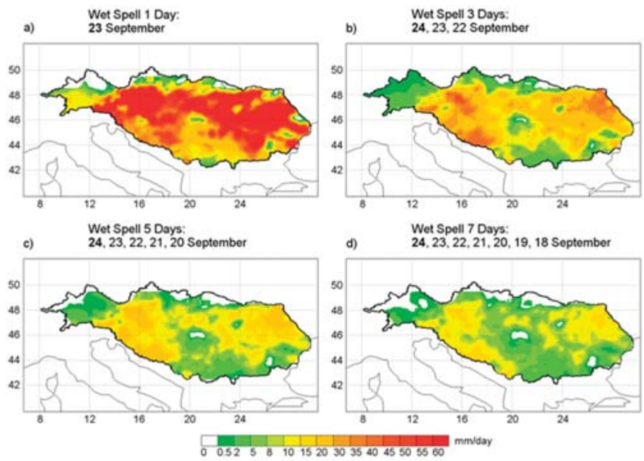

Figure 3. Mean daily values of precipitation anomalies (shaded, mm/day) for wet spell event of 23 September 1996 in duration of one, three, five and seven days, on the area of the DRB (Danube River Basin). Daily data from CHIRPS in a 0.05° degree spatial resolution in latitude and longitude.

3.2.2. Meteorological Configuration

The synoptic situation for the day 23 September 1996 is shown in Figure 4. The field of daily composite mean sea level pressure (SLP) and total 850 hPa geopotential height, and their anomalies related to the wet spell event analysed are plotted. Those panels to the left (Figure 4a,c) show the climatology for 23 September 1981–2015, and the right panels (Figure 4b,d) show the anomalies. The climatological SLP and geopotential at 850 hPa (Figure 4a,c) denote that over the Atlantic region an anticyclone dominates the general pattern, extending the situation over Europe and the Mediterranean region. However, the anomalies (Figure 4b,d) show an intense low-pressure system over the Italian Peninsula, the Adriatic Sea, Croatia and Slovenia. The central low peaks at 988.3 hPa in SLP (1245.18 hPa in 850 hPa geopotential high level). This confirms that the most anomalous wet spell event for the 1-day ranking was characterised by a cyclone over Southern Europe, crossing the area of the Danube River and leading to heavy precipitation in this region. However, one strong anticyclone is positioned over the Northern Atlantic Ocean.

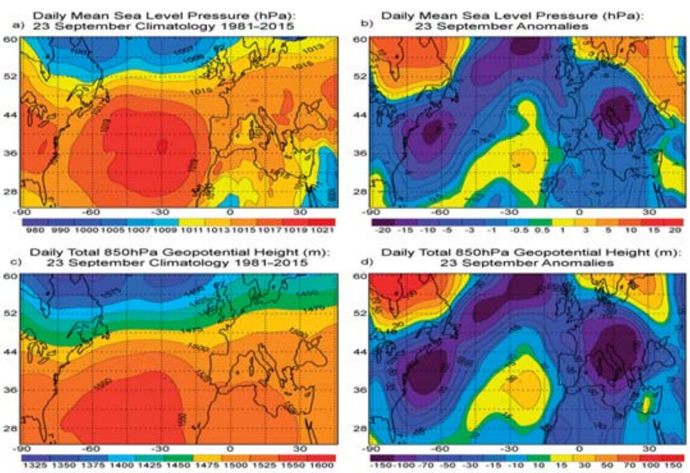

Figure 4. Top: Daily mean seal level pressure (SLP) for the day 23 September 1996 (measured in hPa). Bottom: Daily total geopotential height at 850 hPa, measured for the day 23 September 1996 (in geopotential metres, gpm). Left hand column (**a**,**c**) shows the climatology for 23 September 1981–2015 and right column (**b**,**d**) the anomalies. Data obtained from ERA-Interim at 1° degree in latitude and longitude.

To show the moisture flux and vertical motion, Figure 5 shows plots for the VIMF (Vertically Integrated Moisture Flux) and its divergence for the climatology (Figure 5a) for all those 23 September dates in the period (1981–2015) and the anomaly (Figure 5b) for our studied case (23 September 1996). Between both figures, a larger difference in the distribution of the divergence-converge pattern and its values is notable. The anomalies show (Figure 5a) that over the Danube River Basin area, there is a significant region of convergence (bluish colours) that is concordant with the highest amounts of precipitation (Figures 2 and 3) experienced over the area. Conversely, Figure 5 shows two main areas of anomalous divergence (in red), one over the Mediterranean Sea and another over the Northern Atlantic Ocean, near the NW coast of the Iberian Peninsula. The convergent area over the Danube River Basin and the divergence over the Mediterranean are positioned around the low level pressure shown in Figure 4 (marked in Figure 5 with a black cross). The anomalous anticlockwise circulation is clear in the VIMF plot, showing an NW-SE direction over the area of convergence over the Mediterranean, and an S-N flow over the divergent zone in the Danube area. Over the convergence area in the Atlantic, a NW dominant flux is evident.

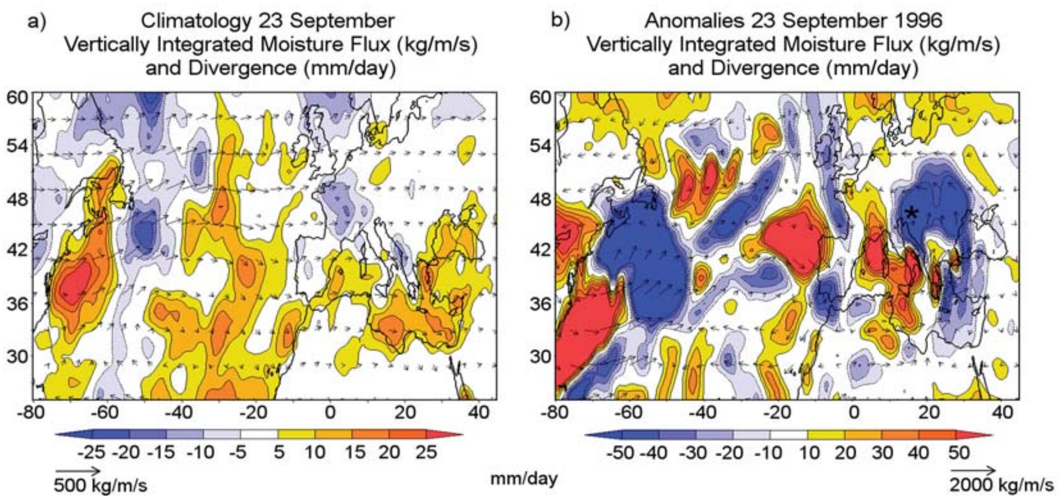

Figure 5. Left hand (**a**): Climatological daily mean Vertically Integrated Moisture Flux (VIMF) values for 23 September during the period 1981–2015. Right hand (**b**): Daily mean anomalies of VIMF values for the day 23 September 1996. Vectors measured in kg m^{-1} s^{-1} and respective divergence shaded and measured in mm day^{-1}. The black asterisk marks the central position of the low. Data from ERA-Interim at 1° degree in latitude and longitude.

3.2.3. Anomalous Moisture Uptake during the 23 September 1996 Wet Spell Event

Once the top-ranked wet spell event was identified for the DRB and the meteorological situation, the next step was to investigate changes in the moisture transport during the lifetime of the extreme event using a Lagrangian approach. Figure 6 shows the mean climatological sources of moisture for the 1-day, 3-day, 5-day and 7-day lengths of the wet spell. The climatology is calculated using a 35-year period (1981–2015) obtained through backward trajectories from the Danube River Basin. The backward analysis allows us to track where the particles gain humidity during their trajectories towards the area of the Danube River Basin. The colours with positive values represent areas where evaporation is greater than precipitation (E − P) > 0; thus, these areas are moisture sources for the DRB. On the other hand, areas where precipitation is greater than evaporation are moisture sinks (E − P < 0). In Figure 6, these areas are marked with bluish colours that represent negative values. For the 1-day length, for instance, to compute the moisture climatological field, all of the values for 23 September along the 35 years are taken into account, and for the 3-day length, the three days involved (22–24 September) for the 35 years are taken into account. The moisture source patterns (Figure 6) for the wet spell event at the different time scales exhibit similar behaviour. For all plots of the regions that show the major positive values of (E − P), the moisture sources are the northern-central and western Mediterranean Sea, the Danube River Basin itself, and the northern and western Black Sea. This result is in concordance with a recently published paper [2] in which the sources of moisture for the DRB were analysed in depth.

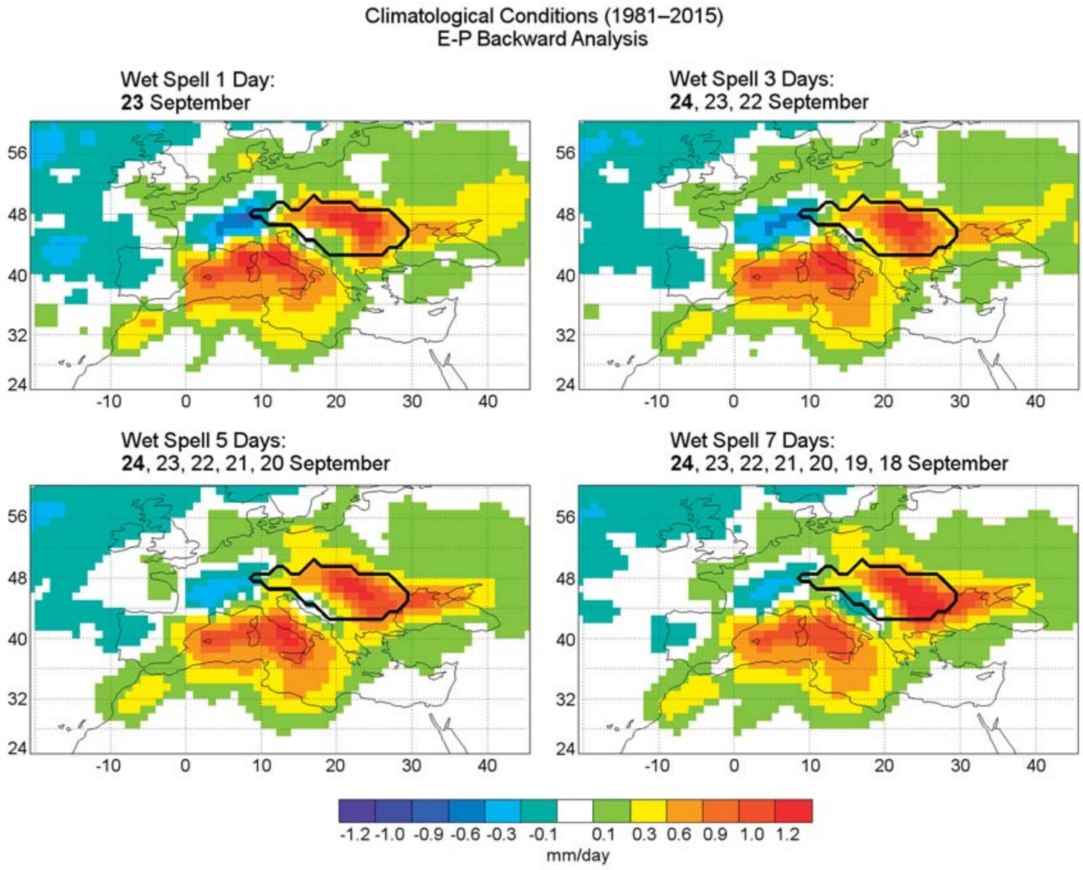

Figure 6. E − P climatological conditions from the backward analysis for 1981–2015 time period for the wet spell events on its different time scales (1, 3, 5 and 7 days). The black line contour corresponds to the Danube River Basin. Scale in mm/day.

In general, for studies about extreme events, it is critical to analyse the differences between the event studied and the climatological conditions. Therefore, the anomalies in the moisture sources field for the 23 September 1996 event on the different time scales were investigated. Figure 7 shows that during this particular wet spell event, some areas reinforced their role as sources of moisture. This phenomenon is observed for the western Black Sea and the southern and most western areas of the Mediterranean Sea. The positive anomalies values reached values higher than 2.5 mm/day over these regions. In addition, it is important to note that a region that climatologically acted as a source can now be a sink, as is the case for the Danube River Basin and the climatological source over the northern Mediterranean Sea (Liguria Sea); and that the areas around central Italy exhibit negative anomalies. Other areas appear as effective sources of moisture, as is the case for the band over the Northern Atlantic Ocean that was not a primary climatological moisture source in the period considered (see Figure 6), but for the event analysed the anomaly pattern showed a positive signal. It is highlighted that for the shorter time scales (1 day) the anomalies are more intense than those for longer lengths (7 days).

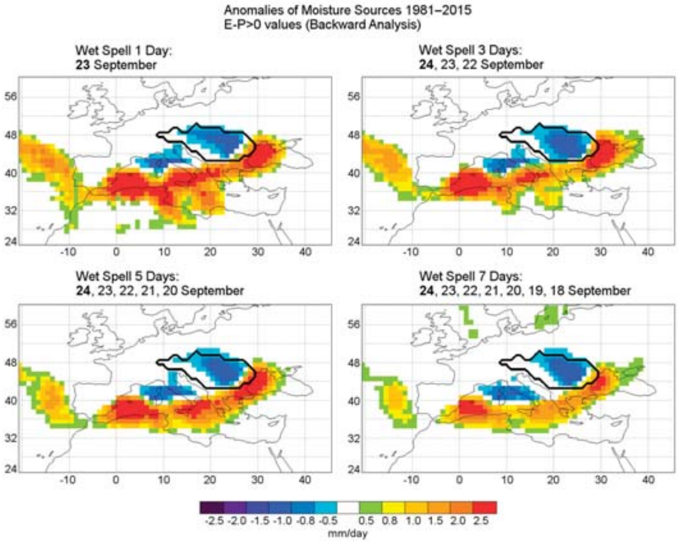

Figure 7. Anomalies of moisture sources obtained from the backward analysis (E − P > 0 values) for the different time scale for the 23 September 1996 wet spell. The black line contour corresponds to the Danube River Basin. Scale in mm/day.

The negative values in the field E − P > 0 anomalies over the Danube River Basin (Figure 7 top right hand) are in concordance with the convergence in Figure 5 (right panel) and the highest amounts of precipitation.

4. Discussion

The configuration with an anticyclone on the left and the intense low level pressure system on the right acts as a belt of transport for the moisture over the Atlantic flowing to the Mediterranean Sea and it is available to penetrate within the storm and activates the processes for intense precipitation over the Danube River Basin (schematic process in Figure 8).

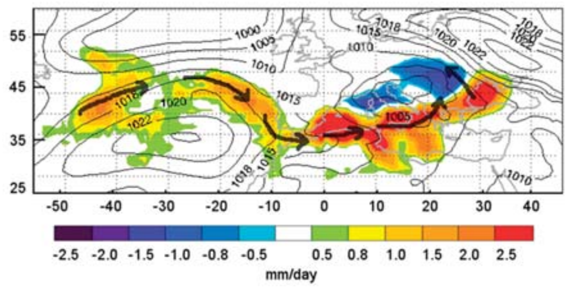

Figure 8. Anomalies of moisture sources (E − P > 0) obtained from the backward analysis during 10 days for the 23 September 1996 wet spell. SLP in black contours for 23 September 1996. Grey arrows indicate schematically the flow of the moisture from the Northern Atlantic Ocean to the DRB crossing the Mediterranean basin.

Despite the Mediterranean being the main moisture source for the event (about 55% of the total), the anomalous moisture from the North Atlantic Ocean deserves a little more attention. During the days prior to the low over the Danube River Basin a hurricane occurred in the North Atlantic Ocean, the Hortense hurricane (3–16 September 1996). It has been shown that the hurricane events over the Atlantic may directly impact not only western Europe (e.g., [40]), but also the Mediterranean region (e.g., [41]). Other studies [42] and references therein] state the important role of intense transports of moist air from the tropical and subtropical Atlantic in the occurrence of cold season extreme precipitation events in the Mediterranean region. These extreme precipitation events may originate from atmospheric processes associated with the formation of hurricanes or intense cyclones over the Atlantic Ocean. The development of these events is characterised by intense convergence of moist air from the tropics [43] that is followed by a fast intrusion of moist air into the Mediterranean region without significant mixing with the surrounding air. A significant number of these events in the Mediterranean region appear to take place during (or immediately after) Atlantic hurricanes or storms [42].

Hortense was a wet hurricane, as the National Hurricane Center reports (http://www.nhc.noaa.gov/data/tcr/AL081996_Hortense.pdf). It started as low-pressure near Africa on 30 August, it moved westward and it became in a tropical storm on 7 September near the Guadeloupe Islands. Hortense became a hurricane on 9 September over Puerto Rico, then it moved northward intensifying, and it became an extratropical low on 15 September. Figure 9 shows the synoptic configuration for SLP, wind and specific humidity at 900hPa using data from ERA-Interim during 14–16 September 1996, the last days during the hurricane situation and the first two days during the transition to an extratropical cyclone. It is clear that the core of the hurricane transported a higher amount of humidity to extratropical latitudes and it was available for its transport during the following 10 days, the period used for computing the E − P anomaly.

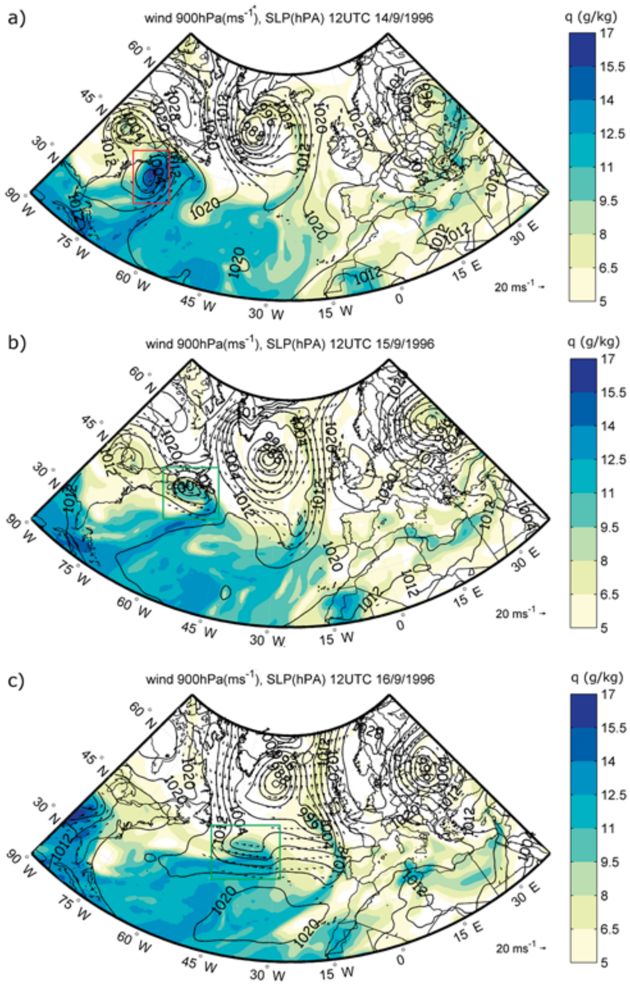

Figure 9. The wind field (vectors, m/s) and specific humidity (shaded, g/kg) at 900 hPa are shown along with the Sea Level Pressure (SLP, contours, hPa) on the (**a**) 14 September 1996 at 12 UTC; (**b**) 15 September 1996 at 12 UTC and (**c**) 16 September 1996 at 12 UTC. In addition, Hurricane Hortense is highlighted with a red square, while it's extra-tropical transition is highlighted with a green square. Only winds speeds above 10 m/s are shown.

The tropical cyclones also impact downstream wave breaking, and this remote impact was demonstrated in some episodes of intense rainfall over the Mediterranean in autumn [41]. This suggests that the interaction of tropical cyclones with a midlatitude flow over the western North Atlantic may be considered a perturbation to, rather than a source of, downstream wave breaking [41].

The extratropical cyclone derived from Hortense disappeared during 19 September 1996 over the northern Iberian Peninsula (see Supplementary Material Video S1 green box), but the low over the Danube River Basin was due to a second cyclone within the wave train (Supplementary Material Video S1 blue box) that started on 18 September 1996 over the middle North Atlantic, reached the Mediterranean Sea during the next day, and it was reinforced when it was situated on the Danube region.

The extra tropical cyclone that occurs immediately after the Hortense (highlighted with the blue box on Supplementary Material Video S1) struck the Northwest Iberian Peninsula on 20 September 1996. Figure 10a shows that associated with it there was a long corridor of vertically integrated horizontal water vapour transport (IVT) with the characteristics of an Atmospheric River (AR) around 38.5ºN. ARs are relatively long, narrow regions in the atmosphere that transport most of the water vapour outside of the tropics, they contain high amounts of water vapour and they could be associated with extreme events in terms of rainfall and floods where they impact [17,43,44]. In fact, the ERA-Interim ARs database developed by Ramos et al. [45] for the Iberian Peninsula identifies this particular AR. Then, this fast corridor of moisture (but with lower intensity) penetrated the Mediterranean basin during the following day (Figure 10b), and on the 23 September 1996 (Figure 10d) the anomalous transport of moisture reached the Danube River Basin, associated with the low situated over our area of study. A close look at the global ARs database of Guan and Waliser [46] indicates that this particular pattern of IVT along the Mediterranean and North Africa towards the Danube is also an AR event.

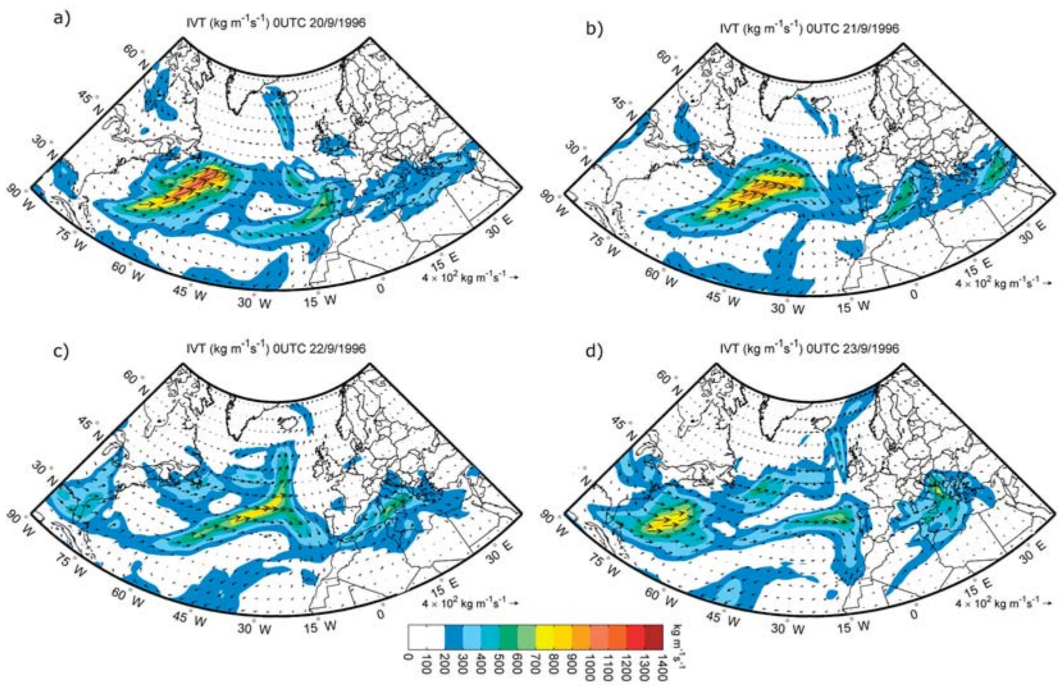

Figure 10. Vertically integrated horizontal water vapour transport (IVT) (vectors) and intensity (kg m^{-1} s^{-1}; color shading) at (**a**) 20 September 1996 00UTC, (**b**) 21 September 1996 00UTC, (**c**) 22 September 1996 00UTC, and (**d**) 23 September 1996 00UTC.

5. Conclusions

In this work, we calculated the top 10 ranking wet spell events over the Danube River Basin region using the CHIRPS daily precipitation dataset at 0.05 degrees spatial resolution and for the temporal period from 1981 until 2015, considering different time scales from 1 to 7 days using a method developed by Ramos et al. [20,21]. The most intense event detected occurred on 23 September 1996. This top ranked wet spell events is present in the first position of the ranking for the length of 1 day but also between the top 10 events on 3-, 5- and 7-day time scales. During this event, the existence of a low level surface pressure (988.3 hPa in SLP) caused a situation of extreme precipitation over the DRB, reaching values up to 100 mm/day with peaks of 150 mm/day. The magnitude of the anomalies fluctuated from 30 to 60 mm/day over the main area of the Danube River Basin.

The analysis of the moisture source anomalies using a Lagrangian model of particles (FLEXPART) showed that the system was fed with anomalous moisture from the western and south-central Mediterranean Sea, the western Black Sea, and the northern Atlantic Ocean. This pattern is a consequence of several synoptic conditions: the occurrence of hurricane Hortense during the days prior to the event, which lets available moisture over the North Atlantic, an anticyclone positioned over the Atlantic during at least 10 days, and a low-level pressure system that occurred immediately after this hurricane with an associated Atmospheric River that directly struck the Iberian Peninsula on 20 September and then reached the DRB through the Mediterranean Sea on 23 September 1996. The dipole in the SLP and geopotential in low tropospheric level fields due the low-level pressure and the anticyclone made this transport possible, and the occurrence of an AR was responsible for the anomalous moisture availability in the area. This anomalous moisture transport affected the Danube Basin on 23 September 1996 and produced the extreme and anomalous precipitation event.

Supplementary Materials: The following are available online at www.mdpi.com/2073-4441/9/8/615/s1.

Acknowledgments: D. Ciric is supported by European Commission under the Erasmus Mundus project Green-Tech-WB: Smart and Green Technologies for Innovative and Sustainable Societies in the Western Balkans (551984-EM-1-2014-1-ES-ERA Mundus-EMA2). A.M. Ramos was supported through a postdoctoral grant (SFRH/BPD/84328/2012) from the Fundação para a Ciência e a Tecnologia (FCT, Portuguese Science Foundation). We also thank the IMDROFLOOD project financed by the Water Works 2014 co-funded call of the European Commission. We thank Bin Guan for providing the AR database and both anonymous referees for their effort and comments that have improved this paper.

Author Contributions: D. Ciric, R. Nieto, and L. Gimeno conceived and designed the experiments; D. Ciric and A.M. Ramos performed the experiments and D. Ciric, R. Nieto, A.M. Ramos, and L. Gimeno analysed the data; D. Ciric, R. Nieto, A. Drumond and A.M. Ramos wrote the paper.

Conflicts of Interest: The authors declare no conflict of interest. The founding sponsors had no role in the design of the study; in the collection, analyses, or interpretation of data; in the writing of the manuscript; and in the decision to publish the results.

References

1. Lehner, B.; Döll, P.; Alcamo, J.; Henrichs, T.; Kaspar, F. Estimating the Impact of Global Change on Flood and Drought Risks in Europe: A Continental, Integrated Analysis. *Chlimatic. Chang.* **2006**, *75*, 273–299. [CrossRef]
2. Ciric, D.; Stojanovic, M.; Drumond, A.; Nieto, R.; Gimeno, L. Tracking the Origin of Moisture over the Danube River Basin Using a Lagrangian Approach. *Atmosphere* **2016**, *7*, 162. [CrossRef]
3. Stancik, A.; Jovanovic, S. *Hidrology of the River Danube*; Priroda: Bratislava, Slovakia, 1988; p. 272.
4. Brilly, M. *Hydrological Processes of the Danube River Basin: Perspective from the Danubian Countries*; Springer Science & Business Media: Ljubljana, Slovenia, 2010; Volume 1, p. 436. [CrossRef]
5. Zolina, O. Multidecadal trends in the duration of wet spells and associated intensity of precipitation as revealed by a very dense observational German network. *Environ. Res. Lett.* **2014**, *9*, 025003. [CrossRef]
6. Kaspar, M.; Müller, M. Selection of historic heavy large-scale rainfall events in the Czech Republic. *Nat. Hazards Earth Syst. Sci.* **2008**, *8*, 1359–2008. [CrossRef]

7. Babić, M.; Babić-Mladenović, M.; Danko, B.; Pavel, B.; Razvan, B.; Lenka, C. *Flood Risk Management Plan for the Danube River Basin District*; International Commission for the Protection of the Danube River: Vienna, Austria, 2015.
8. Blöschl, G.; Nester, T.; Komma, J.; Parajka, J.; Perdigão, R.A.P. The June 2013 flood in the Upper Danube Basin, and comparisons with the 2002, 1954 and 1899 floods. *Hydrol. Earth Syst. Sci.* **2013**, *17*, 5197–5212. [CrossRef]
9. Stadtherr, L.; Coumou, D.; Petoukhov, V.; Petri, S.; Rahmstorf, S. Record Balkan floods of 2014 linked to planetary wave resonance. *Sci. Adv.* **2016**, *2*, e1501428. [CrossRef] [PubMed]
10. EASAC. *Trends in Extreme Weather Events in Europe: Implications for National and European Union Adaptation Strategies*; EASAC Policy Report 22; European Academies Science Advisory Council: Halle, Germany, 2013; Available online: www.easac.eu (accessed on 24 April 2017).
11. Martín, M.L.; Santos-Muñoz, D.; Morata, A.; Luna, M.Y.; Valero, F. An objectively selected case study of a heavy rain event in the Mediterranean Basin: A diagnosis using numerical simulation. *Atmos. Res.* **2006**, *81*, 187–205. [CrossRef]
12. Jansa, A.; Genoves, A. Western Mediterranean cyclones and heavy rain. Part 1: Numerical experiment concerning the Piedmont flood case. *Meteorol. Appl.* **2000**, *7*, 323–333. [CrossRef]
13. Liberato, M.L.R.; Pinto, J.G.; Trigo, I.F.; Trigo, R.M. Klaus, an exceptional winter storm over Northern Iberia and Southern France—A comparison between storm diagnostics. *Weather* **2011**, *66*, 330–334. [CrossRef]
14. Duan, Z.; Bastiaanssen, W.G.M. First results from Version 7 TRMM 3B43 precipitation product in combination with a new downscaling—Calibration procedure. *Remote Sens. Environ.* **2013**, *131*, 1–13. [CrossRef]
15. Ratan, R.; Venugopal, V. Wet and dry spell characteristics of global tropical rainfall. *Water Resour. Res.* **2013**, *49*, 3830–3841. [CrossRef]
16. Singh, D.; Tsiang, M.; Rajaratnam, B.; Diffenbaugh, N.S. Observed changes in extreme wet and dry spells during the South Asian summer monsoon season. *Nat. Clim. Chang.* **2014**, *4*, 456–461. [CrossRef]
17. Gimeno, L.; Dominguez, F.; Nieto, R.; Trigo, R.M.; Drumond, A.; Reason, C.; Taschetto, A.S.; Ramos, A.M.; Kumar, R.; Marengo, J. Major Mechanisms of Atmospheric Moisture Transport and Their Role in Extreme Precipitation Events. *Annu. Rev. Environ. Res.* **2016**, *41*, 117–141. [CrossRef]
18. Gimeno, L.; Drumond, A.; Nieto, R.; Trigo, R.M.; Stohl, A. On the origin of continental precipitation. *Geophys. Res. Lett.* **2010**, *3*, L13804. [CrossRef]
19. Gimeno, L.; Stohl, A.; Trigo, R.M.; Domínguez, F.; Yoshimura, K.; Yu, L.; Drumond, A.; Durán-Quesada, A.M.; Nieto, R. Oceanic and Terrestrial Sources of Continental Precipitation. *Rev. Geophys.* **2012**, *50*, RG4003. [CrossRef]
20. Ramos, A.M.; Trigo, R.M.; Liberato, M.L.R. A ranking of high-resolution daily precipitation extreme events for the Iberian Peninsula. *Atmos. Sci. Lett.* **2014**, *15*, 328–334. [CrossRef]
21. Ramos, A.M.; Trigo, R.M.; Liberato, M.L.R. Ranking of multi-day extreme precipitation events over the Iberian Peninsula. *Int. J. Clim.* **2017**, *37*, 607–620. [CrossRef]
22. Funk, C.; Peterson, P.; Landsfeld, M.; Pedreros, D.; Verdin, J.; Shukla, S.; Husak, G.; Rowland, J.; Harrison, L.; Hoell, A.; et al. The climate hazards infrared precipitation with stations—A new environmental record for monitoring extremes. *Sci. Data* **2015**, *2*, 150066. [CrossRef] [PubMed]
23. Paredes-Trejoa, F.J.; Barbosa, H.A.; Lakshmi Kumar, T.V. Validating CHIRPS-based satellite precipitation estimates in Northeast Brazil. *J. Arid Environ.* **2017**, *139*, 26–40. [CrossRef]
24. Duan, Z.; Liu, J.; Tuo, Y.; Chiogna, G.; Disse, M. Evaluation of eight high spatial resolution gridded precipitation products in Adige Basin (Italy) at multiple temporal and spatial scales. *Sci. Total Environ.* **2016**, *573*, 1536–1553. [CrossRef] [PubMed]
25. Tuo, Y.; Duan, Z.; Disse, M.; Chiogna, G. Evaluation of precipitation input for SWAT modeling in Alpine catchment: A case study in the Adige river basin (Italy). *Sci. Total Environ.* **2016**, *573*, 66–82. [CrossRef] [PubMed]
26. Katsanos, D.; Retalis, A.; Tymvios, F.; Michaelides, S. Analysis of precipitation extremes based on satellite (CHIRPS) and in situ dataset over Cyprus. *Nat. Hazards* **2016**, *83*, 53–63. [CrossRef]
27. Khandu; Awange, J.L.; Forootan, E. An evaluation of high-resolution gridded precipitation products over Bhutan (1998–2012). *Int. J. Climatol.* **2015**, *36*, 1067–1087. [CrossRef]
28. Hart, R.E.; Grumm, R.H. Using normalised climatological anomalies to rank synoptic-scale events objectively. *Mon. Weather Rev.* **2001**, *129*, 2426–2442. [CrossRef]

29. Dee, D.P.; Uppala, S.M.; Simmons, A.J.; Berrisford, P.; Poli, P.; Kobayashi, S.; Andrae, U.; Balmaseda, M.A.; Balsamo, G.; Bauer, P.; et al. The ERA-Interim reanalysis: Configuration and performance of the data assimilation system. *Q. J. R. Meteorol. Soc.* **2011**, *137*, 553–597. [CrossRef]
30. Stohl, A.; James, P. A Lagrangian analysis of the atmospheric branch of the global water cycle. Part I: Method description, validation, and demonstration for the August 2002 flooding in central Europe. *J. Hydrometeorol.* **2004**, *5*, 656–678. [CrossRef]
31. Stohl, A.; James, P. A Lagrangian analysis of the atmospheric branch of the global water cycle: Part II: Moisture transports between Earth's ocean basins and river catchments. *J. Hydrometeorol.* **2005**, *6*, 961–984. [CrossRef]
32. Numaguti, A. Origin and recycling processes of precipitating water over the Eurasian continent: Experiments using an atmospheric general circulation model. *J. Geophys. Res.* **1999**, *104*, 1957–1972. [CrossRef]
33. Drumond, A.; Nieto, R.; Hernandez, E.; Gimeno, L. A Lagrangian analysis of the variation in moisture sources related to drier and wetter conditions in regions around the Mediterranean Basin. *Nat. Hazards Earth Syst. Sci.* **2011**, *11*, 2307–2320. [CrossRef]
34. Duran-Quesada, A.M.; Gimeno, L.; Amador, J.A.; Nieto, R. Moisture sources for Central America: Identification of moisture sources using a Lagrangian analysis technique. *J. Geophys. Res.* **2010**, *115*, D05103. [CrossRef]
35. Gimeno, L.; Nieto, R.; Trigo, R.M.; Vicente-Serrano, S.M.; Lopez-Moreno, J.I. Where Does the Iberian Peninsula Moisture Come from? An Answer Based on a Lagrangian Approach. *J. Hydrometeorol.* **2010**, *11*, 421–436. [CrossRef]
36. Nieto, R.; Gimeno, L.; Gallego, D.; Trigo, R.M. Contributions to the moisture budget of airmasses over Iceland. *Meteorol. Z.* **2007**, *16*, 037–044. [CrossRef]
37. Sodemann, H.; Schwierz, C.; Wernli, H. Interannual variability of Greenland winter precipitation sources: Lagrangian moisture diagnostic and North Atlantic Oscillation influence. *J Geophys. Res.* **2008**, *113*, D03107. [CrossRef]
38. Drumond, A.; Nieto, R.; Gimeno, L. Sources of moisture for China and their variations during drier and wetter conditions in 2000–2004: A Lagrangian approach. *Clim. Res.* **2011**, *50*, 215–225. [CrossRef]
39. Sorí, R.; Nieto, R.; Drumond, R.; Gimeno, L. The Niger River Basin Moisture Sources: A Lagrangian Analysis. *Atmosphere* **2017**, *8*, 38. [CrossRef]
40. Hickey, K.R.; Connolly-Johnston, C. The Impact of Hurricane Debbie (1961) and Hurricane Charley (1986) on Ireland. In *Advances in Hurricane Research—Modelling, Meteorology, Preparedness and Impacts*; Hickey, K., Ed.; InTech: Rijeka, Croatia, 2012; Chapter 9; Volume 1, pp. 183–198. [CrossRef]
41. Pantillon, F.; Chaboureau, J.P.; Richard, E. Remote impact of North Atlantic hurricanes on the Mediterranean during episodes of intense rainfall in autumn 2012. *Q. J. R. Meteorol. Soc.* **2015**, *141*, 967–978. [CrossRef]
42. Krichak, S.O.; Feldstein, S.B.; Alpert, P.; Gualdi, S.; Scoccimarro, E.; Yano, J.I. Discussing the role of tropical and subtropical moisture sources in cold season extreme precipitation events in the Mediterranean region from a climate change perspective. *Nat. Hazards Earth Syst. Sci.* **2016**, *16*, 269–285. [CrossRef]
43. Ralph, F.M.; Dettinger, M.D. Storms, floods, and the science of atmospheric rivers. *EOS Trans. Am. Geophys. Union* **2011**, *92*, 265–272. [CrossRef]
44. Gimeno, L.; Nieto, R.; Vázquez, M.; Lavers, D.A. Atmospheric rivers: A mini-review. *Front. Earth Sci.* **2014**, *2*, 2. [CrossRef]
45. Ramos, A.M.; Trigo, R.M.; Liberato, M.L.R.; Tome, R. Daily precipitation extreme events in the Iberian Peninsula and its association with Atmospheric Rivers. *J. Hydrometeorol.* **2015**, *16*, 579–597. [CrossRef]
46. Guan, B.; Waliser, D.E. Detection of atmospheric rivers: Evaluation and application of an algorithm for global studies. *J. Geophys. Res. Atmos.* **2015**, *120*, 12514–12535. [CrossRef]

water

MDPI

Article

Contribution of Moisture from Mediterranean Sea to Extreme Precipitation Events over Danube River Basin

Danica Ciric [1,*], Raquel Nieto [1,*], Alexandre M. Ramos [2], Anita Drumond [1] and Luis Gimeno [1]

[1] EPhysLab (Environmental Physics Laboratory), Facultade de Ciencias, Universidade de Vigo, 32004 Ourense, Spain; anitadru@uvigo.es (A.D.); l.gimeno@uvigo.es (L.G.)

[2] Instituto Dom Luiz, Universidade de Lisboa, 1749-016 Lisboa, Portugal; amramos@fc.ul.pt

* Correspondence: cdanica@uvigo.es (D.C.); rnieto@uvigo.es (R.N.); Tel.: +34-988-387-248 (R.N.)

Received: 3 August 2018; Accepted: 1 September 2018; Published: 4 September 2018

check for updates

Abstract: In the most recent decades, central Europe and the Danube River Basin area have been affected by an increase in the frequency and intensity of extreme daily rainfall, which has resulted in the more frequent occurrence of significant flood events. This study characterised the link between moisture from the Mediterranean Sea and extreme precipitation events, with varying lengths that were recorded over the Danube River basin between 1981 and 2015, and ranked the events with respect to the different time scales. The contribution of the Mediterranean Sea to the detected extreme precipitation events was then estimated using the Lagrangian FLEXPART dispersion model. Experiments were modelled in its forward mode, and particles leaving the Mediterranean Sea were tracked for a period of time determined with respect to the length of the extreme event. The top 100 extreme events in the ranking with durations of 1, 3, 5, 7, and 10 days were analysed, and it was revealed that most of these events occurred in the winter. For extreme precipitation, positive anomalies of moisture support from the Mediterranean were found to be in the order of 80% or more, but this support reached 100% in summer and spring. The results show that extreme precipitation events with longer durations are more influenced by the extreme Mediterranean anomalous moisture supply than those with shorter lengths. However, it is during shorter events when the Mediterranean Sea contributes higher amounts of moisture compared with its climatological mean values; for longer events, this contribution decreases progressively (but still doubles the climatological moisture contribution from the Mediterranean Sea). Finally, this analysis provides evidence that the optimum time period for accumulated moisture to be modelled by the Lagrangian model is that for which the extreme event is estimated. In future studies, this fine characterisation could assist in modelling moisture contributions from sources in relation to individual extreme events.

Keywords: Danube River Basin; extreme precipitation events; Mediterranean Sea; Lagrangian approach; moisture transport

1. Introduction

There has been a rise in the number of extreme multi-day precipitation events occurring across Europe (including the Danube region), even in areas characterised as being drier on average [1]. These findings are consolidated by the results of other studies, which show that climate change and the presence of a warmer climate result in higher heavy rainfall events with varying durations but a reduction in summer precipitation throughout most parts of Europe [2,3].

The Danube River Basin is an important international basin. It has a length of 2780 km from Central to South-eastern Europe (Figure 1), and is the second-largest catchment area in Europe (approximately 817,000 km^2). It is characterised by diverse topography (including the Alps region) and by the high amount of precipitation received throughout the year, which is due to significant influences from the Mediterranean, Black Sea, the Atlantic Ocean, and the basin itself [4].

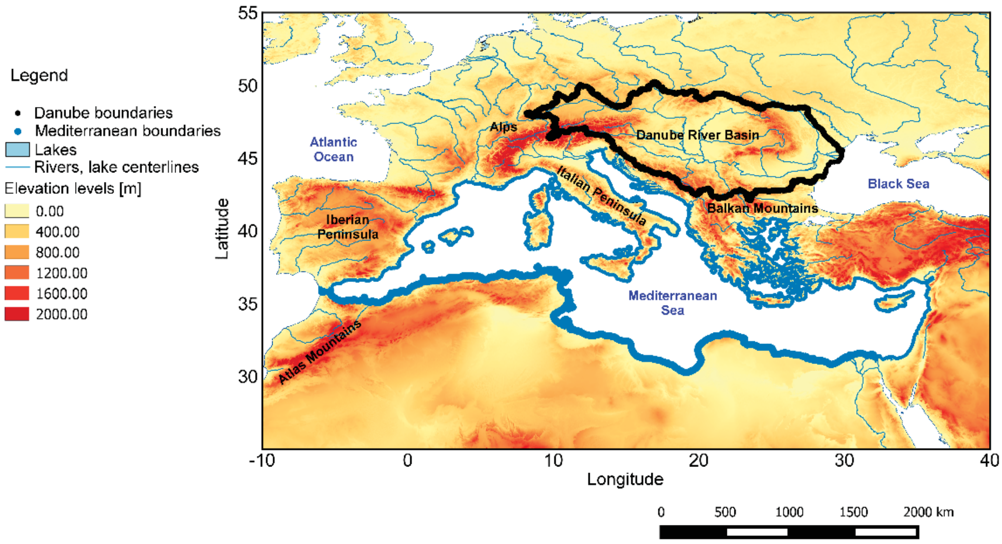

Figure 1. Map of Danube River Basin (black line) and Mediterranean Sea (blue line) as provided by the HydroSHEDS project (hydrological data and maps on shuttle elevation derivatives at multiple scale available online at https://hydrosheds.cr.usygs.gov).

Average annual precipitation is estimated in a range between 2300 mm in the high mountain regions and 400 mm in the Danube Delta [4]. Highest precipitation values of over 2000 mm have been recorded on the southern-oriented mountain chains of the Julian Alps and the Dinaric system, where the effects of humid and warm air masses originating from the Mediterranean and the associated orographic ascent result in convective precipitation [4,5]. In the Danube region, maximum mean climatological precipitation is recorded in the western part of the basin in July (mid-summer) and the minimum is recorded in April (spring) [6], but June and September are also defined as extremely wet months [7]. Wet and dry periods in the area are not temporally and spatially homogeneous and are strongly dependent on cyclone (anticyclone) circulation, convergence (divergence), advection of moist (dry) air and an increase (reduction) in the number of rain days [8].

Extreme hydrological events in the Danube River Basin, such as extreme precipitation and drought events, have become more frequent and more intensive as a consequence of changes in precipitation and temperature [9,10]. In particular, precipitation in the Mediterranean region has shown intra-annual irregularities over the most recent years, and a huge amount of rain has been recorded as falling within a short time frame [11]. Changes in daily precipitation could be related to an above average increase in the intensity and frequency of wet-days and wet-spell lengths [12]. The extreme hydrological events occurring in the Danube River Basin result in abnormal rainfall quantities falling in the region and are one of the main causes of floods in the area [13]. With respect to the three main parts of the Danube region, flood occurrences have mainly been recorded during June–August in the Upper Danube River Basin, in April in the Central part, and during April–May in the Lower Danube River [5]. As an example, and to highlight the importance of the extreme rainfall, a historical flood was recorded in August 2002 in the region, when heavy rain occurred in the southern and eastern parts of Germany, Austria, the Czech Republic and Slovakia, and resulted in devastating inundations that caused billions of euros worth of damage [14]. This extreme rainfall was caused by a V-b cyclone that had been created in the northern Mediterranean and then moved toward Austria, the Czech Republic, and Germany, while also affecting some parts of Poland and Slovakia. The largest precipitation quantities were recorded in Austria; the total rainfall amount for a few days in August exceeded the monthly climatological value by three to four times and provided 40–50% more than the annual average precipitation. In the mountain region between the Czech Republic and Austria, the amount of precipitation recorded was 350% that of the monthly climatological mean [15].

Part of the Danube River Basin is situated in the Mediterranean area, which is a region determined as being one of the most vulnerable to future climate change affects [16], and is considered a "hot-spot" region with respect to future negative climate projections. An analysis of the impact of climate change on extreme precipitation and floods in Slovakia found that climate change will cause an increase in short-term extreme rainfall events with accompanying floods. An increased maximum daily mean flood discharge of up to 43–55% is expected by 2025, up to 94–115% by 2050 and up to 115–166% by 2075 [17]. Another study also confirmed that future intensification of extreme precipitation events can be expected in the Mediterranean region as a consequence of depth-duration-frequency (DDF) curve changes, which may lead to floods with increased severity and intensity [18].

Many studies have investigated extreme precipitation events in the Danube basin region [19–22]. Ciric et al. [22] ranked extreme precipitation events with different durations in the Danube River basin by considering all days within the period 1981–2015. Their study analysed the most extreme precipitation event (23 September 1996), investigated the moisture sources and synoptic conditions leading to this extreme precipitation, and determined that the Mediterranean Sea is one of the most important moisture sources in the region [4,22] and for certain adjacent areas, such as the Balkan Peninsula [23,24] and the Southern Alpine region [25]. It is important to note the importance of the Mediterranean Sea as a source of moisture at a global scale, being one of the major oceanic sources to continental precipitation [26]. However, its impact differs on a seasonal scale over the Danube River Basin; it is the most important in winter whereas the Danube River Basin itself is dominant in summer [4].

In this paper, we use the ranking of extreme precipitation events developed by Ciric et al. [22] to analyse the contribution from the Mediterranean Sea (as a source of moisture) to the 100 most intense precipitation events recorded over the Danube River basin and obtained from the Climate Hazards Group Infra-Red Precipitation with Station dataset (CHIRPS) [27], which have different durations of 1, 3, 5, 7, and 10 days. Using the outputs of the Lagrangian dispersion model FLEXPART V9.0, which was initially developed by Stohl and James [28,29], and was fed with ERA-Interim reanalysis dataset from the ECMWF (European Centre for Medium-Range Weather Forecast) [30]. This dataset is accessible in 1° spatial resolution on 60 vertical levels from 1000 to 0.1 hPa and is available at 6-h time intervals. We forward tracked all particles that initially resided over the Mediterranean Sea and then reached the Danube River basin during all selected events. We then computed the available moisture from the Mediterranean Sea that generated precipitation over the basin as $(E - P) < 0$ (herein, PFLEX) for each event. Comparing anomalies calculated from these PFLEX values with anomalies from CHIRPS precipitation data for each event in the Danube region, the contribution to total precipitation from moisture from the Mediterranean was calculated, and a link between both variables was obtained.

2. Materials and Methods

2.1. Ranking of Extreme Precipitation Events

Following the ranking method developed by Ramos et al. [31,32] and using the daily high resolution (0.05°) CHIRPS, we used the ranking of extreme precipitation events with different durations (1, 3, 5, 7, and 10 days) over the Danube River Basin presented in Ciric et al. [22] to analyse only the most intense wet-spell events (in terms of moisture availability and their associated synoptic configurations).

CHIRPS data are obtained from a quasi-global precipitation database and are available on daily to seasonal time-scales at a high resolution (0.05°). The database is comprised of three main components: High-resolution climatology, time-varying cold cloud duration precipitation estimates, and in situ rain gauge data. The high resolution and 6-h to 3-month aggregates make it suitable for determining extreme precipitation events in certain areas with high precision. The temporal period 1981 until 2015 was used to calculate extreme precipitation events with different durations in the Danube region.

The method developed by Ramos et al. [31,32] assigns a magnitude to each individual extreme precipitation event prior to determining its ranking. The index of the ranking (R) is given daily after multiplying two variables: (i) The area (A) where the precipitation anomaly is above two standard deviations (SDs) (expressed as percentages), and (ii) the mean value of precipitation anomalies (M), where only those grid points in A that have precipitation amounts higher than 1 mm are considered. The ranking index (R) can be expressed using the following equation,

$$R = A \times M. \tag{1}$$

Ranking based on this R index is computed over multi-day periods as the sum of normalised precipitation anomalies for different durations (in our case for lengths of 1, 3, 5, 7, and 10 days). For example, the accumulated precipitation anomalies for an event with a duration of three days corresponds to the sum of the normalised precipitation anomalies of the analysed day and the two previous days, which totals three days. Explanation of this ranking methodology for extreme precipitation events is available in Ramos et al. [31,32] and Ciric et al. [22].

The R index was calculated for all days in the study period 1981–2015, which is a total of 12,775 days. We studied only the top 100 most extreme precipitation events occurring over the Danube River Basin with accumulated durations of 1, 3, 5, 7, and 10 days. The R magnitude for these 100 cases represents, for all durations, the ~0.99 percentile; therefore, we considered events that had the highest intensities. Table 1 provides an example of dates for the first 10 ranked cases, but the complete 100 extreme events for each duration are available in Tables S1–S5 in the Supplementary Material.

For each event, we computed the daily mean and daily anomalies of the precipitation values from CHIRPS data for the specific day/days of each event over the Danube River Basin.

Table 1. List of 10 top extreme precipitation events out of 100 total ranked cases with different durations over the Danube River Basin. The complete list of 100 detected events for all wet-spell durations is shown in the Supplementary Material (Tables S1–S5).

Position of the Ranking	1 Day	3 Days	5 Days	7 Days	10 Days
1	23 Sep 1996	24 Sep 1996	24 Sep 1996	1 Jan 1996	23 Aug 2005
2	28 Dec 2014	23 Sep 1996	25 Sep1996	15 Dec 1990	18 Dec 1990
3	6 Nov 1985	25 Sep 1996	26 Sep 1996	2 Jan 1996	24 Aug 2005
4	1 Mar 2008	11 Feb 1984	14 Dec 1990	14 Dec 1990	4 Jan 1996
5	18 Feb 1994	6 Nov 1985	23 Jan 1998	7 May 1987	15 Dec 1990
6	27 Nov 1983	8 Jan 2010	27 Sep 1996	27 Sep 1996	17 Dec 1990
7	6 May 1987	6 May 1987	23 Sep 1996	24 Sep 1996	16 Dec 1990
8	14 Mar 2013	10 Feb 1984	22 Jan 1998	16 Dec 1990	14 Dec 1990
9	2 Mar 2014	29 Oct 1990	30 Oct 1990	28 Sep 1996	22 Aug 2005
10	27 Mar 1993	31 Oct 1994	31 Oct 1990	25 Sep 1996	12 May 1991

2.2. Lagrangian Analysis of Mediterranean Moisture Contribution to Extreme Precipitation Events in Danube River Basin

In the present study, we analysed the contribution of moisture originating from the Mediterranean Sea and falling in the Danube River Basin during extreme precipitation events with different durations (Table 1). To enable this, we used a Lagrangian dispersion model FLEXPART V9.0, which was initially developed by Stohl and James [28,29], and was fed with ERA-Interim reanalysis data from the ECMWF [30]. This dataset is accessible in 1° spatial resolution on 60 vertical levels from 1000 to 0.1 hPa and is available at 6-h time intervals.

This Lagrangian approach consists in the division of the atmosphere in a large number of particles, for which it is assumed that the mass (*m*) remains constant. Basically, the Lagrangian model consists in calculation of surface freshwater flux (E − P) using the information on the particle's trajectories. To produce trajectories, the input velocity data are interpolated on the present particle position (Lagrangian grid) to advect the particle. Approximately 2 million particles are modelled every 6-h, and the motion of these particles occurs through a 3-D (two horizontal and one vertical dimension) wind field, as well as superimposed stochastic turbulent and convective motions, horizontal and vertical wind components, temperature and specific humidity. Since all three wind components are used to trace the particle path, the trajectories are three dimensional. The trajectory calculation in FLEXPART is based on the simple trajectory equation [33,34]:

$$\frac{\partial}{\partial t,}\vec{X} = \vec{v}\left[\vec{X}(t)\right] \quad (2)$$

where, t is time, $\vec{X}$ is the vector position and $\vec{v}$ is the wind vector.

Changes in specific humidity (q) and of each element (particle) with time, ($e - p = m\ dq/dt$), where m is the mass of particle, enables identification of particles that decrease in moisture through precipitation (p) or evaporation (e) over each particle trajectory. By adding the ($e - p$) of all the tracked particles in the atmosphere over the area of interest, it is possible to obtain the total surface freshwater flux (E − P), where (E) is the evaporation rate and (P) the precipitation rate per unit area, through the equation,

$$\mathrm{E} - \mathrm{P} = \frac{\sum_{k-1}^{k}(e-p)_k}{A}. \quad (3)$$

for all K particles that reside inner the area A [28,29].

Along individual particle trajectories (as on a regular grid) can be identified the surfaces where the particles obtain and loss moisture, using only the particles' information. On this way the source and sinks regions for a selected area can be identified and connected using the trajectory information. Particles are moved by the wind during the assumed average residence time in water vapour within the atmosphere, which is approximately 10 days [35]. A detailed explanation of many physical and dynamical parameters of the model may be found in the technical note by Stohl et al. [36] and in the official FLEXPART webpage (https://www.flexpart.eu/wiki).

This method can be applied in a backward or forward mode to compute the (E − P) budget and analyse main moisture sources for an area of interest and sinks for a defined source, respectively. When running the program backwards, it is possible to determine the sources of moisture and the areas where particles gain humidity as (E − P > 0); and running the program forward enables identification of sink regions where particles lose humidity (E − P < 0). A more detailed explanation of backward and forward analyses can be found in several works recently published that relate to areas near our target region (the Mediterranean basin [37], the Fertile Crescent [38], and the Iberian Peninsula [39]) and areas further north [40,41]. A more complete review can be found in the study of Gimeno et al. [42], which provides a comparison with other approaches used to detect moisture sources and sinks regions (as box and/or isotopes models) and emphasizes that the Lagrangian approach is one of the most suitable for use with these types of calculations. However, although there are many advantages of the Langrangian approach, it has two main associated limitations [42]: (1) The method is not able to calculate E and P separately, and (2) when input data have a limited resolution, the final results are also not as sharp. Nevertheless, the developers of the FLEXPART model, Stohl and James [36], pointed out that the large number of air particles considered in the experiment may cancel out such error types with respect to the given number of particles found in each atmospheric column. A more detailed explanation of the model's advantages and disadvantages can also be found in Gimeno et al. [42].

In this study, to calculate the moisture contribution from the Mediterranean Sea to extreme precipitation events occurring over the Danube River Basin, we computed (E − P) < 0 using the forward mode for each of the top 100 events (which were individually detected by the ranking method and lasted for either 1-day, 3-days, 5-days, 7-days, or 10-days). We selected the specific number of days relating to each precipitation event to compute the mean daily values of E − P < 0 (namely, PFLEX-$_{\text{EVENT}}$) and the mean climatological values for the same days within the 35-years climatology period 1981–2015 (PFLEX-$_{\text{CLI}}$). This enabled us to compute the moisture anomalies supported from the Mediterranean Sea for each event (PFLEX-$_{\text{ANOM}}$), and determine the anomalous moisture contribution from the Mediterranean Sea to each extreme precipitation event. To make a comparison between the percentage moisture contribution from the Mediterranean for each event modelled by FLEXPART (PFLEX-%) and climatology (PFLEX-$_{\text{CLI}}$), the relationship was computed using Equation (4),

$$(\text{PFLEX} - \%) = \frac{(\text{PFLEX}_{-\text{EVENT}} - \text{PFLEX}_{-\text{CLI}})}{\text{PFLEX}_{-\text{CLI}}} \times 100. \tag{4}$$

3. Results

For each extreme precipitation event, we calculated the precipitation characteristics using CHIRPS data and the information obtained from the FLEXPART model (derived from E − P < 0) to improve our knowledge of the relationship between precipitation events occurring over the Danube River Basin and moisture from the Mediterranean Sea. In addition, the percentage moisture from the Mediterranean Sea (PFLEX-%) relating to each event was computed and compared using PFLEX-$_{\text{CLI}}$. All variables for the 100 events analysed are transcribed in the Supplementary Material (Tables S1–S5 for events with lengths of 1-day, 3-days, 5-days, 7-days and 10-days), and the R-index value of the ranking for each event is provided. Table 2 presents the top 10 extreme precipitation events of the total 100 ranked for the 5 different period lengths (1-, 3-, 5-, 7-, and 10-days). The date of an extreme ranked event denotes the last day of each event for a different duration. According to this, the moisture supply (E − P < 0) from the Mediterranean Basin into the Danube River Basin obtained via the FLEXPART outputs (PFLEX values) was computed for the same period length of the ranking. Thus, the integrated days of each event to compute PFLEX in different duration correspond to the same days of the length of the event. Therefore, for events with lengths of 1-day, we forward-integrated the PFLEX values for one day; for those with lengths of 3-days, the integration was performed for three days; and this continued until all durations were integrated.

Table 2. List of the top 10 extreme precipitation events out of a total of 100 cases with different durations ranked for the Danube River Basin. The columns for each event show: The position of the ranking, the date of the event, the daily mean precipitation value (Mean ∑CHIRPS), daily climatological precipitation value (Clim. CHIRPS), daily precipitation Anomaly (Anom. CHIRPS), value of ranking index (R), mean E − P < 0 values from the Mediterranean Sea into the Danube River Basin for day/days of the extreme precipitation event (PFLEX-$_{\text{EVENT}}$), daily climatological E − P < 0 value (PFLEX-$_{\text{CLI}}$), daily anomaly of E − P < 0 values (PFLEX-$_{\text{ANOM}}$), and percentage of Mediterranean contribution for each event calculated by FLEXPART (PFLEX-%). Units of calculations with CHIRPS and PFLEX are in mm/day; R has no units; and the last column is expressed in %. CHRIPS, Climate Hazards Group Infra-Red Precipitation with Station dataset; PFLEX, available moisture from the Mediterranean Sea (E − P < 0 values) obtained via Lagrangian experiment.

Position of the Ranking	Date Event	Mean ∑CHIRPS	Clim. CHIRPS	Anom. CHIRPS	R	PFLEX -EVENT	PFLEX -CLI	PFLEX -ANOM	PFLEX-%
				1 day					
1	23 Sep 1996	45.66	4.13	41.53	198.65	0.59	0.15	0.44	285.69
2	28 Dec 2014	17.76	3.45	14.31	168.81	0.82	0.14	0.68	457.93
3	6 Nov 1985	19.74	1.96	17.79	156.70	0.45	0.21	0.25	118.89
4	1 Mar 2008	13.09	2.42	10.68	155.58	0.20	0.18	0.02	11.87
5	18 Feb 1994	12.05	1.18	10.87	142.60	0.40	0.10	0.30	285.92
6	27 Nov 1983	16.94	1.57	15.38	140.42	0.76	0.16	0.60	383.90
7	6 May 1987	26.90	3.53	23.37	138.02	0.58	0.18	0.40	224.24
8	14 Mar 2013	14.18	1.17	13.01	137.91	1.21	0.07	1.14	1657.75
9	2 Mar 2014	9.67	2.07	7.60	136.17	0.08	0.14	−0.06	−41.29
10	27 Mar 1993	13.32	2.47	10.86	131.77	1.12	0.21	0.90	424.33

Table 2. *Cont.*

Position of the Ranking	Date Event	Mean ∑CHIRPS	Clim. CHIRPS	Anom. CHIRPS	R	PFLEX -EVENT	PFLEX -CLI	PFLEX -ANOM	PFLEX-%
				3 days					
1	24 Sep 1996	19.61	2.59	17.02	249.95	1.37	0.57	0.80	140.94
2	23 Sep 1996	18.54	2.51	16.03	228.27	2.10	0.51	1.59	312.59
3	25 Sep 1996	16.90	2.49	14.41	224.59	0.70	0.59	0.11	18.07
4	11 Feb 1984	6.77	1.70	5.07	206.04	0.54	0.40	0.14	34.63
5	6 Nov 1985	9.50	2.03	7.46	204.39	1.12	0.54	0.58	107.29
6	8 Jan 2010	6.12	1.46	4.67	198.54	0.96	0.30	0.66	217.26
7	6 May 1987	13.52	3.08	10.44	198.36	2.05	0.53	1.52	284.32
8	10 Feb 1984	6.54	1.61	4.93	195.88	1.03	0.38	0.64	169.23
9	29 Oct 1990	11.82	2.03	9.79	195.15	1.07	0.35	0.71	202.75
10	31 Oct 1994	10.10	2.05	8.06	193.43	0.38	0.37	0.01	3.85
				5 days					
1	24 Sep 1996	19.61	2.59	17.02	254.85	1.92	0.74	1.18	160.01
2	25 Sep1996	18.54	2.51	16.03	254.22	1.62	0.77	0.85	110.97
3	26 Sep 1996	16.90	2.49	14.41	251.71	1.14	0.79	0.36	45.42
4	14 Dec 1990	6.77	1.70	5.07	237.58	1.40	0.43	0.96	222.56
5	23 Jan 1998	9.50	2.03	7.46	234.92	1.17	0.48	0.69	145.60
6	27 Sep 1996	6.12	1.46	4.67	231.42	0.60	0.79	−0.20	−24.68
7	23 Sep 1996	13.52	3.08	10.44	230.92	2.13	0.70	1.42	201.84
8	22 Jan 1998	6.54	1.61	4.93	227.95	1.57	0.46	1.11	243.75
9	30 Oct 1990	11.82	2.03	9.79	222.08	1.14	0.47	0.67	142.65
10	31 Oct 1990	10.10	2.05	8.06	221.67	1.13	0.47	0.65	138.03
				7 days					
1	1 Jan 1996	6.52	2.12	4.40	298.19	1.67	0.51	1.16	225.99
2	15 Dec 1990	6.41	1.67	4.74	290.71	1.41	0.51	0.89	173.84
3	2 Jan 1996	5.33	1.96	3.37	277.60	1.36	0.49	0.88	180.10
4	14 Dec 1990	5.84	1.64	4.21	273.79	1.55	0.51	1.04	205.09
5	7 May 1987	7.53	2.67	4.86	260.72	2.16	0.80	1.36	171.43
6	27 Sep 1996	9.15	2.32	6.83	260.69	1.24	0.89	0.35	38.74
7	24 Sep 1996	9.28	2.34	6.94	258.47	1.92	0.86	1.07	124.99
8	16 Dec 1990	5.47	1.62	3.86	257.33	1.26	0.53	0.73	138.16
9	28 Sep 1996	9.07	2.26	6.81	256.91	0.86	0.90	−0.05	−5.41
10	25 Sep 1996	9.08	2.31	6.77	256.87	1.76	0.86	0.89	102.92
				10 days					
1	23 Aug 2005	8.05	2.02	6.03	325.98	1.15	0.79	0.36	45.52
2	18 Dec 1990	4.82	1.76	3.06	317.66	1.22	0.56	0.66	116.23
3	24 Aug 2005	7.49	2.04	5.45	315.91	1.08	0.82	0.26	31.93
4	4 Jan 1996	4.68	1.90	2.78	313.98	1.28	0.51	0.76	147.99
5	15 Dec 1990	4.99	1.63	3.36	313.50	1.55	0.55	0.99	179.03
6	17 Dec 1990	4.68	1.72	2.97	301.29	1.33	0.56	0.77	136.24
7	16 Dec 1990	4.78	1.62	3.16	300.85	1.41	0.56	0.85	152.19
8	14 Dec 1990	4.69	1.66	3.03	298.32	1.64	0.55	1.09	195.89
9	22 Aug 2005	7.45	2.03	5.42	298.17	1.21	0.76	0.45	58.65
10	12 May 1991	6.03	2.67	3.36	290.89	1.44	0.95	0.49	51.64

The Mediterranean Sea is known to be one of the main sources of moisture for its surrounding continental areas (including the Danube region), and this is clear when analysing Table 2 (and Tables S1–S5). Although the amount of precipitations is greater than climatological mean values during extreme events, there are occasions when the moisture transport is not higher than the climatological value, and PFLEX-$_{\mathrm{ANOM}}$ takes negative values. However, for the cases used in this analysis, positive PFLEX-$_{\mathrm{ANOM}}$ values denote that for extreme precipitation events the Mediterranean is an effective source of moisture that provides greater than mean climatological values. Table 3 presents the percentage of these positive contributions on an annual and seasonal scale (winter, spring, summer and autumn), and the total of the events during each season. Although the Mediterranean always acts as a moisture source, it provides higher than mean amounts for between 84% and 93% of events (it contributes less to events of 5-days and more to events of 10-days in length). On a seasonal scale, the Mediterranean Sea has an extra support of moisture to extreme events with all duration lengths during summer (only showing lower percentages for events with lengths of 3-days). It is also evident from Table 3 evidences that the highest number of extreme precipitation events occurred during winter and the lowest number occurred during summer.

Table 3. Numbers of extreme events on annual and seasonal scales (within brackets) and percentages of extreme precipitation events with a higher Mediterranean Sea contribution than the mean annual and seasonal climatological value for all rainy length periods of 1, 3, 5, 7, and 10 days. Results are presented with respect to Mediterranean PFLEX anomalies into the Danube River Basin.

Duration	1 day	3 days	5 days	7 days	10 days
Annual	86% (100)	90% (100)	84% (100)	91% (100)	93% (100)
Winter	83.33% (36)	85.71% (42)	86.96% (46)	97.44% (39)	85.29% (43)
Spring	90% (30)	90.91% (22)	100% (7)	100% (11)	100% (21)
Summer	100% (9)	90% (10)	100% (9)	100% (11)	100% (15)
Autumn	80% (25)	96.15% (26)	73.68% (38)	79.49% (39)	93.33% (30)

Table 2 shows the calculated intensity of the Mediterranean contribution in each ranked extreme precipitation event that is expressed by the variable PFLEX-%. As explained above, this variable denotes how many more times the Mediterranean moisture contributes to each event than during climatological contributions: A contribution of 100% means that this event was fed by twice the amount of moisture derived from the Mediterranean Sea than during climatological contributions. Figure 2 shows the occurrence distribution of this percentage on an annual scale for all extreme event durations. Positive values represent all the cases presented in Table 3. Our results show that the contribution from the Mediterranean was much higher (reaching values over 400%) for events lasting 1-day than for events with other durations. The contribution decreased for precipitation events with longer durations, although it was usually above 50%.

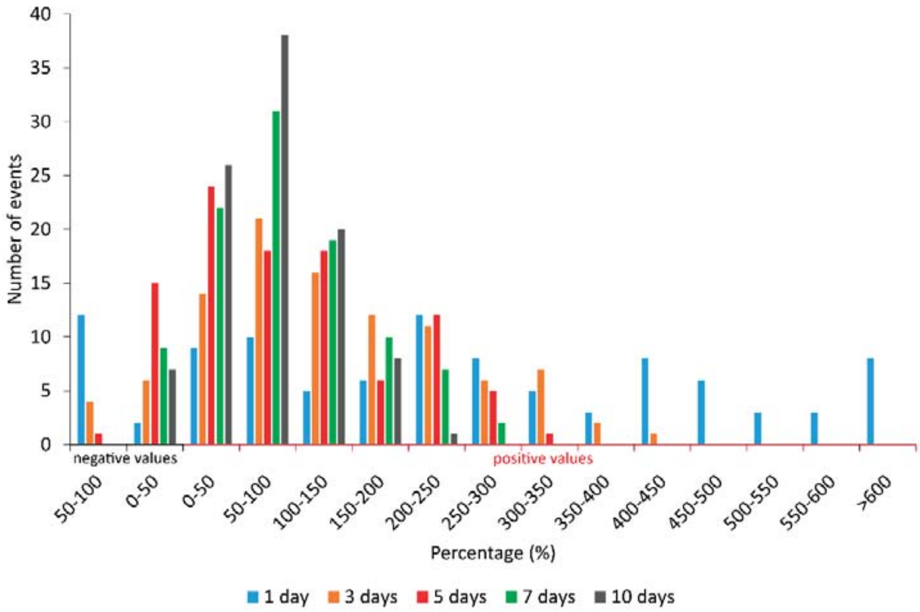

Figure 2. Percentage moisture supply from the Mediterranean Sea relating to each extreme event (PFLEX-%) on an annual scale for the 100 events analysed and all ranked durations: Blue bars represent number of events with 1-day duration; orange bars represent 3-days duration; red bars represent 5-days duration; green bars represent 7-days duration; and grey bars represent 10-days duration.

The computation was repeated to determine results on a seasonal scale (winter, spring, summer and autumn) for all durations, and these results are presented in the Supplementary Material

(Figure S1 for 1-day duration, Figure S2 for 3-days duration, Figure S3 for 5-days duration, Figure S4 for 7-days duration, and Figure S5 for 10-days duration).

One of the main goals of this paper is to determine how much moisture is provided by the Mediterranean Sea to fuel extreme precipitation events over the Danube River Basin. To determine the existence of this relationship, a regression analysis was conducted (Table 4) between precipitation anomalies (Anomalies CHIRPS) and the anomalous contribution from the Mediterranean Sea (PFLEX-$_{ANOM}$). As stated in the methodology, PFLEX-$_{ANOM}$ was calculated for the same different periods used in the ranking and lasting for 1, 3, 5, 7, and 10 days. This enabled us to understand the effect of the moisture supply to each event during the period of the event or/and during the previous days. Table 4 shows the results of linear regression slope values, and significant values (at a level of 90%) are highlighted.

On an annual scale and according to the Student's *t*-test (see Table 4), events lasting 1 day, 3 days, and 7 days were more extreme when they had a higher moisture contribution from the Mediterranean Sea. It is remarkable the importance of the time period for the PFLEX integration, being the relationship significant for the same length of calculation (with the exception for events with 7 days of length). The results show a significant relationship in all seasons for extreme events lasting 7 days; for events of 10 days the relationship is only no significant during summer; but for short-duration events of 1 day, the relationship is significant during spring (accounting the moisture supply for 1 and 3 days) and summer (for all the time periods of moisture integration), and for events lasting 3 days, the relationship is significant during spring and autumn (but only integrating the moisture support for the same time period, 3 days).

Calculated coefficient of determination values (R^2) between Anomalies CHIRPS and PFLEX-$_{ANOM}$ for extreme events are indicated next to the corresponding regression line in Figure 3. The greatest R^2 value (0.73) relate to events with duration of 1-day (Figure 3a) can be observed during summer, and means that 73% of the variability of precipitation anomalies during these events can be explained by positive anomalous moisture support from the Mediterranean Sea (PFLEX-$_{ANOM}$). For other durations of 3-days (Figure 3b), 5-days (Figure 3c) and 10-days (Figure 3d), the highest values are observed during spring ($R^2 = 0.21$, $R^2 = 0.89$ and $R^2 = 0.37$, respectively). These results mean that during spring and summer (for extreme precipitation events lasting 1-day) the highest precipitation anomalies over the Danube River Basin are highly associated with a strong moisture supply anomaly from the Mediterranean Sea that occurs during the event period. However, the positive moisture supply from the Mediterranean does not always correspond with extreme precipitation events, where cases with low R^2 relate to 1-day events in autumn and 3-day events in winter, for example.

Table 4. Slope values of simple linear regression analysis between CHIRPS anomaly values of extreme precipitation for events with different durations (1, 3, 5, 7, and 10 days) with respect to PFLEX-$_{ANOM}$ values (for 1, 3, 5, 7, and 10 integrated days) on annual, winter, spring, summer, and autumn scales. Highlighted numbers represent those values that are significant at 90% when applying Student's *t*-test, and the asterisk denotes 99% significance.

Duration of Extreme Event	**1 Day**					**3 Days**				**5 Days**			**7 Days**		**10 Days**
Period of integration used for PFLEX-$_{ANOM}$ values	1 day	3 days	5 days	7 days	10 days	3 days	5 days	7 days	10 days	5 days	7 days	10 days	7 days	10 days	10 days
Annual	**3.34** *	1.42	0.23	1.13	−0.10	**1.30**	0.28	0.30	0.00	1.05	0.78	0.01	**1.30** *	**0.09** *	0.04
Winter	1.21	−0.15	−0.05	−0.27	−0.39	−0.24	−0.25	−0.30	−0.37	1.19	1.13	1.17	**0.88** *	**1.07** *	**1.05**
Spring	**5.83** *	**4.77** *	1.07	0.69	−0.53	**3.40** *	1.72	0.10	0.83	1.22	1.29	1.29	**1.77** *	**1.87** *	**1.01** *
Summer	**10.10** *	**6.14**	**6.83**	**7.90** *	**7.87**	0.25	0.24	0.16	0.27	−0.42	−0.64	−0.85	**1.97** *	**2.07** *	0.53
Autumn	−0.25	−3.18	−3.27	−0.31	−0.87	**2.38**	1.04	1.48	1.53	2.15	1.36	0.86	**1.51** *	**1.33** *	**0.81**

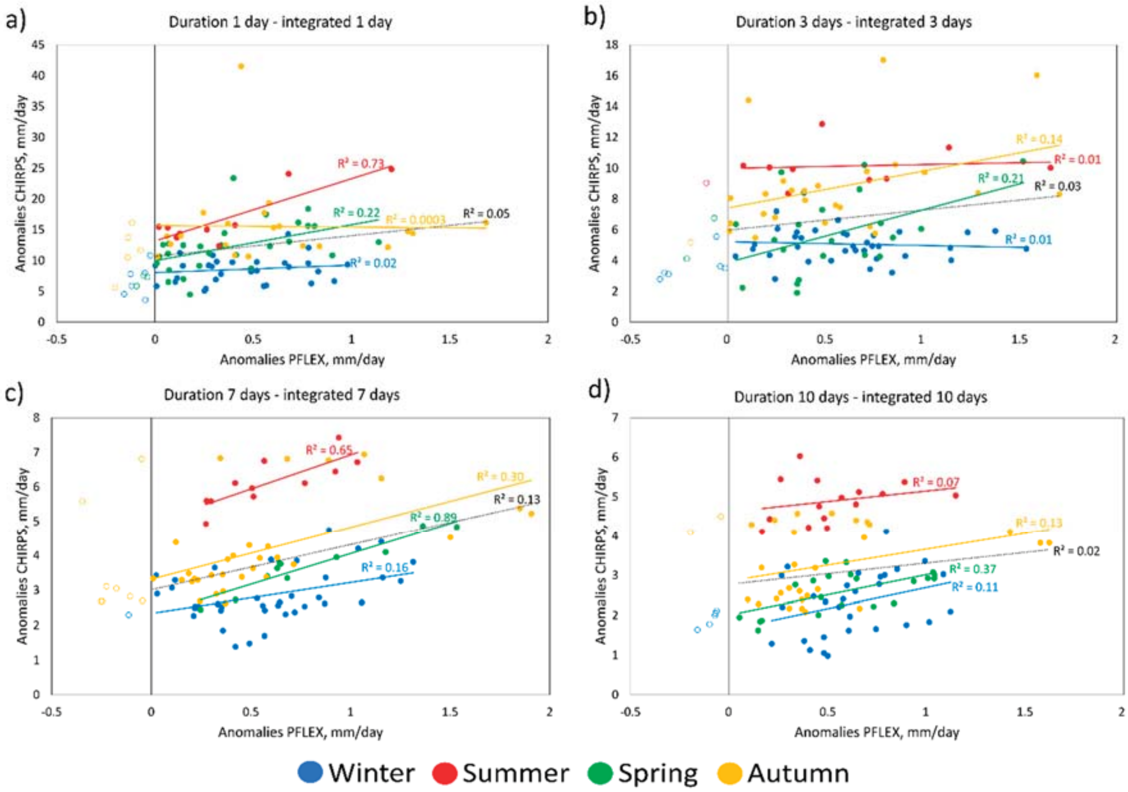

Figure 3. Scatterplot for moisture supply anomalies from Mediterranean Sea (PFLEX-$_{\mathrm{ANOM}}$) (*x*-axe, mm/day) and precipitation anomalies from CHIRPS database (Anomalies CHIRPS, *y*-axe, mm/days) over the Danube River Basin for 100 ranked extreme precipitation events separated on seasonal scales (winter—blue circles; summer—red circles; spring—green circles; autumn—yellow circles). The filled circles represent events with positive PFLEX-$_{\mathrm{ANOM}}$ values and empty circles represent negative values. The corresponding regression line and coefficient of determination (R^2) are also shown for each season (blue, red, green, and yellow lines) and on an annual scale (dashed black line) for events with positive PFLEX-$_{\mathrm{ANOM}}$ values.

4. Discussion and Conclusions

In this study, we investigated the relationship between the anomalous moisture supply from the Mediterranean Sea during extreme precipitation events occurring in the Danube River Basin during the period 1981–2015.

Extreme precipitation events with different durations (1, 3, 5, 7, and 10 days) were ranked using CHIRPS data and by applying the method developed by Ramos et al. [31,32]. The ranked events included all extreme events that occurred during the 35-years period. However, we selected only the top 100 events, which had differing duration lengths (the highest 100 extreme precipitation events). Daily precipitation anomalies were then calculated for each extreme precipitation event.

To investigate the moisture contribution from the Mediterranean Sea to the Danube River Basin during these ranked extreme precipitation events of all durations, a Lagrangian forward analysis was conducted for the same 35-years period using the FLEXPART model, and the accumulated daily anomalous moisture supplies from the Mediterranean Sea for each event were calculated (PFLEX-$_{\mathrm{ANOM}}$) by integrating the moisture contribution during 1, 3, 5, 7, and 10 days.

Some of the results obtained in this study corroborate those of previous studies that were conducted using other methodologies and introduces new methods for exploring the relationship between moisture support from the Mediterranean Sea and extreme rainfall occurring within the Danube River Basin.

According to the ranking results, we can conclude that most extreme precipitation events occurred during winter in the Danube River Basin region (36 events with durations of 1-day; 42 events with durations of 3-days; 46 events with durations of 5-days; 39 events with durations of 7-days; and 43 events with durations of 10-days), when the Mediterranean Sea was found the dominant moisture source [4]. The variation in the Mediterranean moisture contribution to precipitation throughout the year has been observed in many studies, and clear seasonal differences in the moisture contribution have been shown [4,24]. However, in general, the anomalous contribution percentage from the Mediterranean Sea was positive during summer and spring (reaching 100% for several of the duration lengths) when major precipitation and floods where recorded over the region [5,15], and confirms the results of other studies that have characterised these seasons being a favourable period for extreme precipitation in the central Mediterranean region [43,44]. This behaviour, occurring in winter the maxima occurrence of extremes and being summer and spring when the Mediterranean Sea act as the major positive source of moisture is a consequence of the Mediterranean Sea is not the unique climatological source of moisture for the region (for instance, the Danube River Basin itself or the continental surrounding areas [4]), and many extreme events are generated by moisture that has another origin (all those that show negative values in Table 2 and Tables S1—S5), or to the fact that during winter the region is affected by the transition of synoptic systems that enhance the amount of precipitation during longer periods that during summer when the convective and shorter event are more common [45,46].

This study aims to analyse the contribution from the Mediterranean Sea. Therefore, we computed the number of extreme precipitation events (in percentage) that had a higher support from Mediterranean moisture than from the climatological contribution. The highest contribution related to extreme events with durations of 1 day, when the major part of the events, at least, duplicated the support from the Mediterranean (8 of these events received a percentage contribution of more than 600%). The Mediterranean moisture contribution decreased progressively for longer precipitation events, but it generally reached above 50%.

To determine the existence of a significant relationship between the precipitation anomalies of ranked extreme events for all durations and Mediterranean moisture supply anomalies, a simple linear regression analysis and a Student's *t*-test (with a 90% confidence level) were conducted. The results showed that extreme precipitation events with longer durations were more influenced by the Mediterranean anomalous moisture supply than those with shorter lengths, showing higher R^2 values. The significance was greater for extreme precipitation events with lengths of 7-days on an annual and season scale (at more than 90%), with the highest influence from extreme precipitation by the Mediterranean moisture supply occurring in spring (89%) followed by summer (65%). During both seasons, extreme precipitation events with longer durations in the Danube River Basin were usually related to high precipitation quantities that accumulated over a few days in the Danube River Basin location [47]. Our results provide evidence that these events were related to a high anomalous support of moisture from the Mediterranean Sea, and that events were more intense when this contribution was greater. This same effect occurred for shorter length events of 1-day and 3-days on an annual scale, but the effect differed seasonally. For events with lengths of 1-day, the relationship was significant during spring and summer, and for durations of 3-days, the relationship was significant in spring and autumn. However, extreme precipitation events lasting 5 days showed no significant relationship on any scale. Although the results obtained at a 1- or 3-days are significant for a pair of season, they could improve if a subdivision of the Mediterranean could be performed, since it is known that the central part of the basin has a great influence on local convective rainfall, e.g., References [24,48].

The low R^2 values or the lack of significance in the remaining cases indicate that the moisture contribution from the Mediterranean Sea is not the key to modulate, or to produce, the extreme precipitations. The Danube River Basin has another source of moisture (see Introduction and Ciric et al. [4]) that could contribute with higher amounts of moisture than that from the whole

Mediterranean Sea; and even having a higher support of moisture from the Mediterranean it is needed some dynamical factor to start the convection to produce rainfall and to maintain the instability [49].

It is important to note that the integration times used to compute moisture from the Mediterranean Sea from FLEXPART outputs were conducted during different periods (1, 3, 5, 7, and 10 days), showing that for extreme precipitation the common 10 days (the mean life time for the water vapour in the atmosphere [35]), which have been used in several studies (e.g., References [4,9,22–25,30]), does not provide the best results, and it is preferable to use the same time period for which the extreme event has been calculated. Only during 1-day length events in summer, and for those lasting 7-days in all seasons, does moisture from the Mediterranean reach significant values for 1 to 10 days of the trajectories.

It is also of note that extreme events with temporal scales of 1 and 7 days correspond with typical synoptic rainfall occurring in the region. The shorter duration of 1 day is a typical duration for precipitation in the Danube River Basin and is related to slow-spreading convective systems [50] that produce extreme rainfall throughout the entire year. However, the main cause of the formation of longer-length extreme precipitation events (7 days) is a slow-evolving synoptic environment, which is typical of extratropical cyclone transitions and the effects of orographic barriers [51,52] that are associated with advection of warm and moist air from the Mediterranean Sea to the surrounding continental areas (includes the Danube River Basin) and are caused by the formation of marine low-level jets at specific locations in the presence of specific synoptic-scale circulation conditions that produce extreme precipitation [53]. The results of our study also show that the methodology applied capture the typical synoptic conditions in the northern Mediterranean Basin, and our methodology could therefore be applied to other areas of interest to provide an enhanced analysis of individual extreme precipitation events.

Supplementary Materials: The following are available online at http://www.mdpi.com/2073-4441/10/9/1182/s1. Table S1: As Table 2 but for all 100 events, Table S2: As Table 2 but for all events of 3-days duration, Table S3: As Table 2 but for all events of 5-days duration; Table S4: As Table 2 but for all events of 7-days duration, Table S5: As Table 2 but for all events of 10-days duration. Figure S1: PFLEX-% on a seasonal scale for 1-day events duration, Figure S2: PFLEX-% on a seasonal scale for 3-days events duration, Figure S3: PFLEX-% on a seasonal scale for 5-days events duration, Figure S4: PFLEX-% on a seasonal scale for 7-days events duration, Figure S5: PFLEX-% on a seasonal scale for 10-days events duration.

Author Contributions: D.C., R.N., and L.G. conceived and designed the experiments. D.C. performed the experiments. A.M.R. done the precipitation ranking. A.D. reviewed the computations. D.C., R.N. and L.G. analysed the data. R.N. and D.C. wrote the paper.

Funding: This research received no external funding.

Acknowledgments: Danica Ciric is supported by the European Commission under the Erasmus Mundus Project Green-Tech-WB: Smart and Green Technologies for Innovative and Sustainable Societies in the Western Balkans (551984-EM-1-2014-1-ES-ERA Mundus-EMA2). This research was partially supported by Xunta de Galicia under project ED413C 2017/64 “Programa de Consolidacion e Estructuracion de Unidades de Investigacion Competitivas (Grupos de ReferenciaCompetitiva)” co-funded by the European Regional Development Fund (FEDER). Also we want to thanks for support to IMDROFLOOD financed by the Water Works 2014 co-funded call of the European Commission. A.M. Ramos was supported through a postdoctoral grant (SFRH/BPD/84328/2012) from the Fundação para a Ciência e a Tecnologia (FCT, Portuguese Science Foundation).

Conflicts of Interest: The authors declare no conflict of interest. The founding sponsors had no role in the design of the study, in the collection, analyses, or interpretation of data, in the writing of the manuscript, and in the decision to publish the results.

Abbreviations

The following abbreviations are used in this manuscript

∑CHIRPS	Daily mean precipitation value from CHIRPS precipitation dataset
Anom. CHIRPS	Daily precipitation anomaly value from CHIRPS precipitation dataset
CHIRPS	Climate Hazards Group Infra-Red Precipitation with Station data dataset
Clim. CHIRPS	Daily climatological precipitation value from CHIRPS precipitation dataset
ECMWF	European Centre for Medium-Range Weather Forecast
ERA	European Centre for Medium-Range Weather Forecasting Re-Analysis
FLEXPART	FLEXiblePARTicle dispersion model
HydroSHEDS	Hydrological data and maps based on Shuttle elevation derivatives at multiple scales
PFLEX	Available moisture from the Mediterranean Sea ($E - P < 0$ values) obtained via Lagrangian experiment
PFLEX-%	The percentage of the Mediterranean contribution for each event calculated by FLEXPART
PFLEX-$_{ANOM}$	Daily anomalous $(E - P) < 0$ value obtained via Lagrangian experiment
PFLEX-$_{CLI}$	Daily climatological $(E - P) < 0$ value obtained via Lagrangian experiment
PFLEX-$_{EVENT}$	$(E - P) < 0$ mean values from the Mediterranean Sea into the Danube River Basin the day/days of extreme precipitation event obtained via Lagrangian experiment

References

1. Dankers, R.; Hiederer, R. *Extreme Temperatures and Precipitation in Europe: Analysis of a High-Resolution Climate Change Scenario*; JRC Scientific and Technical Reports; European Communities: Luxemburg, 2008; Available online: http://citeseerx.ist.psu.edu/viewdoc/download?doi=10.1.1.397.1054&rep=rep1&type=pdf (accessed on 25 July 2018).
2. Christensen, J.H.; Christensen, O.B. Severe summertime flooding in Europe. *Nature* **2003**, *421*, 805–806. [CrossRef] [PubMed]
3. Christensen, O.B.; Christensen, J.H. Intensification of extreme European summer precipitation in a warmer climate. *Glob. Planet. Chang.* **2004**, *44*, 107–117. [CrossRef]
4. Ciric, D.; Stojanovic, M.; Drumond, A.; Nieto, R.; Gimeno, L. Tracking the Origin of Moisture over the Danube River Basin Using a Lagrangian Approach. *Atmosphere* **2016**, *7*, 162. [CrossRef]
5. Pekárová, P.; Miklánek, P.; Melo, M.; Halmová, D.; Pekár, J.; Mitková, V. *Flood Marks along the Danube River between Passau and Bratislava*; VEDA: Bratislava, Slovakia, 2014; Available online: http://147.213.100.3:81/danubeflood/PDF/kniha9VEDA%20small.pdf (accessed on 24 July 2018).
6. Brilly, M. *Hydrological Processes of the Danube River Basin*; Springer: New York, NY, USA, 2010.
7. Loczy, D. *Geomorphological Impacts of Extreme Weather: Case Studies from Central and Eastern Europe*; Springer Science & Business Media: New York, NY, USA, 2013; pp. 141–146. ISBN 978-94-007-6300-5.
8. Ionita, M.; Scholz, P.; Chelcea, S. Spatio-temporal variability of dryness/wetness in the Danube River Basin. *Hydrol. Process.* **2015**, *29*, 4483–4497. [CrossRef]
9. Stojanovic, M.; Drumond, A.; Nieto, R.; Gimeno, L. Moisture Transport Anomalies over the Danube River Basin during Two Drought Events: A Lagrangian Analysis. *Atmosphere* **2017**, *8*, 193. [CrossRef]
10. Dosio, A. *Climate Change Projections for the Danube River Basin*; European Comission, Join Research Centre (JRC): Vienna, Austria, 2014; Available online: http://drdsi.jrc.ec.europa.eu/data/userstories/ReqNo_JRC92778_reqno_jrc92778_climate_change_projections_for_the_danube_area_final.pdf (accessed on 3 June 2018).
11. Olcina, J.; Pérez Morales, A.; Gil Guirado, S.; López, F.; Rico Amorós, A.M. The significance of vulnerability and exposure in increased flood risk on the mediterranean coast. In *Consorseguros Revista Digital*; Consorcio de Compensación de Seguros (CCS): Madrid, Spain, 2017; Available online: http://www.consorsegurosdigital.com/almacen/pdf/the-significance-of-vulnerability-and-exposure-in-increased-flood-risk-on-the-mediterranean-coast.pdf (accessed on 4 June 2018).
12. Schmidli, J.; Frei, C. Trends of Heavy Precipitation and Wet and Dr y Spells in Switzerland during the 20th Centry. *Int. J. Climatol.* **2005**, *25*, 753–771. [CrossRef]
13. Mikhailova, M. Recent Extreme Floods and Their Transformation along the Danube River. *J. Environ. Res. Eng. Manag.* **2017**, *73*, 20–32. [CrossRef]

14. Petrow, T.; Thieken, A.H.; Kreibich, H.; Bahlburg, C.H.; Merz, B. Improvements on Flood Alleviation in Germany: Lessons Learned from the Elbe Flood in August 2002. *Environ. Manag.* **2006**, *38*, 717–732. [CrossRef] [PubMed]
15. Vasiliev, O.F.; van Gelder, P.H.A.J.M.; Plate, E.J.; Bolgov, M.V. *Extreme Hydrological Events: New Concepts for Security*; Springer: Berlin, Germany, 2007; pp. 418–420. ISBN 1-4020-5741-5.
16. Giorgi, F. Climate change hot-spots. *Geophys. Res. Lett.* **2006**, *33*, L08707. [CrossRef]
17. Hlačova, K.; Lapin, M.; Valent, P.; Szolgay, J.; Kohnova, S.; Rončak, P. Estimation of the impact of climate change-induced extreme precipitation events on floods. *Contrib. Geophys. Geod.* **2015**, *45*, 173–192. [CrossRef]
18. Forestieri, A.; Arnone, E.; Blenkinsop, S.; Candela, A.; Fowler, H.; Noto, L.V. The impact of climate change on extreme precipitation in Sicily, Italy. *Hydrol. Process.* **2018**, *32*, 332–348. [CrossRef]
19. Łupikasza, E.B.; Hanselb, S.; Matschullat, J. Regional and seasonal variability of extreme precipitationtrends in southern Poland and central-eastern Germany 1951–2006. *Int. J. Clim.* **2011**, *31*, 2249–2271. [CrossRef]
20. Scherrer, S.C.; Fischer, E.M.; Posselt, R.; Liniger, M.A.; Croci-Maspoli, M.; Knutti, R. Emerging trends in heavy precipitation and hot temperature extremes in Switzerland. *J. Geophys. Res. Atmos.* **2016**, 121. [CrossRef]
21. Bocheva, L.; Marinova, T.; Simeonov, P.; Gospodinov, I. Variability and trends of extreme precipitation events over Bulgaria (1961–2005). *Atmos. Res.* **2009**, *93*, 490–497. [CrossRef]
22. Ciric, D.; Nieto, R.; Ramos, A.M.; Drumond, A.; Gimeno, L. Wet Spells and Associated Moisture Sources Anomalies across Danube River Basin. *Water* **2017**, *9*, 615. [CrossRef]
23. Drumond, A.; Nieto, R.; Hernández, E.; Gimeno, L. A Lagrangian analysis of the variation in moisture sources related to drier and wetter conditions in regions around the Mediterranean basin. *Nat. Hazards Earth Syst. Sci.* **2011**, *11*, 2307–2320. [CrossRef]
24. Gómez-Hernández, M.; Drumond, A.; Gimeno, L.; Garcia-Herrera, R. Variability of moisture sources in the Mediterranean region during the period 1980–2000. *Water Resour. Res.* **2013**, *49*, 6781–6794. [CrossRef]
25. Sodemann, H.; Zubler, E. Seasonal and inter-annual variability of the moisture sources for Alpine precipitation during 1995–2002. *Int. J. Clim.* **2010**, *30*, 947–961. [CrossRef]
26. Gimeno, L.; Drumond, A.; Nieto, R.; Trigo, R.M.; Stohl, A. On the origin of continental precipitation. *Geophys. Res. Lett.* **2010**, *37*, L13804. [CrossRef]
27. Funk, C.; Peterson, P.; Landsfeld, M.; Pedreros, D.; Verdin, J.; Shukla, S.; Husak, G.; Rowland, J.; Harrison, L.; Hoell, A.; et al. The climate hazards infrared precipitation with stations—A new environmental record for monitoring extremes. *Sci. Data* **2015**, *2*, 150066. [CrossRef] [PubMed]
28. Stohl, A.; James, P. A Lagrangian analysis of the atmospheric branch of the global water cycle. Part I: Method description, validation, and demonstration for the August 2002 flooding in central Europe. *J. Hydrometeorol.* **2004**, *5*, 656–678. [CrossRef]
29. Stohl, A.; James, P. A Lagrangian analysis of the atmospheric branch of the global water cycle: Part II: Moisture transports between Earth's ocean basins and river catchments. *J. Hydrometeorol.* **2005**, *6*, 961–984. [CrossRef]
30. Dee, D.P.; Uppala, S.M.; Simmons, A.J.; Berrisford, P.; Poli, P.; Kobayashi, S.; Andrae, U.; Balmaseda, M.A.; Balsamo, G.; Bauer, P.; et al. The ERA-Interim reanalysis: Configuration and performance of the data assimilation system. *Q. J. R. Meteorol. Soc.* **2011**, *137*, 553–597. [CrossRef]
31. Ramos, A.M.; Trigo, R.M.; Liberato, M.L.R. A ranking of high-resolution daily precipitation extreme events for the Iberian Peninsula. *Atmos. Sci. Lett.* **2014**, *15*, 328–334. [CrossRef]
32. Ramos, A.M.; Trigo, R.M.; Liberato, M.L.R. Ranking of multi-day extreme precipitation events over the Iberian Peninsula. *Int. J. Clim.* **2017**, *37*, 607–620. [CrossRef]
33. Gittu, S. A study on Atmospheric Dispersion Using the Transport Model FLEXPART. University of Oslo, Department of Geosciences—Meteorology and Oceanography Section, 2011. Available online: https://www.duo.uio.no/bitstream/handle/10852/12594/guttu-master.pdf?sequence=1 (accessed on 21 August 2018).
34. An, X.; Yao, B.; Li, Y.; Li, N.; Zhou, L. Tracking source area of Shangdianzi station using Lagrangian particle dispersion model of FLEXPART. *Met. Apps* **2014**, *21*, 466–473. [CrossRef]
35. Numaguti, A. Origin and recycling processes of precipitating water over the Eurasian continent: Experiments using an atmospheric general circulation model. *J. Geophys. Res. Atmos.* **1999**, *104*, 1957–1972. [CrossRef]
36. Stohl, A.; Forster, C.; Frank, A.; Seibert, P.; Wotawa, G. Technical note: The Lagrangian particle dispersion model FLEXPART version 6.2. *Atmos. Chem. Phys.* **2005**, *5*, 2461–2474. [CrossRef]

37. Nieto, R.; Gimeno, L.; Drumond, A.; Hernandez, E. A Lagrangian identification of the main moisture sources and sinks affecting the Mediterranean area. *WSEAS Trans. Environ. Dev.* **2010**, *5*, 365–374.
38. Salah, Z.; Nieto, R.; Drumond, A.; Gimeno, L.; Vicente-Serrano, S.M. A Lagrangian analysis of the moisture budget over the Fertile Crescent during two intense drought episodes. *J. Hydrol.* **2018**, *560*, 382–395. [CrossRef]
39. Gimeno, L.; Nieto, R.; Trigo, R.M.; Vicente-Serrano, S.M.; Lopez-Moreno, J.I. Where Does the Iberian Peninsula Moisture Come from? An Answer Based on a Lagrangian Approach. *J. Hydrometeorol.* **2010**, *11*, 421–436. [CrossRef]
40. Nieto, R.; Gimeno, L.; Gallego, D.; Trigo, R.M. Contributions to the moisture budget of airmasses over Iceland. *Meteorol. Z.* **2007**, *16*, 037–044. [CrossRef]
41. Vázquez, M.; Nieto, R.; Drumond, A.; Gimeno, L. Extreme Sea Ice Loss over the Arctic: An Analysis Based on Anomalous Moisture Transport. *Atmosphere* **2017**, *8*, 32. [CrossRef]
42. Gimeno, L.; Stohl, A.; Trigo, R.M.; Domínguez, F.; Yoshimura, K.; Yu, L.; Drumond, A.; Durán-Quesada, A.M.; Nieto, R. Oceanic and Terrestrial Sources of Continental Precipitation. *Rev. Geophys.* **2012**, *50*, RG4003. [CrossRef]
43. Ivatek-Šahdan, S.; Stanešić, A.; Tudor, M.; Odak Plenković, I.; Janeković, I. Impact of SST on heavy rainfall events on eastern Adriatic during SOP1 of HyMeX. *Atmos. Res.* **2010**, *200*, 36–59. [CrossRef]
44. Cavicchia, L.; Scoccimarro, E.; Gualdi, S.; Marson, P.; Ahrens, B.; Berthou, S.; Dubois, C. Mediterranean extreme precipitation: A multi-model assessment. *Clim. Dyn.* **2016**, 1–13. [CrossRef]
45. Toreti, A.; Xoplaki, E.; Maraun, D.; Kuglitsch, F.G.; Wanner, H.; Luterbacher, J. Characterisation of extreme winter precipitation in the Mediterranean and associated anomalous atmospheric circulation patterns. *Nat. Hazard Earth Syst.* **2010**, *10*, 1037–1050. [CrossRef]
46. Schaller, N.; Otto, F.E.L.; van Oldenborgh, G.J.; Massey, N.R.; Sparrow, S.; Allan, M.R. The heavy precipitation event of May-June 2013 in the upper Danube and Elbe basins. *Bull. Am. Meteorol. Soc.* **2014**, *95*, S69–S72. Available online: https://pdfs.semanticscholar.org/b7f3/90dab80a8363a3ef415e601df5a63800b6ac.pdf (accessed on 21 August 2018).
47. Thévenot, O.; Bouin, M.-N.; Ducrocq, V.; Lebeaupin Brossier, C.; Nuissier, O.; Pianezze, J.; Duffourg, F. Influence of the sea state on Mediterranean heavy precipitation: A case-study from HyMeX SOP1. *Q. J. R. Meteorol. Soc.* **2014**, *142*, 377–389. [CrossRef]
48. Schicker, I.; Radanovics, S.; Seibert, P. Origin and transport of Mediterranean moisture and air. *Atmos. Chem. Phys.* **2010**, *10*, 5089–5105. [CrossRef]
49. Toreti, A.; Giannakaki, P.; Martius, O. Precipitation extremes in the Mediterranean region and associated upper-level synoptic-scale flow structures. *Clim. Dyn.* **2016**, *47*, 1925–1947. [CrossRef]
50. Romanescu, G.; Stoleriu, C.C. Exceptional floods in the Prut basin, Romania, in the context of heavy rains in the summer of 2010. *Nat. Hazards Earth Syst. Sci.* **2017**, *17*, 381–396. [CrossRef]
51. Ricard, D.; Ducrocq, V.; Auger, L. A climatology of mesoscale environment associated with Mediterranean heavy precipitating events over a Northwestern Mediterranean area. *J. Appl. Meteorol. Clim.* **2012**, *51*, 468–488. [CrossRef]
52. Mariani, L.; Prisi, S.G. Extreme Rainfalls in the Mediterranean Area. In *Storminess and Environmental Change: Climate Forcing and Responses in the Mediterranean Region*; Diodato, N., Bellocchi, G., Eds.; Springer: New York, NY, USA, 2014; pp. 17–39. ISBN 978-94-007-7947-1.
53. Pfahl, S. Characterising the relationship between weather extremes in Europe and synoptic circulation features. *Nat. Hazards Earth Syst. Sci.* **2014**, *14*, 1461–1475. [CrossRef]

water

MDPI

Article

The Mediterranean Moisture Contribution to Climatological and Extreme Monthly Continental Precipitation

Danica Ciric *, Raquel Nieto *, Lucia Losada, Anita Drumond and Luis Gimeno

EPhysLab (Environmental Physics Laboratory), Facultade de Ciencias, Universidade de Vigo, 32004 Ourense, Spain; lucialosadar@gmail.com (L.L.); anitadru@uvigo.es (A.D.); l.gimeno@uvigo.es (L.G.)

* Correspondence: cdanica@uvigo.es (D.C.); rnieto@uvigo.es (R.N.); Tel.: +34-988-387-248 (R.N.)

Received: 2 March 2018; Accepted: 19 April 2018; Published: 21 April 2018

check for updates

Abstract: Moisture transport from its sources to surrounding continents is one of the most relevant topics in hydrology, and its role in extreme events is crucial for understanding several processes such as intense precipitation and flooding. In this study, we considered the Mediterranean Sea as the main water source and estimated its contribution to the monthly climatological and extreme precipitation events over the surrounding continental areas. To assess the effect of the Mediterranean Sea on precipitation, we used the Multi-Source Weighted-Ensemble Precipitation (MSWEP) database to characterize precipitation. The Lagrangian dispersion model known as FLEXPART was used to estimate the moisture contribution of this source. This contribution was estimated by tracking particles that leave the Mediterranean basin monthly and then calculating water loss ($E - P < 0$) over the continental region, which was modelled by FLEXPART. The analysis was conducted using data from 1980 to 2015 with a spatial resolution of 0.25°. The results showed that, in general, the spatial pattern of the Mediterranean source's contribution to precipitation, unlike climatology, is similar during extreme precipitation years in the regions under study. However, while the Mediterranean Sea is usually not an important source of climatological precipitation for some European regions, it is a significant source during extreme precipitation years.

Keywords: extreme precipitation; Lagrangian approach; Mediterranean basin; moisture sinks

1. Introduction

Moisture transport from oceans to continents, precipitation, and evaporation are important elements in the hydrological cycle [1]. The connection between evaporation and precipitation on the planet is of great interest to present day meteorologists and hydrologists because of the importance of water resources on the quality of human life [2].

The reasons for precipitation in certain areas versus others may be explained through the presence of one (or more) of these factors: (i) the moisture already present in the atmosphere over the concerned areas, (ii) the transport of moisture by winds from another region, or (iii) moisture recycling. When we study each area over a longer period of time, we find that the contribution of the first source is low. We can, therefore, say that the two major sources of moisture that are responsible for precipitation in a region are advection and local evaporation [3].

Changes in global precipitation and in other categories of precipitation are significant for evaluating global climate change and its impacts. According to some studies, high precipitation events at present show an increasing trend in intensity and/or frequency [4,5]. Extreme events (such as droughts, floods, and landslides) and their changes in frequency and intensity as well as changes in the water cycle lead to major economic losses and human fatalities including in the Mediterranean area, which we study in this paper [6]. In addition, analysis of extreme precipitation trends and changes in water transport from the Mediterranean basin to different areas of the neighbouring continents is relevant for evaluating and predicting high precipitation events.

The Mediterranean region is very important for many sectors and has a huge impact on human life, natural processes, and the availability of water for different purposes [3] especially in Africa, Asia, and Europe [7]. Knowledge of the Mediterranean hydrological cycle and its variability may have a positive effect on the quality of human life in the Mediterranean area and increase socioeconomic benefits to this area.

1.1. Area in Study: The Mediterranean Region

The area of the Mediterranean basin or the Mediterranean area can be determined by considering the countries surrounding the Mediterranean Sea as well as the sea itself. The Mediterranean basin spans 3800 km east to west from the tip of Portugal to the shores of Lebanon and 1000 km north to south from Italy to Morocco and Libya, which have an area of 2.5 million km^2 and an average depth of 1500 m. The climate of the Mediterranean varies by geographic location, but, in general, it is characterized by hot, dry summers and wet, cool winters, which follows a traditional climate classification [8]. The mountainous terrain (the highest peak in the Alps are 4800 m high) around the Mediterranean basin (see Figure 1) has a significant impact on the climate and meteorology in the region. Moreover, the complex land-sea distribution with many islands, peninsulas, and inner seas around the basin [9] makes the region an interesting area in terms of meteorology since it determines important consequences in the atmospheric circulation and is the reason for many sub-regional and mesoscale characteristics.

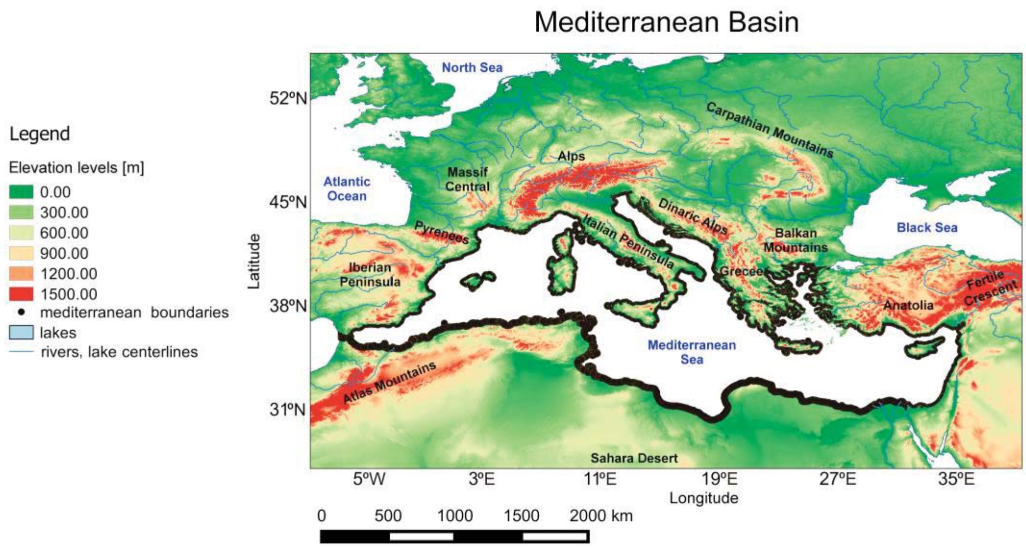

Figure 1. The black line contour indicates the area of the Mediterranean basin. The green-red colored portions represent elevation levels in meters (m). Data is taken from the HydroSHEDS project (Hydrological data and maps based on shuttle elevation derivatives at multiple scales (available online at https://hydrosheds.cr.usgs.gov).

The most significant characteristic of the Mediterranean region is its position between the subtropics and the mid-latitudes, which means it is affected by the regimes of both zones [10]. Some typical mid-latitude variability defines the precipitation pattern in this region. The climate there is mostly affected by the westward movement of storms, which originate from the Atlantic Ocean and affect the western European coasts in the winter [11]. The general precipitation in this region is mostly affected by the North Atlantic Oscillation (NAO) in the western Mediterranean region [12], the East Atlantic Oscillation (EAO) in the northern and eastern areas, and the Scandinavian Patterns or the eastern Atlantic/Western Russia pattern [9,10,13]. However, the subtropical southern part of the Mediterranean basin is affected by systems such as the Hadley Cell throughout its descending branch for many months of the year and by the Asian and African monsoons during the summer [14]. The influences of El Niño Southern Oscillation (ENSO), hurricanes, and the dust intrusions from the Sahara (see Reference [14] for a review or Reference [15]) should not be neglected. In the summer period, a dominant high-pressure system presents a strong positive geopotential anomaly in many parts of Europe including the area of the Mediterranean basin, which leads to a prevalence of dry conditions over the southern Mediterranean region [11]. These highlighted anomalies are associated with blocking conditions, subsidence, stability, a warm lower troposphere, and small pressure gradients at sea level as well as above-normal Mediterranean Sea surface temperatures [16].

1.1.1. Precipitation Patterns and Synoptic Climatological Configuration

The complex morphology of the region and the different interactions between several patterns of climate variability contribute to significant seasonal and annual differences in total precipitation, daily distribution, and geographical distribution [9]. The highest quantities of precipitation occur over the Adriatic coast and the Alpine region mainly during the summer and over the coast of Turkey and the Atlantic Iberian Peninsula border in the winter. During this time, there is more than 1200 mm of precipitation. The lowest quantities occur in the southeast region of the basin and over the northern coast of Africa with less than 400 m of precipitation and over the southern Iberian Peninsula in the summer [17–20].

Large-scale precipitation events in the western, central, and eastern Mediterranean are related to local anomalies of high moisture over the Mediterranean Sea [21] and those are influenced by remote positive source anomalies [22]. Many studies have pointed out the important role of remote sources for the occurrence of extreme precipitation events in the Mediterranean Basin [22–25], which is one of the aims of the present study.

If the Mediterranean basin is characterized by something peculiar, it is the highest number of heavy precipitation events (the aim of this work) with approximately 60% of those events occurring during the extended winter season [26]. During the period between September and May, which is characterized as the most precipitative period of the year, the accumulated rainfall contributes more than 80% of the total annual precipitation [12,27]. This is the case, for instance, in the Alpine region [28]. During the summer (the dry season), some locations in the Balkans and the Caucasus have also recorded significant amounts of precipitation [20]. This type of rainfall over the Mediterranean basin is due to several factors such as mesoscale convective systems, cyclones, upper synoptic-scale-level troughs, and large-scale circulation teleconnection patterns [16,29–32]. At the local scale, the intensity of precipitation depends on the temperature profile, the atmospheric moisture, and the convergence at lower levels. However, moisture content along with intense convection are essential components for generating intense precipitation [33]. Around 90% of heavy precipitation events are associated with cyclones [27]. In general, a higher frequency of extreme precipitation and its impact has been recorded in the north-western part of the basin [34].

Many studies have analyzed trends in the occurrence of extreme precipitation, which points out that their frequency, intensity, and impacts do not show homogenous behavior across the entire area [34,35]. For instance, a significant increasing trend in torrential or heavy rainfall events was reported in the Iberian and Italian Peninsulas while, for both regions, decreasing trends in light and moderate precipitation levels were observed [36]. Other studies on climate extremes have demonstrated that, over the Italian Peninsula, there are positive trends in the number of days with precipitation amounts greater than 10 mm while a negative trend has been demonstrated in the eastern part of the Mediterranean [37]. Another example of this lack of homogeneity is that opposite trends for extreme precipitation have been found over other regions such as Greece [38]. Knowledge of the behavior and the impact of extreme precipitation in the past and present is crucial to understanding future climate change effects, which could be more evident through extreme events [39] under study.

1.1.2. Moisture Transport and Effects

As discussed, precipitation is highly sensitive to the location of the cyclones over the region and variations in climate. However, the role of moisture is also equally important [1]. The Mediterranean Sea was identified in previous works as one of the main sources of moisture for continental precipitation on global [1] and regional scales [2,3,40,41]. In this sense, regional studies show that the Mediterranean basin acts as a moisture source, which contributes to the entire Northern Hemisphere with the greatest amount of precipitation occurring over the Mediterranean Sea itself during the summer [2,3,42] with a higher influence near it. The Mediterranean basin supports significant moisture, for instance among others, over the Danube River Basin [43], the Iberian Peninsula [44], Southern France [45,46], and Southern Switzerland [47]. However, it is important to highlight the different influences by the inner sub-basins. In this sense, the eastern Mediterranean basin mainly affects the Middle East and Northern-east Africa. While the Western Mediterranean basin influences the European continent [42] (mainly over the Iberian, Italian, and Balkan Peninsulas and France) and Northern-Western Africa [3,23] and the Central Mediterranean Sea contributes more to the Italian Peninsula and Northern-Central Africa [3,42], which exhibits a huge influence on extreme precipitation in the Alpine region [48] due to the intensification of the moisture uptake from the Mediterranean basin during the autumn and winter [22]. However, the Mediterranean influence on even more distant regions is also known and the moisture that reaches regions such as the Sahel [49,50], Central Asia, and the Arabian Peninsula [51] is not negligible. In addition, it has been demonstrated that changes in the moisture evaporation from the Mediterranean Sea affect the wetness or dryness of conditions over areas where it sinks [23,52,53].

In the context of a changing climate, measurements over the Mediterranean Sea for the last few decades (from 1958), reveal a positive trend in the balance of surface freshwater fluxes (evaporation minus precipitation) reaching about 182 millimeters per year. However, the tendency is due to a combination of two factors including the decrease in precipitation during the 1980s and the increase in evaporation during more recent decades [54]. These changes also affect the transport of moisture to the continent, which affects trends in extreme precipitation and intensifies the influence of oceanic moisture on continental precipitation [55].

One of the objectives in this study is to analyze the percentage of precipitation over the Mediterranean continental areas during the last four decades (1980 to 2016), which is due to moisture from the Mediterranean Sea. The analysis has been done grid by grid with a high resolution of 0.25° degrees in latitude and longitude, which extends the time-period and the resolution of all the previous analyses. Since the significant characteristic of the region is the presence of high rainfall, we have also computed the changes in the moisture contribution for extreme monthly precipitation to highlight the importance of this source of moisture during the maxima peaks of rainfall. Although the work has been done for all months, in this paper, we discuss the results for January and July, the central months for winter (December, January, and February), and the summer season (June, July, and August) in the Mediterranean region.

To understand and describe features of extreme precipitation for the Mediterranean region, it is important to remark on the processes related to the seasonal variation of precipitation. Therefore, for Europe and North Africa, a typical configuration is the presence of two permanent centers of geopotential action—the Icelandic Low and the Azores High—located around 30° N during January and moving northward toward the British Isles in July [56]. The climate type of the Mediterranean region is in concordance with this latitudinal belt positioned north of the Sahara, which is characterized by rainy winters (above 30° N) and dry summers (below 45° N) [56]. This is why, in this paper, the results are focused in January and July.

So, and in view of the importance of extreme rainfall over the region, the main objectives of this study are: (i) to quantify the monthly contribution of the Mediterranean source of moisture to the precipitation over the surrounding continental areas, and (ii) to analyze the percentage contribution of this source to the extreme precipitation, grid by grid, with the best current resolution.

To estimate the monthly moisture that comes from the Mediterranean Sea and contributes to the precipitation over the continent, we used the Lagrangian tool FLEXPART (FLEXible PARTicle) dispersion model in version 9.0, which was developed initially by Stohl and James [57,58] and fed with ERA-Interim reanalysis data. The high resolution Multi-Source Weighted-Ensemble Precipitation (MSWEP) dataset [59] was used to compute the monthly mean and extreme (by the mean composite of the five monthly higher values between 1980 to 2016) precipitation climatology grid by grid (0.25°) for the first time over the Mediterranean region.

2. Data and Method

2.1. MSWEP Precipitation Dataset

In this study, we used the monthly precipitation dataset, MSWEP [59,60], from January 1980 to December 2015. However, only results for January and July are shown and described in the text. MSWEP is a new precipitation dataset that has been accessible since the beginning of 2017. The MSWEP was developed to merge the highest quality available precipitation data as a function of timescale and location. To determine the regions with the monthly highest precipitation values, taken over a large time period, the resolution and precision of the database used is very important.

The MSWEP database is specially designed for hydrological modeling due its 0.25° × 0.25° spatial resolution in latitude and longitude with accumulated data based on three-hour time periods. The database combines the advantages of a wide range of precipitation information including gauges, satellites, and atmospheric reanalysis models to obtain precipitation information with the highest possible accuracy on a global scale, which makes it unique in comparison with other databases. The database used to characterize the highest precipitation values in the Mediterranean region on a monthly scale cover a temporal period from January 1980 to December 2015, which coincides with the available FLEXPART outputs.

The MSWEP precipitation dataset has been validated on a global scale using observations from approximately 60,000 gauges around the world and hydrological modeling of approximately 9000 catchments [60]. The results showed that MSWEP performs better compared to other precipitation databases such as CHIRPS, CMORPH-CRT, GPCP-1DD, GSMaP, PERSIANN-CCS, PERSIANN-CDR, WFDEI-CRU, and TMPA 3B42.

We have used the MSWEP monthly precipitation dataset to compute the monthly climatological precipitation values over the Mediterranean region between 30° W–65° E and 5° N–70° N. Checking grid by grid for each individual month, we ranked the maximum precipitation. Considering only five years with the most intense precipitation values for each grid point, we composed a study of climatology for the extreme years.

2.2. Sinks for the Mediterranean Sea Moisture Source

In this study, we used a Lagrangian approach to evaluate the role of the moisture transport from the Mediterranean basin. The moisture sink regions are computed using the outputs of a global simulation of the Lagrangian FLEXPART V9.0 model [43,61] with ERA-Interim reanalysis data input from the ECMWF (European Centre for Medium-Range Weather Forecast) [62]. The ERA-Interim dataset has 1° spatial resolutions on 60 vertical levels from 1000 to 0.1 hPa, which is available at each 6-h time interval. The FLEXPART experiment is based on dividing the global atmosphere into approximately 2.0 million particles (air masses or atmospheric particles) of constant mass (m), which are moved along their trajectories using a three-dimensional (3D) wind field while retaining their meteorological characteristics (given by the ERA-Interim data) as well as their individual position (latitude, longitude, and elevation). Therefore, computing changes in specific humidity (q) along the trajectories allows us to identify moisture sources and/or sink regions [57,58] if we follow the particles backward or forward in time, respectively. As commented on previously, the changes in specific humidity (q) allow us to identify those moments when and where the particles obtain moisture through evaporation (e) or lose moisture through precipitation (p). Those changes are outlined in the equation below.

$$e - p = m\,(dq/dt) \tag{1}$$

where m represents the mass of the particle. By adding, day by day, during the 10 days of analysis, the (e−p) for all the particles in the atmosphere over the area of interest, we can obtain instantaneous values of the surface freshwater flux (E − P) where (E) denotes the rate of evaporation and (P) denotes the rate of precipitation per unit area.

To identify the moisture sink regions in the Mediterranean area due to the moisture that comes from the Mediterranean basin, we conducted a forward experiment in time from January 1980 to December 2016. The surface freshwater flux (E − P) takes into account only those particles leaving the Mediterranean basin. Using the forward mode to follow the particles from our area of study, we track the trajectories of the particles for 10 days (the typically mean water vapor lifetime in the atmosphere at mid-latitudes [63]), with the aim to identify the regions where the particles lost humidity. This includes the sink regions where $E - P < 0$.

The Lagrangian approach has been widely used during the last several years in moisture transport analysis for the identification of moisture sources and sinks all around the globe [1,64]. The model includes many physical and dynamical parametrizations (see [65] for a technical description and the continuously update FLEXPART webpage https://www.flexpart.eu/wiki). In comparison to the other approaches applied to moisture transport analysis (for example, box models and isotopes), the Lagrangian approach is one of the most suitable tools for computing moisture source-sink relationships, which was pointed out by Gimeno et al. [64]. However, this model has some limitations. For instance, the quality of input data is crucial for reliable results. To minimize these type of errors, the choice of ERA-Interim may be justified in terms of its performance in reproducing the hydrological cycle and water balance closure better than other available reanalysis products [66,67]. Another main disadvantage is that the model cannot make calculations of E and P separately and E and P should always be taken into consideration as part of a balance between them [57,58,64]. Therefore, this P calculated from $E - P < 0$ is not exactly equal to real precipitation [57]. It represents the moisture transported for precipitation. Other sources of error are the limited resolution, uncertainties, and the interpolation of input data. Additionally, the trajectory errors could be higher especially in areas with low meteorological data coverage [68,69]. The developers of the model [57] state that such errors may cancel each other out given the large number of trajectories considered in the experiment and given the number of particles found in the typical grid used. For a complete description of the advantages and disadvantages, we recommend the review by Gimeno et al. [64].

With regard to the precipitation analysis, January and July results for the sinks of moisture from the Mediterranean Sea are shown in the main text while all the months are included in the supplementary material.

3. Results and Discussion

3.1. Climatological and Extreme MSWEP Monthly Precipitation

To calculate the climatological value of monthly precipitation (namely MSWEP-Cli), we used the global precipitation database from MSWEP. The analysis covers the temporal period from 1980 to 2015. In this work, we put the focus on January and July (see Figure 2) (see the results in the Supplementary Materials for all months, Figure S1).

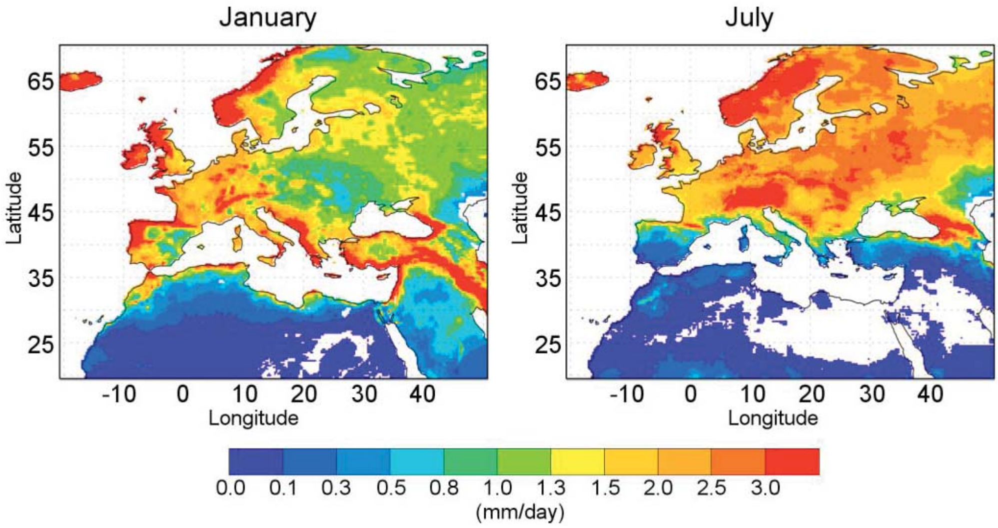

Figure 2. Monthly climatological values from MSWEP (0.25°) global precipitation database (MSWEP-Cli) for January (right panel) and July (left panel) over the area of Mediterranean basin for 1980–2015. Units in mm/day. White color over continents indicates where the MSWEP database does not report values.

Results show that the highest climatological precipitation values (greater than 2 mm/day) in January are recorded along the Atlantic coast from the Iberian Peninsula to the Scandinavian lands and over Central Europe, the Italian Peninsula, the Balkans, the Middle East, the Anatolian Peninsula coasts, and the Fertile Crescent arch. Most of the precipitation over the Atlantic coast and northern Europe is typically due to fronts associated with the transit of mid-latitude cyclones. In addition, if they flow over the continent, they can continue eastward up to the Middle East [70]. Higher precipitation in the Northern Mediterranean basin and northern Africa is also due to convective events [22] and those over the Fertile Crescent are associated with cyclone systems that reach the region from the Mediterranean Sea combined with a dominant moisture southern flux [71,72]. Yet, very low values of precipitation (lower than 0.3 mm/day) occur in the semi-arid and arid regions of Africa and Asia. During July, the highest climatological values of precipitation are recorded northward of 42° latitude including practically the entire Eurasian continent with the exception of the Iberian Peninsula (where very low values of less than 0.3 mm/day are recorded), Northern Africa, and Western Asia.

Since the Mediterranean region is characterized by intense precipitation, after identifying the climatological values, we have computed, grid by grid, the precipitation values of the five years that exhibit the greatest values during both January and July (see Figure S2 in Supplementary Materials for the remaining months). The maps concerning the mean values of these five years (hereafter MSWEP-extreme) are shown in Figure 3.

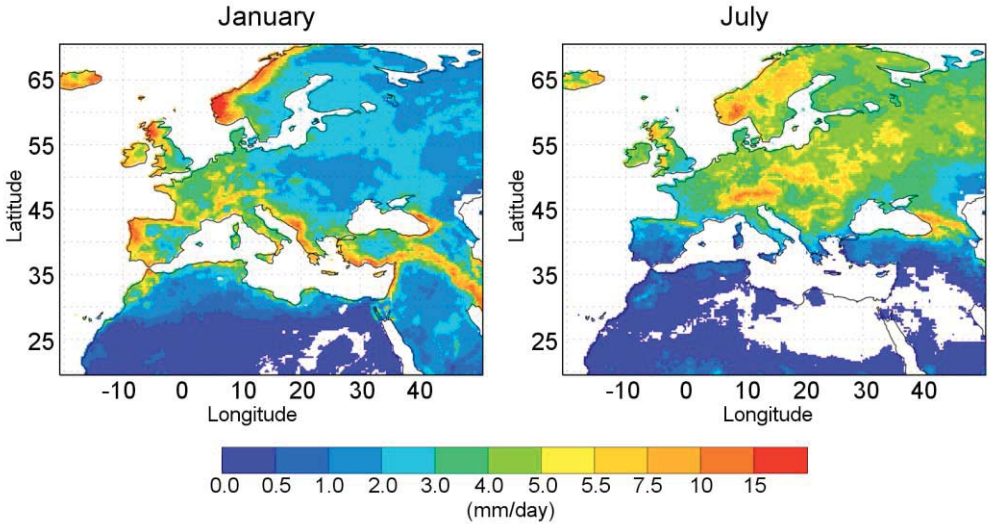

Figure 3. Mean precipitation for each grid point for the identified five years with the highest value of precipitation (MSWEP-extreme) for January (right panel) and July (left panel). Results are obtained from the MSWEP precipitation dataset, which considers a 36-year temporal period (1980–2015). Units in mm/day. White color over continents indicates where the MSWEP database does not report values during any of the five months computed.

This pattern during both months exhibits a similar configuration compared to climatological conditions (see Figure 2). The highest values (greater than 5.5 mm/day, orange colors) in January are observed over the western Iberian and Scandinavian Peninsulas, the eastern coast of the Adriatic Sea, the eastern Mediterranean coast and Fertile Crescent, and over some areas of the Italian Peninsula. In Eastern Europe and northern Asia, the MSWEP-extreme values are lower and range between 0.5 and 2 mm/day. During July, the highest values of MSWEP-extreme (>5.5 mm/day) are mainly exhibited in the central part of the Euro-Asiatic continent, which highlights elevated terrains as the Alpine region, the Scandinavian Peninsula, and regions over the Carpathian Mountains. The plot also shows higher values over Central Africa below 15° N. However, this area is outside the Mediterranean region.

The ratio between these precipitation measurements (MSWEP-Cli divided by MSWEP-extreme) are plotted in Figure 4. This ratio highlights the areas where there is a greater difference between the climatology and the extreme precipitation (indicating that extreme precipitation occurs in a few isolated events but is important in quantity). However, ratio values around one (ratio $\approx$ 1) show the areas where precipitation quantities do not exhibit considerable change over the studied time period. For both months (see Figure S3 in Supplementary Materials for the remaining months), the results generally show that the ratio is higher in the arid and semiarid regions of Northern Africa, the Middle East, and the southern Iberian Peninsula where MSWEP-Cli values are very low (especially during July). In these areas, precipitation for extreme years can be as high as five times the climatological values. During January, values for MSWEP-extreme are twice the climatological values over central Europe, which shows that extreme precipitation modulates the mean climatological value. It is particularly interesting that the MSWEP-extreme over the Mediterranean coast of the Balkan, Greek, and Anatolian Peninsulas is twice the value of MSWEP-Cli. The South-western Iberian Peninsula also shows a particular behaviour. This region is characterized by higher values in both measurements and the ratio is also elevated with values over three. Therefore, in January, this region was affected by systems that bring extreme precipitation, which mostly determine its climatological value. In July, the highest ratio values, in addition to the already discussed dry areas, are located along the northern Mediterranean coast including the coast of France, Italy, Greece, and Turkey. In the Alpine regions such as the Scandinavian and Carpathian mountains where climatological precipitation values reached a maximum in both cases, the ratio is among the lowest, which indicates that these areas commonly experience extreme precipitation during the summer.

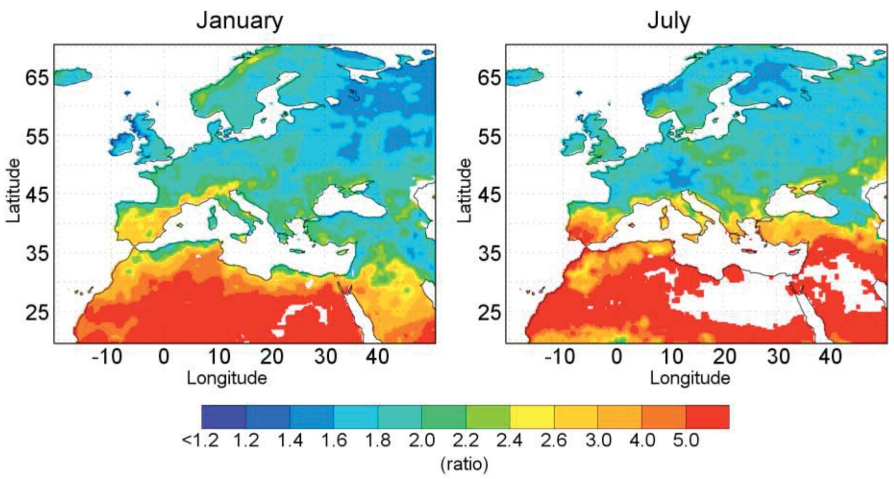

Figure 4. Ratio between MSWEP-extreme and MSWEP-Cli during January (right panel) and July (left panel). White areas over the continent indicate where the MSWEP database does not report values.

3.2. Climatological and Extreme FLEXPART Monthly Precipitation with Origin in the Mediterranean Sea

To identify the major climatological monthly moisture sinks for the Mediterranean region, we tracked the air masses (the particles) residing in the atmosphere over the Mediterranean Sea forward in time for ten days from 1980 to 2016 every six hours. We computed month by month the balance of $E - P$ for each grid point (as described in the methodology using the outputs of the FLEXPART model) and we maintained only monthly negative values ($(E - P) < 0$) to identify those areas where precipitation (P) exceeds evaporation (E) in the net moisture budget. Monthly positive values are removed. The final mean accumulated $(E - P) < 0$ over land (hereafter, PFLEX-Cli in this paper) shows the moisture sink regions for the moisture that comes from the Mediterranean Sea and produces precipitation over the neighborhood continental areas. January and July PFLEX-Cli values are shown in Figure 5 (see the results in the Supplementary Materials for all months, Figure S4). Colored areas are the sink for the Mediterranean moisture including those regions with precipitation.

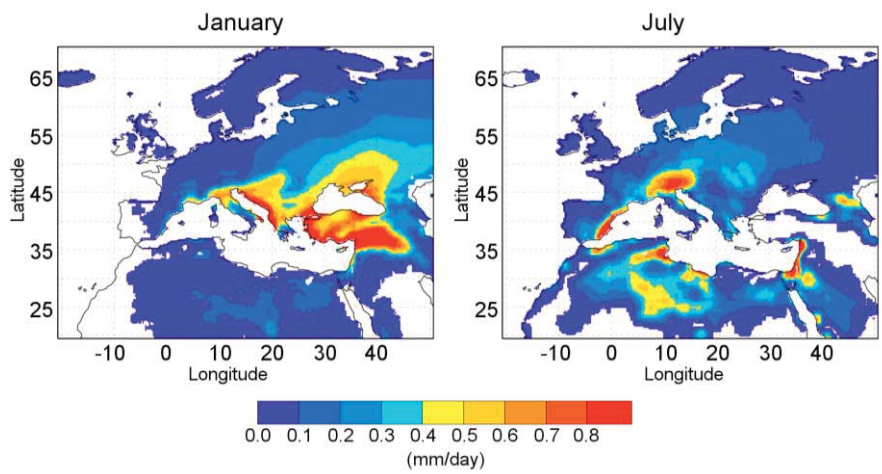

Figure 5. Monthly-averaged value of $E - P < 0$ integrated over ten days (PFLEX-Cli) between 1980 to 2015 obtained from the forward Lagrangian experiment for Mediterranean Sea during January (right panel) and July (left panel). Units in mm/day. White areas over continent are regions not influenced by the Mediterranean moisture.

During January, the pattern of PFLEX-Cli has an eastern shift, which follows the mean winter general circulation in this latitude. The main moisture Mediterranean influence for precipitation occurs over the eastern areas. The highest values are found over the regions close to the Mediterranean Sea (reddish colours, >0.5 mm/day) over the Balkan Peninsula, pre-Alpine region, the Middle East, Turkey, the Fertile Crescent, and the northern Black Sea. By contrast, during July, the highest values do not exhibit this displacement and the PFLEX-Cli is based on the local source of moisture. The main affected areas are recorded over the eastern Iberian Peninsula, the Alps, the western Middle East, and Northern Africa (Saharan regions to the north of Ahaggar and Tibesti massifs that include Algeria, Tunisia, and Libya).

We have also conducted a grid-by-grid computation of the precipitation generated by moisture coming from the Mediterranean Sea and calculated by the Lagrangian experiment for the same five years of maximum precipitation used to compute MSWEP-extreme. These extreme $E - P < 0$ monthly values, hereafter PFLEX-extreme, for January and July are shown in Figure 6 (see Figure S5 in Supplementary Materials for the remaining months). Both patterns exhibit a similar geographical distribution to those recorded by PFLEX-Cli.

Compared to MSWEP maps (see Figures 2 and 3), both PFLEX values are, as expected, lower because they exhibit only the portion of the precipitation that originates in the Mediterranean Sea.

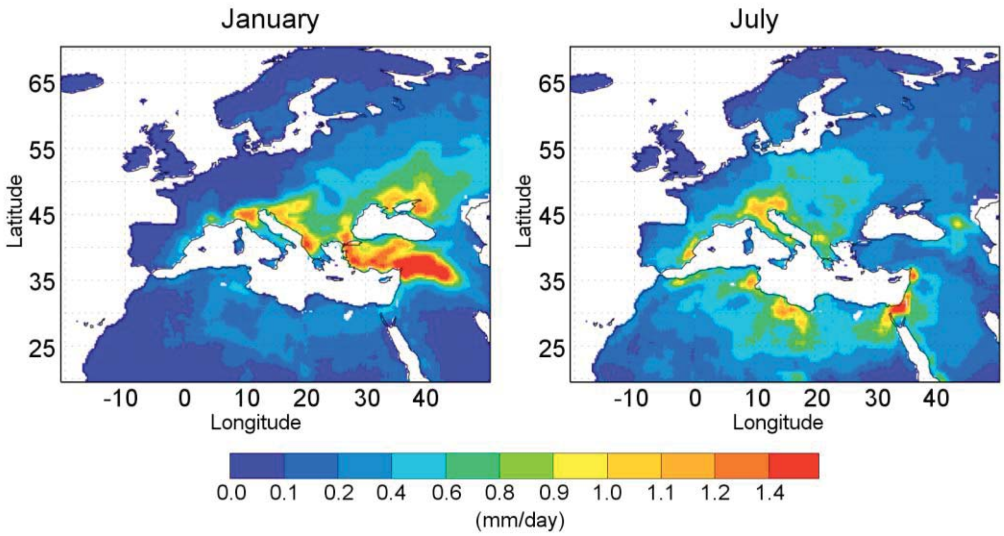

Figure 6. Mean precipitation for each grid point was calculated by the Lagrangian experiment for moisture originating from the Mediterranean Sea (PFLEX-extreme) for the same five years, which was identified as MSWEP-extreme in January (right panel) and July (left panel) for a 36-year temporal period (1980–2016). Units in mm/day. White color over continents indicates where the PFLEX does not report values during any of the five months computed.

As for MSWEP data, we show in Figure 7 the ratio between PFLEX-Cli and PFLEX-extreme.

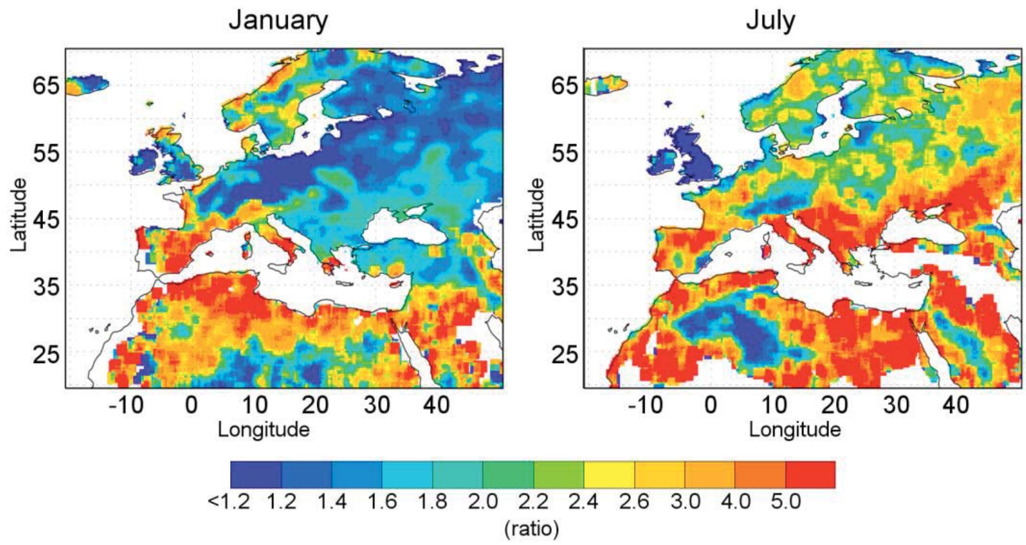

Figure 7. Ratio between the mean values of the observed five years with highest values of E − P < 0, calculated using FLEXPART (PFLEX-extreme), and the mean climatological values of E − P < 0 (PFLEX-Cli) during January (right panel) and July (left panel), which is calculated for each grid point. Period: 1980–2016. White areas over the continent indicate where the PFLEX-Cli does not report values.

For both central months, January in the winter and July in the summer (see Figure S6 in Supplementary Materials for the remaining months), the results show that the ratio has higher values (reddish colors, greater than 3) in the semi-arid and arid regions of Northern Africa, Middle Eastern coast, and Iberian and Italian Peninsulas. These high ratio values denote that, in those areas, a greater amount of moisture comes from the Mediterranean Sea when compared to local sources during extreme events (PMWEP-extreme). It is important to emphasize the differences between January and July over the Alpine region, the Balkans, and the Greek areas as well as the eastern longitudes. Both exhibit contrary behavior in the sense that the contribution by the Mediterranean moisture is very important for the extreme precipitation over the Alpine region (ratio values up to 5) during the winter while the contribution to extreme precipitation is close to the PFLEX-Cli values (ratio values around 1, bluish colors) during the summer.

However, during July, PFLEX-extreme exhibits notable differences compared to PFLEX-Cli over the Balkan Peninsula, Ukraine, Georgia, and western Turkey (reddish colors), which indicates that in these areas, extreme precipitation events are mostly present during the summer period when the moisture comes from the Mediterranean Sea.

Very similar amounts of precipitation during PFLEX-Cli and PFLEX-extreme are recorded in Central and Western Europe in January. During July, the difference is more notable since PFLEX-extreme values are more than twice the PFLEX-Cli values (ratio up to 2).

3.3. Identification of Differences between FLEXPART and MSWEP Climatological Monthly Precipitation and Extreme Monthly Precipitation

To show the influence of the Mediterranean Sea moisture in the rainfall tracked during the winter (January) and the summer (July) (see the results in the Supplementary Materials for all months, Figure S7), we have calculated the percentage between the mean climatological value of precipitation obtained via the forward Lagrangian experiment (PFLEX-Cli) and the monthly climatological precipitation in the Mediterranean region (MSWEP-Cli) using the MSWEP precipitation dataset (see Figure 8).

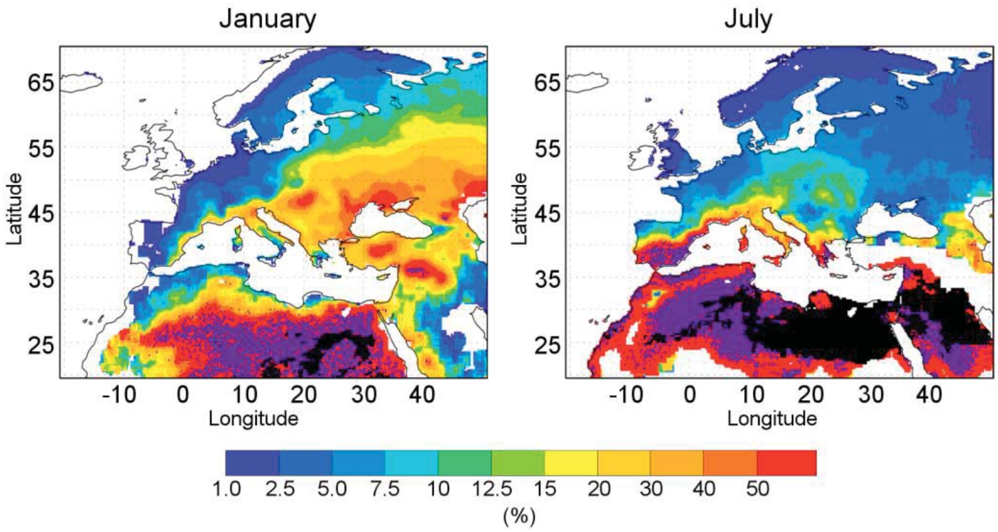

Figure 8. Monthly climatological percentage of the Mediterranean moisture contribution (PFLEX-Cli) to precipitation (MSWEP-Cli) during January (right panel) and July (left panel). Violet represents percentage values of 100% and a black color indicates those regions where the MSWEP precipitation dataset does not show values. White areas are those regions where PFLEX-Cli does not report values.

The results show that, for both months, the Mediterranean moisture had the highest contribution to the total precipitation over semiarid and arid regions in Africa (values greater than 40%, reddish colors). These results are in concordance with other studies that suggest the Mediterranean Sea is an important moisture source of precipitation over Eastern-North Africa [52]. Focusing on the European continent, during January, higher values were recorded over Ukraine, Turkey, some parts of Russia, Kazakhstan, Uzbekistan, and the Middle East. The amount of precipitation from these areas is more than twice the moisture that comes from the Mediterranean Sea. However, more than 20% of the precipitation of Eastern Europe comes from the Mediterranean moisture. This pattern changes during the summer (July) when the Mediterranean Sea contributes more rain (up to 40%) to the mean climatological precipitation in areas around the southern Iberian Peninsula, Italian Peninsula, and Middle East coasts. These regions are typically sinks for moisture originating from the Mediterranean [42,46,52,73].

The same computation was done to check the percentage difference between monthly extreme precipitation values (PFLEX-extreme versus MSWEP-extreme) over five years with maximum grid-by-grid values during January and July (see Figure 9) (see Figure S8 in Supplementary Materials for the remaining months).

The patterns of these results are quite similar to that exhibited in Figure 8. This indicates that the moisture contribution from the Mediterranean Sea to extreme precipitation events are of the same proportion as the contribution to the mean climatology. However, they also explain that extreme precipitation in the area is caused by moisture from the Mediterranean source over North Africa, Eastern Europe, and the Anatolian Peninsula during January and the influence is most concentrated along the Mediterranean Sea borders during July.

To highlight the different Mediterranean precipitation contributions by percentage toward extreme events and climatology, Figure 10 shows the differences between the plots in Figures 8 and 9 (see Figure S9 in Supplementary Materials for the remaining months).

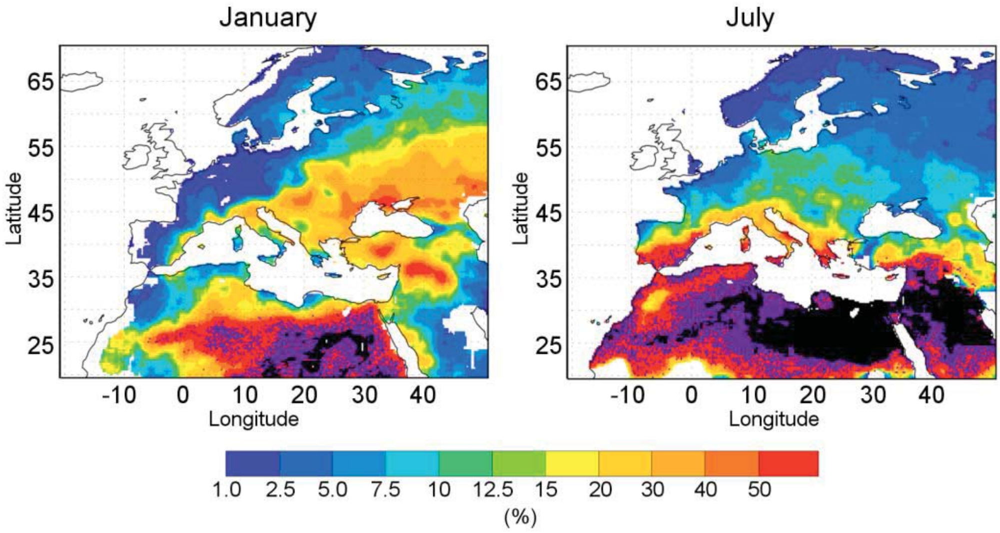

Figure 9. Similar to Figure 8 but comparing the percentage between PFLEX-extreme and MSWEP-extreme during January (right panel) and July (left panel). White areas over the continent indicate where the PFLEX-Cli does not report values. Violet represents percentage values of 100% and the black color indicates those regions where the MSWEP precipitation dataset does not show values.

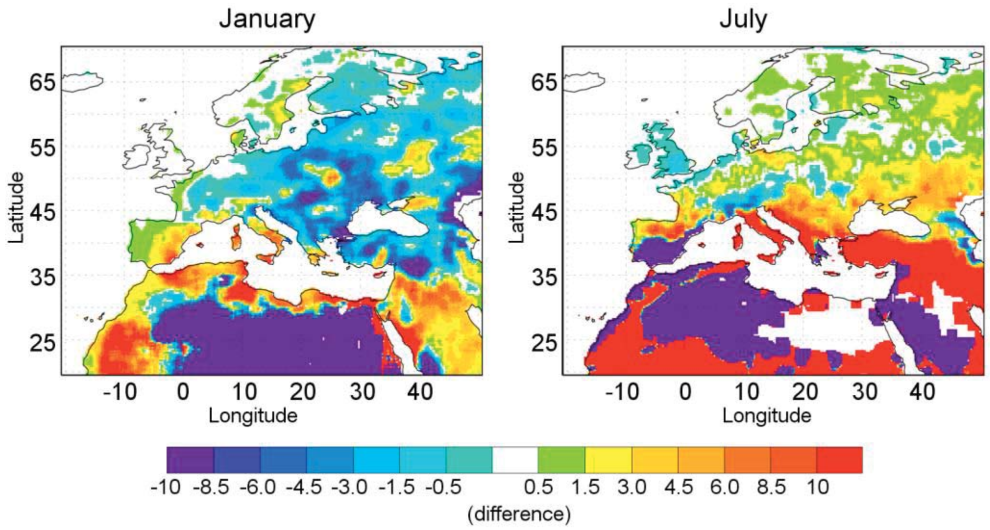

Figure 10. Difference between the percentages of the moisture from the Mediterranean Sea supplied to extreme events (see Figure 9) and to the mean climatology (see Figure 8).

This last figure shows where the Mediterranean moisture supplied to extreme events was higher (or lower) than the climatological mean values. Generally, the Mediterranean supplies more moisture to extreme events (reddish colors) in the southern and western borders of the basin during January and over the northern side during July. The contribution to the mean values (bluish colors) was highest over central Europe in January and over the Alps and the Carpathian Mountains as well as the British Isles during June. The arid regions over Africa always received a smaller percentage of contribution during extreme events.

4. Summary and Conclusions

In this work, we estimated the contribution of the Mediterranean Sea as the main moisture source of the monthly precipitation over the surrounding continental areas. We analyzed both the mean climatological behavior and the extreme values. The analysis was done in three steps. First, we characterized the precipitation patterns for both the 1980–2015 climatology and the five extreme years, grid by grid, by using the MSWEP database. Next, we estimated the moisture contribution from the Mediterranean basin to the precipitation through the Lagrangian FLEXPART model for both monthly climatological values and five-year values, grid by grid, which was demonstrated in step one. Finally, we compared both patterns, precipitation and contribution, by calculating the differences between them.

The monthly mean climatological precipitation (MSWEP-Cli) shows a clear dichotomy between the winter and summer. During January, the highest rainfall values were recorded along the European Atlantic coast and parts of Central Europe due to the typical frontal precipitation associated with cyclones over the northern and eastern limits of the basin and the Fertile Crescent due to convective systems. However, during July, the pattern shows its maximum values for covering practically the entire Eurasian continent with the exception of the Iberian and Anatolian Peninsulas and northern Africa. The analysis of the monthly mean extreme values of precipitation (MSWEP-extreme) shows that the pattern is similar to the climatological one. The highest values in January occur over areas in the Western Iberian Peninsula, Northern British Isles, Scandinavia, the eastern coast of the Adriatic Sea, Southern Anatolian Peninsula, and the Fertile Crescent reaching north of the Persian Gulf. During July, higher values of MSWEP-extreme are also expressed in the central part of the Euro-Asiatic continent, which highlights the peaks over the Alps and the Carpathian and Scandinavian Mountains. When the ratio of the climatology and extreme events is analyzed, it becomes evident that extreme precipitation is modulated over some parts of the continental Mediterranean region compared to the mean climatological values. This behavior is clear over arid and semi-arid regions including southern Iberian Peninsula during both seasons when the extreme events yield values greater than three times the mean precipitation. Over the Anatolian and southern Greek Peninsulas, this event occurs in July. However, it is also remarkable that, in the same areas, this ratio reaches lower values, which indicates that, throughout the analyzed period (36 years), precipitation is quite regular. This occurs over elevated terrains such as the Alps and the Carpathian and Scandinavian Mountains, which commonly experience extreme precipitation.

The analysis of the contribution of the Mediterranean basin to the precipitation over land showed that climatologically (PFLEX-Cli) during January, the main moisture sink areas for the moisture coming from the Mediterranean basin are found over the North-eastern Mediterranean region with a clear eastern shift caused by westerly winds. During July, when the values are smaller, the areas affected are more local (with a high impact over the Alpine region, the eastern Iberian Peninsula, Middle East, and northern Africa).

The contribution of the Mediterranean moisture to the extreme precipitation (PFLEX-extreme) shows similar geographical distribution patterns in both months as those recorded by PFLEX-Cli. The arid regions could be positively biased by the overestimation of PFLEX-Cli and PFLEX-extreme if we compare the precipitation simulated by the model and the MSWEP data. PFLEX represents the moisture available for precipitation since it is pointed in the methodology.

When MSWEP-extreme and PFLEX-extreme precipitation values are compared, PFLEX-extreme values are, as expected, lower because PFLEX only computes those amounts of continental precipitation with origin in the Mediterranean Sea. The ratio between PFLEX-Cli and PFLEX-extreme shows that the contribution of the Mediterranean Sea to extreme events during both boreal months is most pronounced over the Iberian and Italian Peninsula, Middle East coast, and in the desert regions of Northern Africa where the ratio can be up to three times the climatological precipitation values. An interesting case appears over the Alpine regions and over the Balkan and the Greek Peninsulas where the ratio exhibits opposite behavior during the winter and summer. During the winter, the Mediterranean Sea is the most important provider of moisture (ratio approximately 5) for extreme precipitation while, during the summer, the contribution is quite similar to PFLEX-Cli (ratio approximately 1). In Central and Western Europe, a similar pattern is recorded in January when the ratio is around 1. These values show that PFLEX-Cli and PFLEX-extreme exhibit quite similar amounts of precipitation.

The Mediterranean contribution and the precipitation was compared with respect to the difference between MSWEP and PFLEX climatological monthly and extreme monthly recorded precipitation. The difference was analyzed for two fields of the precipitation, which includes the percentage difference between PFLEX-Cli and MSWEP-Cli and the percentage difference between PFLEX-extreme and MSWEP-extreme. The results show that, for the first case, the Mediterranean Sea contributes significantly to total precipitation (around 40%) in both months in semi-arid and arid regions of Africa while the European continent results differ depending on the season. Therefore, during January, the Mediterranean Sea contributes more than twice the precipitation recorded in areas over Ukraine, Turkey, and the European part of Russia. In July, the Italian and Iberian Peninsulas are the most affected areas where the moisture originating from the Mediterranean Sea can be greater than 40%, which was confirmed by numerous studies conducted in these regions. The Mediterranean Sea has been detected as the main moisture source [42,52]. For the second case, the percentage between PFLEX-extreme and MSWEP-extreme exhibits quite similar behavior to the percentage between monthly climatological precipitation values. From the climatological point of view, during the winter season, the rainfall contribution from the Mediterranean Sea is highest over Central Europe (the Alps and the Carpathian Mountains), but, in the summer, the precipitation values originating from the Mediterranean are highest around the British Isles. During extreme events, the Mediterranean Sea is declared as the main moisture provider in the southern and western parts of the basin during January while, during July, this contribution is exhibited more over the northern side. The semi-arid and arid regions in Africa are areas where the Mediterranean contributes the least to extreme precipitation.

To summarize, the results showed that the spatial pattern of rainfall contribution from the Mediterranean source is similar for extreme precipitation years when compared to climatology. However, significant differences could occur locally particularly in any European region where the Mediterranean is not an important regular source for climatological precipitation but is a significant source in extreme precipitation years.

Supplementary Materials: The following are available online at http://www.mdpi.com/2073-4441/10/4/519/s1, Figure S1: As Figure 2 but for all months, Figure S2: As Figure 3 but for all months, Figure S3: As Figure 4 but for all months, Figure S4: As Figure 5 but for all months, Figure S5: As Figure 6 but for all months, Figure S6: As Figure 7 but for all months, Figure S7: As Figure 8 but for all months, Figure S8: As Figure 9 but for all months, and Figure S9: As Figure 10 but for all months.

Funding: Danica Ciric is supported by the European Commission under the Erasmus Mundus Project Green-Tech-WB: Smart and Green Technologies for Innovative and Sustainable Societies in the Western Balkans (551984-EM-1-2014-1-ES-ERA Mundus-EMA2). This research was partially supported by Xunta de Galicia under project ED413C 2017/64 “Programa de Consolidacion e Estructuracion de Unidades de Investigacion Competitivas (Grupos de Referencia Competitiva)” co-funded by the European Regional Development Fund (FEDER).

Author Contributions: Danica Ciric, Raquel Nieto, and Luis Gimeno conceived and designed the experiments. Danica Ciric and Lucia Losada performed the experiments. Danica Ciric, Raquel Nieto, Anita Drumond, and Luis Gimeno analyzed the data. Danica Ciric and Raquel Nieto wrote the paper.

Conflicts of Interest: The authors declare no conflict of interest. The founding sponsors had no role in the design of the study, in the collection, analyses, or interpretation of data, in the writing of the manuscript, and in the decision to publish the results.

Abbreviations

The following abbreviations are used in this manuscript:

ECMWF	European Centre for Medium-Range Weather Forecast
ERA	European Centre for Medium-Range Weather Forecasting Re-Analysis
FLEXPART	FLEXible PARTicle dispersion model
HydroSHEDS	Hydrological data and maps based on Shuttle elevation derivatives at multiple scales
MSWEP	Multi-Source Weighted-Ensemble Precipitation
MSWEP-Cli	Monthly climatological value from MSWEP global precipitation database

MSWEP-extreme	Mean precipitation for the identified 5 years with the highest value of precipitation from MSWEP global precipitation database
PFLEX-Cli	Monthly averaged value of E - P < 0 integrated over 10 days obtained from the forward Lagrangian experiment
PFLEX-extreme	Mean precipitation for the identified 5 years with the highest value of precipitation from FLEXPART monthly precipitation data

References

1. Gimeno, L.; Drumond, A.; Nieto, R.; Trigo, R.M.; Stohl, A. On the origin of continental precipitation. *Geophys. Res. Lett.* **2010**, *3*, L13804. [CrossRef]
2. Gomez-Hernandez, M.; Drumond, A.; Gimeno, L.; Garcia-Herrera, R. Variability of moisture sources in the Mediterranean region during the period 1980–2000. *Water Resour. Res.* **2013**, *49*, 6781–6794. [CrossRef]
3. Nieto, R.; Gimeno, L.; Drumond, A.; Hernandez, E. A Lagrangian identification of the main moisture sources and sinks affecting the Mediterranean area. *WSEAS Ttrans. Environ. Dev.* **2010**, *6*, 1790–5079.
4. Westra, S.; Alexander, L.V.; Zwiers, F.W. Global Increasing Trends in Annual Maximum Daily Precipitation. *J. Clim.* **2013**, *26*, 3904–3918. [CrossRef]
5. Alexander, L.V.; Zhang, X.; Peterson, T.C.; Caesar, J.; Gleason, B.; Klein Tank, A.M.G.; Haylock, M.; Collins, D.; Trewin, B.; Rahimzadeh, F.; et al. Global observed changes in daily climate extremes of temperature and precipitation. *J. Geophys. Res.* **2006**, *111*, D05109. [CrossRef]
6. EASAC. *Trends in Extreme Weather Events in Europe: Implications for National and European Union Adaptation Strategies*; EASAC Policy Report 22; European Academies Science Advisory Council: Halle, Germany, 2013. Available online: www.easac.eu (accessed on 30 October 2017).
7. Gualdi, S.; Somot, S.; Li, L.; Artale, V.; Adani, M.; Bellucci, A.; Braun, A.; Calmanti, S.; Carillo, A.; Dell'Aquila, A.; et al. The CIRCE Simulations Regional Climate Change Projections with Realistic Representation of the Mediterranean Sea. *Bull. Am. Meteorol. Soc.* **2013**, *94*, 65–81. [CrossRef]
8. Köppen, W. Versuch einer Klassifikation der Klimate, vorzugsweise nach ihren Beziehungen zur Pflanzenwelt. *Geographische Zeitschrift* **1990**, *6*, 593–611.
9. Lionello, P.; Malanotte-Rizzoli, P.; Boscolo, R.; Alpert, P.; Artale, V.; Li, L.; Luterbacher, J.; May, W.; Trigo, R.; Tsimplis, M.; et al. The Mediterranean climate: An overview of the main characteristics and issues, Mediterranean Climate Variability. *Dev. Earth Environ. Sci.* **2006**, *4*, 1–26. [CrossRef]
10. Trigo, R.; Xoplaki, E.; Zorita, E.; Luterbacher, J.; Krichak, S.O.; Alpert, P.; Jacobeit, J.; Saenz, J.; Fernandez, J.; González-Rouco, F.; et al. Relations between variability in the Mediterranean region and mid-latitude variability. *Dev. Earth Environ. Sci.* **2006**, *4*, 179–226. [CrossRef]
11. Giorgi, F.; Lionello, P. Climate Change Projections for the Mediterranean Region. *Glob. Planet. Chang.* **2008**, *63*, 90–104. Available online: https://www.researchgate.net/publication/223492610_Climate_change_projections_for_the_Mediterranean_region#pff (accessed on 28 September 2017). [CrossRef]
12. Hurrell, J.W. Decadal trends in the North Atlantic Oscillation: Regional temperature and precipitation. *Science* **1995**, *269*, 676–679. [CrossRef] [PubMed]
13. Trigo, R.M.; Valente, M.A.; Trigo, I.F.; Miranda, P.; Ramos, A.M.; Paredes, D.; Garcıa-Herrera, R. North Atlantic wind and cyclone trends and their impact in the European precipitation and Atlantic significant wave height. *Ann. N.Y. Acad. Sci.* **2008**, *1146*, 212–234. [CrossRef] [PubMed]
14. Alpert, P.; Baldi, M.; Ilany, R.; Krichak, S.; Price, C.; Rodo, X.; Saaroni, H.; Ziv, B.; Kishcha, P.; Barkan, J.; et al. Relations between climate variability in the Mediterranean region and the tropics: ENSO, South Asian and African monsoons, hurricanes and Saharan dust. *Dev. Earth Environ. Sci.* **2006**, *4*, 149–177. [CrossRef]
15. Krichak, S.; Breitgand, J.S.; Gualdi, S.; Feldstein, S.B. Teleconnection–extreme precipitation relationships over the Mediterranean region. *Theor. Appl. Climatol.* **2014**, *117*, 679–692. [CrossRef]
16. Xoplaki, E.; González-Rouco, J.F.; Luterbacher, J.; Wanner, H. Wet season Mediterranean precipitation variability: Influence of large-scale dynamics and trends. *Clim. Dyn.* **2004**, *23*, 63–78. [CrossRef]
17. Schönwiese, C.D.; Rapp, J. *Climate Trend Atlas of Europe Based on Observations 1891–1990*; Kluwer Academic Publishers: Dordrecht, Netherlands; Boston, MA, USA; London, UK, 1997.
18. Kadoglu, M.; Tulunay, Y.; Borhan, Y. Variability of Turkish precipitation compared to E1 Niño Events. *Geophys. Res. Lett.* **1991**, *26*, 1597–1600. [CrossRef]

19. Trigo, R.M.; Palutikof, J.P. Precipitation Scenarios over Iberia: A Comparison between Direct GCM Output and Different Downscaling Techniques. *J. Clim.* **2001**, *14*, 4422–4446. [CrossRef]
20. Lelieveld, J.; Hadjinicolaou, P.; Kostopoulou, E.; Chenoweth, J.; El Maayar, M.; Giannakopoulos, C.; Hannides, C.; Lange, M.A.; Tanarhte, M.; Tyrlis, E.; et al. Climate change and impacts in the Eastern Mediterranean and the Middle East. *Clim. Chang.* **2012**, *114*, 667–687. [CrossRef] [PubMed]
21. Raveh-Rubin, S.; Wernli, H. Large-scale wind and precipitation extremes in the Mediterranean: A climatological analysis for 1979–2012. *Q. J. R. Meteorol. Soc.* **2015**, *141*, 2404–2417. [CrossRef]
22. Winschall, A.; Sodemann, H.; Pfahl, S.; Wernli, H. How important is intensified evaporation for Mediterranean precipitation extremes? *J. Geophys. Res. Atmos.* **2014**, *119*, 5240–5256. [CrossRef]
23. Ciric, D.; Nieto, R.; Ramos, A.M.; Drumond, A.; Gimeno, L. Wet Spells and Associated Moisture Sources Anomalies across Danube River Basin. *Water* **2017**, *9*, 615. [CrossRef]
24. Knippertz, P.; Martin, J.E. Tropical plumes and extreme precipitation in subtropical and tropical West Africa. *Q. J. R. Meteorol. Soc.* **2005**, *131*, 2337–2365. [CrossRef]
25. Pinto, J.G.; Ulbrich, S.; Parodi, A.; Rudari, R.; Boni, G.; Ulbrich, U. Identification and ranking of extraordinary rainfall events over Northwest Italy: The role of Atlantic moisture. *J. Geophys. Res. Atmos.* **2013**, *118*, 2085–2097. [CrossRef]
26. Toreti, A.; Xoplaki, E.; Maraun, D.; Kuglitsch, F.G.; Wanner, H.; Luterbacher, J. Characterisation of extreme winter precipitation in the Mediterranean and associated anomalous atmospheric circulation patterns. *Nat. Hazard Earth Syst.* **2010**, *10*, 1037–1050. [CrossRef]
27. Gaetani, M.; Baldi, M.; Dalu, G.A.; Maracchi, G. Jetstream and rainfall distribution in the Mediterranean region. *Nat. Hazard Earth Syst. Sci.* **2011**, *11*, 2469–2481. [CrossRef]
28. Molinié, G.; Ceresetti, D.; Anquetin, S.; Dominique Creutin, J.; Boudevillain, B. Rainfall Regime of a Mountainous Mediterranean Region: Statistical Analysis at Short Time Steps. *J. Appl. Meteorol. Climatol.* **2012**, *51*, 429–448. [CrossRef]
29. Dayan, U.; Nissen, K.; Ulbrich, U. Review Article: Atmospheric conditions inducing extreme precipitation over the eastern and western Mediterranean. *Nat. Hazards Earth Syst. Sci.* **2015**, *15*, 2525–2544. [CrossRef]
30. Dayan, U.; Ziv, B.; Margalit, A.; Morin, E.; Sharon, D. A severe autumn storm over the Middle-East: Synoptic and Mesoscale convection. *Theor. Appl. Climatol.* **2001**, *69*, 103–122. [CrossRef]
31. Homar, V.; Stensrud, D.J. Sensitivities of an intense Mediterranean cyclone: Analysis and validation. *Q. J. R. Meteorol. Soc.* **2004**, *130*, 2519–2540. [CrossRef]
32. Kotroni, V.; Lagouvardos, K.; Defer, E.; Dietrich, S.; Porcu, F.; Medaglia, C.M.; Demirtas, M. The Antalya 5 December 2002 storm: Observations and model analysis. *J. Appl. Meteorol. Climatol.* **2006**, *45*, 576–590. [CrossRef]
33. Massacand, A.C.; Wernli, H.; Davies, H.C. Heavy precipitation on the alpine southside: An upper-level precursor. *Geophys. Res. Lett.* **1998**, *25*, 1435–1438. [CrossRef]
34. Llasat, M.C.; Llasat-Botija, M.; Prat, M.A.; Porcu, F.; Price, C.; Mugnai, A.; Lagouvardos, K.; Kotroni, V.; Katsanos, D. High-impact floods and flash floods in Mediterranean countries: The FLASH preliminary database. *Adv. Geosci.* **2010**, *23*, 47–55. [CrossRef]
35. Rodrigo, F.S.; Trigo, R.M. Trends in daily rainfall in the Iberian Peninsula from 1951 to 2002. *Int. J. Climatol.* **2007**, *27*, 513–529. [CrossRef]
36. Alpert, P.; Ben-Gai, T.; Baharad, A.; Benjamini, Y.; Yekutieli, D.; Colacino, M.; Diodato, L.; Ramis, C.; Homar, V.; Romero, R.; et al. The paradoxical increase of Mediterranean extreme daily rainfall in spite of decrease in total values. *Geophys. Res. Lett.* **2002**, *29*. [CrossRef]
37. Kostopoulou, E.; Jones, P.D. Assessment of climate extremes in the Eastern Mediterranean. *Meteorol. Atmos. Phys.* **2005**, *89*, 69–85. [CrossRef]
38. Norrant, C.; Douguedroit, A. Monthly and daily precipitation trends in the Mediterranean (1950–2000). *Theor. Appl. Climatol.* **2006**, *83*, 89–106. [CrossRef]
39. IPCC. *Managing the Risks of Extreme Events and Disasters to Advance Climate Change Adaptation. A Special Report of Working Groups I and II of the Intergovernmental Panel on Climate Change*; Field, C.B.V., Barros, T.F., Stocker, D., Qin, D.J., Dokken, K.L., Ebi, M.D., Mastrandrea, K.J., Mach, G.-K., Plattner, S.K., Allen, M., et al., Eds.; Cambridge University Press: New York, NY, USA, 2012; p. 582.
40. Mariotti, A.; Struglia, M.V.; Zeng, N.; Lau, K.-M. The hydrological cycle in the Mediterranean region and implications for the water budget of the Mediterranean Sea. *J. Clim.* **2002**, *15*, 1674–1690. [CrossRef]

41. Fernandez, J.; Saenz, J.; Zorita, E. Analysis of the wintertime atmosphere moisture transport and its variability over the Mediterranean Basin. *Clim. Res.* **2003**, *23*, 195–215. [CrossRef]
42. Schicker, I.; Radanovics, S. and Seibert, P. Origin and transport of Mediterranean moisture and air. *Atmos. Chem. Phys.* **2010**, *10*, 5089–5105. [CrossRef]
43. Stojanovic, M.; Drumond, A.; Nieto, R.; Gimeno, L. Moisture Transport Anomalies over the Danube River Basin during Two Drought Events: A Lagrangian Analysis. *Atmosphere* **2017**, *8*, 193. [CrossRef]
44. Trigo, R.M.; Añel, J.A.; Barriopedro, D.; Garcia-Herrera, R.; Gimeno, L.; Nieto, R.; Castillo, R.; Allen, M.R.; Massey, N. The record winter drought of 2011–2012 in the Iberian Peninsula. *Bull. Am. Meteorol. Soc.* **2013**, *94*, S41–S45.
45. Nuissier, O.; Ducroq, V.; Ricard, D.; Lebeaupin, C.; Anquetin, S. A numerical study of three catastrophic precipitating evens over southern France. I: N numerical framework and synoptic ingredients. *Q. J. R. Meteorol. Soc.* **2008**, *134*, 111–130. [CrossRef]
46. Ricard, D.; Ducroq, V.; Auger, L. A climatology of the mesoscale environment associated with heavily precipitating events over a northwestern Mediterranean area. *J. Appl. Meteorol. Climatol.* **2012**, *51*, 468–488. [CrossRef]
47. Sodemann, H.; Zubler, E. Seasonal and inter-annual variability of the moisture sources for Alpine precipitation during 1995–2002. *Int. J. Climatol.* **2010**, *30*, 947–961. [CrossRef]
48. Martius, O.; Schwierz, C.; Davies, H.C. Far-upstream precursors of heavy precipitation events on the alpine south-side. *Q. J. R. Meteorol. Soc.* **2008**, *134*, 417–428. [CrossRef]
49. Salih, A.A.M.; Zhang, Q.; Pausata, F.S.R.; Tjernström, M. Sources of Sahelian-Sudan moisture: Insights from a moisture-tracing atmospheric model. *J. Geophys. Res. Atmos.* **2016**, *121*, 7819–7832. [CrossRef]
50. Nieto, R.; Vázquez, M.; Algarra, I.; Gimeno, L. An Analysis of the Water Cycle in the Sahel through a Lagrangian Perspective. In Proceedings of the 1st International Electronic Conference on Atmospheric Sciences, 16–31 July 2016.
51. Nieto, R.; Castillo, R.; Drumond, A.; Gimeno, L. A catalog of moisture sources for continental climatic regions. *Water Resour. Res.* **2014**, *50*, 5322–5328. [CrossRef]
52. Drumond, A.; Nieto, R.; Hernández, E.; Gimeno, L. A Lagrangian analysis of the variation in moisture sources related to drier and wetter conditions in regions around the Mediterranean basin. *Nat. Hazards Earth Sys. Sci.* **2011**, *11*, 2307–2320. [CrossRef]
53. Druyan, L.M.; Koster, R.D. Sources of Sahel Precipitation for Simulated Drought and Rainy Seasons. *J. Clim.* **1989**, *2*, 1438–1446. [CrossRef]
54. Lionello, P. *The Climate of the Mediterranean Region, from the Past to the Future*, 1st ed.; Elsevier: Amsterdam, The Netherlands, 2012; p. 502, ISBN 9780124160422.
55. Gimeno, L.; Nieto, R.; Drumond, A.; Castillo, R.; Trigo, R. Influence of the intensification of the major oceanic moisture sources on continental precipitation. *Geophys. Res. Lett.* **2013**, *40*, 1443–1450. [CrossRef]
56. Rego, F.C.; Rocha, M.S. Climatic Patterns in the Mediterranean Region. *Ecol. Mediterr.* **2014**, *40*, 50. Available online: http://www.isa.utl.pt/ceabn/uploads/docs/publicacoes/FR_e_MR_Ecologia_Mediterranea_2014.pdf (accessed on 21 November 2017).
57. Stohl, A.; James, P. A Lagrangian analysis of the atmospheric branch of the global water cycle. Part I: Method description, validation, and demonstration for the August 2002 flooding in central Europe. *J. Hydrometeorol.* **2004**, *5*, 656–678. [CrossRef]
58. Stohl, A.; James, P. A Lagrangian analysis of the atmospheric branch of the global water cycle: Part II: Moisture transports between Earth's ocean basins and river catchments. *J. Hydrometeorol.* **2005**, *6*, 961–984. [CrossRef]
59. Beck, H.E.; van Dijk, A.I.J.M.; Levizzani, V.; Schellekens, J.; Miralles, D.G.; Martens, B.; de Roo, A. MSWEP: 3-hourly 0.25° global gridded precipitation (1979–2015) by merging gauge, satellite, and reanalysis data. *Hydrol. Earth Syst. Sci.* **2017**, *21*, 589–615. [CrossRef]
60. Beck, H.E.; Vergopolan, N.; Pan, M.; Levizzani, V.; van Dijk, A.I.J.M.; Weedon, G.P.; Brocca, L.; Pappenberger, F.; Huffman, G.J.; Wood, E.F. Global-scale evaluation of 23 precipitation datasets using gauge observations and hydrological modeling. *Hydrol. Earth Syst. Sci. Discuss.* **2017**, *21*, 6201. [CrossRef]
61. Ciric, D.; Stojanovic, M.; Drumond, A.; Nieto, R.; Gimeno, L. Tracking the Origin of Moisture over the Danube River Basin Using a Lagrangian Approach. *Atmosphere* **2016**, *7*, 162. [CrossRef]

62. Dee, D.P.; Uppala, S.M.; Simmons, A.J.; Berrisford, P.; Poli, P.; Kobayashi, S.; Andrae, U.; Balmaseda, M.A.; Balsamo, G.; Bauer, P.; et al. The ERA-Interim reanalysis: Configuration and performance of the data assimilation system. *Q. J. R. Meteorol. Soc.* **2011**, *137*, 553–597. [CrossRef]
63. Numaguti, A. Origin and recycling processes of precipitating water over the Eurasian continent: Experiments using an atmospheric general circulation model. *J. Geophys. Res.* **1999**, *104*, 1957–1972. [CrossRef]
64. Gimeno, L.; Stohl, A.; Trigo, R.M.; Domínguez, F.; Yoshimura, K.; Yu, L.; Drumond, A.; Durán-Quesada, A.M.; Nieto, R. Oceanic and Terrestrial Sources of Continental Precipitation. *Rev. Geophys.* **2012**, *50*, RG4003. [CrossRef]
65. Stohl, A.; Forster, C.; Frank, A.; Seibert, P.; Wotawa, G. Technical note: The Lagrangian particle dispersion model FLEXPART version 6.2. *Atmos. Chem. Phys.* **2005**, *5*, 2461–2474. [CrossRef]
66. Trenberth, K.E.; Fasullo, J.T.; Mackaro, J. Atmospheric Moisture Transports from Ocean to Land and Global Energy Flows in Reanalyses. *J. Clim.* **2011**, *24*, 4907–4924. [CrossRef]
67. Lorenz, C.; Kunstmann, H. The Hydrological Cycle in Three State-of-the-Art Reanalyses: Intercomparison and Performance Analysis. *J. Hydrometeorol.* **2012**, *13*, 1397–1420. [CrossRef]
68. Schlosser, E.; Oerter, H.; Masson-Delmotte, V.; Reijmer, C. Atmospheric influence on the deuterium excess signal in polar firn: Implications for ice-core interpretation. *J. Glaciol.* **2008**, *54*, 117–124. [CrossRef]
69. Scarchilli, C.; Frezzotti, M.; Ruti, P.M. Snow precipitation at four ice core sites in East Antarctica: Provenance, seasonality and blocking factors. *Clim. Dyn.* **2011**, *37*, 2107–2125. [CrossRef]
70. Mehta, A.V.; Yang, S. Precipitation climatology over Mediterranean Basin from ten years of TRMM measurements. *Adv. Geosci.* **2008**, *17*, 87–91. [CrossRef]
71. Evans, J.P.; Smith, R.B.; Oglesby, R.J. Middle East climate simulation and dominant precipitation processes. *Int. J. Climatol.* **2004**, *24*, 1671–1694. [CrossRef]
72. Salah, Z.; Nieto, R.; Drumond, A.; Gimeno, L.; Vicente-Serrano, S.M. A Lagrangian analysis of the moisture budget over the Fertile Crescent during two intense drought episodes. *J. Hydrol.* **2018**, *560*, 382–395. [CrossRef]
73. Peixoto, J.P.; De Almeida, M.; Rosen, R.D.; Salstein, D.A. Atmospheric moisture transport and the water balance of the Mediterranean Sea. *Water Resour. Res.* **1982**, *18*, 83–90. [CrossRef]

5

A global Atlas of precipitation and contribution of the main moisture sources in the peak precipitation month

5.1 Introduction

Extreme precipitation events are a major natural disaster around the world and are the seed for flooding events. The aim of this Atlas is not only to collect maps of global extreme values, but also to enhance understanding of the role of the major sources of moisture (oceanic and continental) over the most intense precipitation months. This is done at the finest resolution for which data is available (0.25° × 0.25° latitude and longitude) for the period 1980-2015.

To construct this extensive Atlas, monthly data from MSWEP and outputs from Lagrangian modelling were used. Separate maps are presented for each month. In the following pages of this doctoral dissertation, maps for January and July are shown, but the complete monthly climatology can be found in Appendix A: Supplementary Material (Figures A.4.1 to A.4.12).

The order of the maps that make up the Atlas is as follows:

- The annual climatological precipitation values from MSWEP database.
- The monthly climatological precipitation values obtained from MSWEP database, presented for each month.
- A map showing the Peak Precipitation Month (PPM) based on monthly gridded MSWEP data.
- The monthly climatological precipitation values of the detected PPM (PMSWEP).
- Climatological monthly moisture contribution, obtained via the forward Lagrangian experiment, from all main moisture sources in the PPM (PFLEX).
- Percentage of the moisture contribution from all sources (PFLEX) to precipitation in the PPM (PMSWEP).
- A map indicating the preferred moisture source (PS) in the PPM.
- Moisture contribution of preferred moisture source in the PPM (PFLEX-PS).
- Percentage of the moisture contribution from the PS (PFLEX-PS) to precipitation in the PPM (PMSWEP).
- Mean precipitation, gridded, for the five years with a) maximum precipitation and b) minimum precipitation, measured from the MSWEP database in the PPM (PMSWEP-Max and PMSWEP-Min, respectively).
- Ratio between PMSWEP-Max and PMSWEP and between PMSWEP-Min and PMSWEP.
- Mean precipitation values of the PS, obtained by the Lagrangian experiment for the same five years of maximum and minimum precipitation, detected from MSWEP data (PFLEX-PSMax and PFLEX-PSMin).
- Ratio expressed in percentage between PFLEX-PSMax and PMSWEP, and between PFLEX-PSMin and PMSWEP.

5.2 Characterisation of global monthly moisture sources and sinks

To investigate the monthly role of the major moisture sources for the peak precipitation months (PPM) for each 0.25° grid square, it was first necessary to identify these moisture sources and sinks. This was done following the methodology of Gimeno et al. (2010).

This sub-chapter represents a review and an extension of the work by Gimeno et al. (2010; 2013) and Castillo et al. (2014), in which annual sources of moisture were detected. Thus, in the present study, we applied a methodology based on maximum climatological monthly vertical integrated moisture flux (VIMF) divergence to identify major monthly moisture sources, instead of the annual climatology method used in Gimeno et al. (2010). The ERA-Interim (Dee et al., 2011) reanalysis data from the ECMWF was used from January 1980 to December 2016 on a 1° × 1° latitude-longitude grid. The threshold that was applied to define moisture sources was based on the fiftieth percentile of VIMF divergence for oceanic sources and on the fortieth percentile for continental sources. This differs from Gimeno et al. (2010), who imposed a fixed threshold of 750 and 500 mm/year for oceanic and land sources, respectively. The choice of the fiftieth and fortieth percentiles was based on the attempt to find the closest common percentile to the threshold used by Gimeno et al. (2010). In the present work, the values of VIMF divergence differ month to month and between oceanic and continental sources (see Table 5.1).

Table 5.1. Monthly values for oceanic (fiftieth percentile) and continental (fortieth percentile) sources.

Month	Oceanic sources (p50) mm/year	Land sources (p40) mm/year
January	830.8	498.3
February	768.4	496.8
March	699.9	447.7
April	656.3	466.9
May	670.4	440.7
June	838.3	474.1
July	849.6	477.5
August	748.3	489.5
September	659.2	447.9
October	721.3	501.0
November	768.7	508.4
December	807.4	480.8

A total of 14 moisture sources were identified. Eleven were oceanic, namely NPAC (North Pacific), SPAC (South Pacific), MEXCAR (Gulf of Mexico and Caribbean Sea), NATL (North Atlantic), SATL (South Atlantic), ZANAR (Zanzibar Current and Arabian Sea), AGU (Agulhas Current), IND (Indian Ocean), CORALS (Coral Sea), MED (Mediterranean Sea), and REDS (Red Sea). Three were continental: SAM (South America), SAHEL (Sahel region), and SAFR (South Africa). As MED and RED take up practically the whole area inside their basins, these two sources were defined using their physical boundaries. The left panels of Figure 5.1 show an example: oceanic and terrestrial moisture source regions for January and July (mid-winter and mid-summer months). The remaining monthly figures can be found in Appendix A: Supplementary Material in Figures A.4.1 to A.4.12.

The contribution of the detected sources to continental precipitation was estimated using the forward mode in the Lagrangian dispersion model FLEXPART's outputs (Stohl et al., 2005) for the period 1980-2016. This is another main difference to the work of Gimeno et al. (2010), which analysed only a five-year period (2000-2004), although this work was then updated by Castillo et al. (2014) to 2012. The selected particles over each source of moisture were followed forward along their trajectories with a limited transport time of 10 days (Numaguti, 1999). The particles' information was recorded at 6 h time intervals (00, 06, 12 and 18 UTC). Based on the methodology described by Stohl and James (2004; 2005) and in the methodology chapter of this dissertation, the loss of moisture over the continental regions coming from each source was indicated by negative values of E-P. This calculation was performed for every month, but for simplicity the results and explanation are presented only for January and July (Figure 5.1, right column). The results for all other months can be found in Appendix A: Supplementary Material, in Figures A.4.1 to A.4.12.

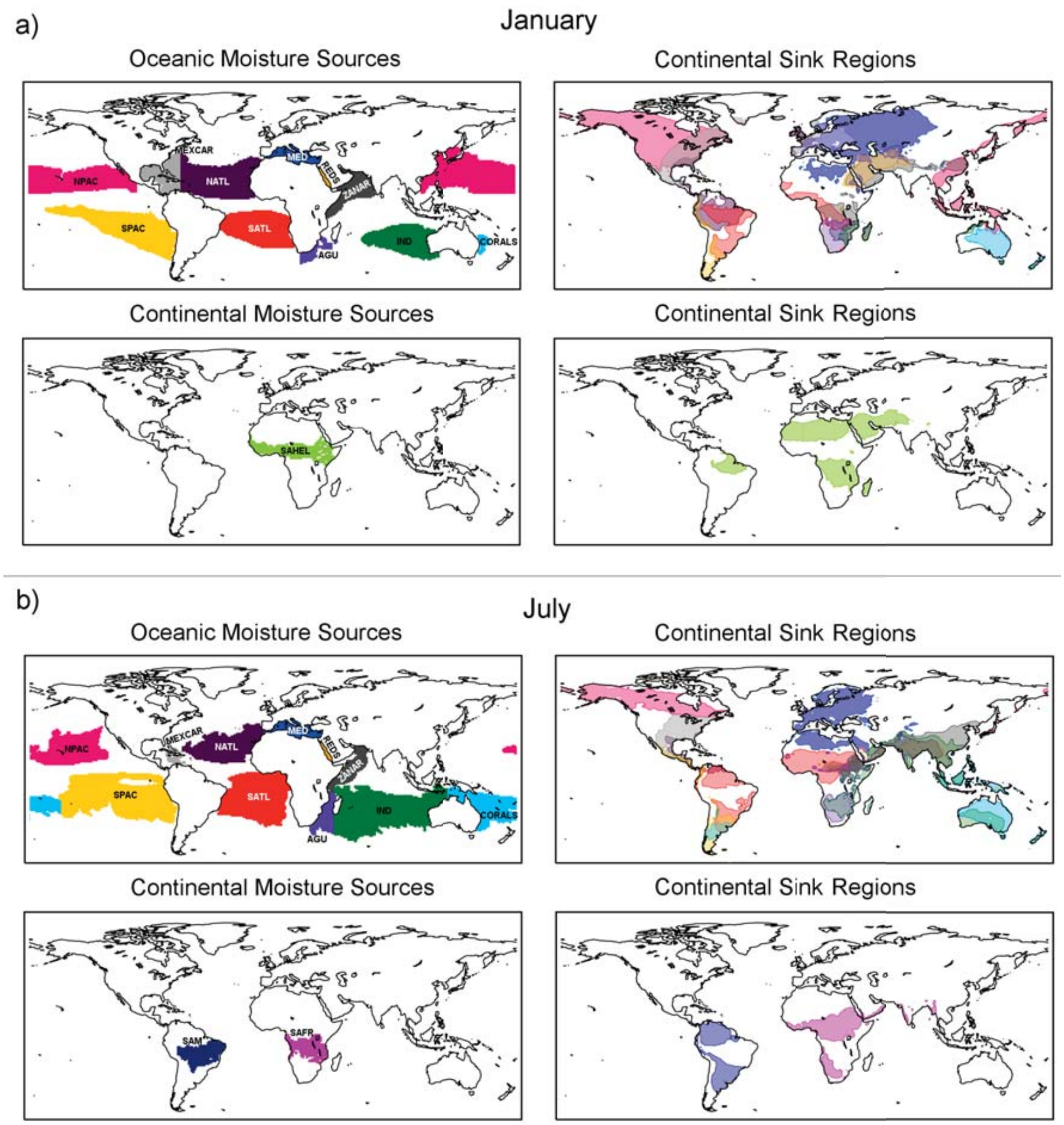

Figure 5.1. Left column: Monthly oceanic and terrestrial moisture source regions for January (a) and July (b). Right column: Sink regions for each moisture source. The sink regions (E-P < 0 values identified from forward tracking) on the continents are plotted for values higher than -0.05 mm/day for all the detected sources.

In general, the moisture sources we identified at monthly scale are quite similar to those found by Gimeno et al. (2010) and Castillo et al. (2014). Moreover, it is interesting to note that, in the work presented here, the moisture sources are not stationary. They show variation in intensity across the months, which is reflected in their spatial extension and thus also in the associated sink. At the global scale, the highest number of detected moisture sources are located over tropical and subtropical oceanic areas, including the continental areas of South America, South Africa, and the Sahel regions.

In terms of annual variation, some sources are present throughout the year, while others are greatly reduced or completely absent in some months. For example, in both the northern and southern hemispheres, the PAC and ATL sources are present during both January and July and also during all other months (see Appendix A: Supplementary Material). ZANAR, in the northern hemisphere, and IND, in the southern hemisphere, also provide moisture throughout the year. On the other hand, some sources vary through the year. CORALS is one such source – it practically disappears in January, while in July it is a strong moisture source. MEXCAR (Mexico Caribbean) is another example of this behaviour. From January to April, this source dominates in moisture evaporation; it then weakens from May until August and completely disappears in September. From October, it appears again as an important moisture source (for the complete annual evolution see Appendix A: Supplementary Material). Similar patterns are also observed with all defined continental sources: SAM, SAF, and SAHEL. Figure 5.1 shows that in January, the SAHEL is the only moisture source on land, but it disappears during July when SAFR and SAM appear. The SAHEL source exhibits a clear seasonal dichotomy; during summer (April-September) it is absent as a moisture source, while during winter (October-March) it is an important source. Moreover, SAM is a bigger moisture source between April and October but is completely reduced in September and October, appearing only over the north-eastern part of Brazil.

The sinks of moisture associated with each source are shown in Figure 5.1 (right panels) and in the Supplementary Material. Our results show that oceanic subtropical areas dominate as moisture providers (as in Gimeno et al., 2010). Thus, the North Atlantic Ocean (NATL) is the dominant moisture source during January, providing the moisture for precipitation on three continents: Europe, Eastern North America, and South America. In July, its influence is weakened, and it contributes to only small parts of Mexico, Central America, and Northern South America. On the other hand, the South Atlantic Ocean (SATL) contributes to the precipitation during January and July, mainly providing the moisture for Brazil and Central Africa. There is no rule that major moisture sources necessarily provide precipitation to huge continental areas; for example, the Indian and South Pacific Oceans demonstrate this during both January and July. In contrast, there are some small moisture source regions which provide a huge amount of moisture for precipitation in comparison with their size. For example, the Mediterranean Sea is an important water source for Europe and North Africa during both January and July, and the Red Sea provides great quantities of precipitation for the whole Middle East coast, Syria, Iraq, and Iran during January. The MEXCAR (Mexico Caribbean) source is the dominant moisture source for precipitation over Europe and Eastern North America during January, extending its influence across the Northern American continent in July, although with reduced intensity. There are also areas, including Australia and Canada, which mainly receive precipitation from a single source throughout the year. The dominant moisture source for Australia is CORALS (Coral Sea) during both January and July, while for Canada it is the North Pacific Ocean (NPAC). Moreover, continental moisture sources are important providers of precipitation in months when they appear as significant moisture source regions. For instance, during January the Sahel region provides precipitation for vast continental areas including North and South African regions, the coast of the Middle East, and the north-eastern part of Brazil. In contrast, SAM and SAF are important moisture sources for precipitation during January for South America and Central and South Africa, respectively. The monthly variation of all detected moisture source regions' contribution to precipitation can be found in Appendix A: Supplementary Material.

5.3 Detection of the peak precipitation month

In order to describe global precipitation features in terms of annual and monthly maximum precipitation climatology, the MSWEP database (Beck et al., 2017a) was used. The MSWEP database covers the temporal period from 1980 to 2015 and is available at 0.25° × 0.25° latitude and longitude spatial resolution. Detailed information about this dataset and its advantages and characteristics may be found in the methodology section of this dissertation.

Figure 5.2 presents MSWEP global annual climatological precipitation. As anticipated, the precipitation pattern shows the highest precipitation values in the tropical and subtropical zones positioned between 0° and 20° north and south, located over areas of South America, Central South Africa, South Asia (India, Thailand, Cambodia), Indonesia, and Papa New Guinea. Areas further north such as the West Coast of Canada, Central Europe, and Norway also had among the highest precipitation values, with amounts of 4 mm/day or more. The lowest precipitation values were observed in semi-arid and arid regions of Africa, the coast of the Middle East, Central Asia, and Australia, with less than 0.3 mm/day. Moderate precipitation values, between 1.5 and 2.5 mm/day, were mostly recorded over Europe, West Russia, and the eastern United States and Canada. The general distribution of precipitation from the MSWEP database is similar to other climatological precipitation datasets, such as the Global Precipitation Climatology Project (GPCP) (Huffman et al., 1997) and ERA-Interim (Simmons et al., 2007; Sun et al., 2018).

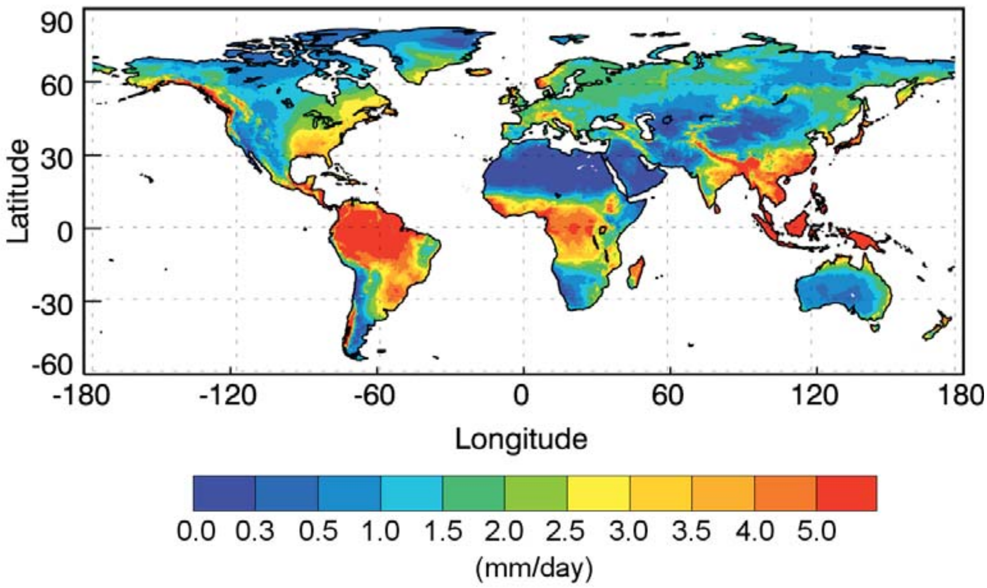

Figure 5.2. Annual climatological precipitation values (1980-2015) from the Multi-Source Weighted-Ensemble Precipitation database.

Using the monthly precipitation climatology data from MSWEP (Figure 5.3) and using a 0.25˚ grid allowed us to detect the month which exhibits the maximum precipitation (Figure 5.4) – hereafter, the Peak Precipitation Month (PPM). The results show clearly that the movement of the Inter Tropical Convergence Zone (ITCZ) causes PPMs during December to February (austral summer) around latitudes from 10°S to 30°S over central South America, South Africa, and northern Australia; and during July and August (boreal summer) over southern Asia, the Sahel, and Central Africa, and between 5°N to 30°N in America.

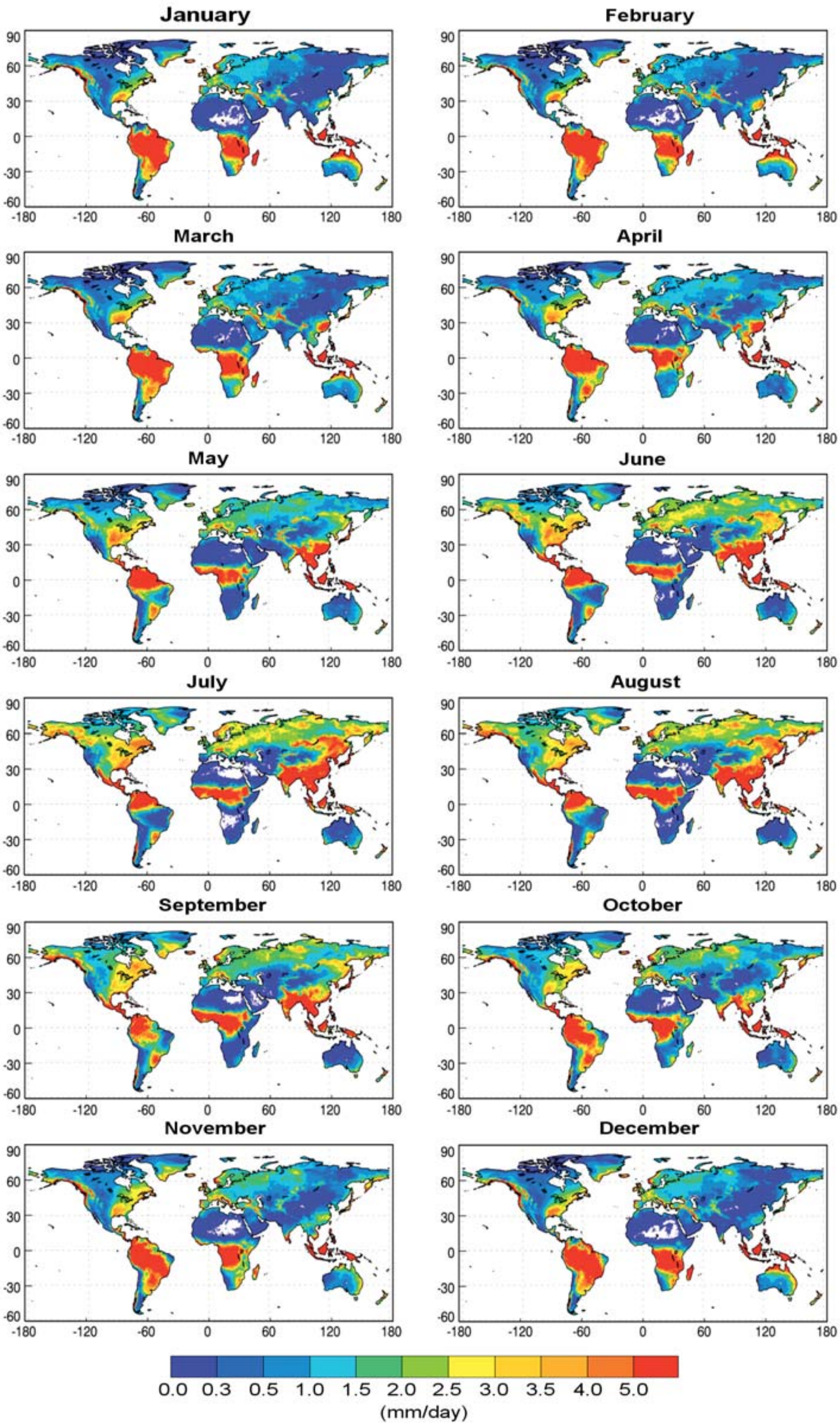

Figure 5.3. Monthly precipitation climatology (1980-2015) from the Multi-Source Weighted-Ensemble Precipitation database.

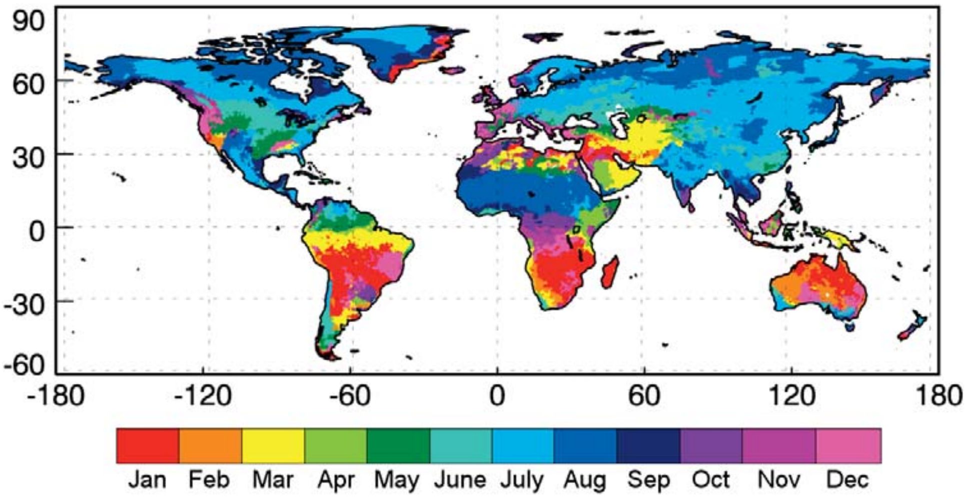

Figure 5.4. Peak Precipitation Month (PPM) based on monthly Multi-Source Weighted-Ensemble Precipitation database data.

Further north, across most of the Asian continent, northern Europe, and northern and central North America, the PPMs occur between June and August. March predominates as the PPM over the eastern Middle East and the band between 1°S to 10°S over South America. It is interesting to note that the Mediterranean and central north America exhibit the most diverse pattern. The PPMs along the European Atlantic coast occur during boreal winter months, which is the time with the most active precipitation, associated with storm tracks; this is also the case in the Pacific coast of North America.

Figure 5.5 shows the climatological monthly precipitation value during the PPM using MSWEP data. The areas around the equator and those affected by the ITCZ show the highest precipitation quantities, with precipitation values during the PPMs higher than 8 mm/day. This is double the mean annual values (4-5 mm/day, see Figure 5.2). On the other hand, arid or semiarid regions of Africa, the Middle East, central Asia, or Australia receive the smallest precipitation quantities (less than 1 mm/day) during the PPMs. In the most areas worldwide, the PPM precipitation values are double the mean annual value.

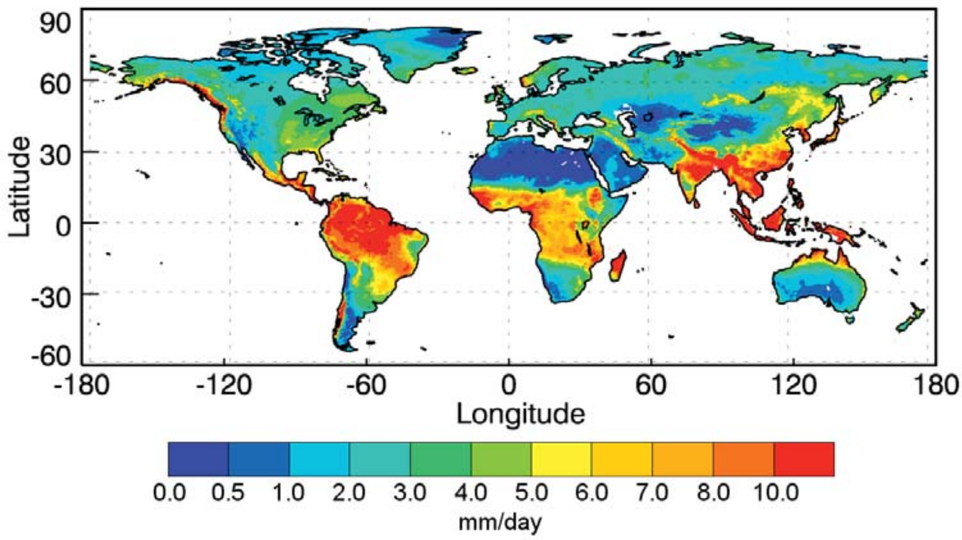

Figure 5.5. Monthly climatological precipitation values, using Multi-Source Weighted-Ensemble Precipitation data, for the detected peak precipitation month (PPM).

5.4 Moisture sources' contribution to precipitation in the PPM

Figure 5.6 is a map of the total precipitation that comes from the moisture sources (Figure 5.1 and Appendix A: Supplementary Material Figure A.4.1 to Figure A.4.12) over each grid point during the PPM. To estimate the contribution of each detected moisture source to precipitation over each grid square, fields where precipitation exceeded evaporation (E-P < 0) were constructed using the FLEXPART outputs for the period 1980-2016 (PFLEX). A detailed explanation of this is given in the methodology section. To create Figure 5.6, the values where E-P < 0 were added for all the detected sources for each PPM. For example, in the area of North America that has July as the PPM is affected by a single source, the NPAC (North Pacific) (see Figure 5.1 for July). Thus, the precipitation values in Figure 5.6 for that region are only those from NPAC. On the other hand, there are regions where two or more moisture sources contribute to precipitation during the PPM. For example, this is the case over the South Arabian Peninsula, Iraq, Iran and Kazakhstan regions where the PPM is March (see Figure 5.4 in yellow colour), and the precipitation in March was supported by moisture coming from REDS (Red Sea) and ZANAR (Zanzibar Current and Arabian Sea). Therefore, for each grid point, the total precipitation contribution of both sources was added.

The general pattern shown in Figure 5.6 is similar to Figure 5.5. However, in Figure 5.6 only precipitation from the major oceanic and continental moisture sources is represented (Figure 1.1 and Figure A.4.1 to Figure A.4.12 in Appendix A: Supplementary Material). The missing quantity is made up of the remaining oceanic and continental evaporative areas that are not included as major moisture sources.

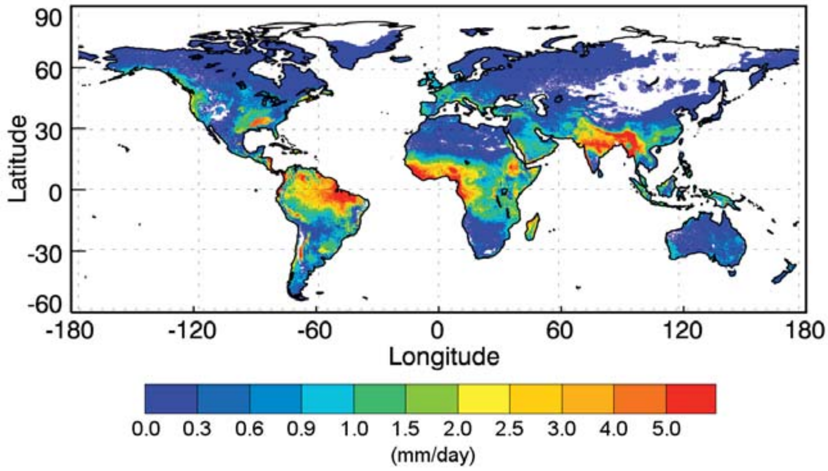

Figure 5.6. Gridded precipitation contribution of all detected moisture source regions during the peak precipitation months identified via Lagrangian experiment (PFLEX).

Figure 5.7 plots the ratio between the precipitation values coming from the major moisture sources (PFLEX, Figure 5.6) and the climatological values of precipitation (PMSWEP, Figure 5.5) during the PPMs. It is important to stress that for the percentage calculation, PMSWEP values lower than 0.1 mm/day were not considered. The purpose of this calculation is to show which percentage of precipitation in the PPM is from moisture originating from the detected moisture sources.

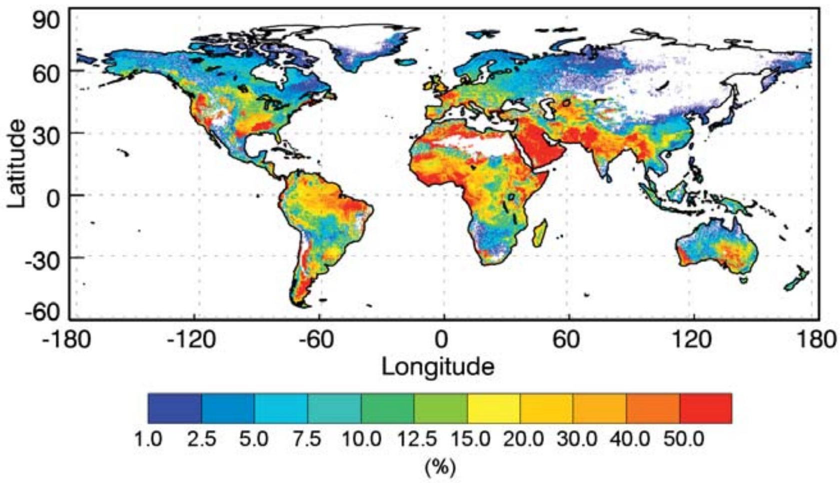

Figure 5.7. Percentage of continental precipitation originating from the major sources of moisture (PFLEX) compared with the total precipitation measured by Multi-Source Weighted-Ensemble Precipitation (PMSEWP) for the peak precipitation month over each 0.25° grid square.

5.5 Characterisation of preferred moisture source

The next step in the construction of this Atlas is to show the Preferred Moisture Source for the Peak Precipitation Month (PPM) at each grid square. The source of moisture that contributes the most to the precipitation over each grid square is denoted as the Preferred Source (PS) (Figure 5.8). The map shows that in the European Atlantic coast, from the Iberian to the Scandinavian Peninsula, the preferred moisture source is NATL (North Atlantic Ocean), while for North Europe to Eurasia, and also North Africa, the preferred source of moisture is MED (the Mediterranean Sea). In most of Australia, the PS is the Coral Sea. For the southern cone of South America and for Central America, the SPAC contributes the highest precipitation amount during the PPM. NATL is the PS over the Amazon River Basin, while the SATL prevails over most of eastern South America and Central Africa. On the other hand, for South Africa the PS is the Agulhas Current (AGU). In the North American continent, two PS appear: the NPAC (North Pacific) dominates in Alaska, Canada, and the northern United States, extending its influence to some regions in Russia; while MEXCAR (Mexico Caribbean) is the PS for the eastern cone of the United States and some parts of Mexico. It is interesting to note that in Central and East Asia, including the Middle Eastern coast, the detected preferred source is ZANAR (Zanzibar Current and Arabian Sea). IND (Indian Ocean), as expected, dominates in India and extends its influence over eastern Africa.

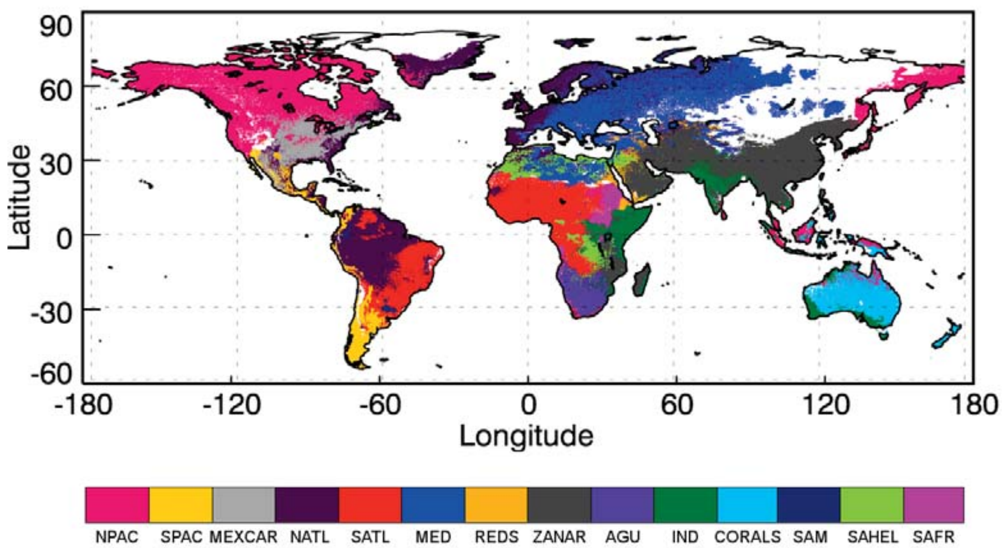

Figure 5.8. Preferred sources of moisture for precipitation during the peak precipitation month of each location.

After the detection of these Preferred Moisture Sources (PS) for the Peak Precipitation Months (PPM), the precipitation values (calculated from the Lagrangian approach, PFLEX) associated with each of them (PFLEX-PS) are presented, gridded, in Figure 5.9. This map shows a similar spatial pattern compared with the precipitation linked with all sources (Figure 5.6), but with lower values. This is as expected, given that Figure 5.9 takes into account only one source for each grid square, while Figure 5.6 shows the total amount from all the sources.

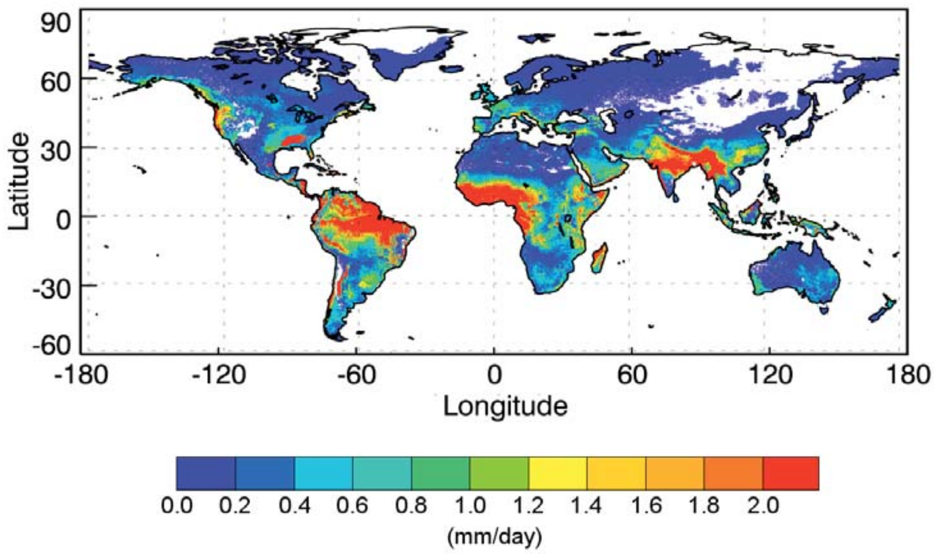

Figure 5.9. Precipitation from the moisture of the Preferred Source (PFLEX-PS) during the peak precipitation month, obtained through the Lagrangian experiment.

The next map of this Atlas, Figure 5.10, shows the percentage of the precipitation in the PPM that was contributed by the Preferred Moisture Source compared to all detected sources, for each grid square. The highest percentage values denote areas in which the preferred source is strongly dominant in providing precipitation during the Peak Precipitation Months.

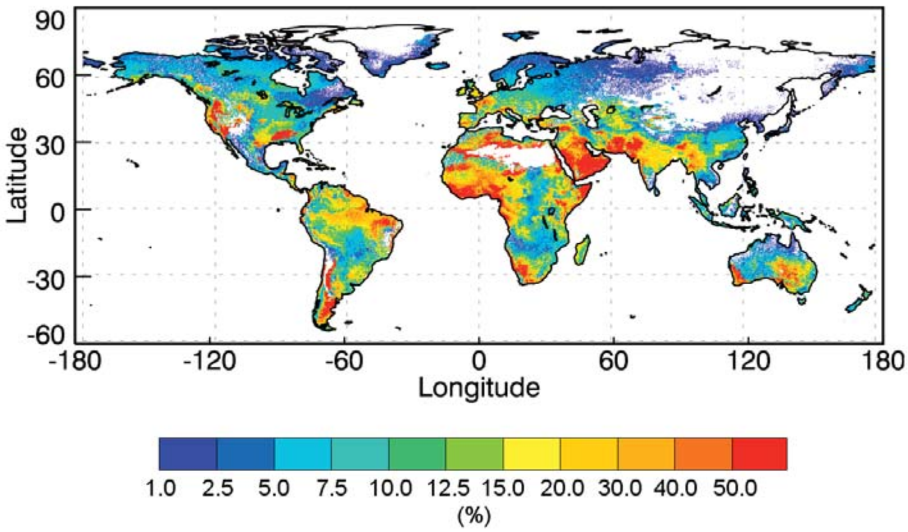

Figure 5.10. Percentage of precipitation contributed by the preferred source (PFLEX-PS) during the peak precipitation month (PMSWEP).

5.6 The five years with maximum and minimum precipitation for the PPM

The mean precipitation for the 5 years that exhibit the maximum and minimum precipitation values during the PPM (hereafter, PMSWEP-Max and PMSWEP-Min, respectively) using MSWEP data are plotted in Figure 5.11. It is important to stress that for the identification the 5 minimum years, grid points with values of 0 mm/day were not considered.

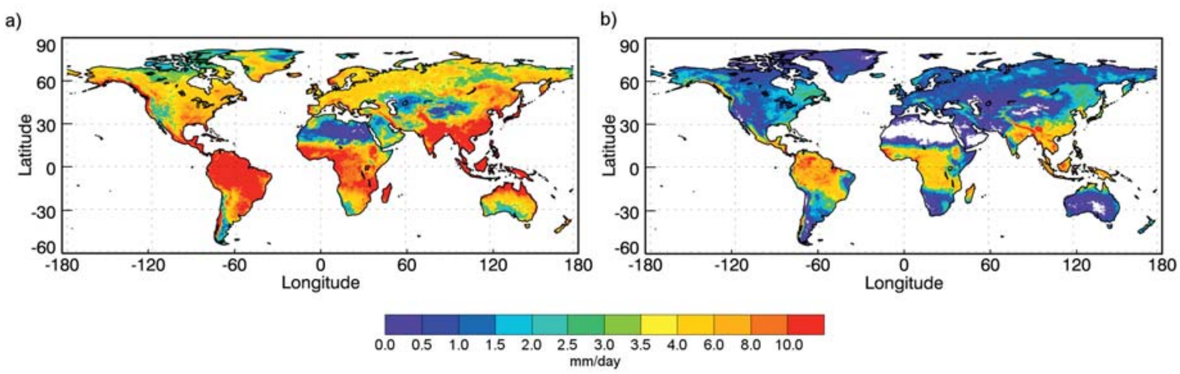

Figure 5.11. Mean precipitation, gridded, for the five years with (a) maximum precipitation (PMSWEP-Max), and (b) minimum precipitation (PMSWEP-Min) during the peak precipitation month. The Multi-Source Weighted-Ensemble Precipitation database was used to derive data. Grid points with values of 0 mm/day were not considered (shown in white in b).

The precipitation pattern for both PMSWEP-Max and PMSWEP-Min shows that Central and South America, India, and south-eastern Asia – which are the climatic areas (Figure 5.2) of maximum precipitation (equatorial zones) – had the highest precipitation values. This indicates that even in the minimum years, the precipitation values there are still high. Moreover, there are areas where the precipitation is very low (less than 1 mm/day) in the years of minimum precipitation (Figure 5.11b): Central Canada; the Mediterranean region, extending to North Europe and Eurasia; the southern cone of South America; South Africa; and Australia.

The ratio between the precipitation values of the minimum and maximum periods and the monthly climatological value of the PPMs is plotted in Figure 5.12. These values indicate to what extent the PMSWEP-Max and PMSWEP-Min vary in relation to the climatology. In the driest areas of the world, PMSWEP-Max values are double or triple climatological values (Figure 5.12a). Moreover, there are also areas where PMSWEP-Max is close or equal to the climatology (expressed by ratios ~1). Those are over Central America, North and South America (the Amazon and Orinoco river basins), western and Central Africa (the Sahel and Congo river basin), and south-eastern Asia. Over these regions, the 5 maximum precipitation years during the PPMs is almost identical to the climatological values during the PPMs, indicating that precipitation is always abundant and does not show a lot of variability. This is confirmed by the PMSWEP-Min ratios in these areas (Figure 5.12b), which is also close to 1 (more than 0.7 mm/day).

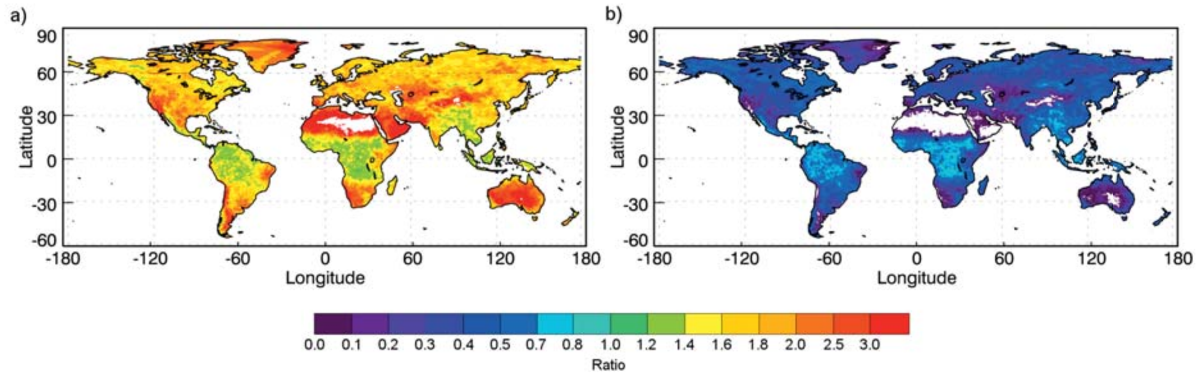

Figure 5.12. Ratio between (a) PMSWEP-Max and PMSWEP and (b) PMSWEP-Min and PMSWEP. PPM: peak precipitation month; PMSWEP: monthly climatological precipitation values of the PPM; PMSWEP-Max: the five years with maximum precipitation during the PPM; PMSWEP-Min: the five years with minimum precipitation during the PPM.

5.7 Precipitation supported by the preferred moisture source for the five-year period of maximum and minimum precipitation for the peak precipitation months

Using the monthly climatological precipitation computed from the Lagrangian FLEXPART model (PFLEX) for the detected preferred sources, we calculated the mean precipitation for the 5 years of PMSWEP-Max and PMSWEP-Min in the peak precipitation months (hereafter, PFLEX-PSMax and PFLEX-PSMin, respectively). These fields are plotted in Figure 5.12. Both maps show a similar geographical distribution of precipitation. Compared with Figure 5.11, which shows the same 5-year periods for maximum and minimum MSWEP, the values are lower (in some regions by half) because Figure 5.12 represents only the precipitation from the preferred source in each grid square.

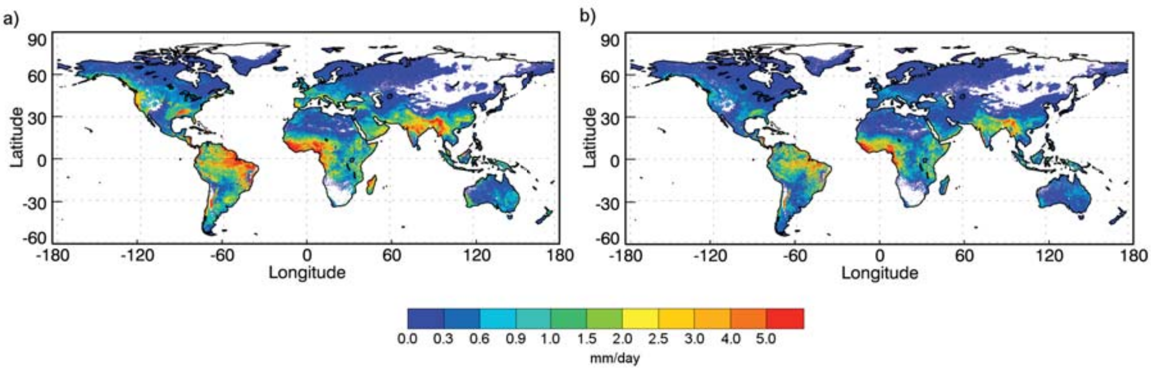

Figure 5.13. Mean monthly climatological precipitation values computed from the Lagrangian FLEXPART model, coming from the preferred source, for the five years of (a) maximum and (b) and minimum precipitation detected from Multi-Source Weighted-Ensemble Precipitation database.

As in Figure 5.10, the ratio between PFLEX-PSMax and PFLEX-PSMin and the monthly climatological precipitation (PMSWEP) for the peak months is presented in Figure 5.14. The highest difference in the contribution by the preferred source between Figure 5.14a and Figure 5.14b is in subtropical latitudes. For example, over the Iberian Peninsula and France the preferred source contributes more than 50% (red colours) of moisture for precipitation in the peak month in the maximum precipitation years, while for the minimum precipitation years, this decreases to almost 10% (green colours). The same pattern also is detected in monsoonal climate zones; for example, over India 40% or more of precipitation in the PPM during maximum precipitation years comes from the preferred sources, while in the minimum years this number drops to around 10%.

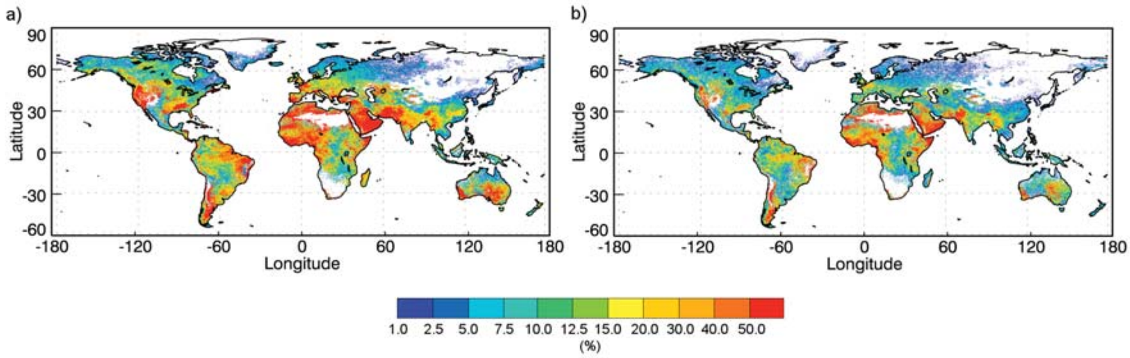

Figure 5.14. Percentage of the moisture contributed by the preferred source to total precipitation during the peak precipitation month for the 5 years with (a) maximum precipitation (PFLEX-PSMax) and (b) minimum precipitation (PFLEX-PSMin).

It is interesting to note that in some regions, the preferred source is a high contributor during both maximum and minimum precipitation years. These areas are mostly tropical climate zones, which are constantly influenced by high quantities of precipitation.

Generally, the pattern is similar for both Figure 5.14(a) and (b). This indicates that the FLEXPART model and the methodology to calculate the moisture that comes from major moisture sources to contribute to continental precipitation is valid for both higher and lower amounts of precipitation.

6

Summary, conclusions, and further research

Precipitation is characterised as one of the most important parts of the hydrological cycle, but also presents one of the greatest challenges to researchers in terms of predicting, monitoring, and estimating (Beck et al., 2017b). Moreover, precipitation is known to vary strongly across space and time, meaning that many areas throughout the year receive much more rainfall than the climatological standard (Michaelides et al., 2009). Extreme precipitation events associated with a high magnitude of precipitation may be a serious source of risk at all spatial scales, from regional to global.

The main purpose of this PhD thesis was to investigate the atmospheric branch of the hydrological cycle by linking the main moisture source regions with extreme precipitation over continental areas. The methodology was based on a Lagrangian technique, which is a suitable way to identify sources of moisture and evaluate continental precipitation from moisture that comes from both oceanic and continental sources of moisture. To assess this undertaking, the outputs of the FLEXPART model were used. The FLEXPART model models a large set of particles (about 2 million) at 6 h intervals around the world that are moved with 3D winds and records their position and specific humidity. In summary, we identified the main sources of moisture by tracing particles from a given moisture sink backwards along their trajectory and calculating changes in their specific humidity. We also tracked particles forward from their moisture source and identified changes in their specific humidity, allowing us to see where their final sink was. For both tracking modes, the particles were followed for 10 days, which is the widely used in climate research as the mean water lifetime in the atmosphere.

Research on the origin of extreme precipitation that occurs over land was conducted first at the regional and then at the global scale. Firstly, we analysed the Danube River Basin, then expanded the research to the whole Mediterranean region, and finally characterised extreme precipitation at the global scale. From the global scale research, we developed an Atlas that shows how the main global oceanic and continental moisture sources contribute to extreme precipitation worldwide.

The main conclusive remarks derived from this thesis are presented below, following the same sequence of the articles presented in Chapter 4:

(1) Identification of the sink-source moisture relationship for the Danube River Basin

As stated, this study began at the regional scale, analysing one of the biggest river basins on the European continent, the Danube River Basin (DRB). The analysis was done for 1980 to 2014 and used global particle tracks from the FLEXPART experiment. The most important results in terms of the sink-source moisture relationship are listed below:

- Seven main climatological sources for precipitation at the annual scale were detected: the Mediterranean Sea; Black Sea; Caspian Sea; Danube River Basin; North Atlantic Ocean; and two continental sources, one in North Africa and the land around the Danube River Basin.

- At seasonal scale, the contribution of each source changes depending on the time of year. During the summer season (April-September), the highest contribution came from the Danube River basin itself (51%), followed by the rest of the land surrounding the basin (21%). Together, these sources accounted for more than 70%. In winter (October-March), the Mediterranean Sea supports 31% of precipitation and is the dominant moisture source for this season, followed by the Black Sea with 19%. In winter months, the basin contribution reduces to 16%, almost half of that in summer.

- The sources supply different amounts of moisture along the 10 days considered. It should be therefore pointed out that at the beginning of the period the Mediterranean Sea, the Danube itself, and the surrounding land areas contribute the highest amount of moisture, while at the end of the 10 days the North Atlantic Ocean is the most important source. At a seasonal scale, the Mediterranean Sea and North Atlantic play the most important role in moisture contribution during the winter, reaching their maximum support at the 3rd and 7th days, respectively, before the particles reach the sink area over the Danube River Basin. In contrast, during the summer the Danube basin itself and the continental areas around it supply the highest amount of moisture during the 1st day and supply a significant amount of moisture until the 6th day; thereafter, until the 10th day, these areas provide only reduced quantities of moisture.
- Considering the contribution of each source to precipitation over the Danube basin by using the forward mode to follow the particles shows that, in general, the Mediterranean Sea is the major contributor during summer and winter, but with a different spatial distribution in the two seasons. In winter, the Mediterranean Sea's contribution extends to the whole Danube area, while in summer it mainly contributes to precipitation over the western part of the basin. The Black and Caspian Seas are the lowest contributors to moisture for precipitation in both seasons.

(2) Characterising extreme precipitation events (wet spells) over the Danube River Basin

We characterised extreme precipitation events (wet spells) over the Danube River Basin using the ranking methodology developed by Ramos et al. (2014; 2017) for the period 1981-2015 (a total of 12775 days). The ranking used daily precipitation data from the CHIRPS database. The first step of this research was ranking the extreme precipitation events over the Danube River Basin for different time scales (1, 3, 5, 7, and 10 days).

Using this ranking, a pair of papers was published (see Chapter 4 of this PhD thesis). The former was an analysis focused on the most intense wet spell event detected, which occurred on 23 September 1996. After that, in a second paper, the analysis was extended to consider the most extreme 100 events of each duration.

2.1 *Analysis of the most extreme precipitation event:*

- The extreme precipitation amount that occurred was caused by an anomalous moisture supply from three maritime sources for the Danube basin: the Mediterranean Sea, Black Sea, and North Atlantic Ocean.

- The anomalous moisture transport was supported with some specific synoptic conditions: i) an anticyclone situated, during at least the 10 days before the event, over the Atlantic Ocean; ii) the occurrence of Hurricane Hortense during the days prior to the event (9-14 September 1996), which released available moisture over the North Atlantic Ocean; and iii) a secondary, low-level pressure system that occurred immediately after the hurricane associated with an atmospheric river that took moisture released by the hurricane and transported it to the Danube River Basin.

2.2 *Analysis of the 100 most extreme precipitation events:*

Using the ranked list of wet spell events over the Danube River Basin, the analysis was expanded to consider the 100 top events of each different duration (1, 3, 5, 7, and 10 days). In this case, the aim of the analysis was to find what role the Mediterranean Sea played in supplying moisture for these extreme precipitation events. The most significant findings are presented below:

- The highest number of extreme events for all durations occurred during the winter season in the Danube basin, when the Mediterranean Sea acts as the most important moisture source.

- The importance of the Mediterranean Sea as a source for extreme precipitation is confirmed by the finding that between 84 and 93% of the analysed events were supplied by anomalous moisture from this source.

- During summer and spring the Mediterranean Sea was a moisture source for 100% of wet spells regardless of time scale, with the exception of long-lasting events of 3 days in the summer, for which it was a source for 90%.
- Computing the intensity of the Mediterranean's moisture contribution for each extreme event indicated that the highest contribution is found to 1 day events. For events of longer time scales, the contribution decreases but remains higher than 50%.
- For extreme precipitation events of 1, 3, and 7 days, a positive relationship (significant at 90% or more) was identified at the annual scale between precipitation anomalies and anomalous moisture from the Mediterranean.
- In addition to the importance of the Mediterranean Sea for extreme precipitation over the Danube River Basin, this study highlights another significant finding: the huge importance that the integrated time period of particle tracking plays in establishing a positive relationship when tracking particles from the Mediterranean Sea with the FLEXPART model. The most suitable integrated time period was found to be the length of the event.

(3) Moisture contribution from the Mediterranean Sea to climatological and extreme monthly precipitation over the surrounding continents

The monthly moisture contribution of the Mediterranean Sea to monthly precipitation over the neighbouring continental areas (its sinks of moisture) was calculated. The mean climatological behaviour and extreme precipitation values (the five years of highest precipitation) were analysed over a grid for the period 1980-2015. To compute precipitation, the MSWEP monthly precipitation database was used; to identify the role of the Mediterranean Sea, we tracked air particles forward from the Mediterranean Sea using the Lagrangian model FLEXPART v9.0.

The most important results – with January and July as representative months for boreal winter and summer, respectively – are listed below:

- The precipitation patterns for both climatological and extreme precipitation show a similar geographic distribution during winter and summer.

- During winter, the most intense precipitation values were observed over the Adriatic coast, western side of the Iberian and Scandinavian Peninsulas, and Fertile Crescent; while during summer, the highest precipitation amount was recorded over the Alps, Scandinavian Peninsula, and Carpathian Mountains.
- The ratio between climatological and extreme monthly precipitation over the Mediterranean denotes regions where the extreme precipitation is much greater than the monthly climatological precipitation values. For both seasons, the ratio was greatest over the Iberian Peninsula, Middle East, and North Africa, where extreme precipitation was up to five times higher than the monthly mean.
- Some areas have almost the same quantities of climatological and extreme precipitation, such as the Scandinavian and Carpathian regions during July.
- During January, the climatological pattern for precipitation coming from the Mediterranean Sea exhibits a clear eastern shift, with the highest values over the north-eastern continental region around the Mediterranean Sea. During July, the Mediterranean moisture contribution is focused on local areas closest to the basin itself, such as the Middle East, North Africa, Alpine region, and eastern Iberian Peninsula.
- The Mediterranean moisture contribution to extreme precipitation over continental areas shows a similar pattern as its contribution to climatological precipitation during both January and July.
- The ratio between the amount of moisture that the Mediterranean supplies to extreme precipitation and climatological precipitation shows that, for both January and July, extreme precipitation was supported up to 3 times more than climatological precipitation over the Italian and Iberian Peninsulas, coast of the Middle East, and in arid regions of Africa.
- Finally, the highest difference between the contribution of the Mediterranean to climatological and extreme precipitation is recorded in some parts of Europe. In these areas, the Mediterranean Sea is not the most important provider of

moisture for climatological precipitation, but is the most significant source of moisture for extreme precipitation.

(4) Global Atlas of precipitation and contribution of the main moisture sources in the peak precipitation month

To form this Global Atlas, we used MSWEP monthly precipitation data and outputs from the FLEXPART Lagrangian model. The Atlas provides a comprehensive analysis of moisture transport from the main global moisture sources, connected with the occurrence of extreme precipitation over continental areas at the global scale. The body of the Atlas incorporates maps concerning global monthly moisture sources, detection of the peak precipitation month, maximum and minimum precipitation values in the PPM, and identification of the preferred moisture source for precipitation in the PPM.

Previously, the main global monthly moisture source regions were characterised. Fourteen sources were identified: NPAC (North Pacific), SPAC (South Pacific), MEXCAR (Gulf of Mexico and Caribbean Sea), NATL (North Atlantic), SATL (South Atlantic), ZANAR (Zanzibar Current and Arabian Sea), AGU (Agulhas Current), IND (Indian Ocean), CORALS (Coral Sea), MED (Mediterranean Sea), REDS (Red Sea), SAM (South America), SAHEL (Sahel region), and SAFR (South Africa). This characterisation was performed for each month, producing 12 maps. However, for simplicity, only the maps for January and July are presented in Chapter 5 of this dissertation; the maps for the remaining months can be found in Appendix A: Supplementary Material as Figures A.4.1 to A.4.12.

The areas identified as major moisture source regions were then connected with average and extreme precipitation patterns over continental areas for each 0.25° grid square. A total of 14 figures are presented in the Atlas connected with the topics described in this section.

Although more information can be derived from each figure in the Atlas, an overall conclusion is that using the FLEXPART model to track moisture from major sources to continental precipitation sinks produces a pattern that strongly resembles the pattern of observed global precipitation, in terms of both climatological and extreme precipitation.

Further Research

Following the same line of research, it could be very interesting to develop a catalogue of extreme precipitation events (wet spells) during the last four decades (1980-2017), either at the global scale, or for regions that show major variability in precipitation or frequently experience extreme precipitation or floods. This catalogue could be executed automatically using reanalysis data and/or different precipitation databases such as the ERA-Interim (Dee et al., 2011), the GPCP (Adler et al., 2003), MSWEP (Beck et al., 2017a) or CHIRPS (Funk et al., 2015). This would enable researchers to find differences between the databases.

Once the areas of interest were identified, the next step would be to analyse the role of the major oceanic and continental moisture sources in providing moisture for regional anomalous extreme precipitation. Determining the moisture contribution of each source would be realized using of the outputs of the Lagrangian model FLEXPART. Finally, attention would be focused on detecting the link between anomalous moisture transport from moisture source regions and the specific synoptic conditions related to extreme precipitation events.

This information could be very useful for further studies in climate change, as changes in the behaviour of moisture support from the sources could affect the frequency and/or intensity of extreme precipitation events.

A

Supplementary Material

In this section is presented the supplementary material linked to each article that makes the main part of this Ph.D dissertation. The supplementary material that corresponds to the "Global Atlas of Precipitation and Contribution of the Main Moisture Sources in the Peak Precipitation Month" presented in Chapter 5 also is included. All material related with published articles is available online by each journal.

A.1. Wet Spells and Associated Moisture Sources Anomalies across Danube River Basin (2017), Water.

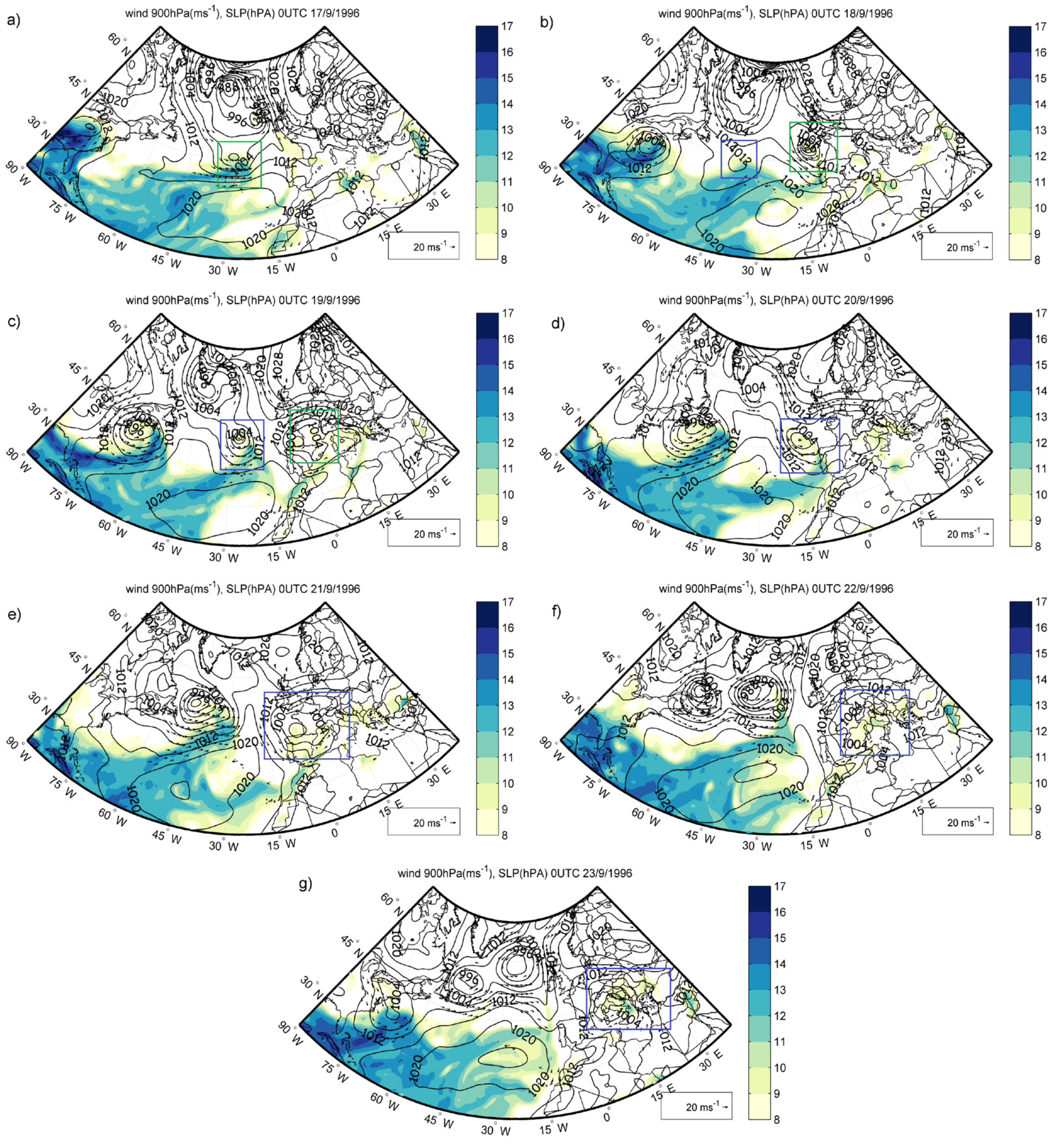

Figure A.1.1. Individual figures from the video presented in supplementary material related with paper "Wet Spells and Associated Moisture Sources Anomalies across Danube River Basin" published in Water (2017).

A.2. Contribution of Moisture from Mediterranean Sea to Extreme Precipitation Events over Danube River Basin (2018), Water.

Table A.2.1. Complete list of top 100 ranked extreme precipitation events in duration of 1-day.

Position of the ranking	Event	∑CHIRPS	Clim. CHIRPS	Anom. CHIRPS	R	∑PFLEX	Clim. PFLEX	Anom. PFLEX	%
1	23 Sep 1996	45.66	4.13	41.53	198.65	0.59	0.15	0.44	285.69
2	28 Dec 2014	17.76	3.45	14.31	168.81	0.82	0.14	0.68	467.93
3	6 Nov 1985	19.74	1.96	17.79	156.70	0.45	0.21	0.25	118.89
4	1 Mar 2008	13.09	2.42	10.68	155.58	0.20	0.18	0.02	11.87
5	18 Feb 1994	12.05	1.18	10.87	142.60	0.40	0.10	0.30	285.92
6	27 Nov 1983	16.94	1.57	15.38	140.42	0.76	0.16	0.60	383.90
7	6 May 1987	26.90	3.53	23.37	138.02	0.58	0.18	0.40	224.24
8	14 Mar 2013	14.18	1.17	13.01	137.91	1.21	0.07	1.14	1657.75
9	2 Mar 2014	9.67	2.07	7.60	136.17	0.08	0.14	-0.06	-41.29
10	27 Mar 1993	13.32	2.47	10.86	131.77	1.12	0.21	0.90	424.33
11	8 Jan 2010	11.10	1.53	9.57	123.27	0.90	0.12	0.78	638.71
12	17 Nov 1995	21.01	1.65	19.35	123.23	0.82	0.24	0.58	241.53
13	2 Apr 1996	17.98	2.40	15.58	120.30	0.95	0.14	0.81	599.77
14	6 Jan 2012	11.52	1.91	9.60	119.68	0.81	0.15	0.66	443.51
15	29 Oct 1994	19.60	1.88	17.73	118.84	0.72	0.17	0.56	333.54
16	23 Dec 1996	11.06	2.07	8.99	117.15	0.81	0.13	0.68	518.01
17	2 Feb 1986	8.67	1.50	7.17	115.85	0.20	0.09	0.11	131.67
18	7 Oct 2011	18.77	2.79	15.98	113.75	0.54	0.17	0.37	219.65
19	11 Aug 2002	28.71	3.87	24.84	113.59	1.32	0.11	1.20	1069.29
20	12 Mar 2003	8.77	1.44	7.33	111.92	0.03	0.07	-0.04	-55.08
21	19 Dec 1987	12.35	1.52	10.83	111.38	0.15	0.17	-0.02	-13.89
22	13 Feb 2007	12.11	2.26	9.85	110.20	0.41	0.09	0.31	332.13
23	14 Nov 2004	16.49	2.07	14.43	109.49	1.55	0.23	1.31	560.80
24	10 Feb 1984	9.19	1.36	7.83	109.20	0.03	0.15	-0.12	-82.42
25	28 Aug 1995	27.69	3.62	24.07	108.05	0.84	0.16	0.68	421.75
26	26 Apr 1995	13.99	1.42	12.57	107.90	0.13	0.09	0.04	44.29
27	26 Feb 1988	9.58	1.36	8.23	107.68	1.03	0.20	0.83	413.62
28	23 Mar 2007	13.60	2.47	11.13	107.24	0.17	0.11	0.07	61.60
29	18 Apr 1991	21.11	2.71	18.40	103.42	0.95	0.17	0.78	459.76
30	6 Apr 1994	15.35	2.63	12.72	103.10	0.19	0.12	0.07	58.91
31	9 Dec 1992	13.62	1.53	12.09	102.77	0.93	0.15	0.78	517.50
32	16 Aug 2005	19.20	3.72	15.48	102.56	0.10	0.08	0.02	26.13
33	1 Jan 1996	11.66	1.92	9.74	98.43	0.54	0.14	0.39	274.39
34	27 Jan 1996	10.41	2.41	8.00	96.56	0.03	0.08	-0.05	-61.35
35	11 Oct 2003	19.53	3.39	16.14	93.08	0.01	0.12	-0.12	-93.90

36	19 Mar 1997	12.95	2.05	10.89	91.70	0.52	0.11	0.41	380.05
37	28 Jan 2009	10.91	1.72	9.19	91.42	0.11	0.11	0.00	1.20
38	6 Nov 1993	16.00	1.96	14.04	90.08	0.34	0.21	0.13	63.23
39	2 Mar 1986	11.23	2.07	9.16	90.05	0.36	0.14	0.23	162.25
40	7 Apr 1990	17.61	1.96	15.65	88.78	0.90	0.12	0.78	629.78
41	12 Dec 1990	10.73	1.50	9.23	88.17	0.38	0.11	0.27	248.28
42	12 Oct 1993	17.02	3.27	13.76	87.87	0.05	0.19	-0.14	-72.21
43	17 Dec 1984	11.11	1.96	9.15	87.71	0.32	0.18	0.14	80.57
44	22 Feb 1999	12.42	2.66	9.76	86.05	0.69	0.17	0.52	309.57
45	22 Jan 1998	7.53	1.68	5.85	85.93	0.11	0.10	0.01	8.05
46	10 Apr 2004	15.01	2.53	12.48	85.51	0.34	0.20	0.14	71.98
47	26 Jan 2001	9.52	1.70	7.82	84.94	0.46	0.12	0.34	272.84
48	7 May 1991	14.64	2.17	12.47	82.08	0.43	0.10	0.34	344.48
49	2 Apr 1984	14.74	2.40	12.34	82.07	0.72	0.14	0.58	431.93
50	2 Mar 1987	9.07	2.07	7.01	80.27	0.28	0.14	0.14	104.07
51	14 Jan 2013	6.99	1.12	5.87	80.25	0.67	0.12	0.55	456.71
52	27 Dec 1995	11.12	2.77	8.34	80.02	0.70	0.19	0.52	279.37
53	19 Mar 2002	11.76	2.21	9.55	79.83	0.12	0.11	0.01	8.66
54	16 Oct 2013	16.46	2.54	13.92	79.17	0.24	0.17	0.06	35.19
55	2 Jan 2006	10.76	1.72	9.04	78.95	0.41	0.12	0.29	239.19
56	1 Apr 1987	13.97	1.67	12.30	78.09	0.35	0.12	0.23	192.86
57	12 Oct 2009	17.26	2.52	14.74	77.95	1.52	0.23	1.29	558.41
58	27 Dec 1999	14.03	2.77	11.25	76.69	0.31	0.19	0.13	68.59
59	13 May 1995	20.53	3.03	17.50	76.38	0.68	0.12	0.57	476.08
60	15 Jan 1987	7.04	1.07	5.96	76.25	0.65	0.09	0.57	665.85
61	9 Feb 1984	8.03	1.73	6.30	75.67	0.94	0.15	0.80	538.64
62	21 May 1987	12.15	3.69	8.46	75.59	0.22	0.15	0.07	47.60
63	12 Feb 2009	6.85	2.27	4.58	75.32	0.03	0.18	-0.16	-86.15
64	21 Oct 1991	14.66	2.26	12.40	74.39	0.95	0.20	0.75	376.62
65	6 Dec 2005	8.74	1.82	6.93	73.74	0.43	0.12	0.31	247.91
66	13 Nov 1997	14.07	1.91	12.17	73.71	1.43	0.25	1.19	483.46
67	1 Jul 2005	18.76	3.73	15.03	73.08	0.36	0.09	0.26	279.36
68	13 Oct 2009	13.22	1.52	11.70	72.84	0.05	0.12	-0.07	-59.74
69	31 Jan 1988	5.14	1.51	3.62	71.88	0.01	0.06	-0.05	-88.70
70	4 Feb 2003	10.67	1.29	9.38	71.76	1.11	0.13	0.98	762.73
71	27 Mar 1996	11.47	2.74	8.72	71.51	0.70	0.21	0.49	230.01
72	18 Dec 2008	13.11	2.11	11.00	71.37	0.48	0.19	0.29	149.68
73	11 Apr 1998	12.59	1.74	10.86	71.32	0.64	0.23	0.41	174.03
74	21 Jan 2009	8.16	1.49	6.67	71.29	1.04	0.13	0.91	690.28
75	27 Mar 2015	7.24	2.74	4.49	70.91	0.39	0.21	0.18	83.71
76	28 Nov 2015	7.38	1.75	5.63	70.90	0.01	0.21	-0.20	-96.35
77	3 May 2014	14.03	2.79	11.24	70.16	0.44	0.16	0.27	166.29
78	9 Jul 1999	17.90	2.52	15.38	69.04	0.14	0.08	0.06	81.88
79	21 Jun 2010	16.94	3.20	13.74	68.56	0.22	0.11	0.11	100.23

80	21 Nov 2015	18.20	2.64	15.56	67.96	0.87	0.24	0.63	263.17
81	6 Sep 1998	15.13	2.44	12.68	67.16	0.13	0.05	0.08	150.22
82	3 May 1991	18.97	2.79	16.18	66.54	0.89	0.16	0.73	442.61
83	4 Sep 1995	15.30	2.83	12.47	66.01	0.54	0.18	0.36	203.75
84	26 Nov 1990	12.98	2.32	10.66	64.49	0.68	0.21	0.48	230.99
85	19 Mar 1981	8.73	2.21	6.52	64.24	0.18	0.11	0.07	63.02
86	9 Feb 1986	6.83	1.73	5.10	64.21	0.40	0.15	0.25	170.91
87	21 Jan 2012	7.37	1.49	5.88	64.05	0.01	0.13	-0.12	-89.49
88	17 Aug 2015	16.51	2.12	14.39	63.33	0.18	0.06	0.13	231.56
89	28 Oct 1990	12.59	1.90	10.69	62.53	0.15	0.13	0.01	11.11
90	11 May 2014	17.02	2.56	14.46	62.10	0.49	0.14	0.35	259.04
91	6 Apr 2015	8.21	2.34	5.87	62.05	0.03	0.12	-0.09	-78.81
92	15 Oct 2015	14.38	2.06	12.32	61.99	1.02	0.19	0.84	445.27
93	6 Feb 2015	7.11	1.68	5.43	60.57	0.37	0.11	0.26	243.27
94	21 Apr 1997	15.27	2.18	13.09	59.82	0.84	0.16	0.68	430.11
95	4 Dec 2010	8.63	2.07	6.56	58.82	0.25	0.14	0.10	72.75
96	28 Aug 1989	16.38	4.01	12.37	58.70	0.49	0.16	0.33	201.78
97	1 Jun 1995	19.50	3.75	15.75	58.15	0.54	0.13	0.41	312.41
98	5 Oct 2008	11.92	1.42	10.50	58.09	0.04	0.18	-0.14	-78.84
99	17 Feb 2000	9.65	1.44	8.20	58.02	0.59	0.11	0.49	464.60
100	12 Sep 1998	18.89	2.73	16.16	57.78	1.87	0.19	1.68	891.79

Table A.2.2. Complete list of top 100 ranked extreme precipitation events in duration of 3-days.

Position of the ranking	Event	∑CHIRPS	Clim. CHIRPS	Anom. CHIRPS	R	∑PFLEX	Clim. PFLEX	Anom. PFLEX	%
1	24 Sep 1996	19.61	2.59	17.02	249.95	1.37	0.57	0.80	140.94
2	23 Sep 1996	18.54	2.51	16.03	228.27	2.10	0.51	1.59	312.59
3	25 Sep 1996	16.90	2.49	14.41	224.59	0.70	0.59	0.11	18.07
4	11 Feb 1984	6.77	1.70	5.07	206.04	0.54	0.40	0.14	34.63
5	6 Nov 1985	9.50	2.03	7.46	204.39	1.12	0.54	0.58	107.29
6	8 Jan 2010	6.12	1.46	4.67	198.54	0.96	0.30	0.66	217.26
7	6 May 1987	13.52	3.08	10.44	198.36	2.05	0.53	1.52	284.32
8	10 Feb 1984	6.54	1.61	4.93	195.88	1.03	0.38	0.64	169.23
9	29 Oct 1990	11.82	2.03	9.79	195.15	1.07	0.35	0.71	202.75
10	31 Oct 1994	10.10	2.05	8.06	193.43	0.38	0.37	0.01	3.85
11	30 Oct 1994	10.99	2.13	8.85	191.17	0.82	0.36	0.46	130.79
12	18 Nov1995	10.95	2.40	8.55	187.50	0.82	0.49	0.33	66.58
13	29 Dec 2014	9.60	2.40	7.20	187.08	0.59	0.34	0.25	72.98
14	30 Dec 2014	7.58	2.02	5.56	185.61	0.29	0.34	-0.06	-16.90

15	13 Oct 1909	11.90	2.17	9.73	182.86	1.52	0.51	1.01	199.80
16	29 Jan 2009	7.32	1.76	5.55	182.47	0.62	0.27	0.35	126.60
17	14 Dec 1990	7.36	1.57	5.79	182.29	0.95	0.35	0.60	168.74
18	28 Nov1983	9.08	2.05	7.02	181.46	0.75	0.57	0.19	32.76
19	7 Nov 1985	8.80	2.00	6.80	180.98	0.77	0.53	0.24	45.94
20	2 Jan 1996	7.50	1.63	5.87	180.67	1.26	0.38	0.88	234.37
21	25 Dec 1996	6.74	1.81	4.93	179.69	1.19	0.41	0.78	187.90
22	6 Feb 2003	6.91	1.44	5.47	177.66	0.69	0.31	0.38	120.48
23	17 Nov1995	10.32	2.40	7.92	175.32	0.92	0.52	0.40	76.22
24	28 Jan 2009	6.93	1.76	5.17	171.50	1.00	0.29	0.72	248.96
25	28 Dec 1999	11.14	2.74	8.40	168.31	0.79	0.40	0.39	98.10
26	21 Oct 1991	12.17	1.94	10.23	166.90	1.48	0.62	0.86	139.41
27	22 Jan 1998	6.11	1.48	4.64	165.90	0.98	0.37	0.60	161.20
28	27 Nov1983	7.50	2.02	5.48	165.70	0.63	0.49	0.14	29.19
29	31 Jan 1988	6.65	1.71	4.94	165.38	0.98	0.24	0.74	309.91
30	1 Jan 1996	7.53	1.61	5.92	163.93	1.77	0.40	1.38	345.24
31	7 Jan 2012	7.56	1.59	5.97	163.40	0.77	0.32	0.45	141.94
32	22 Oct 1991	10.55	2.22	8.33	162.85	0.82	0.62	0.19	31.29
33	24 Dec 1996	5.81	1.78	4.03	162.66	1.52	0.37	1.15	313.45
34	14 Oct 2009	10.42	1.89	8.53	161.91	0.88	0.49	0.39	80.69
35	7 May1987	11.48	2.85	8.63	161.10	1.14	0.46	0.68	146.86
36	18 Aug2005	11.16	2.11	9.04	160.75	0.21	0.32	-0.11	-33.74
37	02 Mar 2014	4.50	2.02	2.49	160.46	0.75	0.39	0.36	90.93
38	30 Oct 1990	9.72	2.13	7.59	160.35	0.92	0.36	0.56	154.33
39	05 Feb 2003	6.92	1.23	5.69	159.68	0.93	0.32	0.61	190.19
40	03 Mar 2014	5.04	2.29	2.74	159.62	0.77	0.41	0.37	90.21
41	10 Dec 1992	8.40	1.78	6.62	158.95	0.92	0.35	0.57	159.72
42	28 Dec 2014	8.81	2.74	6.07	158.74	0.66	0.40	0.26	63.80
43	8 Aug 1985	15.60	2.73	12.87	157.20	0.88	0.39	0.49	124.46
44	08 Nov1985	7.13	1.95	5.18	156.25	0.32	0.51	-0.19	-37.21
45	20 Feb 1994	5.65	1.38	4.27	153.69	0.35	0.31	0.04	13.07
46	17 Aug2005	12.46	2.31	10.16	152.98	0.41	0.33	0.08	24.74
47	29 Nov1983	7.73	1.81	5.92	152.01	0.57	0.56	0.01	1.63
48	12 Aug2002	13.69	2.35	11.34	148.88	1.53	0.40	1.14	287.68
49	09 Nov2011	10.95	1.78	9.16	148.65	0.77	0.49	0.29	58.52
50	12 Apr 2004	8.28	3.02	5.27	147.63	1.08	0.54	0.53	98.14
51	8 May 1987	9.82	3.05	6.77	147.47	0.34	0.41	-0.07	-16.90
52	2 Feb 1986	6.04	1.39	4.65	147.46	0.93	0.23	0.70	304.06
53	3 Mar 2008	4.53	2.29	2.24	147.36	0.48	0.41	0.08	18.85
54	2 Mar 1986	6.39	2.02	4.37	147.33	1.10	0.39	0.71	179.39
55	20 Dec 1987	5.41	2.20	3.21	144.88	0.07	0.39	-0.33	-83.20
56	19 Feb 1994	5.81	1.46	4.35	142.71	0.51	0.29	0.22	73.69
57	6 Jan 2012	7.25	1.61	5.64	141.69	1.10	0.35	0.75	216.95
58	29 Aug1989	12.45	3.13	9.32	141.26	1.32	0.50	0.82	163.53

59	19 Nov1995	8.58	2.16	6.42	141.10	0.47	0.45	0.01	3.20
60	13 Aug2002	12.47	2.53	9.94	141.07	0.68	0.35	0.34	96.45
61	23 Jan 1998	5.11	1.49	3.63	141.05	0.35	0.39	-0.04	-9.75
62	8 Jan 2012	4.96	1.46	3.50	140.58	0.30	0.31	-0.01	-4.27
63	12 Dec 1990	7.44	1.60	5.83	139.80	1.55	0.32	1.23	390.63
64	27 Feb 1988	5.55	1.26	4.30	139.01	1.24	0.32	0.91	282.62
65	13 May1995	13.17	2.96	10.21	138.70	1.18	0.48	0.70	145.90
66	16 Nov2015	10.45	2.07	8.38	137.40	1.80	0.51	1.29	251.37
67	4 Apr 1996	9.28	1.99	7.29	137.12	0.95	0.46	0.49	104.53
68	15 Jan 1987	5.13	1.00	4.12	136.95	1.02	0.26	0.77	299.31
69	21 Nov1999	7.94	2.18	5.76	136.74	1.28	0.52	0.76	144.54
70	19 Dec 1987	5.06	2.27	2.79	136.12	0.07	0.42	-0.35	-83.40
71	8 Nov 1989	8.40	1.95	6.45	135.01	1.01	0.51	0.50	98.64
72	3 Feb 1986	5.17	1.23	3.94	134.79	0.68	0.26	0.42	159.09
73	11 Apr 2004	8.78	2.45	6.33	134.73	0.89	0.52	0.36	69.75
74	18 Aug2015	11.35	2.11	9.24	134.45	1.06	0.33	0.73	219.89
75	11 Dec 1992	6.45	1.70	4.75	134.20	0.45	0.32	0.13	40.37
76	3 Mar 1986	6.60	2.29	4.30	134.00	0.90	0.41	0.49	120.90
77	14 May1995	12.63	2.89	9.74	133.94	0.76	0.49	0.28	56.45
78	3 Apr 1996	7.92	1.86	6.06	132.92	1.42	0.42	1.00	235.97
79	4 Apr 1988	6.75	1.84	4.90	132.35	0.80	0.44	0.36	81.53
80	16 Aug2005	12.20	2.15	10.05	132.04	0.54	0.33	0.21	65.50
81	11 Aug2002	12.49	2.47	10.02	131.69	2.08	0.42	1.66	392.20
82	29 Oct 1994	8.24	2.03	6.21	130.86	1.09	0.36	0.73	204.46
83	30 Aug1989	11.33	2.97	8.37	130.45	0.77	0.46	0.31	67.97
84	15 Nov2015	10.04	1.73	8.31	130.31	2.19	0.49	1.71	348.95
85	27 Mar 1993	6.40	2.13	4.27	130.10	1.32	0.54	0.78	145.08
86	21 Dec 1987	5.08	1.97	3.11	130.09	0.05	0.35	-0.30	-85.81
87	27 Apr 1995	6.90	1.57	5.33	130.02	0.64	0.40	0.24	59.74
88	18 Feb 1994	4.21	1.41	2.81	129.75	0.53	0.29	0.24	84.24
89	4 Mar 2014	4.01	2.10	1.91	126.98	0.74	0.38	0.36	93.67
90	28 Apr 1995	5.83	1.71	4.13	126.70	0.20	0.41	-0.21	-51.00
91	26 Apr 1995	6.98	1.49	5.50	126.22	1.24	0.39	0.85	216.30
92	16 Apr 1982	8.41	2.05	6.36	125.97	0.51	0.47	0.04	8.90
93	16 Jan 1987	4.94	0.94	4.00	125.64	0.79	0.26	0.53	207.63
94	26 Feb 1988	6.20	1.43	4.77	125.44	1.91	0.38	1.54	409.29
95	16 Mar 2013	5.73	1.00	4.73	125.13	0.53	0.25	0.29	115.77
96	10 Jan 2010	4.74	1.29	3.45	125.11	1.03	0.30	0.73	243.95
97	29 Dec 1999	8.24	2.40	5.84	124.95	0.70	0.35	0.36	102.08
98	2 Jan 2006	6.46	1.63	4.83	124.56	1.52	0.38	1.14	301.31
99	23 Mar 2007	8.11	1.67	6.44	124.23	1.20	0.41	0.79	191.78
100	9 Jan 2010	4.54	1.31	3.23	124.20	1.16	0.31	0.85	272.74

Table A.2.3. Complete list of top 100 ranked extreme precipitation events in duration of 5-days.

Position of the ranking	Event	∑CHIRPS	Clim. CHIRPS	Anom. CHIRPS	R	∑PFLEX	Clim. PFLEX	Anom. PFLEX	%
1	24 Sep 1996	12.46	2.47	9.99	254.85	1.92	0.74	1.18	160.01
2	25 Sep1996	12.13	2.36	9.77	254.22	1.62	0.77	0.85	110.97
3	26 Sep 1996	12.15	2.39	9.76	251.71	1.14	0.79	0.36	45.42
4	14 Dec 1990	6.74	1.53	5.21	237.58	1.40	0.43	0.96	222.56
5	23 Jan 1998	5.64	1.46	4.18	234.92	1.17	0.48	0.69	145.60
6	27 Sep 1996	10.82	2.38	8.44	231.42	0.60	0.79	-0.20	-24.68
7	23 Sep 1996	11.71	2.39	9.32	230.92	2.13	0.70	1.42	201.84
8	22 Jan 1998	5.42	1.48	3.94	227.95	1.57	0.46	1.11	243.75
9	30 Oct 1990	8.02	1.95	6.07	222.08	1.14	0.47	0.67	142.65
10	31 Oct 1990	7.89	1.97	5.92	221.67	1.13	0.47	0.65	138.03
11	7 May 1987	9.28	2.91	6.37	220.10	2.01	0.69	1.32	191.95
12	6 Nov 1985	6.64	1.69	4.95	219.06	0.94	0.65	0.29	43.92
13	8 Jan 2010	4.70	1.48	3.22	217.31	1.16	0.38	0.78	202.85
14	6 May 1987	9.06	2.79	6.27	216.29	2.47	0.72	1.75	243.22
15	9 Jan 2010	5.12	1.49	3.64	216.16	1.26	0.38	0.87	227.21
16	11 Feb 1984	5.15	1.63	3.52	213.17	0.85	0.47	0.38	82.26
17	10 Feb 1984	4.98	1.60	3.37	210.03	0.90	0.45	0.45	100.75
18	31 Oct 1994	7.09	1.97	5.12	207.34	0.80	0.47	0.33	69.36
19	8 May 1987	8.62	2.89	5.74	206.97	1.48	0.65	0.83	127.84
20	7 Nov 1985	5.90	1.76	4.13	204.56	0.80	0.67	0.13	18.82
21	8 Nov1985	6.03	1.84	4.19	204.12	0.86	0.68	0.19	27.60
22	26 Dec 1996	5.12	1.98	3.13	203.62	1.15	0.50	0.65	130.89
23	1 Nov1994	6.98	1.89	5.08	202.19	0.71	0.50	0.21	42.50
24	27 Dec 1996	4.80	2.20	2.60	199.77	0.94	0.50	0.44	89.06
25	23 Nov 1999	7.03	2.29	4.75	199.51	1.08	0.68	0.41	59.85
26	6 Dec 1988	5.65	1.91	3.74	199.50	0.59	0.53	0.06	10.83
27	12 Feb 1984	4.86	1.78	3.07	198.73	0.69	0.47	0.22	46.67
28	18 Aug 2005	10.18	2.02	8.16	196.49	0.65	0.50	0.16	31.59
29	10 Jan 2010	4.30	1.39	2.90	196.09	0.99	0.37	0.62	168.20
30	29 Oct 1990	7.28	1.80	5.48	195.89	1.18	0.48	0.70	146.21
31	15 Jan 1987	4.59	0.98	3.61	195.84	1.10	0.31	0.79	252.43
32	5 Dec 1988	6.25	2.02	4.23	195.06	0.80	0.57	0.23	40.75
33	30 Oct 1994	6.99	1.95	5.04	194.88	0.94	0.47	0.47	101.03
34	22 Nov 1999	6.73	2.23	4.50	194.54	1.31	0.66	0.64	96.61
35	19 Nov 1995	7.14	2.18	4.97	194.19	0.60	0.61	-0.01	-1.21
36	18 Jan 1987	4.53	1.09	3.44	193.66	0.67	0.36	0.31	84.53
37	16 Dec 1990	5.34	1.68	3.66	193.15	0.91	0.49	0.43	87.35
38	13 Feb 1984	4.53	1.83	2.70	193.03	0.39	0.44	-0.05	-10.93

39	20 Nov 1995	7.05	2.22	4.83	192.16	0.50	0.61	-0.11	-18.42
40	22 Oct 1991	8.68	1.87	6.80	192.04	1.28	0.79	0.49	62.98
41	2 Nov 1994	6.10	1.77	4.33	190.77	0.51	0.52	-0.01	-1.01
42	18 Nov 1995	6.91	2.26	4.65	190.55	0.66	0.63	0.02	3.44
43	19 Aug 2005	8.81	1.94	6.86	189.80	0.70	0.51	0.19	37.88
44	15 Dec 1990	5.58	1.60	3.98	189.60	1.14	0.46	0.68	146.03
45	12 Dec 1992	6.50	1.73	4.77	188.82	0.58	0.42	0.16	38.51
46	31 Dec 2014	5.79	2.06	3.72	187.06	0.36	0.45	-0.10	-21.06
47	1 Jan 2015	4.57	1.85	2.72	185.48	0.17	0.46	-0.29	-62.57
48	13 Dec 1990	6.43	1.64	4.79	184.68	1.61	0.41	1.20	290.50
49	15 Oct 2009	7.37	2.04	5.33	184.48	1.28	0.68	0.60	89.08
50	5 Dec 2010	7.20	2.02	5.18	184.09	1.11	0.57	0.54	94.48
51	25 Dec 1996	4.44	1.71	2.73	183.80	1.31	0.47	0.85	182.43
52	14 Oct 2009	7.56	1.97	5.58	182.48	1.62	0.68	0.94	139.75
53	8 Feb 2003	4.41	1.47	2.93	182.42	0.48	0.41	0.07	16.55
54	9 Nov 1985	5.55	1.83	3.72	182.36	0.85	0.66	0.19	28.35
55	6 Feb 2003	4.65	1.38	3.27	182.19	0.65	0.37	0.27	72.72
56	13 Oct 2009	7.59	1.89	5.70	182.03	2.00	0.66	1.34	201.72
57	7 Feb 2003	4.70	1.37	3.33	181.78	0.63	0.39	0.24	61.96
58	4 Jan 1996	4.52	1.48	3.05	180.60	0.93	0.42	0.51	120.62
59	30 Nov 1983	5.69	1.85	3.84	180.47	0.46	0.60	-0.14	-22.96
60	31 Jan 2009	4.46	1.72	2.74	179.48	0.48	0.31	0.16	52.77
61	7 May 1991	8.03	2.91	5.12	179.43	1.41	0.69	0.72	105.06
62	30 Dec 2014	6.28	2.32	3.96	179.25	0.40	0.46	-0.06	-13.78
63	21 Oct 1991	8.36	1.68	6.67	178.59	1.56	0.79	0.77	97.06
64	3 Jan 2006	5.95	1.55	4.41	178.16	1.64	0.43	1.21	279.09
65	28 Nov 1983	5.52	1.97	3.55	178.13	0.56	0.70	-0.14	-20.49
66	22 Jun 2010	10.36	3.15	7.20	178.13	1.16	0.79	0.37	46.93
67	11 Aug 2002	10.25	2.53	7.72	178.01	1.82	0.59	1.23	208.84
68	29 Nov 1983	5.75	1.88	3.87	177.61	0.52	0.68	-0.16	-23.16
69	23 Oct 1991	7.77	2.08	5.70	177.48	0.90	0.75	0.14	18.84
70	30 Jan 2009	4.70	1.78	2.92	177.37	0.73	0.34	0.39	114.63
71	15 Oct 2015	8.48	2.04	6.44	177.15	2.27	0.68	1.60	236.30
72	2 Jan 1996	5.18	1.66	3.52	176.16	1.49	0.46	1.04	227.76
73	17 Nov 1995	6.33	2.28	4.06	175.70	0.70	0.66	0.04	5.83
74	12 Dec 1990	5.91	1.73	4.18	175.64	1.64	0.42	1.22	288.58
75	20 Aug 2005	7.69	1.86	5.83	175.63	0.87	0.52	0.35	67.30
76	29 Dec 2014	6.46	2.35	4.11	174.21	0.42	0.47	-0.05	-10.96
77	24 Jan 1998	4.14	1.58	2.56	173.70	0.61	0.47	0.14	28.89
78	3 Jan 1996	4.75	1.55	3.20	173.24	1.28	0.43	0.84	194.69
79	4 Dec 2010	7.29	1.88	5.41	172.46	1.20	0.51	0.69	135.95
80	16 Oct 2009	6.83	2.05	4.78	171.30	0.99	0.68	0.31	45.60
81	2 Jan 2006	5.93	1.66	4.27	170.71	1.87	0.46	1.42	310.89
82	21 Jun 2010	10.28	3.26	7.02	170.07	1.54	0.76	0.78	103.23

83	31 Jan 1988	4.35	1.72	2.63	169.56	0.88	0.31	0.57	182.66
84	20 Aug 2015	8.40	1.86	6.54	168.84	0.93	0.52	0.41	79.01
85	15 May 2014	10.01	2.72	7.29	167.82	1.79	0.73	1.06	143.86
86	13 Dec 1992	5.37	1.64	3.72	167.27	0.31	0.41	-0.10	-25.19
87	14 Apr 2004	5.95	2.62	3.33	167.19	0.94	0.66	0.28	41.84
88	1 Nov 1990	6.34	1.89	4.45	166.97	1.04	0.50	0.54	109.41
89	27 Nov 1983	4.50	2.04	2.46	165.70	0.48	0.69	-0.21	-30.90
90	17 Aug 2005	9.27	2.21	7.06	165.69	0.60	0.48	0.12	25.22
91	1 Jan 1996	5.03	1.85	3.18	165.26	1.62	0.46	1.17	255.68
92	12 Aug 2002	9.52	2.37	7.15	163.60	1.74	0.58	1.17	202.85
93	8 Jan 2012	5.02	1.48	3.54	163.43	0.68	0.38	0.29	76.51
94	10 Nov 1985	4.78	1.81	2.97	163.40	0.70	0.64	0.06	9.11
95	11 Oct 2011	7.37	1.91	5.46	163.24	0.49	0.69	-0.21	-29.62
96	24 Oct 1991	6.41	2.07	4.34	162.85	0.49	0.69	-0.20	-28.83
97	9 Jan 2012	4.66	1.49	3.17	162.46	0.47	0.38	0.08	21.26
98	9 May 1987	7.01	2.68	4.34	162.16	1.03	0.63	0.40	64.20
99	24 Dec 1996	4.24	1.72	2.52	162.00	1.44	0.45	0.99	222.90
100	30 Dec 1999	6.84	2.32	4.51	161.95	0.69	0.46	0.22	48.51

Table A.2.4. Complete list of top 100 ranked extreme precipitation events in duration of 7-days.

Position of the ranking	Event	∑CHIRPS	Clim. CHIRPS	Anom. CHIRPS	R	∑PFLEX	Clim. PFLEX	Anom. PFLEX	%
1	1 Jan 1996	6.52	2.12	4.40	298.19	1.67	0.51	1.16	225.99
2	15 Dec 1990	6.41	1.67	4.74	290.71	1.41	0.51	0.89	173.84
3	2 Jan 1996	5.33	1.96	3.37	277.60	1.36	0.49	0.88	180.10
4	14 Dec 1990	5.84	1.64	4.21	273.79	1.55	0.51	1.04	205.09
5	7 May 1987	7.53	2.67	4.86	260.72	2.16	0.80	1.36	171.43
6	27 Sep 1996	9.15	2.32	6.83	260.69	1.24	0.89	0.35	38.74
7	24 Sep 1996	9.28	2.34	6.94	258.47	1.92	0.86	1.07	124.99
8	16 Dec 1990	5.47	1.62	3.86	257.33	1.26	0.53	0.73	138.16
9	28 Sep 1996	9.07	2.26	6.81	256.91	0.86	0.90	-0.05	-5.41
10	25 Sep 1996	9.08	2.31	6.77	256.87	1.76	0.86	0.89	102.92
11	26 Sep 1996	9.17	2.36	6.81	256.73	1.56	0.88	0.68	77.69
12	22 Aug 2005	7.98	2.01	5.97	252.96	1.19	0.68	0.51	74.10
13	6 May 1987	7.33	2.50	4.84	249.36	2.34	0.80	1.53	190.55
14	2 Apr 1996	5.41	2.01	3.40	246.28	1.23	0.65	0.58	90.07
15	22 Jun 2010	9.99	3.24	6.75	239.59	1.47	0.90	0.57	63.04
16	12 Aug 2002	9.95	2.52	7.43	237.97	1.63	0.68	0.94	137.46
17	23 Jan 1998	4.21	1.42	2.79	235.76	1.34	0.50	0.84	168.02
18	24 Jan 1998	4.21	1.56	2.65	234.78	1.15	0.50	0.65	127.77

19	25 Jan 1998	4.03	1.51	2.53	233.71	0.85	0.50	0.35	70.68
20	23 Sep 1996	8.62	2.37	6.25	232.77	2.00	0.84	1.16	137.11
21	29 Sep 1996	7.88	2.30	5.59	231.89	0.56	0.90	-0.35	-38.32
22	2 Nov 1990	6.09	1.79	4.30	229.33	1.08	0.59	0.49	83.46
23	1 Nov 1990	6.09	1.83	4.26	228.84	1.16	0.57	0.59	101.96
24	22 Jan 1998	3.94	1.29	2.65	227.38	1.54	0.48	1.06	218.64
25	21 Aug 2005	7.70	1.97	5.73	226.86	1.17	0.65	0.51	78.43
26	6 Dec 1988	4.99	1.92	3.07	225.28	0.65	0.55	0.10	18.97
27	8 May 1987	6.84	2.74	4.10	224.91	1.97	0.79	1.18	148.81
28	2 Mar 1986	4.08	1.63	2.45	222.93	0.78	0.53	0.25	46.78
29	30 Oct 1990	5.74	1.81	3.93	222.41	1.10	0.55	0.55	98.34
30	31 Oct 1990	5.77	1.82	3.94	222.41	1.19	0.56	0.63	112.89
31	9 May 1987	6.72	2.77	3.95	221.04	1.72	0.79	0.93	117.88
32	22 Nov 1999	5.75	2.36	3.38	220.65	1.31	0.73	0.58	79.12
33	8 Nov 1985	4.98	1.65	3.33	220.23	0.95	0.74	0.22	29.43
34	11 Jan 2010	3.85	1.42	2.43	220.11	0.97	0.40	0.57	141.10
35	18 Dec 1990	4.22	1.79	2.42	218.33	0.90	0.55	0.35	63.15
36	7 Nov 1985	4.90	1.64	3.25	217.17	0.93	0.73	0.20	28.09
37	7 Dec 1988	4.76	1.86	2.90	216.63	0.62	0.59	0.03	5.04
38	9 Jan 2010	3.97	1.43	2.54	216.62	1.19	0.42	0.77	185.07
39	30 Oct 1994	5.81	1.81	4.00	216.45	0.97	0.55	0.41	74.30
40	20 Aug 2005	7.98	1.86	6.12	215.43	1.05	0.63	0.42	66.90
41	10 Jan 2010	3.80	1.43	2.37	214.89	1.14	0.42	0.72	173.29
42	21 Jun 2010	9.57	3.12	6.45	214.22	1.80	0.87	0.92	105.78
43	10 Nov 1985	4.67	1.77	2.90	212.73	1.06	0.74	0.33	44.28
44	12 Feb 1984	4.22	1.73	2.49	211.67	0.71	0.50	0.22	44.22
45	6 Nov 1985	5.54	1.65	3.90	211.18	1.09	0.71	0.38	54.26
46	11 Aug 2002	9.34	2.62	6.72	210.16	1.74	0.70	1.03	147.82
47	8 Jan 2010	4.04	1.48	2.57	208.92	1.05	0.41	0.64	155.39
48	24 Nov 1999	5.67	2.18	3.49	208.37	0.95	0.76	0.19	24.59
49	31 Oct 1994	5.27	1.82	3.45	208.21	0.92	0.56	0.36	63.92
50	10 May 1987	6.22	2.58	3.63	207.15	1.42	0.79	0.63	80.19
51	11 Feb 1984	4.14	1.60	2.54	206.64	0.71	0.48	0.22	45.54
52	1 Nov 1994	5.26	1.83	3.44	206.12	0.88	0.57	0.30	52.66
53	25 Nov 1999	5.50	2.16	3.34	205.72	0.79	0.78	0.01	1.25
54	9 Nov 1985	4.40	1.71	2.69	205.56	0.99	0.74	0.24	32.95
55	5 Dec 1988	5.18	1.88	3.29	205.25	0.67	0.55	0.12	21.58
56	2 Nov 1994	5.09	1.79	3.30	204.62	0.82	0.59	0.23	39.44
57	16 Oct 2015	7.45	2.06	5.38	204.52	2.64	0.79	1.85	233.54
58	13 Aug 2002	8.57	2.45	6.11	204.26	1.43	0.66	0.77	116.52
59	27 Dec 1996	3.71	2.01	1.70	203.94	1.09	0.52	0.57	109.55
60	28 Dec 1996	3.67	2.19	1.48	203.52	1.01	0.52	0.49	95.09
61	12 Dec 1990	4.92	1.65	3.27	203.25	1.74	0.49	1.25	255.46
62	23 Nov 1999	5.27	2.30	2.97	203.03	1.09	0.73	0.36	49.22

63	8 May 1991	6.50	2.74	3.76	202.96	1.44	0.79	0.65	82.16
64	19 Aug 2005	7.57	1.98	5.59	202.80	0.91	0.61	0.30	49.07
65	18 Aug 2005	7.69	2.09	5.60	202.66	0.88	0.60	0.28	46.35
66	29 Dec 1996	3.59	2.20	1.39	202.33	0.94	0.52	0.42	81.66
67	26 Dec 1996	4.20	1.88	2.32	201.89	1.19	0.52	0.67	129.72
68	3 Nov 1994	4.99	1.69	3.30	201.87	0.77	0.61	0.15	24.92
69	12 Jan 2010	3.12	1.27	1.85	201.06	0.74	0.38	0.36	93.60
70	13 Feb 1984	4.01	1.74	2.27	200.68	0.70	0.49	0.21	43.85
71	17 Dec 1990	4.25	1.69	2.56	200.50	1.10	0.54	0.56	103.11
72	12 May 1991	5.40	2.67	2.73	200.36	1.22	0.80	0.42	52.80
73	8 Dec 1988	4.06	1.76	2.30	199.68	0.45	0.56	-0.11	-20.13
74	16 Jan 1987	3.80	0.97	2.84	198.66	1.07	0.37	0.70	190.89
75	1 Jan 2000	5.54	2.12	3.43	197.40	0.54	0.51	0.02	4.85
76	23 Jun 2010	8.19	3.26	4.93	197.37	1.18	0.90	0.27	30.42
77	11 Nov 1985	4.38	1.75	2.62	197.04	1.09	0.72	0.37	51.63
78	15 Jan 1987	3.69	1.07	2.62	196.39	1.24	0.37	0.87	233.07
79	15 Oct 2015	7.11	1.88	5.23	196.26	2.68	0.77	1.91	247.80
80	7 May 1991	6.46	2.67	3.79	196.06	1.44	0.80	0.64	80.93
81	29 Oct 1990	5.20	1.81	3.39	195.89	1.03	0.58	0.46	78.88
82	18 Jan 1987	3.59	0.99	2.60	195.59	0.74	0.40	0.33	83.08
83	21 Nov 1995	5.05	2.36	2.69	195.41	0.46	0.72	-0.25	-35.36
84	20 Nov 1995	5.28	2.17	3.11	195.30	0.48	0.70	-0.23	-32.07
85	9 May 1991	6.12	2.77	3.35	195.13	1.47	0.79	0.68	86.47
86	13 Dec 1990	4.93	1.57	3.37	194.88	1.66	0.49	1.16	234.77
87	19 Nov 1995	5.20	2.15	3.05	194.55	0.54	0.71	-0.18	-24.65
88	12 Dec 1992	5.30	1.65	3.65	194.52	0.81	0.49	0.32	65.01
89	17 Oct 2009	5.67	2.04	3.64	193.88	1.31	0.80	0.51	63.68
90	10 Feb 1984	3.97	1.52	2.45	193.75	0.73	0.48	0.25	50.96
91	3 Jan 2006	5.55	1.74	3.81	193.55	1.79	0.47	1.31	278.78
92	19 Jan 1987	3.63	1.09	2.54	193.21	0.67	0.43	0.24	54.28
93	22 Nov 1995	5.05	2.36	2.69	192.55	0.48	0.73	-0.25	-33.67
94	11 Dec 1992	5.58	1.70	3.88	192.42	1.10	0.50	0.60	120.71
95	16 Oct 2009	5.81	2.06	3.75	192.12	1.51	0.79	0.72	90.26
96	24 Oct 1991	6.25	1.86	4.39	191.99	0.92	0.80	0.12	15.44
97	18 Nov 1995	4.94	2.11	2.83	190.55	0.61	0.72	-0.11	-14.86
98	4 Nov 1994	4.36	1.66	2.70	190.55	0.61	0.65	-0.04	-6.73
99	17 Oct 2015	6.56	2.04	4.53	190.27	2.30	0.80	1.50	187.37
100	17 Jan 1987	3.70	0.93	2.77	190.02	0.92	0.39	0.53	137.74

Table A.2.5. Complete list of top 100 ranked extreme precipitation events in duration of 10-days.

Position of the ranking	Event	∑CHIRPS	Clim. CHIRPS	Anom. CHIRPS	R	∑PFLEX	Clim. PFLEX	Anom. PFLEX	%
1	23 Aug 2005	8.05	2.02	6.03	325.98	1.15	0.79	0.36	45.52
2	18 Dec 1990	4.82	1.76	3.06	317.66	1.22	0.56	0.66	116.23
3	24 Aug 2005	7.49	2.04	5.45	315.91	1.08	0.82	0.26	31.93
4	4 Jan 1996	4.68	1.90	2.78	313.98	1.28	0.51	0.76	147.99
5	15 Dec 1990	4.99	1.63	3.36	313.50	1.55	0.55	0.99	179.03
6	17 Dec 1990	4.68	1.72	2.97	301.29	1.33	0.56	0.77	136.24
7	16 Dec 1990	4.78	1.62	3.16	300.85	1.41	0.56	0.85	152.19
8	14 Dec 1990	4.69	1.66	3.03	298.32	1.64	0.55	1.09	195.89
9	22 Aug 2005	7.45	2.03	5.42	298.17	1.21	0.76	0.45	58.65
10	12 May 1991	6.03	2.67	3.36	290.89	1.44	0.95	0.49	51.64
11	25 Aug 2005	6.52	2.09	4.43	289.40	1.05	0.85	0.21	24.32
12	1 Jan 1996	6.14	2.03	4.12	286.63	1.36	0.57	0.80	140.78
13	19 Dec 1990	4.15	1.81	2.34	284.92	1.06	0.57	0.49	85.63
14	5 Jan 1996	3.74	1.77	1.97	277.43	1.11	0.50	0.61	123.22
15	13 May 1987	5.62	2.70	2.92	276.03	1.60	0.95	0.65	67.75
16	8 Jan 2010	4.26	1.51	2.75	275.35	1.07	0.47	0.60	126.02
17	9 Jan 2010	4.08	1.48	2.60	270.85	1.11	0.47	0.64	136.85
18	27 Sep 1996	6.86	2.27	4.58	265.72	1.49	0.97	0.52	53.87
19	28 Sep 1996	6.81	2.23	4.57	264.25	1.32	0.97	0.35	35.53
20	1 Oct 1996	6.71	2.21	4.50	264.22	0.96	1.00	-0.04	-4.16
21	29 Sep 1996	6.70	2.29	4.41	261.90	1.21	0.98	0.23	23.55
22	24 Sep 1996	6.72	2.43	4.29	261.85	1.68	0.97	0.71	73.53
23	25 Sep 1996	6.68	2.32	4.36	261.71	1.67	0.97	0.70	72.38
24	10 May 1987	5.36	2.50	2.85	261.59	1.85	0.91	0.94	102.55
25	30 Sep 1996	6.52	2.22	4.29	261.17	1.10	0.99	0.11	11.53
26	26 Sep 1996	6.71	2.31	4.40	261.16	1.61	0.97	0.64	66.63
27	3 Jan 1996	4.96	1.95	3.01	260.96	1.32	0.53	0.79	149.24
28	8 May 1987	5.39	2.39	3.00	258.18	1.92	0.88	1.04	118.70
29	9 May 1987	5.41	2.48	2.93	258.16	1.90	0.89	1.01	112.84
30	7 May 1987	5.35	2.27	3.08	257.36	1.91	0.87	1.03	118.48
31	10 Jan 2010	3.68	1.47	2.21	257.32	1.00	0.45	0.56	124.73
32	4 Apr 1996	4.85	1.98	2.87	257.26	1.17	0.74	0.43	57.31
33	18 Jan 1987	3.48	1.08	2.40	256.85	1.03	0.45	0.58	129.23
34	22 Jun 2010	8.50	3.13	5.37	256.66	1.86	0.97	0.89	91.46
35	5 Apr 1996	4.79	2.02	2.77	255.72	1.07	0.73	0.34	45.92
36	19 jan 1987	3.55	1.07	2.47	255.25	0.88	0.45	0.43	94.39
37	2 Oct 1996	6.28	2.18	4.09	252.98	0.82	1.01	-0.20	-19.30
38	3 Apr 1996	4.39	1.93	2.45	252.68	1.21	0.74	0.47	62.77

39	23 Jun 2010	7.95	3.14	4.81	251.60	1.62	0.98	0.64	65.69
40	6 Sep 1995	6.69	2.60	4.10	250.25	1.13	0.80	0.33	41.28
41	20 Jan 1987	3.30	1.10	2.20	249.84	0.74	0.47	0.27	57.41
42	25 Jun 2010	7.20	3.09	4.11	249.42	1.14	0.97	0.17	17.22
43	6 May 1987	5.13	2.21	2.92	249.36	1.92	0.88	1.04	118.63
44	2 Mar 1986	3.53	1.66	1.87	249.06	0.76	0.59	0.17	28.14
45	11 May 1991	5.56	2.54	3.02	248.71	1.55	0.94	0.62	65.89
46	4 Nov 1990	4.96	1.69	3.27	248.55	1.03	0.70	0.33	47.60
47	5 Nov 1990	4.89	1.70	3.20	248.47	0.88	0.71	0.16	23.02
48	21 Aug 2005	6.46	2.00	4.45	248.23	1.22	0.74	0.48	64.92
49	3 Nov 1990	4.84	1.65	3.19	247.96	1.11	0.68	0.44	64.59
50	24 Jun 2010	7.32	3.11	4.21	243.74	1.38	0.98	0.40	41.13
51	2 Apr 1996	3.97	1.96	2.01	242.74	1.19	0.74	0.45	61.42
52	31 Oct 1994	4.50	1.89	2.61	240.92	1.04	0.68	0.36	52.62
53	15 Aug 2002	7.15	2.39	4.76	240.41	1.20	0.75	0.46	61.17
54	3 Mar 1986	3.51	1.67	1.85	239.53	0.74	0.58	0.16	27.18
55	12 Aug 2002	7.76	2.69	5.08	238.65	1.56	0.78	0.78	99.56
56	13 Aug 2002	7.75	2.62	5.12	237.93	1.42	0.76	0.66	86.33
57	14 Aug 2002	7.43	2.45	4.98	237.32	1.32	0.75	0.57	75.63
58	19 Oct 2015	5.97	1.87	4.10	237.07	2.32	0.89	1.42	159.44
59	23 Sep 1996	6.45	2.48	3.96	236.22	1.65	0.97	0.68	70.94
60	25 Nov 1999	4.63	2.23	2.40	235.05	0.93	0.84	0.09	11.25
61	1 Nov 1994	4.47	1.79	2.68	234.80	0.97	0.67	0.30	45.42
62	9 Dec 1988	3.61	1.83	1.78	234.77	0.48	0.58	-0.10	-17.14
63	27 Jan 1998	2.95	1.59	1.36	234.61	0.89	0.51	0.38	75.12
64	11 Nov 1985	3.80	1.64	2.16	234.57	1.16	0.79	0.37	46.84
65	24 Nov 1999	4.66	2.25	2.42	234.47	1.08	0.84	0.24	28.71
66	26 Jan 1998	2.95	1.50	1.45	234.37	1.00	0.52	0.48	92.80
67	25 Jan 1998	3.00	1.38	1.62	234.23	1.12	0.52	0.61	117.03
68	20 Aug 2005	6.27	2.06	4.21	233.83	1.23	0.73	0.50	67.87
69	23 Jan 1998	3.03	1.27	1.76	232.72	1.41	0.51	0.90	176.11
70	24 Jan 1998	3.02	1.36	1.66	232.47	1.26	0.52	0.74	143.87
71	4 Mar 1986	3.27	1.64	1.62	232.39	0.71	0.57	0.15	25.86
72	28 Jan 1998	2.87	1.58	1.29	232.10	0.71	0.50	0.22	43.50
73	21 Jun 2010	8.15	3.11	5.04	231.87	2.11	0.96	1.15	119.37
74	14 Dec 1992	4.66	1.66	3.00	231.20	0.82	0.55	0.27	47.97
75	16 May 1991	4.39	2.44	1.95	231.13	1.06	1.01	0.05	5.22
76	16 Oct 2015	5.80	1.98	3.82	231.06	2.49	0.86	1.62	188.23
77	13 Mar 2006	4.78	1.45	3.33	230.88	1.02	0.43	0.59	138.36
78	23 Nov 1999	4.36	2.27	2.08	230.03	1.22	0.83	0.39	46.41
79	2 Nov 1990	4.36	1.70	2.65	229.91	1.12	0.67	0.45	67.53
80	31 Dec 1996	3.08	2.02	1.05	229.65	1.04	0.56	0.48	85.98
81	1 Nov 1990	4.28	1.79	2.49	229.13	1.07	0.67	0.40	59.00
82	10 Dec 1988	3.47	1.84	1.64	228.19	0.45	0.61	-0.16	-26.37

83	14 Mar 2006	4.36	1.39	2.98	228.07	0.92	0.42	0.50	121.00
84	30 Dec 1996	3.00	2.02	0.98	227.90	1.05	0.55	0.50	90.85
85	12 May 1987	4.89	2.67	2.22	227.86	1.68	0.95	0.73	77.31
86	2 Nov 1994	4.26	1.70	2.56	227.74	0.93	0.67	0.26	39.35
87	1 Jan 1997	3.15	2.03	1.13	227.44	0.98	0.57	0.41	72.43
88	10 Nov 1985	3.79	1.62	2.17	227.01	1.10	0.79	0.31	38.55
89	30 Oct 1994	4.35	1.95	2.39	226.47	1.06	0.69	0.37	53.21
90	7 Dec 1988	3.90	1.79	2.11	226.37	0.53	0.60	-0.06	-10.59
91	8 Dec 1988	3.83	1.77	2.06	225.99	0.51	0.58	-0.07	-12.02
92	6 Dec 1988	3.89	1.88	2.00	225.99	0.55	0.62	-0.07	-11.65
93	13 Nov 1985	3.92	1.75	2.17	225.81	1.47	0.80	0.66	82.36
94	14 May 1987	4.87	2.61	2.25	225.42	1.53	0.96	0.57	59.36
95	11 May 1987	4.83	2.54	2.30	225.16	1.77	0.94	0.84	89.35
96	15 Oct 2015	5.72	1.90	3.82	224.55	2.44	0.86	1.58	182.42
97	22 Jan 1998	3.11	1.27	1.83	224.50	1.51	0.50	1.01	204.18
98	22 Dec 1990	3.86	1.76	2.10	223.83	1.69	0.57	1.12	197.58
99	30 Oct 1990	4.23	1.95	2.28	222.79	0.84	0.69	0.15	21.50
100	2 Jan 1996	5.22	2.00	3.22	222.72	0.84	0.55	0.30	54.31

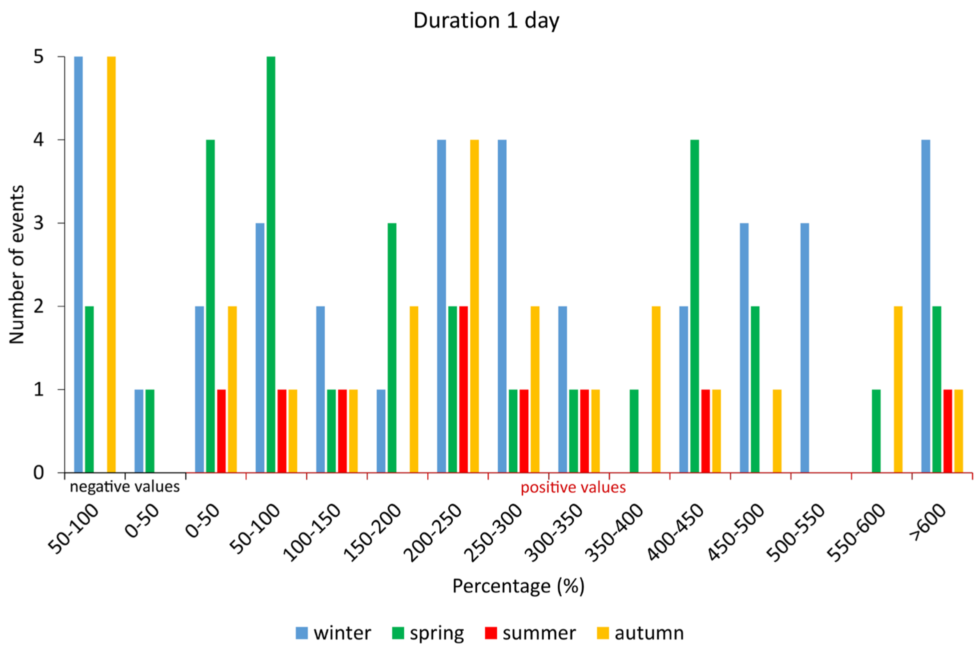

Figure A.2.1. Percentage moisture supply from the Mediterranean Sea relating to each extreme event (PFLEX-%) on a seasonal scale for the 100 events analysed in duration of 1 day.

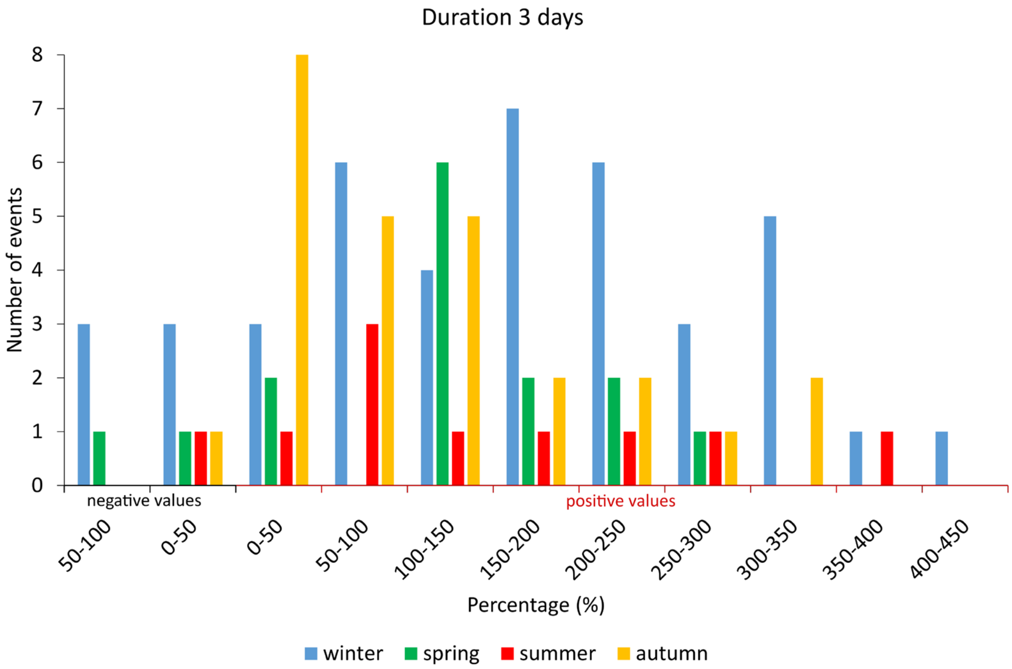

Figure A.2.2. As Figure A.2.1 but for events in duration of 3 days.

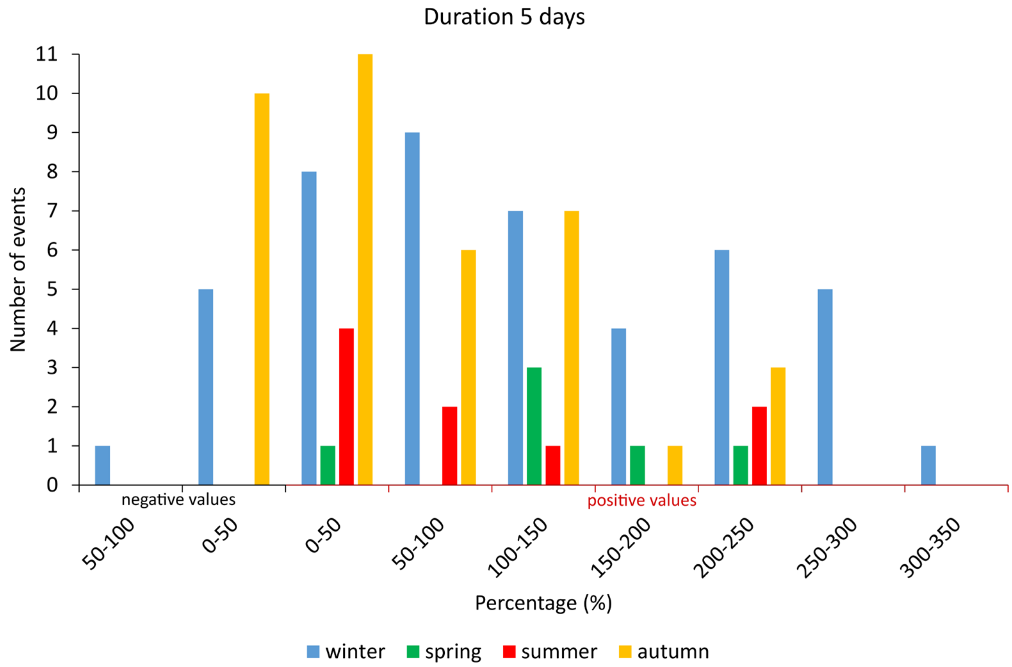

Figure A.2.3. As Figure A.2.1 but for events in duration of 5 days.

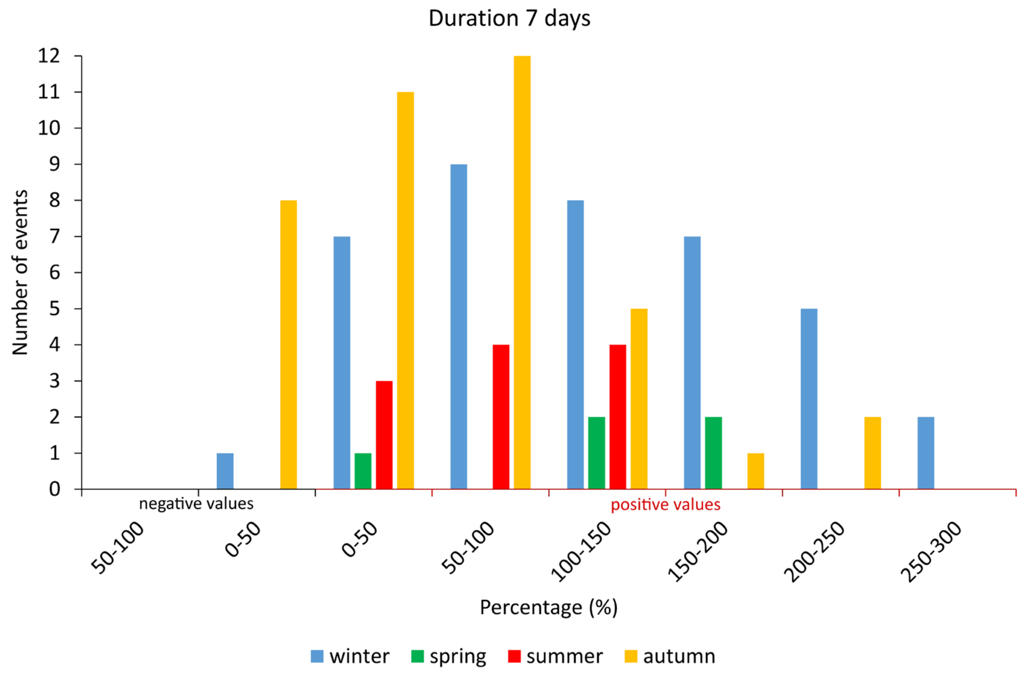

Figure A.2.4. As Figure A.2.1 but for events in duration of 7 days.

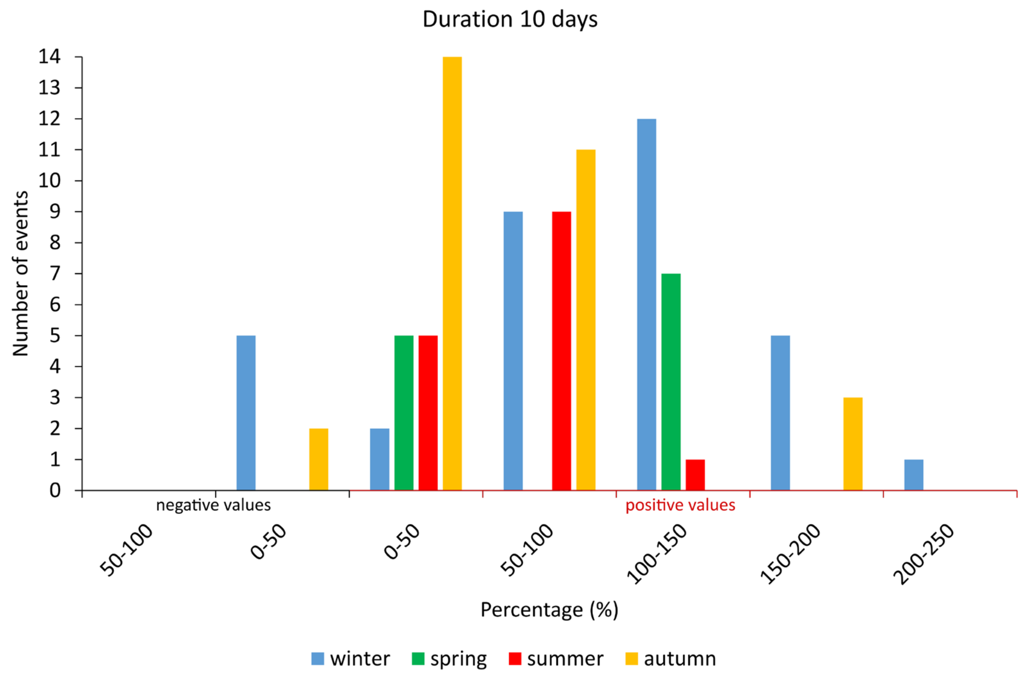

Figure A.2.5. As Figure A.2.1 but for events in duration of 10 days.

A.3. The Mediterranean Moisture Contribution to Climatological and Extreme Monthly Continental Precipitation (2018), Water.

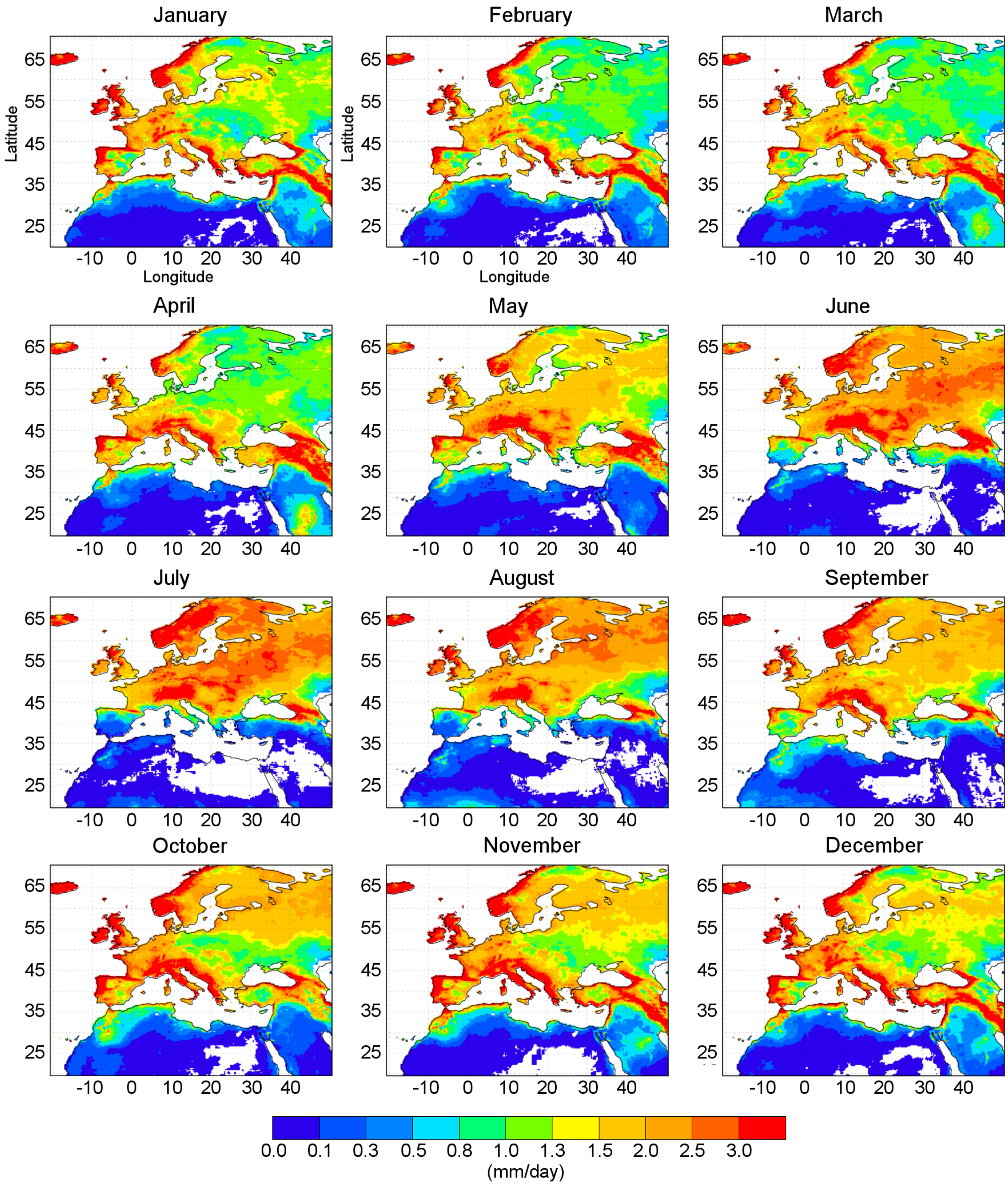

Figure A.3.1. Monthly climatological values (mm/day) from MSWEP global precipitation database (MSWEP-Cli) for all months over the area of Mediterranean basin for 1980-2015.

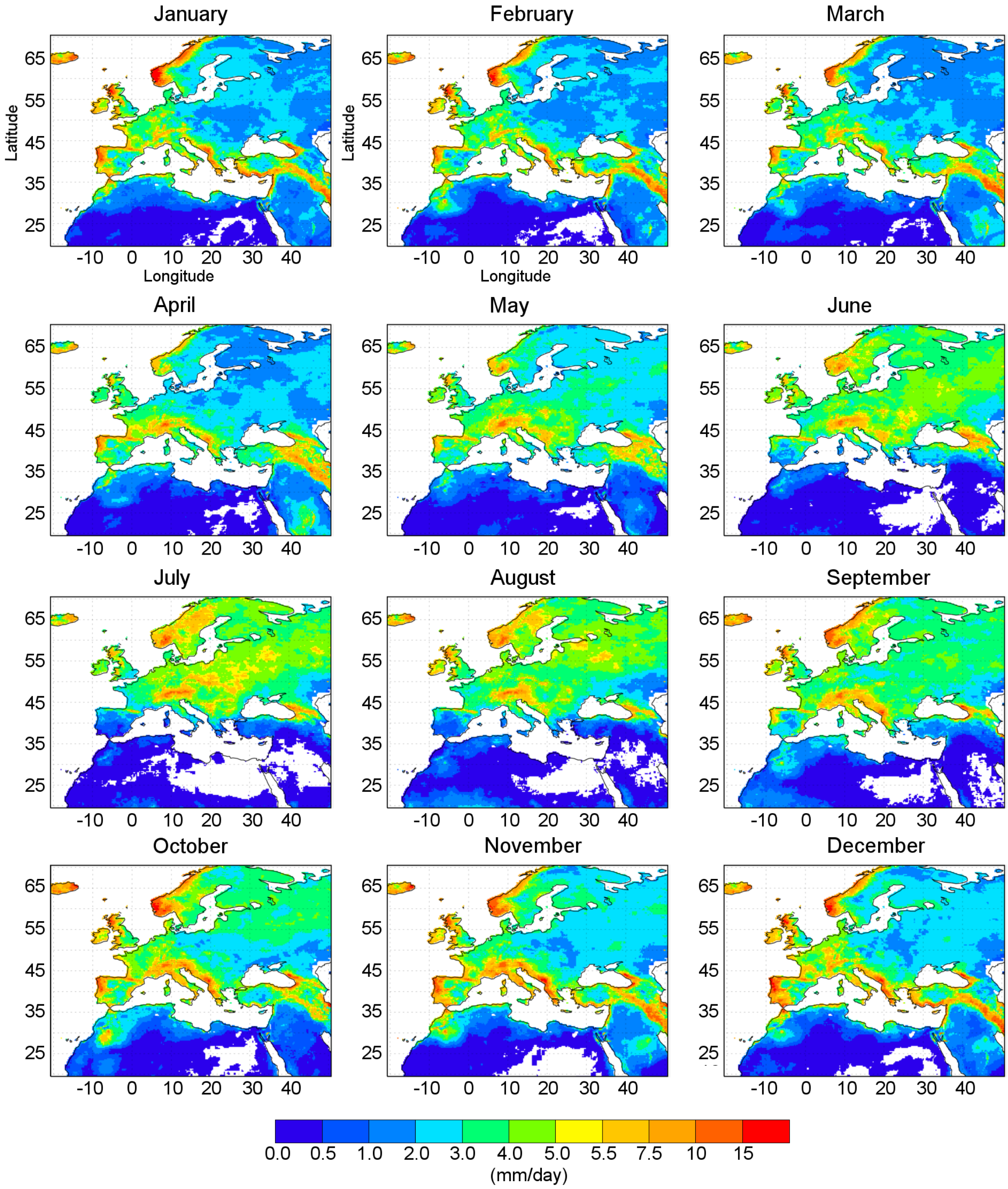

Figure A.3.2. Mean precipitation (mm/day) for each grid point for the identified five years with the highest value of precipitation (MSWEP-extreme) for all months.

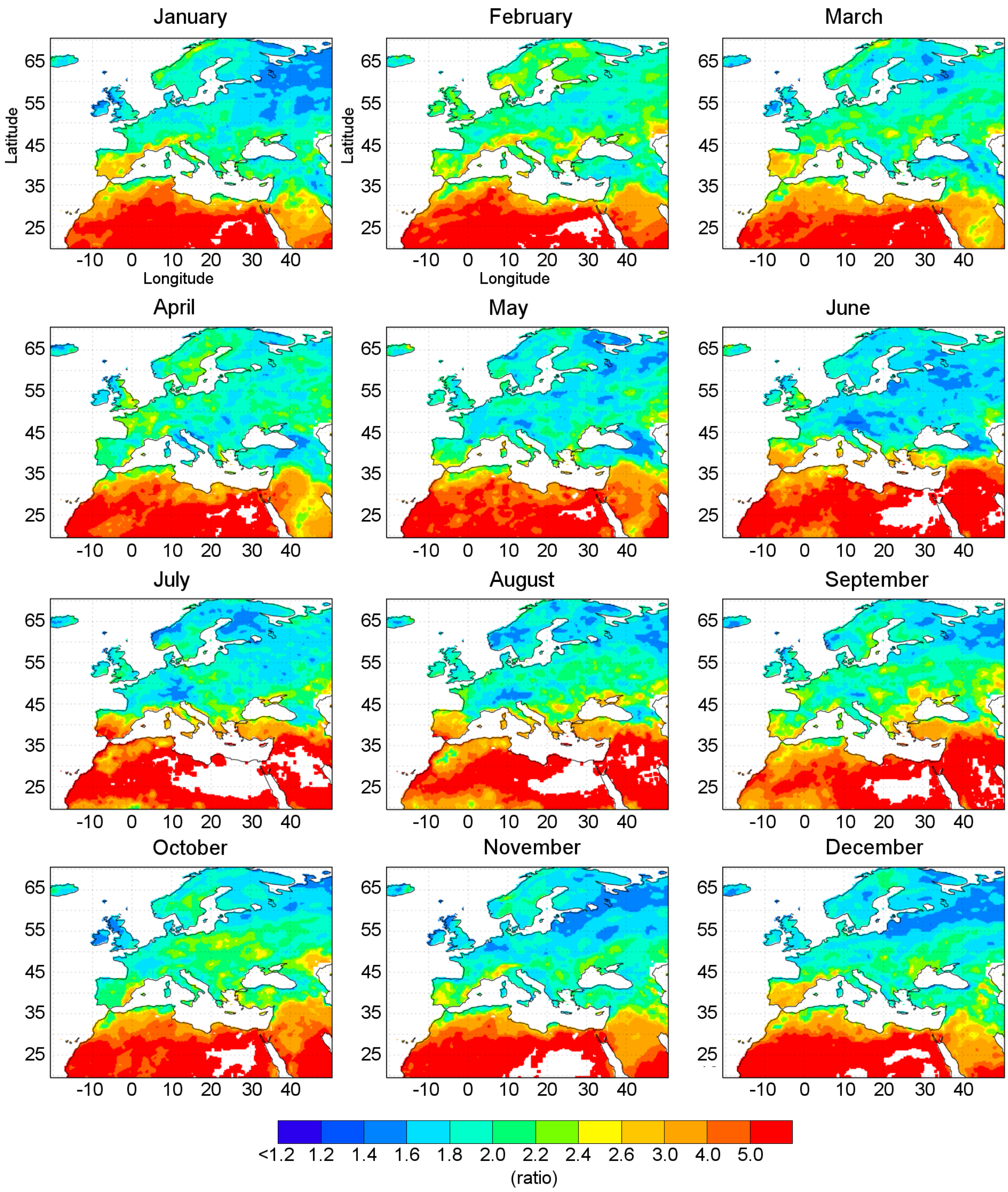

Figure A.3.3. Ratio between MSWEP-extreme and MSWEP-Cli for all months.

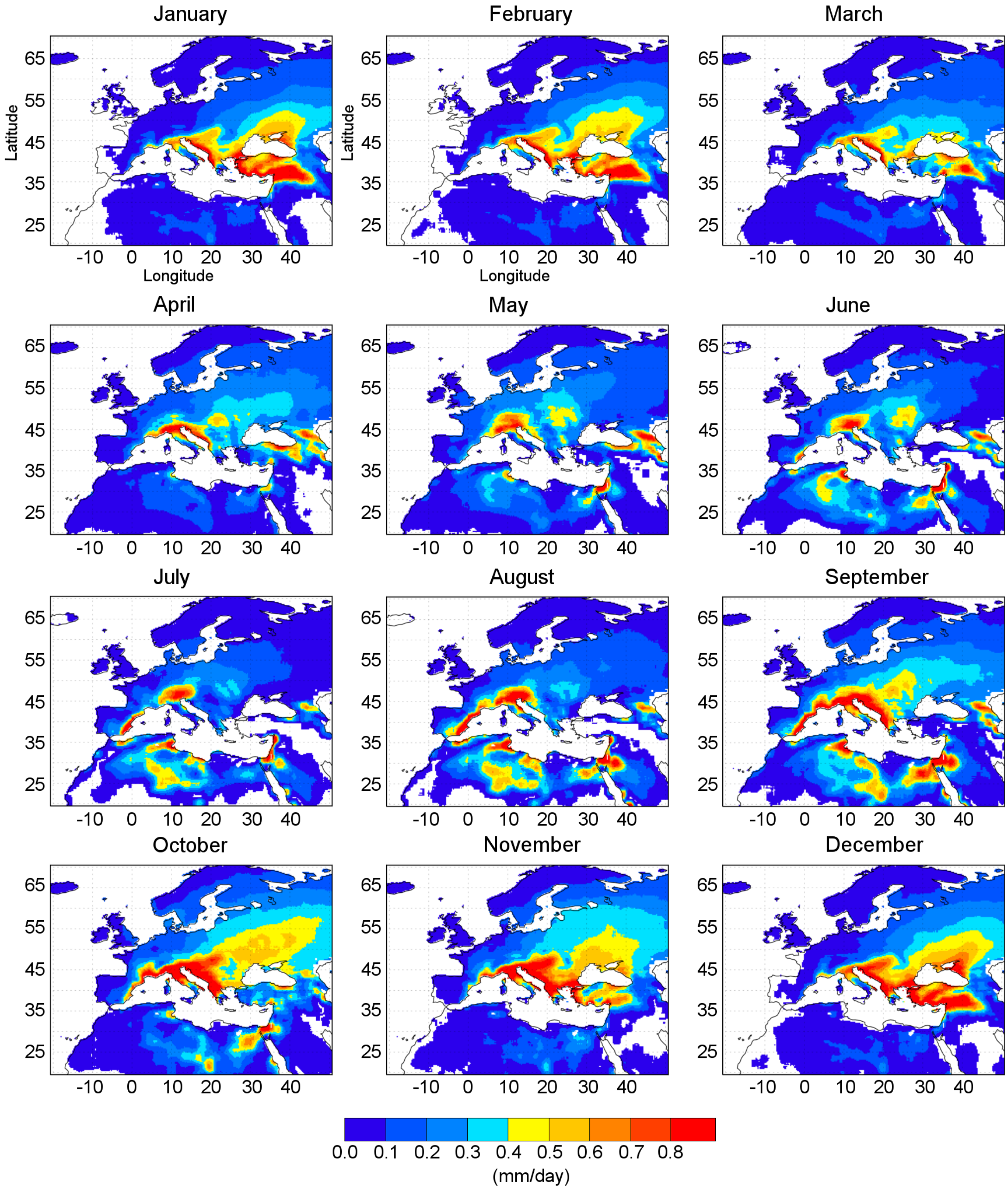

Figure A.3.4. Monthly-averaged value of E-P < 0 integrated over ten days (PFLEX-Cli) between 1980 to 2015 obtained from the forward Lagrangian experiment for Mediterranean Sea for all months. Units in mm/day.

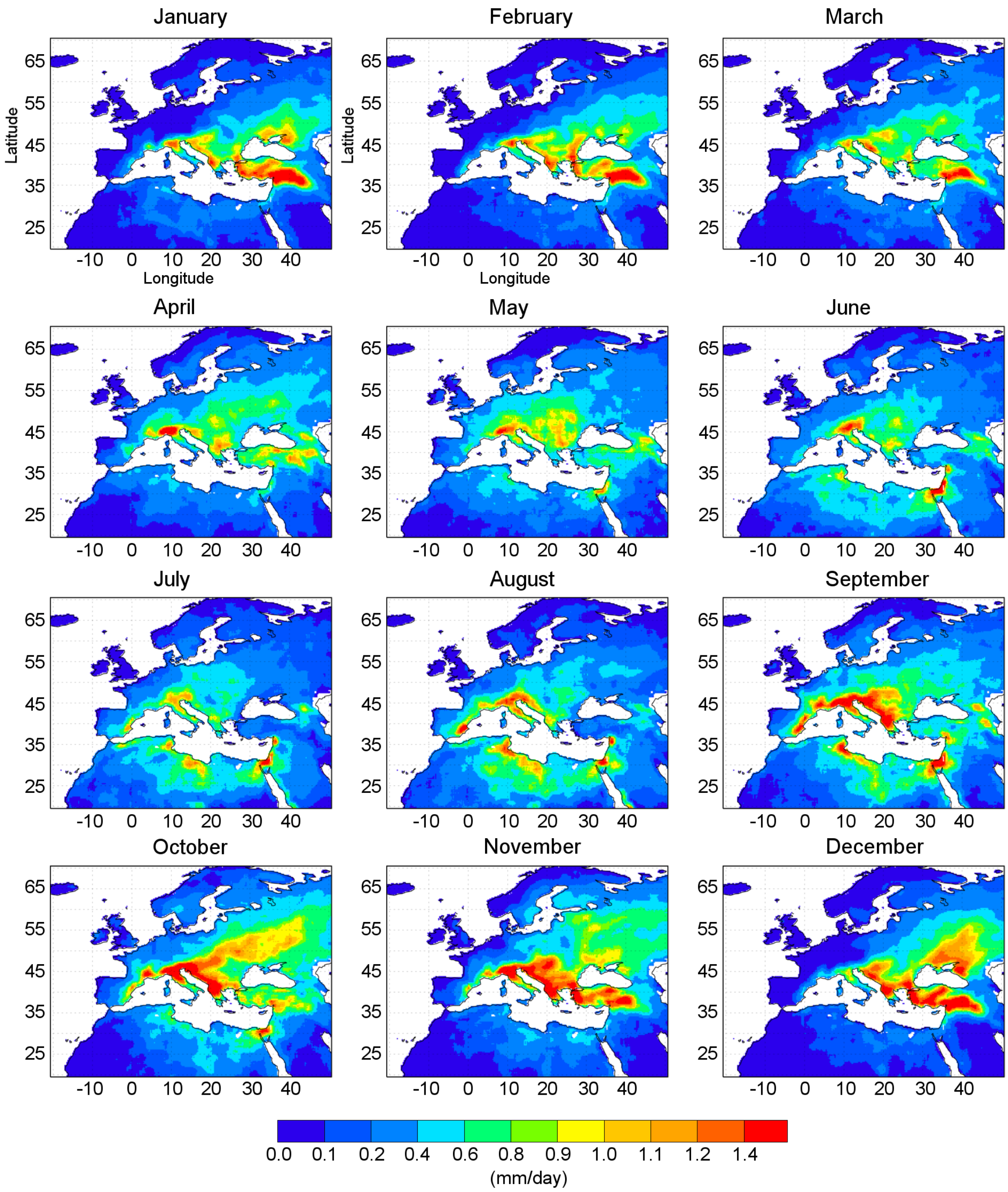

Figure A.3.5. Mean precipitation (mm/day) for each grid point was calculated by the Lagrangian experiment for moisture originating from the Mediterranean Sea (PFLEX-extreme) for the same five years, which was identified as MSWEP-extreme for a 36-year temporal period (1980–2016).

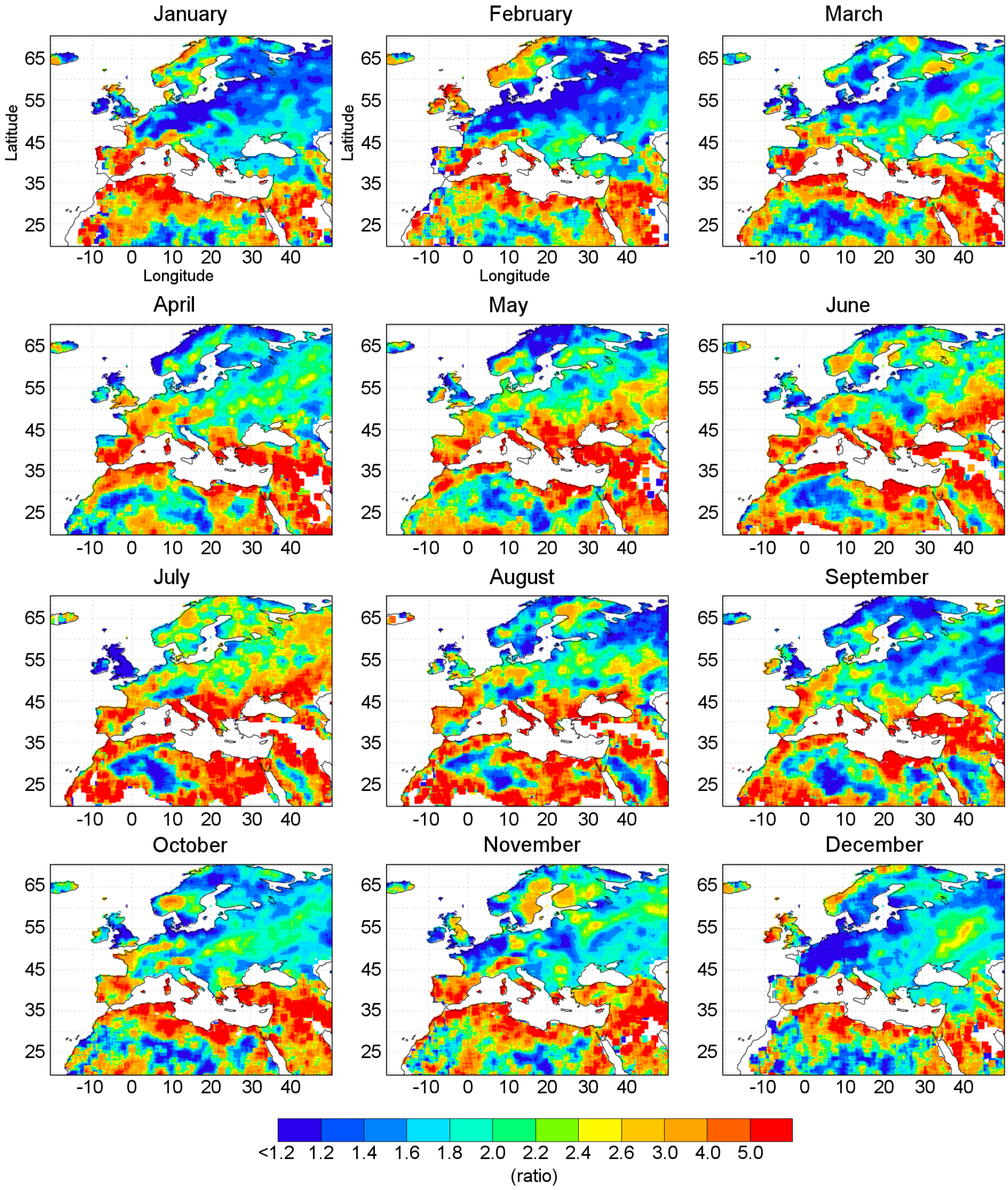

Figure A.3.6. Ratio between the mean values of the observed five years with highest values of E-P < 0, calculated using FLEXPART (PFLEX-extreme), and the mean climatological values of E-P < 0 (PFLEX-Cli) during the all months which is calculated for each grid point during the period: 1980-2016.

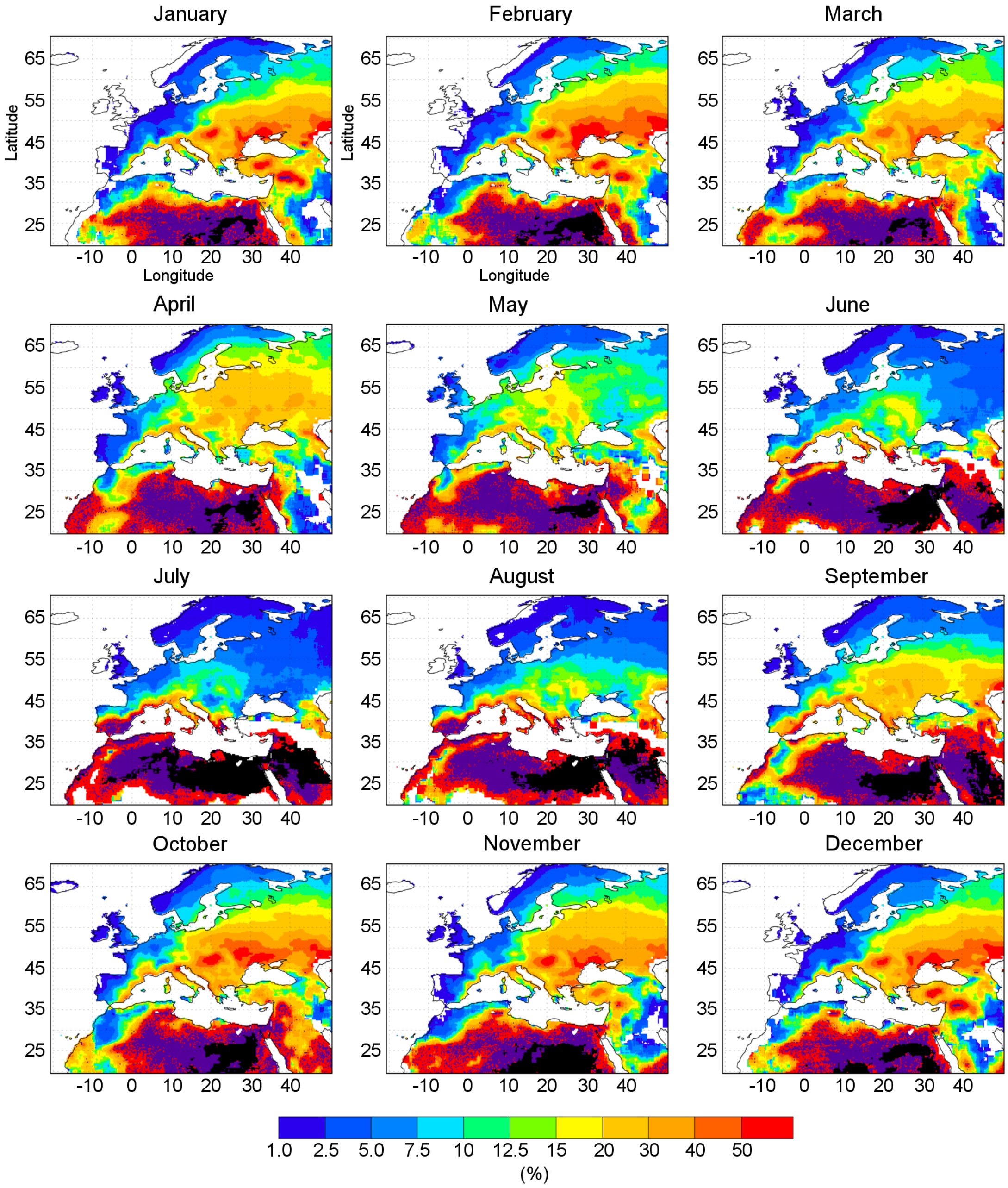

Figure A.3.7. Monthly climatological percentage of the Mediterranean moisture contribution (PFLEX-Cli) to precipitation (MSWEP-Cli) during all months.

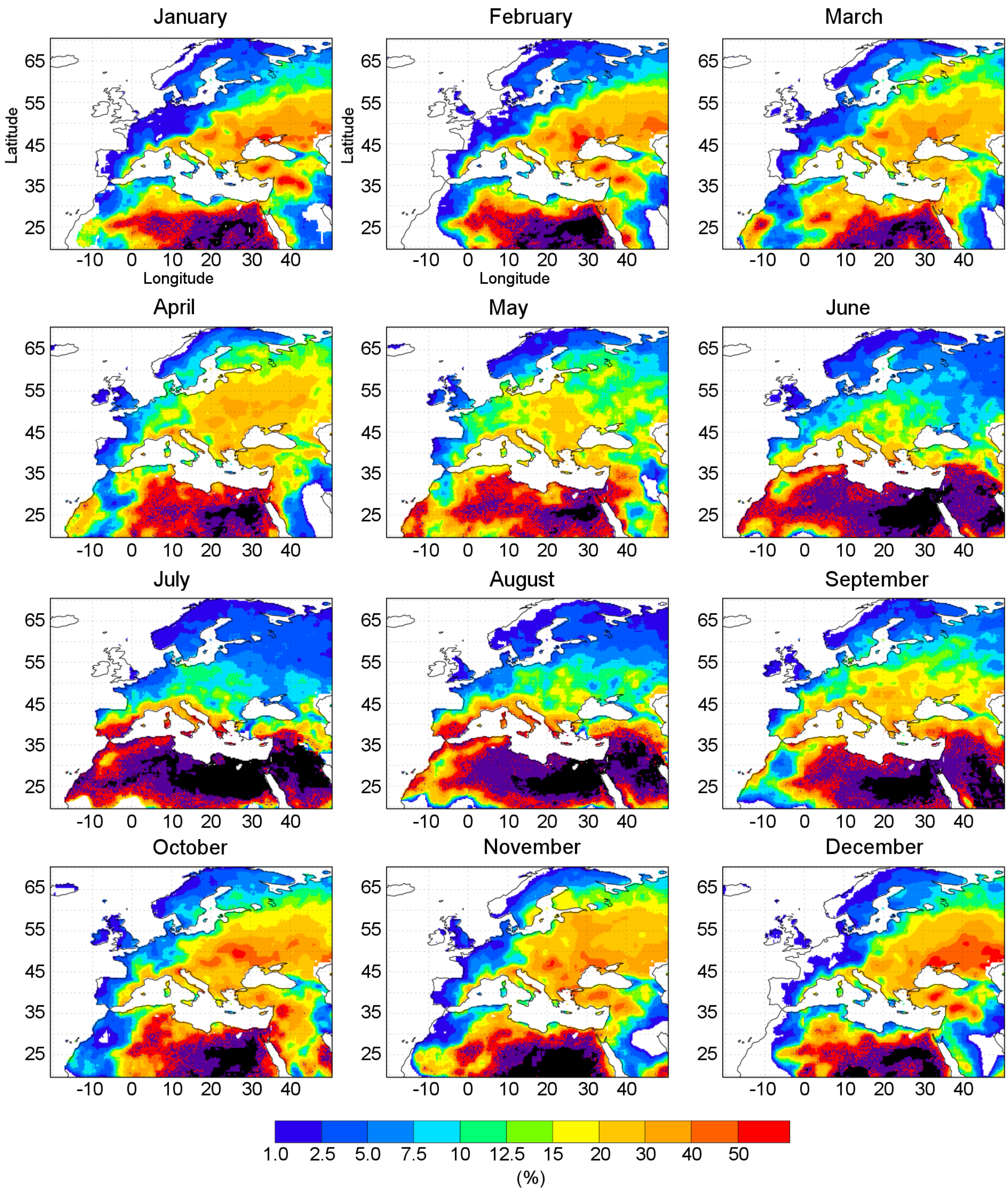

Figure A.3.8. Similar to Figure A.3.7 but comparing the percentage betwenn PFLEX-extreme and MSWEP-extreme during the all months.

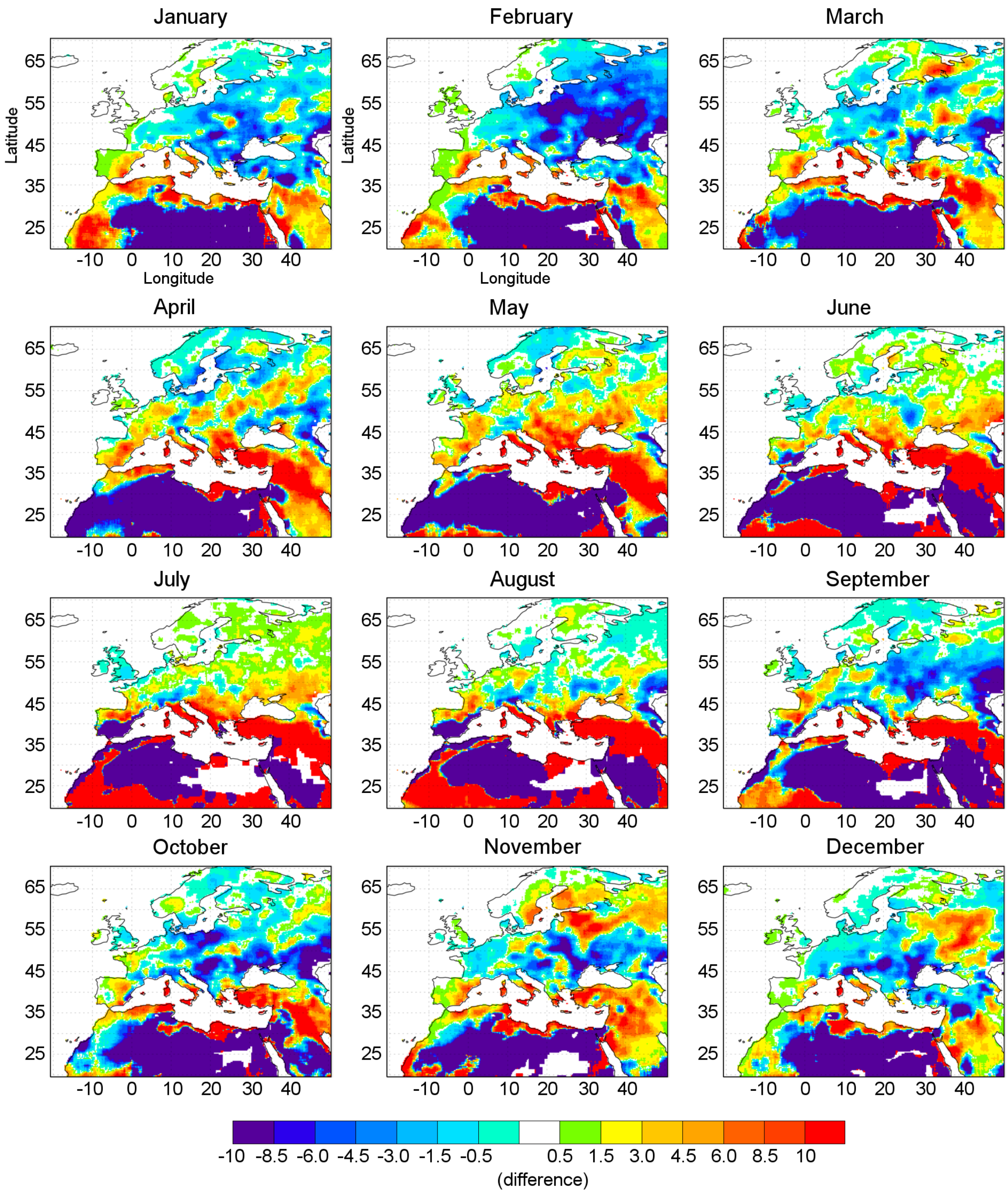

Figure A.3.9. Difference between the percentages of the moisture from the Mediterranean Sea supplied to extreme events (Figure A.3.8) and to the mean climatology (see Figure A.3.7) for all months.

A.4. A global Atlas of precipitation and contribution of the main moisture sources in the peak precipitation month.

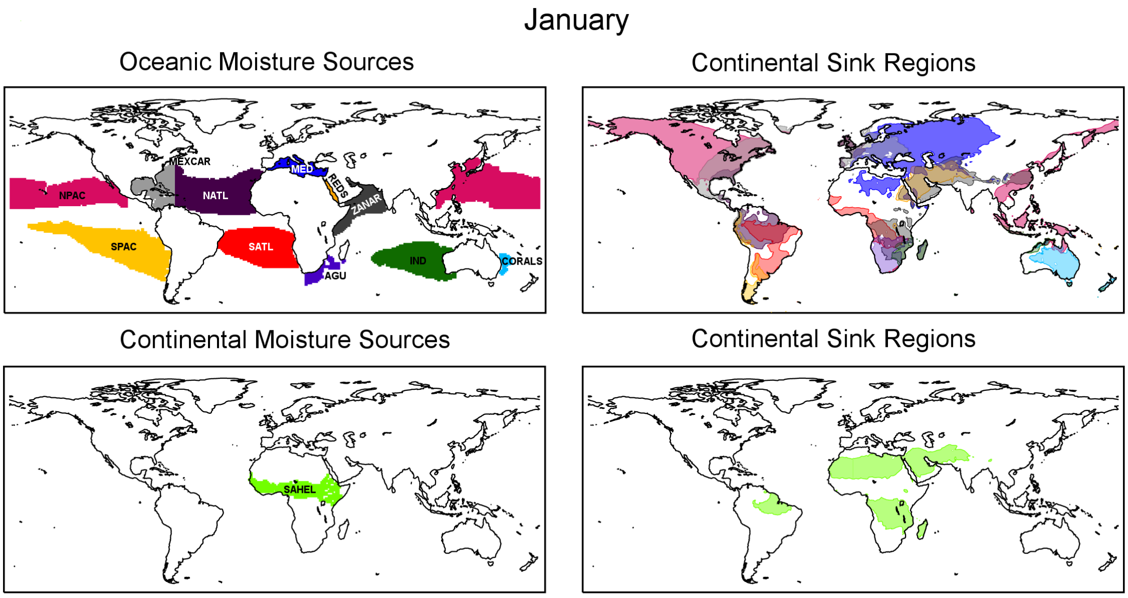

Figure A.4.1. Left column: Schematic monthly oceanic and terrestrial moisture sources regions for January. Right column: Sink regions for each moisture source. The sink regions (only E-P < 0 values from forward tracking) on the continents are plotted for values higher than -0.05 mm/day for all the sources detected.

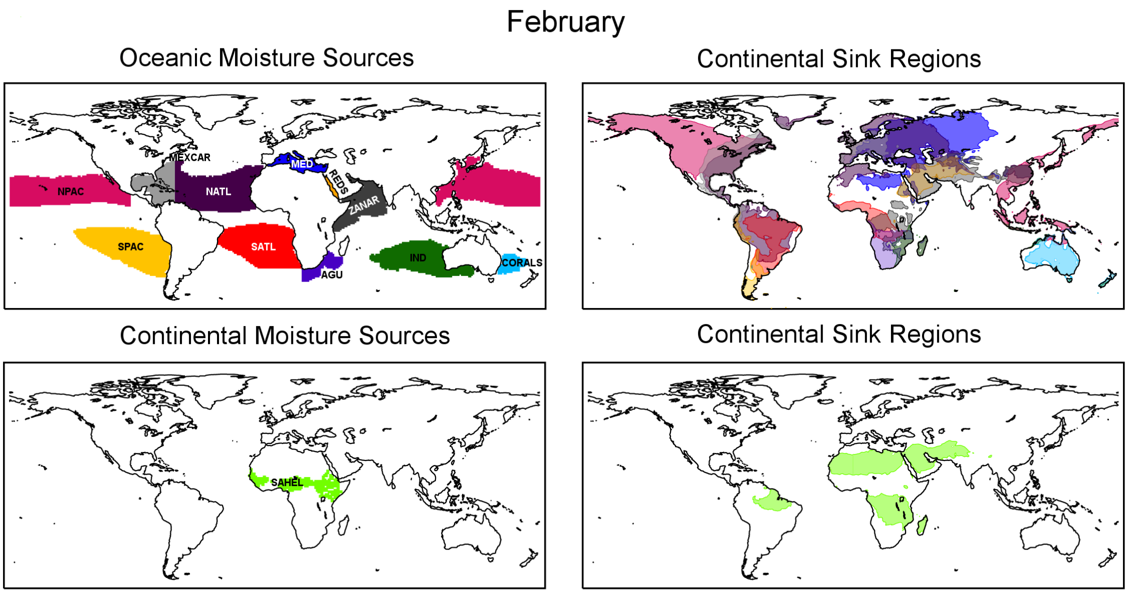

Figure A.4.2. As Figure A.4.1 but for February.

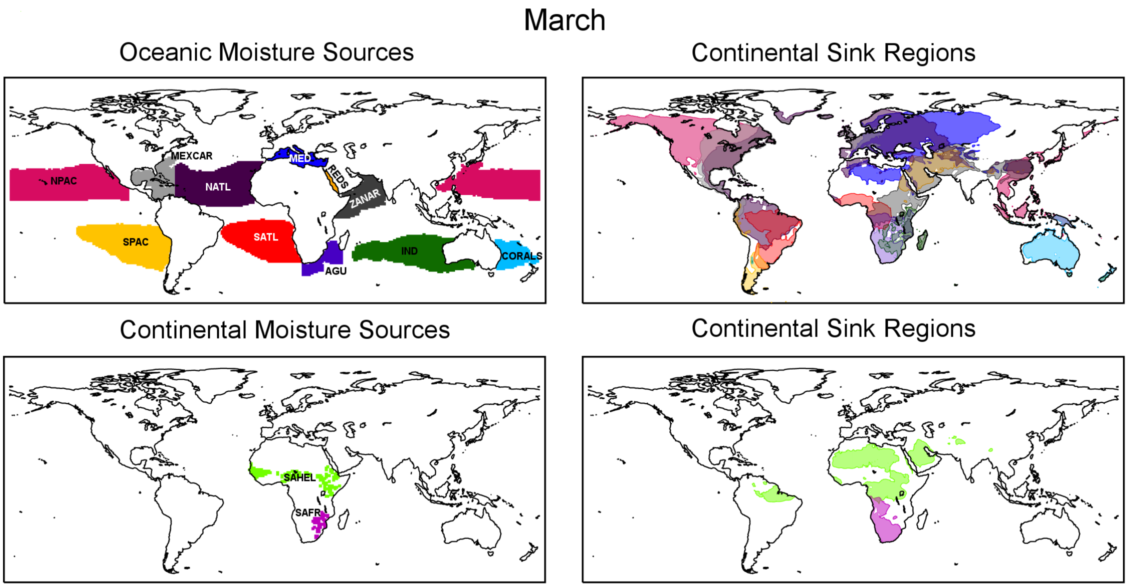

Figure A.4.3. As Figure A.4.1 but for March.

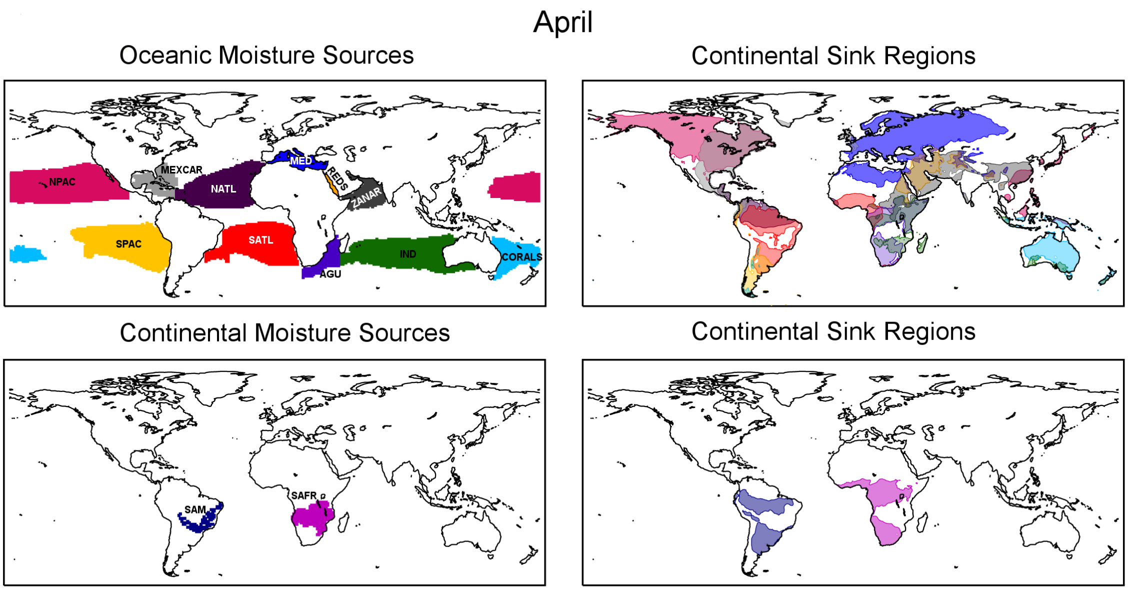

Figure A.4.4. As Figure A.4.1 but for April.

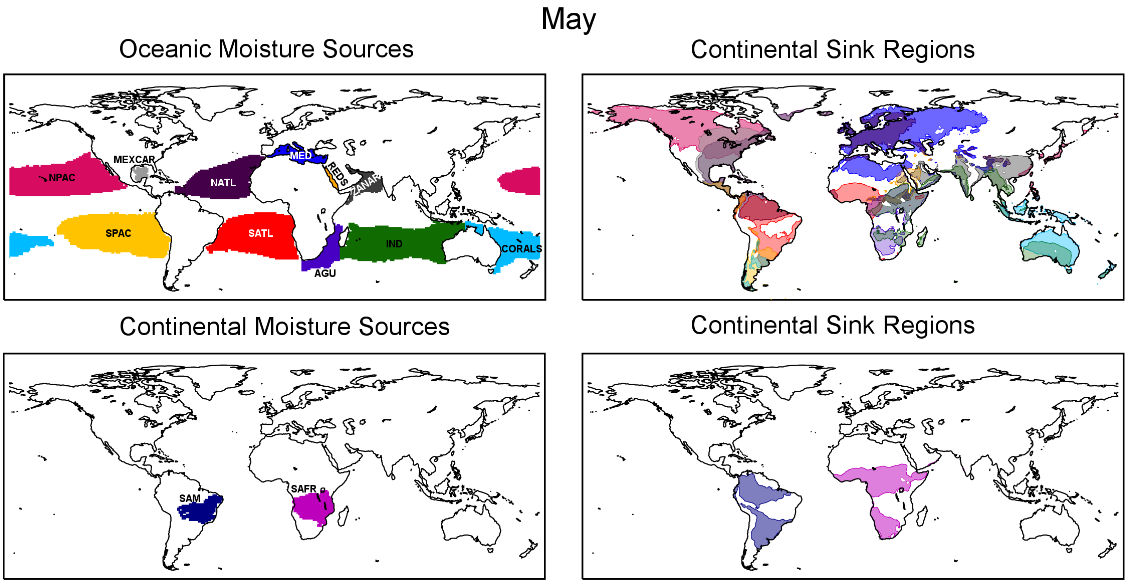

Figure A.4.5. As Figure A.4.1 but for May.

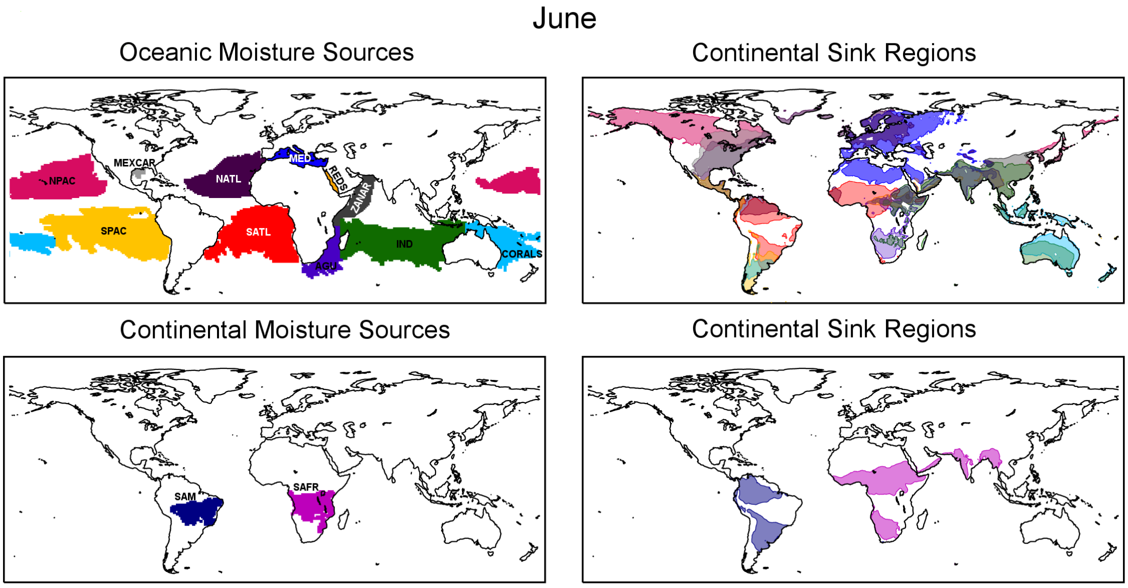

Figure A.4.6. As Figure A.4.1 but for June.

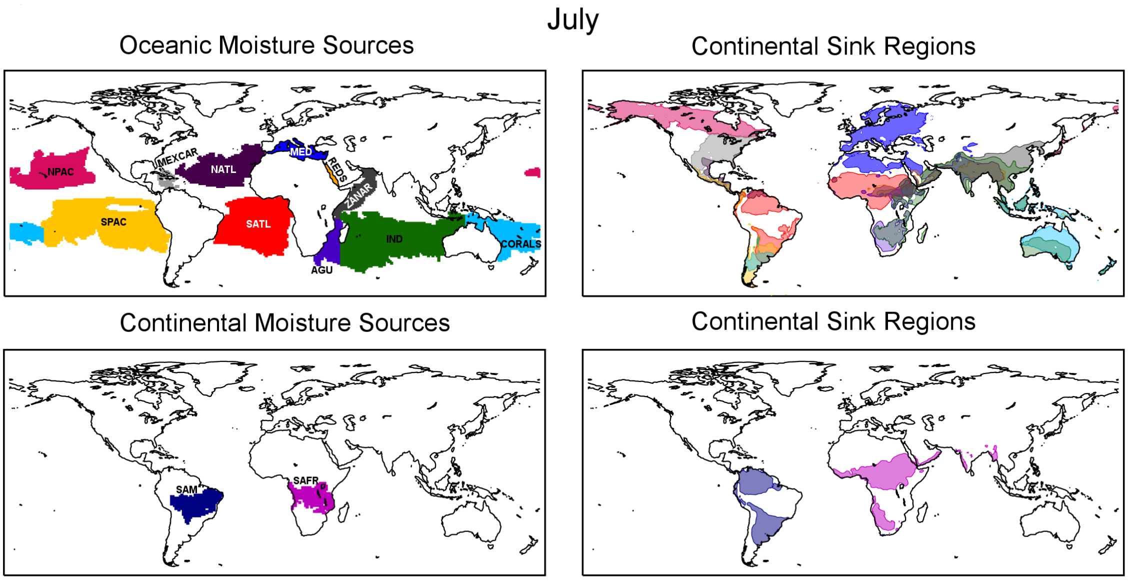

Figure A.4.7. As Figure A.4.1 but for July.

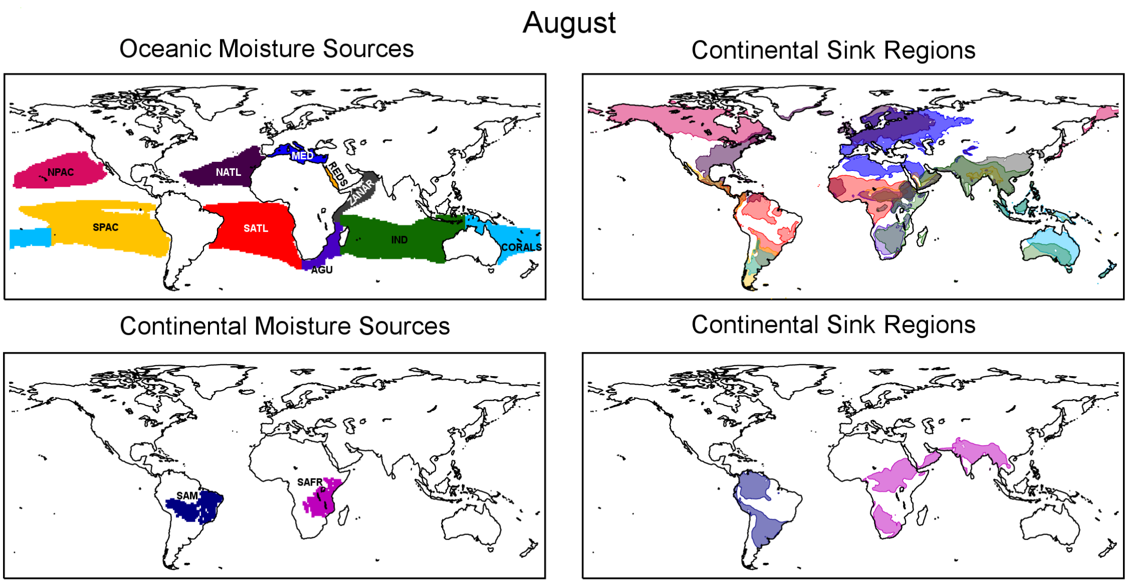

Figure A.4.8. As Figure A.4.1 but for August.

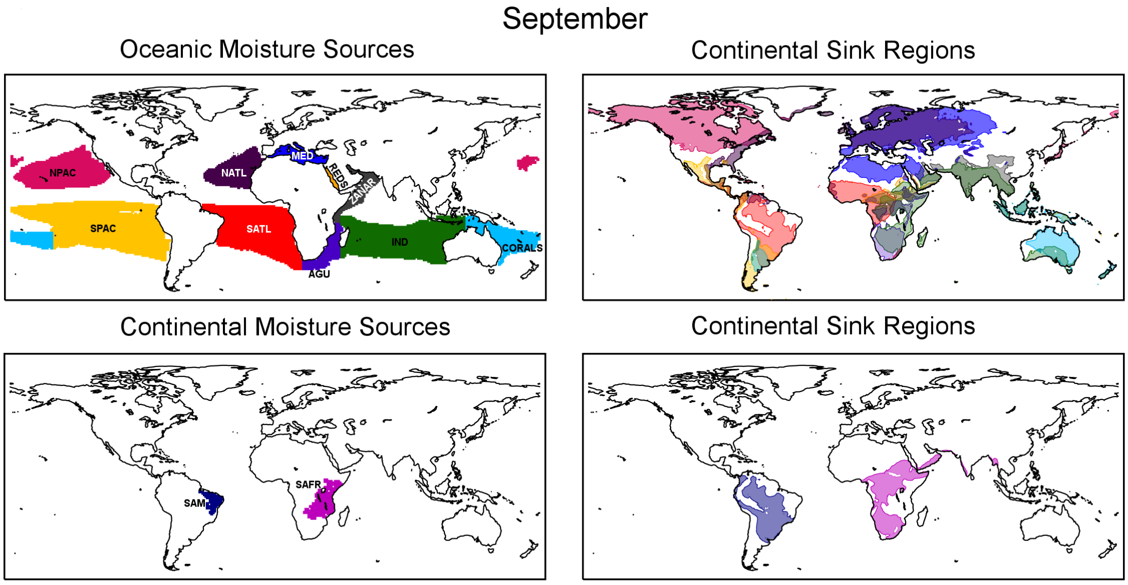

Figure A.4.9. As Figure A.4.1 but for September.

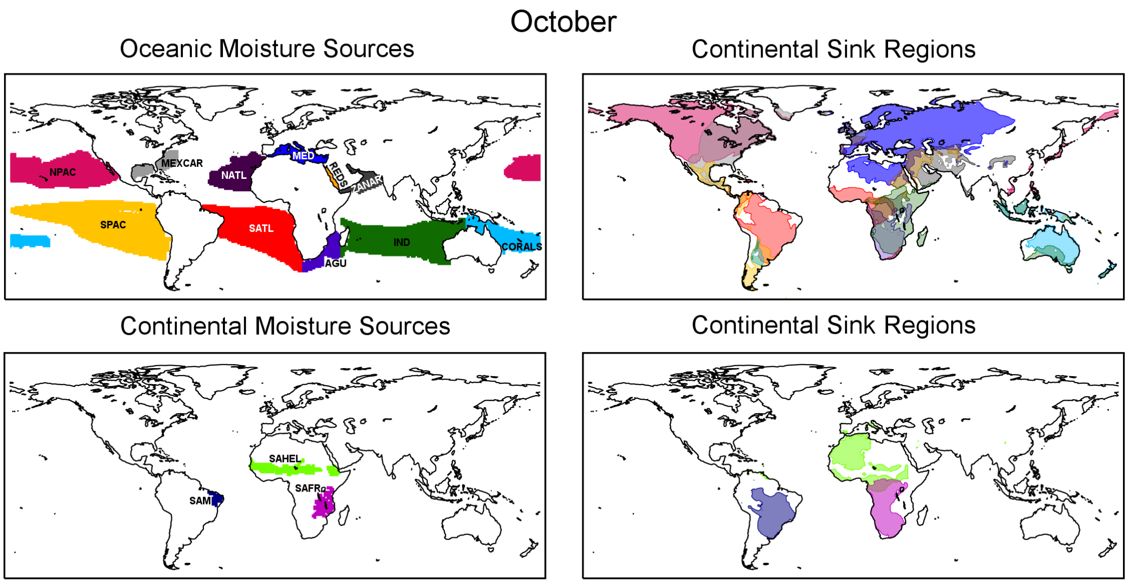

Figure A.4.10. As Figure A.4.1 but for October.

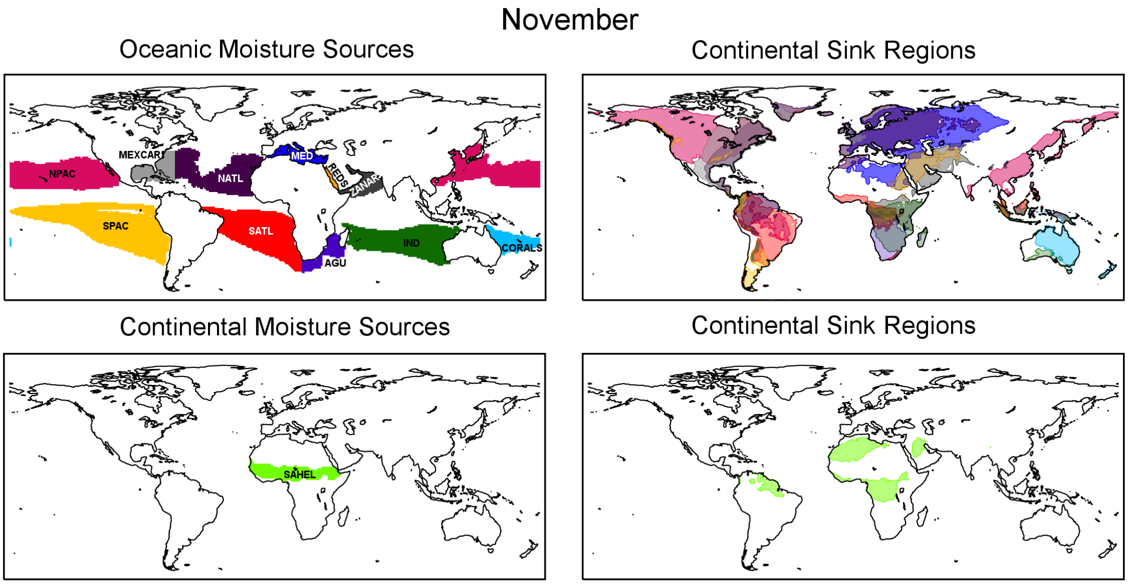

Figure A.4.11. As Figure A.4.1 but for November.

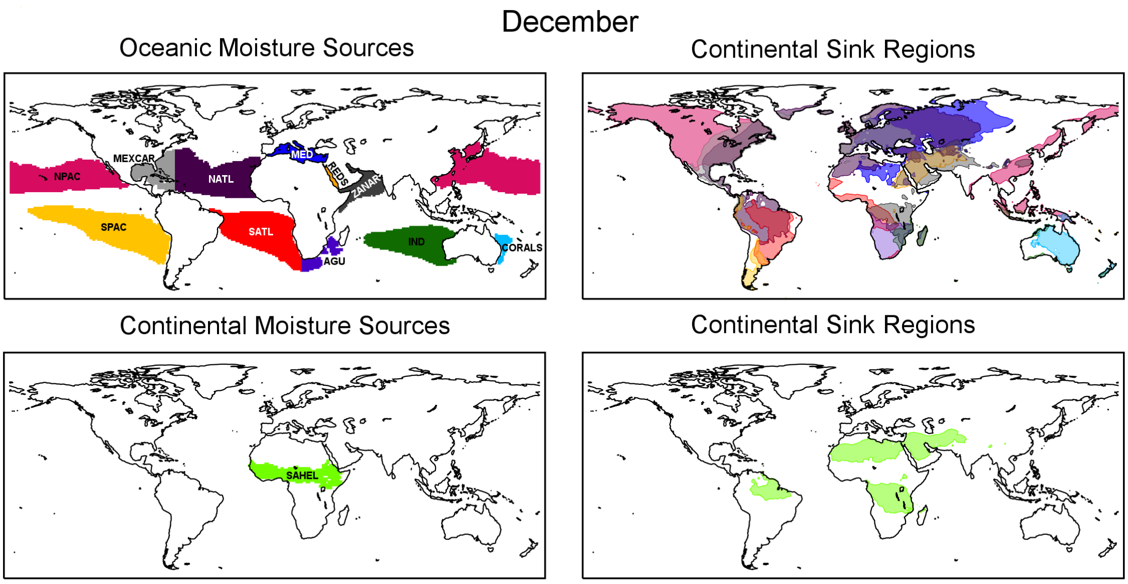

Figure A.4.12. As Figure A.4.1 but for December.

References

Adler, R.F., Huffman, G.J., Chang, A., Ferraro, R., Xie, P., Janowiak, J., Rudolf, B., Schneider, U., Curtis, S., Bolvin, D., Gruber, A., Susskind, J., and Arkin, P. (2003). The Version 2 Global Precipitation Climatology Project (GPCP) Monthly Precipitation Analysis (1979-Present). *Journal of Hydrometeorology*, 4(6), 1147–116, doi: 10.1175/1525-7541(2003)004<1147:TVGPCP>2.0.CO;2.

Beck, H.E., van Dijk, A.I.J.M., Levizzani, V., Schellekens, J., Miralles, D.G., Martens, B., and de Roo, A. (2017a). MSWEP: 3-hourly 0.25º global gridded precipitation (1979–2015) by merging gauge, satellite, and reanalysis data. *Hydrology and Earth System Science*, 21, 589–615, doi: 10.5194/hess-21-589-2017.

Beck, H.E., Vergopolan, N., Pan, M., Levizzani, V., van Dijk, A.I.J.M., Weedon, G.P., Brocca, L., Pappenberger, F., Huffman, G.J., and Wood, E.F. (2017b). Global-scale evaluation of 22 precipitation datasets using gauge observations and hydrological modeling. *Hydrology and Earth System Sciences*, 21, 6201–6217, doi: 10.5194/hess-21-6201-2017.

Becker, A., Finger, P., Meyer-Christoffer, A., Rudolf, B., Schamm, K., Schneider, U., and Ziese, M. (2012). A description of the global land-surface precipitation data products of the Global Precipitation Climatology Centre with sample applications including centennial (trend) analysis from 1901–present. *Earth System Science Data Discussions*, 5, 921–998, doi: 10.5194/essdd-5-921-2012.

Bengtsson, L. (2010). The global atmospheric water cycle. *Environmental Research Letter*, 5, 025202, doi: 10.1088/1748-9326/5/2/025202.

Bengtsson, L., Hagemann, S., and Hodges, K.I. (2004). Can climate trends be calculated from reanalysis data? *Journal of Geophysical Research*, 109, D11111, doi: 10.1029/2004JD004536.

Blanc, D., and Perez, R. (2007). The relationship between rainfall and human density and its implications for future water stress in sub-Saharan Africa. Department of Economic and Social Affairs: DESA Working Paper No. 57. Available online: http://www.un.org/esa/desa/papers/2007/wp57_2007.pdf.

Bohlinger, P., Sorteberg, A., and Sodemann, H. (2017). Synoptic conditions and moisture sources actuating extreme precipitation in Nepal. *Journal of Geophysical Research: Atmospheres*, 122, 12653–12671, doi: 10.1002/2017JD027543.

Bourqui, M.S. (2006). Stratosphere-troposphere exchange from the Lagrangian perspective: a case study and method sensitivities. *Atmospheric Chemistry and Physics*, 6, 2651–2670. doi: 10.5194/acp-6-2651-2006.

Brilly, M. (2010), Hydrological Processes of the Danube River Basin: Perspective from the Danubian Countries; Springer Science & Business Media: Ljubljana, Slovenia, Vol 1, pp 436.

Brioude, J., Arnold, D., Stohl, A., Cassiani, M., Morton, D., Seibert, P., Angevine, W., et al. (2013). The Lagrangian particle dispersion model FLEXPART-WRF version 3.1. *Geoscientific Model Development*, 6, 1889–1904, doi: 10.5194/gmd-6–1889-2013.

Burde, G.I., and Zangvil, A. (2001). The Estimation of Regional Precipitation Recycling. Part I: Review of Recycling Models. *Journal of Climate*, 14, 2497–2508, doi: 10.1175/1520-0442(2001)014<2497:TEORPR>2.0.CO;2.

Carvalho, L.M., Jones, C., and Liebmann, B. (2002). Extreme Precipitation Events in Southeastern South America and Large-Scale Convective Patterns in the South Atlantic Convergence Zone. *Journal of Climate*, 15, 2377–2394, doi: 10.1175/1520-0442(2002)015<2377:EPEISS>2.0.CO;2.

Castillo, R., Nieto, R., Drumond, A., and Gimeno, L. (2014). The role of the ENSO cycle in the modulation of moisture transport from major oceanic moisture sources. *Water Resources Research*, 50, 1046–1058, doi: 10.1002/2013WR013900.

Castro, P., Velarde, M., Ardao, J., Perlado, J.M., and Sedano, L. (2011). Consequences of Different Meteorological Scenarios in the Environmental Impact Assessment of Tritium Release. *Fusion Science and Technology*, 6(4), 1284–1287, doi: 10.13182/FST11-A12665.

Chen, T., Huang, W., and Takle, E.S. (2004). Annual Variation of Midlatitude Precipitation. *Journal of Climate*, 17, 4291–4298, doi: 10.1175/JCLI3201.1.

Chen, B., Xu, X.D., and Zhao, T.L. (2013). Main moisture sources affecting lower Yangtze River Basin in boreal summers during 2004–2009. *International Journal of Climatology*, 33, 1035–1046, doi:10.1002/joc.3495.

Christensen, J. H., et al. (2007). Regional climate projections, in Climate Change 2007: The Physical Science Basis. Contribution of Working Group I to the Fourth Assessment Report of the Intergovernmental Panelon Climate Change, edited by S. Solomon et al., Cambridge Univ. Press, Cambridge, U. K.

Ciric, D., Nieto, R., Ramos, A.M., Drumond, A., and Gimeno, L. (2017). Wet Spells and Associated Moisture Sources Anomalies across Danube River Basin, *Water*, 9, 615, doi: 10.3390/w9080615.

Costello, M.J., Cheung, A., and De Hauwere, N. (2010). Topography statistics for the surface and seabed area, volume, depth and slope, of the world's seas, oceans and countries. *Environmental Science and Technology*, 44(23), 8821–8828, doi: 10.1021/es1012752.

Dayan, U., Nissen, K., and Ulbrich, U. (2015). Review Article: Atmospheric conditions inducing extreme precipitation over the eastern and western Mediterranean. *Natural Hazards and Earth System Sciences*, 15, 2525–2544, doi: 10.5194/nhess-15-2525-2015.

Decremer, D., Chung, C.E., Ekman, A.M.L., and Brandefelt, J. (2014). Which significance test performs the best in climate simulations? *Tellus A: Dynamic Meteorology and Oceanography*, 66(1), 23139, doi: 10.3402/tellusa.v66.23139.

Dee, D., Uppala, S.M., Simmons, A.J., Berrisford, P., Poli, P., Kobayashi, S., Andraee, U., et al. (2011). The ERA Interim reanalysis: Configuration and performance of the data assimilation system. *Quarterly Journal of the Royal Meteorological Society*, 137, 553–597, doi:10.1002/qj.828.

Dirmeyer, P.A., and Brubaker, K. L. (2007). Characterization of the global hydrologic cycle from a back-trajectory analysis of atmospheric water vapor. *Journal of Hydrometeorology*, 8(1), 20–37, doi: 10.1175/JHM557.1.

Dore, M.H. (2005). Climate change and changes in global precipitation patterns: what do we know? *Environment International*, 31, 1167–1181, doi: 10.1016/j.envint.2005.03.004.

Drumond, A., Nieto, R., and Gimeno, L. (2016). A Lagrangian approach for investigating anomalies in the moisture transport during drought episodes. *Cuadernos de Investigación Geográfica*, 42, 113–125, doi: 10.18172/cig.2925.

Drumond, A., Marengo, J., Ambrizzi, T., Nieto, R., Moreira, L., and Gimeno, L. (2014). The role of Amazon Basin moisture on the atmospheric branch of the hydrological cycle: a Lagrangian analysis. *Hydrology and Earth System Sciences*, 18, 2577–2598, doi: 10.5194/hessd-18-2577-2598.

Drumond, A., Nieto, R., Gimeno, L., and Ambrizzi T. (2008). A Lagrangian identification of major sources of moisture over Central Brazil and La Plata Basin. *Journal of Geophysical Research*, 113, D14128, doi: 10.1029/2007JD009547.

Drumond, A., Nieto, R., Gimeno, L., Trigo, R.M., Ambrizzi, T., and De Souza, E. (2010). A Lagrangian identification of the sources of moisture over Northeastern Brazil during its pre-rainy and rainy seasons. *PLoS ONE*, 5(6), e11205, doi: 10.1371/journal.pone.0011205.

Duran-Quesada, A.M., Gimeno, L., Amador, J.A., and Nieto, R. (2010). Moisture sources for Central America: Identification of moisture sources using a Lagrangian analysis technique. *Journal of Geophysical Research*, 115, D05103, doi: 10.1029/2009JD012455.

EASAC, 2013: Trends in Extreme Weather Events in Europe: Implications for National and European Union Adaptation Strategies; EASAC Policy Report 22; European Academies Science Advisory Council: Halle, Germany, 2013. Available online: www.easac.eu.

Easterling, D.R., Evans, J.L., Groisman, P.Y., Karl, T.R., Kunkel, K.E., and Ambenje, P. (2000). Observed Variability and Trends in Extreme Climate Events: A Brief Review. *Bulletin of the American Meteorological Society*, 81, 417–426, doi: 10.1175/1520-0477(2000)081<0417:OVATIE>2.3.CO;2.

Ebi, K.L., and Bowen, K. (2016). Extreme events as sources of health vulnerability: Drought as an example. *Weather and Climate Extremes*, 11, 95–102, doi: 10.1016/j.wace.2015.10.001.

EEA (European Environment Agency), 2017. Blaz Kurnik. Heavy precipitación. Denmark, Chopenhagen. Available online: https://www.eea.europa.eu.

Eshel, G., and Farrell, B.F. (2000). Mechanisms of Eastern Mediterranean Rainfall Variability. *Journal of Atmospheric Sciences*, 57, 3219–3232, doi: 10.1175/1520-0469(2000)057<3219:MOEMRV>2.0.CO;2.

Faccini, F., Giostrella, P., Lazzeri, R., Melillo, M., Raso, E., and Roccati, A. (2015). The 10th November 2014 flash-flood event in Chiavari city (Eastern Liguria, Italy). *Rendiconti Online Societa Geologica Italiana*, 35, 124–127, doi: 10.3301/ROL.2015.80.

Fowler, H.J., and Ekström, M. (2009). Multi-model ensemble estimates of climate change impacts on UK seasonal precipitation extremes. *International Journal of Climatology*, 29(3), 385–416, doi: 10.1002/joc.1827.

Frei, C., Davies, H.C., Gurtz, J., and Schär, C. (2000). Climate dynamics and extreme precipitation and flood events in Central Europe. *Integrated Assessment*, 1, 281–300, doi: 10.1023/A:1018983226334.

Frich, P., Alexander, L.V., Della-Marta, P., Gleason, B., Haylock, M., Klein Tank, A., and Peterson, T. (2001). Observed coherent changes in climatic extremes during the second half of the 20th century. *Climate Research*, 219, 193–212. doi: 10.3354/cr019193.

Funk, C., Peterson, P., Landsfeld, M., Pedreros, D., Verdin, J., Shukla, S., Husak, G., Rowland, J., Harrison, L., Hoell, A., et al. (2015). The climate hazards infrared precipitation with stations—A new environmental record for monitoring extremes. *Scientific Data*, 2, 150066, doi: 10.1038/sdata.2015.66.

Gimeno, L., Drumond, A., Nieto, R., Trigo, R.M., and Stohl, A. (2010). On the origin of continental precipitation. *Geophysical Research Letters*, 37, L13804, doi: 10.1029/2010GL043712.

Gimeno, L., Stohl, A., Trigo, R.M., Dominguez, F., Yoshimura, K., Yu, L., Drumond, A., Durán-Quesada, A.M., and Nieto, R. (2012). Oceanic and terrestrial sources of continental precipitation. *Reviews of Geophysics*, 50, RG4003, doi: 10.1029/2012RG000389.

Gimeno, L. (2014). Oceanic sources of continental precipitation. *Water Resources Research*, 50, 3647–3649, doi: 10.1002/2014WR015477.

Gimeno, L., Nieto, R., Drumond, A., Castillo, R., and Trigo, R. (2013). Influence of the intensification of the major oceanic moisture sources on continental precipitation. *Geophysical Research Letters*, 40, 1443–1450, doi:10.1002/grl.50338.

Gimeno, L. (2013). Grand challenges in atmospheric science. *Frontiers in Earth Science*, 1, 1–5, doi: 10.3389/feart.2013.00001.

Gimeno, L., Vázquez, M., Nieto, R., and Trigo, R.M. (2015). Atmospheric moisture transport: the bridge between ocean evaporation and Arctic ice melting. *Earth System Dynamics*, 2, 583-589, doi: 10.5194/esd-6-583-2015.

Gimeno-Sotelo, L., Nieto, R., Vázquez, M., and Gimeno, L. (2018). A new pattern of the moisture transport for precipitation related to the drastic decline in Arctic sea ice extent. *Earth System Dynamics*, 9, 611-625, doi: 10.5194/esd-9-611-2018.

Gomez-Hernandez, M., Drumond, A., Gimeno, L., and Garcia-Herrera, R. (2013). Variability of moisture sources in the Mediterranean region during the period 1980–2000. *Water Resources Research*, 49, 6781–6794, doi:10.1002/wrcr.20538.

Gomez-Hernandez, M. (2013). Analisis de las fuentes de humedad en la cuenca Mediterranea en el periodo 1980-2000. Tesis Doctoral. Universidad Complutense de Madrid, Facultad de Ciencias Fisicas. Dpto. Astrofisica y CC. de la Atmosfera.

Gunawardhana, L.N., Al-Rawas, G.A., Kwarteng, A.Y., Al-Wardy, M., and Charabi, Y. (2018). Potential changes in the number of wet days and its effect on future intense and annual precipitation in northern Oman. *Hydrology Research*, 49(1), 237–250, doi: 10.2166/nh.2017.188.

Held, I.M., and Soden, B.J. (2006). Robust responses of the hydrological cycle to global warming. *Journal of Climate*, 19(21), 5686–5699, doi: 10.1175/JCLI3990.1.

Hennessy, K.J., Suppiah, R., and Page, C.M. (1999). Australian rainfall changes, 1910–1995. *Australian Meteorological Magazine*, 48, 1–13. Available online: http://www.cmar.csiro.au/e-print/internal/hennessy_x1999a.pdf.

Hertig, E., Seubert, S., Paxian, A., Vogt, G., Paeth, H., and Jacobeit, J. (2013). Statistical modelling of extreme precipitation indices for the Mediterranean area under future climate change. *International Journal of Climatology*, 34, 1132–1156, doi: 10.1002/joc.3751.

Huang, Y., and Cui, X. (2015). Moisture sources of an extreme precipitation event in Sichuan, China, based on the Lagrangian method. *Atmospheric Science Letters*, 16, 177–183, doi: 10.1002/asl2.562.

Huffman, G.J., Adler, R.F., Arkin, P., Chang, A., Ferraro, R., Gruber, A., Janowiak, J., McNab, A., Rudolf, B., and Schneider, U. (1997). The Global Precipitation Climatology Project (GPCP) Combined Precipitation Dataset. *Bulletin of the American Meteorological Society*, 78, 5–20, doi: 10.1175/1520-0477(1997)078<0005:TGPCPG>2.0.CO;2.

Huntington, T.G., and Williams, R.S., Jr. (2012). The global hydrologic cycle. Supplemental Cryosphere Note 2 in Williams, R.S., Jr., and Ferrigno, J.G., *eds*., Satellite image atlas of glaciers of the world: U.S. Geological Survey Professional Paper 1386-A (State of the Earth's Cryosphere at the Beginning of the 21st Century: Glaciers, Snow Cover, Floating Ice, and Permafrost and Periglacial Environments).

IPCC, 2007: Climate Change 2007: The Physical Science Basis. Contribution of Working Group I to the Fourth Assessment Report of the Intergovernmental Panel on Climate Change [Solomon, S., D. Qin, M. Manning, Z. Chen, M. Marquis, K.B. Averyt, M. Tignor, and H.L. Miller (eds.)]. Cambridge University Press, Cambridge, United Kingdom and New York, NY, USA, 996 pp.

IPCC, 2012: Managing the Risks of Extreme Events and Disasters to Advance Climate Change Adaptation. A Special Report of Working Groups I and II of the Intergovernmental Panel on Climate Change. In: Field, C.B., Barros, V., Stocker, T.F., Qin, D., Dokken, D.J., Ebi, K.L., Mastrandrea, M.D., Mach, K.J., Plattner, G.-K., Allen, S.K., Tignor, M., Midgley, P.M. (Eds.). Cambridge University Press Cambridge, UK, and New York, NY, USA, 582 pp.

Katsanos, D., Retalis, A., Tymvios, F., and Michaelides, S. (2016). Analysis of precipitation extremes based on satellite (CHIRPS) and in situ dataset over Cyprus. *Natural Hazards*, 83, 53–63, doi: 10.1007/s11069-016-2335-8.

Khlebnikova, E.I. (2009). Middle-Latitude Climate Zones and Climate Types. Environmental Structure and Function: Climate System, Vol. 2. Paris, France: EOLSS Publications. Available online: https://www.eolss.net/sample-chapters/C01/E4-03-06-02.pdf.

Kidda, C., and Huffman, G. (2011). Review Global precipitation measurement. *Meteorological Applications*, 18, 334–353. doi: 10.1002/met.284.

Kovats, R.S., Valentini, R., Bouwer, L.M., Georgopoulou, E., Jacob, D., Martin, E., Rounsevell, M., and Soussana, J.-F. (2014). In: Climate Change 2014: Impacts, Adaptation, and Vulnerability. Part B: Regional Aspects. Contribution of Working

Group II to the Fifth Assessment Report of the Intergovernmental Panel on Climate Change [Barros, V.R., C.B. Field, D.J. Dokken, M.D. Mastrandrea, K.J. Mach, T.E. Bilir, M. Chatterjee, K.L. Ebi, Y.O. Estrada, R.C. Genova, B. Girma, E.S. Kissel, A.N. Levy, S. MacCracken, P.R. Mastrandrea, and L.L.White (eds.)]. Cambridge University Press, Cambridge, United Kingdom and New York, NY, USA, pp. 1267-1326.

Kundzewicz, Z.W., Radziejewski, M., and Pinskwar, I. (2006). Precipitation extremes in the changing climate of Europe. *Climate Research*, 31, 51–58. doi: 10.3354/cr031051.

Läderach, A., and Sodemann, H. (2016). A revised picture of the atmospheric moisture residence time. *Geophysical Research Letters*, 43, 2, doi: 10.1002/2015GL067449.

Lasda, O., Dikou, A., and Papapanagiotou, E. (2010). Flash flooding in Attika, Greece: climatic change or urbanization? *Ambio*, 39(8), 608–11, doi: 10.1007/s13280-010-0050-3.

Legates, D.R., and Willmott, C.J. (1990). Mean seasonal and spatial variability in gauge-corrected, global precipitation. *International Journal of Climatology*, 10, 111–127, doi: 10.1002/joc.3370100202.

Lionello, P., Malanotte-Rizzoli, P., Boscolo R., Alpert, P., Artale, V., Li, L., Luterbacher, J., et al. (2006). The Mediterranean Climate: An overview of the main characteristics and issues. *Developments in Earth Environmental Sciences*, 4, 1–26, doi: 10.1016/S1571-9197(06)80003-0.

Llasat, M.C., Marcos, R., Turco, M., Gilabert, J., and Llasat-Botija, M. (2014). Trends in flash flood events versus convective precipitation in the Mediterranean region: The case of Catalonia. *Journal of Hydrology*, 541, 24–37, doi: 10.1016/j.jhydrol.2016.05.040.

Lorenz, C., and Kunstmann, H. (2012). The hydrological cycle in three state-of-the-art reanalyses: Intercomparison and performance analysis. *Journal of Hydrometeorology*, 13, 1397–1420, doi:10.1175/jhm-d-11–088.1.

Lucarini, V., Danihlik, R., Kriegerova, I., and Speranza, A. (2008). Hydrological cycle in the Danube basin in present-day and XXII century simulations by IPCCAR4 global climate models. *Journal of Geophysical Research*, 113, D09107, doi: 10.1029/2007JD009167.

Marengo, J.A., Jones, R., Alvesa, L.M., and Valverdea, M.C. (2009). Future change of temperature and precipitation extremes in South America as derived from the PRECIS regional climate modeling system. *International Journal of Climatology*, 29, 2241–2255, doi: 10.1002/joc.1863.

Martin-Gómez, V., Hernandez-Garcia, E., Barreiro, M., and López, C. (2016). Interdecadal Variability of Southeastern South America Rainfall and Moisture Sources during the Austral Summertime. *Journal of Climate*, 29, 6751–6763, doi: 10.1175/JCLI-D-15-0803.1.

Mehta, A.V., and Yang, S. (2008). Precipitation Climatology over Mediterranean Basin from Ten Years of TRMM Measurements. *Advances in Geosciences*, 17, 87–91, doi: 10.5194/adgeo-17-87-2008.

Michaelides, S., Levizzani, V., Anagnostou, E., Bauer, P., Kasparis, T., and Lane, J.E. (2009). Precipitation: measurement remote sensing, climatology and modelling. *Atmospheric Research*, 94, 512–533, doi: 10.1016/j.atmosres.2009.08.017.

Milelli, M., Llasat, M.C., and Ducroq, V. (2006). The cases of June 2000, November 2002 and September 2002 as examples of Mediterranean floods. *Natural Hazards and Earth System Sciences*, 6, 271–284, doi: 10.5194/nhess-6-271-2006.

New, M., Todd, M., Hulme, M., and Jones, P. (2001). Precipitation measurements and trends in the twentieth century. *International Journal of Climatology*, 21, 1899–1922, doi: 10.1002/joc.680.

Nieto, R., Gimeno, L., Drumond, A., and Hernandez, E. (2010a). A Lagrangian identification of the main moisture sources and sinks affecting the Mediterranean area. *WSEAS Transactions on Environment and Development*, 5, 365–374, ISSN: 1790-5079.

Nieto, R., Gimeno, L., and Trigo, R.M. (2006). A Lagrangian identification of major sources of Sahel moisture. *Geophysical Research Letters*, 33, L18707, doi: 10.1029/2006GL027232.

Nieto, R., Duran-Quesada, A.M., and Gimeno, L. (2010b). Major sources of moisture over Antarctic ice-core sites identified through a Lagrangian approach. *Climate Research*, 41, 45–49, doi: 10.3354/cr00842.

Numaguti, A. (1999). Origin and recycling processes of precipitating water over the Eurasian continent: Experiments using an atmospheric general circulation model. *Journal of Geophysical Research*, 104, 1957–1972, doi: 10.1029/1998jd200026.

Ogino, S., Yamanaka, M.D., Mori, S., and Matsumoto, J. (2016). How Much is the Precipitation Amount over the Tropical Coastal Region? *Journal of Climate*, 29, 1231–1236, doi: 10.1175/JCLI-D-15-0484.1.

Oki, T., and Kanae, S. (2006). Global Hydrological Cycles and World Water Resources. *Science*, 313(5790), 1068–1072, doi: 10.1126/science.1128845.

Palazzi, E., and Provenzale, A. (2016). Water in the climate system. In: Provenzale, A., Palazzi, E., Fraedrich K. (eds) The Fluid Dynamics of Climate. CISM International Centre for Mechanical Sciences, vol 564. Springer, Vienna.

Pan, X.L., Kanaya, Y., Wang, Z.F., Tang, X., Takigawa, M., Pakpong, P., Taketani, F., and Akimoto, H. (2014). Using Bayesian optimization method and FLEXPART tracer model to evaluate CO emission in East China in springtime. *Environmental Science and Pollution Research*, 21, 3873, doi: 10.1007/s11356-013-2317-2.

Parry, M.L. (2000). Assessment of potential effects and adaptations for climate change in Europe: the Europe ACACIA Project. University of East Anglia, Norwich.

Peixoto, J.P., and Oort, A.H. (1992). Physics of Climate, AIP-Press, New York, NY, Springer Verlag, New York Press.

Ramos, A.M., Trigo, R.M., and Liberato, M.L.R. (2014). A ranking of high-resolution daily precipitation extreme events for the Iberian Peninsula. *Atmospheric Science Letters*, 15, 328–334, doi: 10.1002/asl2.507.

Ramos, A.M., Trigo, R.M., and Liberato, M.L.R. (2017). Ranking of multi-day extreme precipitation events over the Iberian Peninsula. *International Journal of Climate*, 37, 607–620, doi: 10.1002/joc.4726.

Salah, Z., Nieto, R., Drumond, A., Gimeno, L., and Vicente-Serrano, S.M. (2018). A Lagrangian analysis of the moisre budget over the Fertile Crescent during two intense drought episodes. *Journal of Hydrology*, 560, 382–395, doi: 10.1016/j.jhydrol.2018.03.021.

Santos, C., and Costa dos, A. (2014). Recent changes in temperature and precipitation extremes in an ecological reserve in Federal District, Brazil. *Revista Brasileira de Meteorologia*, 29(1), 13–20, doi: 10.1590/S0102-77862014000100002.

Seibert, P., and Frank, A. (2004). Source-receptor matrix calculation with a Lagrangian particle dispersion model in backward mode. *Atmospheric Chemistry and Physics*, 4, 51–63, doi: 10.5194/acp-4-51-2004.

Serreze, M.C., and Hurst, C.M. (2000). Representation of Mean Arctic Precipitation from NCEP–NCAR and ERA Reanalyses. *Journal of Climate*, 13, 182–201, doi: 10.1175/1520-0442(2000)013<0182:ROMAPF>2.0.CO;2.

Shmakin, A.B., and Popova, V.V. (2006). Dynamics of climate extremes in northern Eurasia in the late 20th century. *Izvestiya, Atmospheric and Oceanic Physics*, 42, 138–147, doi: 10.1134/S0001433806020022.

Simmons, A., Uppala, S., Dee, D., and Kobayashi, S. (2007). ERA-Interim: New ECMWF Reanalysis Products from 1989 Onwards. *ECMWF Newsletter*, 110, 25–35, doi: 10.21957/pocnex23c6.

Smalley, M., and L'Ecuyer, T. (2015). A Global Assessment of the Spatial Distribution of Precipitation Occurrence. *Journal of Applied Meteorology and Climatology*, 54, 2179–2197, doi: 10.1175/JAMC-D-15-0019.1.

Sodemann, H., and Zubler, E. (2010). Seasonal and inter-annual variability of the moisture sources for Alpine precipitation during 1995–2002. *International Journal of Climatology*, 30, 947–961, doi: 10.1002/joc.1932.

Sodemann, H., and Stohl, A. (2009). Asymmetries in the moisture origin of Antarctic precipitation. *Geophysical Research Letters*, 36, L22803, doi: 10.1029/2009GL040242.

Sodemann, H., Wernli, H., and Schwierz, C. (2009). Sources of water vapour contributing to the Elbe flood in August 2002: A tagging study in a mesoscale model. *Quarterly Journal of the Royal Meteorological Society*, 135, 205–223, doi:10.1002/qj.374.

Sorí, R., Nieto, R., Drumond, A., Vicente-Serrano, S.M., and Gimeno, L. (2017a). The atmospheric branch of the hydrological cycle over the Indus, Ganges, and Brahmaputra river basins. *Hydrology and Earth System Sciences*, 21, 6379–6399, doi: 10.5194/hess-21-6379-2017.

Sorí, R., Nieto, R., Vicente-Serrano, S.M., Drumond, A., and Gimeno, L. (2017b). A Lagrangian Perspective of the Hydrological Cycle in the Congo River Basin, *Earth System Dynamics*, 8, 653–675, doi: 10.5194/esd-2017-21.

Sorí, R., Nieto, R., Drumond, A. and Gimeno, L., (2017c). The Niger River Basin Moisture Sources: A Lagrangian Analysis. *Atmosphere*, 8(2), 38, doi: 10.3390/atmos8020038.

Sorí, R., Marengo, J., Nieto, R., Drumond, A., and Gimeno, L. (2018). The Atmospheric Branch of the Hydrological Cycle over the Negro and Madeira River Basins in the Amazon Region, *Water*, 10(6), 738, doi: 10.3390/w10060738.

Stadtherr, L., Coumou, D., Petoukhov, V., Petri, S., and Rahmstorf, S. (2016). Record Balkan floods of 2014 linked to planetary wave resonance. *Science Advances*, 2, e1501428, doi: 10.1126/sciadv.1501428.

Stewart, R.H. (2008). Introduction to Physical Oceanography. Department of Oceanography, Texas A. and M. University.

Stohl, A., Hittenberger, M., and Wotawa, G. (1998). Validation of the lagrangian particle dispersion model FLEXPART against large-scale trace experiment data. *Atmospheric Environment*, 32(24), 4245–4264, doi: 10.1016/s1352-2310(98)00184-8.

Stohl, A, Forster, C, Frank, A, Seibert, P., and Wotawa, G. (2005). Technical note: The Lagrangian particle dispersion model FLEXPART 6.2. *Atmospheric Chemistry and Physics*, 5, 2461–2474, doi: 10.5194/acp-5-2461-2005.

Stohl, A., Forster, C., Eckhardt, S., Spichtinger, N., Huntrieser, H., Heland, J., Schlager, H., Wilhelm, S., Arnold, F., and Cooper, O. (2003). A backward modeling study of intercontinental pollution transport using aircraft measurements. *Journal of Geophysical Research*, 108, 4370. doi: 10.1029/2002JD002862.

Stohl, A. (1999). The Flexpart Particle Dispersion Model Version 3.1. User Guide. University of Munich, Germany. Available online: https://folk.nilu.no/~andreas/flexpart/flexpart31.pdf.

Stohl, A., and James, P. (2005). A Lagrangian analysis of the atmospheric branch of the global water cycle: Part II: Moisture transports between Earth's ocean basins and river catchments. *Journal of Hydrometeorology*, 6, 961–984, doi:10.1175/JHM470.1.

Stohl, A., and James, P. (2004). A Lagrangian analysis of the atmospheric branch of the global water cycle. Part I: Method description, validation, and demonstration for the August 2002 flooding in central Europe. *Journal of Hydrometeorology*, 5, 656–678, doi: 10.1175/1525-7541(2004)005<0656:ALAOTA>2.0.CO;2.

Sun, Q., Miao, C., Duan, Q., Ashouri, H., Sorooshian, S., and Hsu, K.-L. (2018). A review of global precipitation data sets: Data sources, estimation, and inter-comparisons. *Reviews of Geophysics*, 56, 79–107, doi: 10.1002/2017RG000574.

Toteri, A., and Desiato, F. (2008). Changes in temperature extremes over Italy in the last 44 years. *International Journal of Climatology*, 28, 733–745. doi: 10.1002/joc.1576.

Trenberth, K.E., Dai, A., Rasmussen, R.M., and Parsons, D.B. (2003). The changing character of precipitation. *Bulletin of the American Meteorological Society*, 84(9), 1205–1217, doi: 10.1175/BAMS-84-9-1205.

Trenberth, K.E. (2011). Changes in precipitation with climate change. *Climate Research*, 47, 123–138, doi: 10.3354/cr00953.

Trenberth, K.E., Fasullo, J.T., and Mackaro, J. (2011). Atmospheric moisture transports from ocean to land and global energy flows in reanalyses. *Journal of Climate*, 24(18), 4907–4924, doi:10.1175/2011jcli4171.1.

Trenberth, K.E. (1999). Atmospheric moisture recycling: Role of advection and local evaporation. *Journal of Climate*, 12, 1368–1381, doi: 10.1175/1520-0442(1999)012<1368:AMRROA>2.0.CO;2.

Trigo, R., Xoplaki, E., Zorita, E., Luterbacher, J., Krichak, S.O., Alpert, P., Jacobeit, J., Saenz, J., Fernandez, J., González-Rouco, F., et al. (2006). Relations between variability in the Mediterranean region and mid-latitude variability. *Developments in Earth Environmental Sciences*, 4, 179–226, doi: 10.1016/S1571-9197(06)80006-6.

Tu, J.-Y., and Chou, C. (2013). Changes in precipitation frequency and intensity in the vicinity of Taiwan: typhoon versus non-typhoon events. *Environmental Research Letters*, 8, 014023, doi: 10.1088/1748-9326/8/1/014023.

Turner, J., and Marshall, G.J. (2011). Climate Change in the Polar Regions. Cambridge, Cambridge University Press, 434 pp, ISBN 978-0-521-85010-0.

van der Ent, R.J., and Savenije, H.H.G. (2013). Oceanic sources of continental precipitation and the correlation with sea surface temperature. *Water Resources Research*, 49, 3993–4004, doi: 10.1002/wrcr.20296.

van der Ent, R.J., Savenije, H.H.G., Schaefli, B., and Steele-Dunne, S.C. (2010). Origin and fate of atmospheric moisture over continents. *Water Resources Research*, 46, W09525, doi: 10.1029/2010WR009127.

van der Ent, R., and Tuinenburg, O.A. (2017). The residence time of water in the atmosphere revisited. *Hydrology and Earth System Science*, 21, 779–790, doi: 10.5194/hess-21-779-2017.

Vázquez, M., Nieto, R., Drumond, A., and Gimeno, L. (2016). Moisture transport into the Arctic: Source-receptor relationships and the roles of atmospheric circulation and evaporation. *Journal of Geophysical Research: Atmospheres*, 121, doi: 10.1002/2016JD025400.

Vázquez, M., Nieto, R., Drumond, A., and Gimeno, L. (2017). Extreme Sea Ice Loss over the Arctic: An Analysis Based on Anomalous Moisture Transport. *Atmosphere*, 8(2), 32, doi: 10.3390/atmos8020032.

Vázquez, M., Nieto, R., Drumond, A., and Gimeno, L. (2018). Moisture transport from the Arctic: a characterization from a Lagrangian perspective. *Cuadernos de Investigación Geográfica*, 1–12, doi:10.18172/cig.3477.

Wang. Y., and Zhou, L. (2005). Observed trends in extreme precipitation events in China during 1961–2001 and the associated changes in large-scale circulation. *Geophysical Research Letters*, 32, L09707, doi: 10.1029/2005GL022574.

Wegman, M., Orsolini, Y., Vázquez, M., Gimeno, L., Nieto, R., Bulygina, O., Jaiser, R., Handorf, D., Rinke, A., Dethloff, K., Sterin, A., and Brönnimann, S. (2015). Arctic moisture source for Eurasian snow cover variations in autumn. *Environmental Research Letters*, 10, 054015, doi: 10.1088/1748-9326/10/5/054015.

Xoplaki, E., Gonzalez-Rouco, J.F., Luterbacher, J., and Wanner, H. (2004). Wet season Mediterranean precipitation variability: influence of large-scale dynamics and trends. *Climate Dynamics*, 23, 63–78, doi: 10.1007/s00382-004-0422-0.

Zhao, G.-J., Hörmann, G., Fohrer, N., Gao, J.-F., Zhai, J.-Q., and Zhang, Z.-X. (2009). Spatial and temporal characteristics of wet spells in the Yangtze River Basin from 1961 to 2003. *Theoretical and Applied Climatology*, 98, 107–117, doi: 10.1007/s00704-008-0099-0.

Zolotokrylin, A., and Cherenkova, E. (2017). Seasonal Changes in Precipitation Extremes in Russia for the Last Several Decades and Their Impact on Vital Activities of the Human Population. *Geography, Environment, Sustainability*, 10, 69–82. doi: 10.24057/2071-9388-2017-10-4-69-82.